UCRL-15420
S/C 6448509

NOTICE
PORTIONS OF THIS REPORT ARE ILLEGIBLE.
It has been reproduced from the best available copy to permit the broadest possible availability.

UCRL--15420

DE82 011066

DESIGN GUIDE FOR COMPOSITE-MATERIAL FLYWHEELS: ROTOR DYNAMIC CONSIDERATIONS PART I - SYSTEM WHIRLING AND STABILITY

C. W. Bert
G. Ramunujam

School of Aerospace, Mechanical and Nuclear Engineering
The University of Oklahoma
Norman, Oklahoma 73019

MASTER

September 1981

Lawrence Livermore Laboratory

This document is
PUBLICLY RELEASABLE
Barry Steele
Authorizing Official
Date: 8-29-07

DISTRIBUTION OF THIS DOCUMENT IS UNLIMITED

DISCLAIMER

This report was prepared as an account of work sponsored by an agency of the United States Government. Neither the United States Government nor any agency Thereof, nor any of their employees, makes any warranty, express or implied, or assumes any legal liability or responsibility for the accuracy, completeness, or usefulness of any information, apparatus, product, or process disclosed, or represents that its use would not infringe privately owned rights. Reference herein to any specific commercial product, process, or service by trade name, trademark, manufacturer, or otherwise does not necessarily constitute or imply its endorsement, recommendation, or favoring by the United States Government or any agency thereof. The views and opinions of authors expressed herein do not necessarily state or reflect those of the United States Government or any agency thereof.

DISCLAIMER

Portions of this document may be illegible in electronic image products. Images are produced from the best available original document.

Research Report
OU-AMNE-81-5

DESIGN GUIDE FOR COMPOSITE-MATERIAL FLYWHEELS: ROTOR DYNAMIC CONSIDERATIONS PART I - SYSTEM WHIRLING AND STABILITY

Final Report on
Subcontract No. 6448509

by

C.W. Bert and G. Ramanujam
School of Aerospace, Mechanical and Nuclear Engineering
The University of Oklahoma
Norman, Oklahoma 73019

Prepared for

University of California
Lawrence Livermore National Laboratory
Livermore, California 94550

September 1981

DISCLAIMER

This book was prepared as an account of work sponsored by an agency of the United States Government. Neither the United States Government nor any agency thereof, nor any of their employees, makes any warranty, express or implied, or assumes any legal liability or responsibility for the accuracy, completeness, or usefulness of any information, apparatus, product, or process disclosed, or represents that its use would not infringe privately owned rights. Reference herein to any specific commercial product, process, or service by trade name, trademark, manufacturer, or otherwise, does not necessarily constitute or imply its endorsement, recommendation, or favoring by the United States Government or any agency thereof. The views and opinions of authors expressed herein do not necessarily state or reflect those of the United States Government or any agency thereof.

DISTRIBUTION OF THIS DOCUMENT IS UNLIMITED

MGW

FOREWORD

This report has been prepared under Lawrence Livermore National Laboratory Subcontract No. 6448509 with the University of Oklahoma. Work accomplished herein is part of the Flywheel Rotor and Containment Technology Task of the Mechanical Energy Storage Project. Professor Charles W. Bert was the Principal Investigator and Dr. Satish V. Kulkarni was the LLNL Project Engineer.

ABSTRACT

This report is the first part of a design guide for composite-material flywheel dynamics. In this report, the flywheel itself is considered as a rigid body, although shaft flexibilities are considered. In Part II, three types of flexible flywheels are considered.

The objective of this report is to provide information to designers of flywheels which will enable them to predict many aspects of the dynamic behavior of their flywheel systems when spin-tested with a quill-shaft support and driven by an air turbine.

Computer programs are presented for the following dynamic analyses to obtain the results indicated:

1. Free whirling: natural frequencies versus rotational speed (or for brevity critical speeds of various orders) and the associated mode shapes.

2. Routh-type stability analysis: to determine the stability limits, i.e., the speed range within which small perturbations attenuate rather than causing catastrophic failure.

3. Forced whirling analysis: to estimate the response of major components of the system to flywheel mass eccentricity and initial tilt.

For the first and third kinds of analyses, two different mathematical models of the generic system are investigated. One is a seven-degree-of-freedom lumped-parameter analysis, while the other is a combined distributed- and lumped-parameter analysis. When applied to an existing flywheel system (the Garrett AiResearch multi-ring design), the two models yielded numerical values for the lowest first-order forward critical speed in very close agreement with each other and with experimental results obtained in spin tests.

Thus, in the interests of computational economy, for the second kind of analysis, only the lumped-parameter model is implemented.

Qualitative discussions as to why forced retrograde whirling is not as severe as forward whirling are also presented.

The analyses are applied to three specific prototype flywheel systems: the multi-material ring type mentioned above, a constant-thickness-disk ring type (General Electric), and a tapered-thickness-disk type (Lawrence Livermore National Laboratory). In addition, the effects of the following flywheel design parameters on system dynamics are investigated:

1. Flywheel mass
2. Flywheel diametral and polar mass moments of inertia
3. Location of flywheel mass center from the lower end of the quill shaft
4. Quill shaft length
5. Lower turbine-bearing support stiffness
6. Equivalent viscous damping coefficient of the external damper
7. Flywheel dead weight
8. Torque applied at the turbine

TABLE OF CONTENTS

	Page
FOREWORD	ii
ABSTRACT	iii
GLOSSARY OF TERMS	vii
1. INTRODUCTION	1
2. LUMPED-PARAMETER MODEL	5
2.1 Description of Model	5
2.2 Free Whirling Analysis	7
2.3 Stability Analysis	10
2.4 Forced Whirling Analysis	11
3. COMBINED (DISTRIBUTED- AND LUMPED-PARAMETER) MODEL	13
3.1 Description of Model	13
3.2 Free Whirling Analysis	15
3.3 Forced Whirling Analysis	16
4. NUMERICAL RESULTS FOR A BASELINE FLYWHEEL SYSTEM	17
4.1 Free Whirling: Campbell Diagrams and Mode Shapes	17
4.2 Stability Growth Factor	31
4.3 Forced Whirling Response	39
5. PARAMETRIC STUDIES	46
5.1 Forward Critical Speeds	46
5.2 Instability Limits	54
5.3 Forced Whirling Response of Forward Branches	55
5.4 Forced Whirling Response of Retrograde Branches	59
6. CONCLUSIONS	60
ACKNOWLEDGMENTS	64
REFERENCES	65
APPENDICES:	
A DETAILED DERIVATIONS FOR LUMPED-PARAMETER MODEL	69
B DERIVATIONS RELATED TO THE COMBINED MODEL	80

Page

C COMPUTER CODES, FLOW CHARTS, AND NOTES FOR USERS 102

C.1 Free Whirling & Stability Using the Lumped Model 102
C.2 Forced Whirling Using the Lumped Model 130
C.3 Free Whirling Analysis Using the Combined Model 138
C.4 Simplified Program for Critical Speeds Using the Combined Model 160
C.5 Forced Whirling Analysis Using the Combined Model 166

D EFFECTS OF FLYWHEEL DEAD WEIGHT AND TORQUE ON THE LOWEST FIRST FORWARD CRITICAL SPEED OF A PENDULOUSLY SUPPORTED FLYWHEEL 174

D.1 Effect of Flywheel Dead Weight 174
D.2 Effect of Load Torque 178

E LIST OF SYMBOLS 180

F SUGGESTIONS FOR FURTHER RESEARCH ON ANALYSIS OF FLYWHEEL ROTOR DYNAMICS 187

GLOSSARY OF TERMS*

Different investigators in the field of rotor dynamics have used certain terms in quite a variety of different contexts. Therefore, for purposes of clarity, most of the specialized terms for this field are defined, in the way that they are used in this design guide, in this section. The terms are arranged in alphabetical order.

Bearing - any support, with low rotational friction, which carries the rotor and offers radial restraint.

Branch - in a plot of whirling frequency of a given mode (see Mode) versus rotational speed, there is only one curve at zero rotational speed; however, as rotational speed is increased, this single curve splits into two curves (unless there is negligible gyroscopic action associated with this particular mode). Each of these curves is referred to as a branch. The higher-frequency branch is associated with forward whirling (see Forward Whirling) and the lower-frequency one with retrograde whirling (see Retrograde Whirling).

Campbell Diagram - a plot of curves of whirling frequencies of various modes and branches versus rotational speed.

Combined Analysis - a rotor dynamic analysis (see Rotor Dynamics) containing both distributed-parameter and lumped-parameter models of various components of a rotor (see Rotor).

---

*A Complete list of symbols used in this design guide is presented in Appendix E.

Critical Speed - a rotational speed (Ω) at which a resonance occurs; usually this occurs when the whirling frequency (ω) is equal to $n\Omega$, where n is the order of the excitation (usually an integer, either positive or negative).

Damping - a velocity-dependent action (force or couple) resisting motion; see External Damping and Internal Damping.

Diametral Mass Moment of Inertia - the mass moment of inertia (see Mass Moment of Inertia), about a diameter passing through the component's mass center, of a rotor component in the form of a body of revolution.

Distributed-Parameter Analysis (Model) - a rotor dynamic analysis (or model) in which all of the components of the rotor are modeled as having distributed mass, damping, and/or stiffness.

Dynamic Unbalance - the type of unbalance in which rotational speed sets up an unbalanced couple; an example is a flywheel system in which the flywheel axis has an initial tilt with respect to the axis of rotation.

Eccentricity - distance from the mass center of a body at rest to the axis of rotation.

External Damping - damping (see Damping) between a rotating member and a stationary member; in a flywheel system, the largest source of such damping is intentionally introduced in an external damping device that acts on the flywheel shaft.

Flywheel - the main energy-storage element of a flywheel system.

Flywheel Shaft - the shaft on which the flywheel is mounted; called the quill shaft on Barbour Stockwell air-turbine-drive spin-test facilities.

Flywheel System - a complete mechanical-energy-storage system in which energy is stored in the form of kinetic energy.

Forced Whirling - the response of a system, to an unbalance excitation due to static or dynamic unbalance or both.

Forward Critical Speed - critical speed (see Critical Speed) associated with forward whirling and in which the order (see Order) is positive.

Forward Whirling - whirling (see Whirling) in which the direction of whirling coincides with the direction of rotor rotation, due to forward-precession gyroscopic action.

Free Whirling - whirling of a rotor (see Rotor) without an excitation; analogous to free vibration of a nonrotating system.

Frequency - the number of cycles of vibration (in this case, whirling) per unit time.

Generalized Displacement - translation or tilt.

Generalized Force - force or couple.

Growth Factor - a Routh-type stability parameter which indicates an unstable exponential growth with time if positive and a stable exponential decay if negative.

Gyroscopic Action - a modification of the basic transverse whirling action, due to the gyroscopic couple associated with tilting of a massive component of a rotor (such as the flywheel or the air turbine).

Initial Tilt - angle between the geometric axis of a rotor component and the axis of rotation of the rotor; this angle is measured when the rotor is at rest.

Instability - opposite of stability (see Stability); highly undesirable from the standpoint of system safety and reliability.

Internal Damping - damping (see Damping) within any of the rotating parts of a flywheel system; in such a system, the principal source of this kind of damping is internal material damping (sometimes called hysteretic damping).

Lumped-Parameter Analysis (Model) - a rotor dynamic analysis (or model) in which all of the components of the system are modeled by lumped (concentrated) mass damping, and/or stiffness.

Mass - the inertial coefficient (m) in Newton's second law for translational motion.

Mass Moment of Inertia - the inertial coefficient in Euler's equations for rotational motion, given by the following volumetric intregral

$$I_x = \iiint_V \rho r_x^2 \, dV$$

where ρ is the material density, r_x is the distance of an arbitrary point from the axis of rotation, and V is the volume.

Material Damping - see Internal Damping.

Mode - a distinct vibration configuration with associated natural frequency and mode shape; a discrete system with N degrees of freedom has N modes of vibration (or less if the system has one or more degrees of freedom associated with rigid body motion); a continuous system theoretically has an infinite number of degrees of freedom.

Mode Shape - a plot of the generalized displacements (translation and tilt), associated with a given mode, versus position in the system.

Natural Frequency - the number of cycles per unit time at which a system undergoes free whirling (or free vibration).

Operating Speed Range - speed range over which a flywheel is expected to be operated, usually from 25% (or 50%) of maximum to maximum operating speed.

Order - frequency of an excitation source, measured in multiples of rotational speed, i.e., ω/Ω.

Polar Mass Moment of Inertia - the mass moment of inertia (see Mass Moment of Inertia)(of a rotor component in the form of a body of revolution) about its axis of revolution.

Quill Shaft - the flywheel shaft on a pendulously supported flywheel system under spin test on a Barbour Stockwell air-turbine-drive system.

Resonance - the forced-vibration (or forced-whirling) phenomenon in which a peak response occurs.

Restoring Action - a generalized force (force or couple) tending to restore a system to equilibrium.

Retrograde Critical Speed - critical speed (see Critical Speed) associated with retrograde whirling (see Retrograde Whirling) and in which the order (see Order) is positive.

Retrograde Whirling - whirling (see Whirling) in which the direction of whirling is backward, i.e., opposite to the direction of rotor rotation, due to backward-precession gyroscopic action.

Rotational Speed - the speed at which the rotating components of the flywheel system turn in the bearings; also called running speed.

Rotor - a generic term referring to all of the rotating components.

Rotor Dynamics - the dynamic behavior of a rotor.

Shaft - a flexible beam (usually circular in cross section) which connects any two components of a rotor; see Flywheel Shaft, Quill Shaft, and Turbine Shaft.

Shear Factor - a correction factor used with Timoshenko beam theory to more accurately account for the distribution of transverse shear strain across a shaft cross section.

Stability - the tendency for the response of a system (to a small, sudden perturbation) to decay with time; this, of course, is a highly desirable characteristic.

Static Unbalance - the type of unbalance in which rotational speed sets up an unbalanced force; may be specified either as eccentricity of the local mass center or its product with the local mass.

Stiffness - the derivative of generalized restoring force with respect to generalized displacement, i.e., the spring constant.

Synchronous Whirl - a forward whirling in which the shaft rotational speed equals the shaft whirling frequency; i.e., it has an order of +1.

System - the interacting combination of rotor(s), bearings, pedestals, etc.

Tilt - angle between the geometric axis of a rotor component and the axis of rotation of the rotor.

Turbine Shaft - shaft, supported on bearings, to which the air turbine and quill shaft are attached.

Unbalance - see Dynamic Unbalance and Static Unbalance.

Whirl - rotor transverse orbital motion about the static equilibrium position at any location along the length of the rotor(s).

Whirl Map - see Campbell Diagram.

Whirling Frequencies - frequency of whirling action (see Whirl).

1. INTRODUCTION

The use of a rotating wheel, called a flywheel, to store mechanical energy dates back to antiquity in the form of the potter's wheel, believed to be approximately 5,500 years old [1]. In the present century, flywheels have been used in buses, spacecraft auxiliary power systems, regenerative braking systems for railroad trains, and automobiles.

The scarcity and rising costs of petroleum have motivated international interest in reducing the use of petroleum-derived fuels. In view of the large number of automobiles in service and the nearly universal use of gasoline or diesel fuel to power them, an important means of reducing petroleum usage could be by introducing hybrid automobiles using flywheels for energy storage. Until just recently, practically all of the flywheels developed have been constructed of materials that are essentially homogeneous and isotropic, such as steel and titanium alloy. Thus, these flywheels have been quite heavy and not competitive with storage batteries in energy storage per unit weight.

Recently, with the continuing development and commercialization of improved filamentary composite materials, there has been considerable interest in the possibility of using these high-strength lightweight materials to construct flywheels that are lighter in weight and more compact in size and yet having excellent energy-storage capacity. It is well established that in designing for steady centrifugal stresses, the only material parameter affecting the energy storage per unit weight is the governing failure strength per unit density [2]. Thus, a variety of high-performance flywheel systems under development in the United States for automotive energy storage use fiber-reinforced, polymer-matrix composite materials [3]. However, to actually achieve

this higher energy-storage potential of composite-material flywheels, it is imperative that they be operated at much higher rotational speeds than is feasible for flywheels constructed of conventional homogeneous materials. Unfortunately, however, this higher speed requirement has been very difficult to achieve in practice because of rotor-dynamic considerations.

In view of the preceding discussion, it is apparent that the success of the U.S. high-performance flywheel program depends very critically upon the rotor-dynamic characteristics of such systems. The rotor-dynamics field has a long history extending over a century to the work of Rankine in 1869 [4], and including numerous treatises and monographs [5-10]. However, these works, as well as numerous research papers, have been concerned almost exclusively with geometrical configurations typical of steam and gas turbines, compressors, and electric motors.

Probably the first rotor-dynamic analysis appropriate to flywheel systems is due to Thomson, Younger, and Gordon in 1977 [11]. They analyzed whirling of a single-mass system with a single vertical shaft mounted on flexible bearing supports and compared the predicted critical speeds with experimental results obtained from two different small models. The system was modeled as a lumped-parameter system having two degrees of freedom: flywheel lateral translation and flywheel tilt. Shortly thereafter, McKinnon [12] made a lumped-parameter analysis including these three degrees of freedom: lateral translation and tilting of the flywheel hub and tilting of the flywheel rim. Unfortunately, some program errors were found in [12], making its results questionable. This work was corrected and extended by Bert et al. [13] to include one more degree of freedom: lateral translation of the flywheel rim with respect to the hub.

In the majority* of the major spin-testing facilities in the United States, the flywheel is pendulously supported by a vertical quill shaft, which in turn is mounted concentrically at its top end to an air-turbine drive system. The first analysis to consider the turbine-wheel dynamics and the flexibility of the turbine shaft on its bearing supports was the work of Bert and Chen [17]. This was a lumped-parameter analysis which included six degrees of freedom: lateral translation and tilt of the flywheel rim, flywheel hub, and turbine wheel. This analysis was later extended by Chen and Bert [18] to include two more degrees of freedom: translation and tilt of an external viscous damper mounted between the flywheel shaft and ground. Further studies of this system, with a more refined variable-coefficient model of the damper, were reported in [19].

All of the FRD (flywheel rotor dynamics) analyses mentioned so far have been lumped-parameter analyses. To the best of the present investigators' knowledge, the only FRD analyses which considered the distributed nature of the stiffness and mass of the shafts were the limited applications of finite-element codes reported in [16,20].

The purpose of this report is to present FRD analyses of flywheels supported in a manner typical of current flywheel test facilities, i.e., with the flywheel pendulously supported by a quill shaft concentric to a ball-bearing-supported air turbine and provided with oil-type external damping. Based on the studies in [18-19,21], it can be concluded that the internal flexibility between the flywheel rim and hub, even in such a flexible band system as in the Sandia

*These include: Johns Hopkins University Applied Physics Laboratory, Laurel, MD [14]; Oak Ridge Flywheel Evaluation Laboratory, Y-12 Plant, Oak Ridge, TN [15]; Sandia National Laboratories, Livermore, CA [16]; and General Electric Co., Corporate Research and Development, Schenectady, NY. One exception is the Rocketdyne facility at Canoga Park, CA, which has provisions for a horizontal shaft mounted on a fixed bearing support at each end.

20-inch-diameter flywheel, has a negligible effect on rotor dynamics for speeds up to design burst speeds.* Furthermore, in view of the long length of the damper on the 4-inch Barbour Stockwell air turbine as used in the Oak Ridge Flywheel Evaluation Laboratory [15], it was decided to assume that the damper is constrained to move only laterally (no tilting). Thus, one system model used in the present investigation is a seven-degree-of-freedom lumped-parameter analysis. The other is a combined model consisting of three shafts modeled as distributed-parameter elements and the remaining rigid-body mass elements.

The three kinds of analyses conducted are the same three considered in [18]:

1. Free whirling
2. Routh-type stability criteria
3. Forced whirling due to both mass eccentricity and initial tilt of the flywheel

However, here, in the free whirling analysis, results are presented for mode shapes as well as Campbell diagrams (whirl maps of frequency versus running speed).

Detailed numerical results are given for a baseline flywheel system. Then the results of parametric studies are presented to show the effects of a variety of system parameters.

Suggestions for further research in the area of flywheel rotor dynamics are presented in Appendix F.

---

*Internal flexibilities of various flywheel systems are studies in Part II of this project.

2. LUMPED-PARAMETER MODEL

The most widely used approach to model mathematically the lateral dynamic behavior of rotating machinery is the lumped-parameter model. In this approach, each of the bulky masses of the system is treated as a rigid body and each of the flexible, dissipative shafts is treated as a lumped complex-stiffness spring. Since the system is a rotational one, the combination of centrifugal force and gyroscopic action must be included, as first suggested by Stodola [22] in 1918; see also [6]. A very clear discussion of the rotor dynamics of single-shaft, single-rotor systems was presented by Hartog [23].

The literature contains a few lumped-parameter analyses of more complicated systems involving more than one rigid body and/or flexible shaft, for example, [18, 24 - 28]. The methodology used here follows that presented in [18].

2.1 Description of Model

The flywheel system,mounted in an air-turbine-driven flywheel testing facility,is modeled as shown schematically in Fig. 2.1. The turbine is modeled as a rigid-body mass clamped to a turbine shaft which is mounted on ball bearings, assumed to act as momentless elastic supports. Concentric within the turbine shaft is the flywheel or quill shaft. It is clamped at its upper end to the turbine, and also is assumed to be supported by the bottom end of the turbine shaft, due to the very small clearance at that point. At a relatively short distance below the lower turbine bearing, an oil-type damper connects the quill shaft to ground. Due to the high length-to-diameter ratio of the damper assembly, it is assumed that the damper restrains the quill shaft from tilting, so that it is free to move only radially. The flywheel itself is modeled as a rigid-body mass clamped to the lower end of the quill shaft.

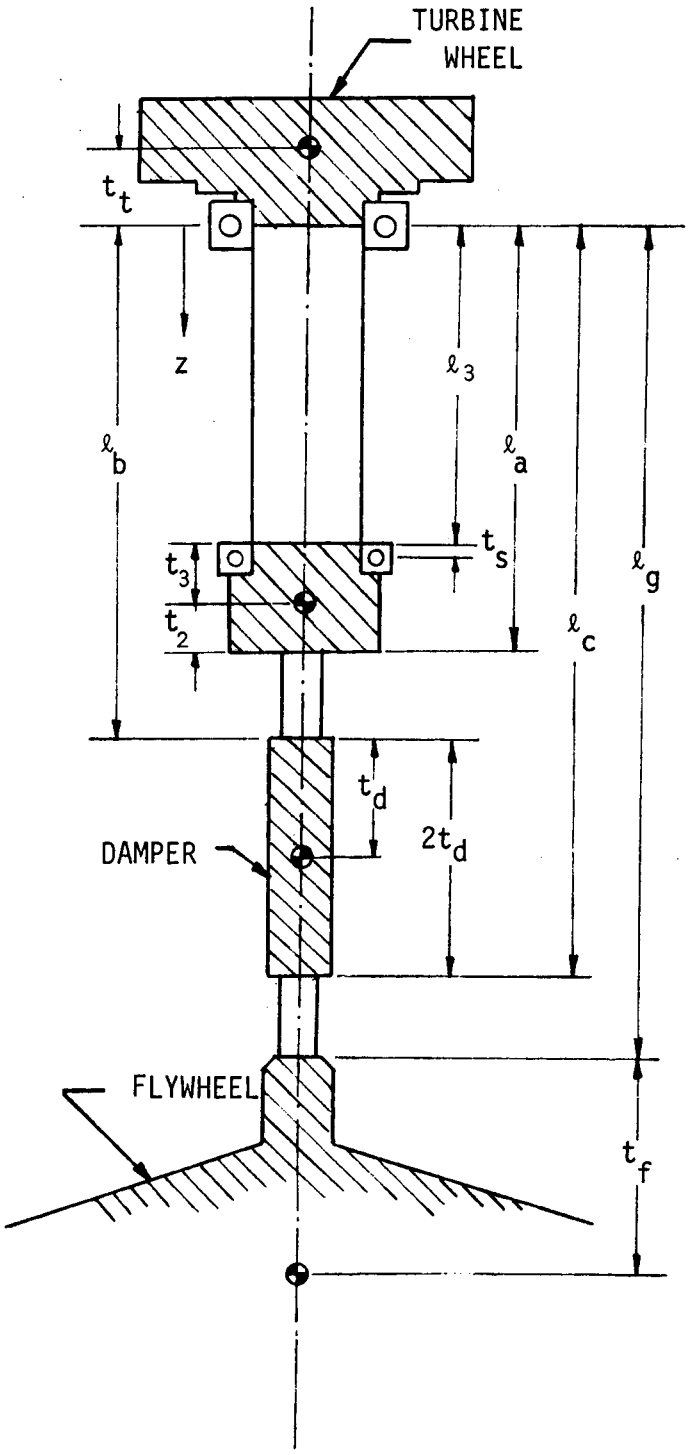

Fig. 2.1. Schematic diagram of the lumped-parameter model with dimensions. Drawing not to scale.

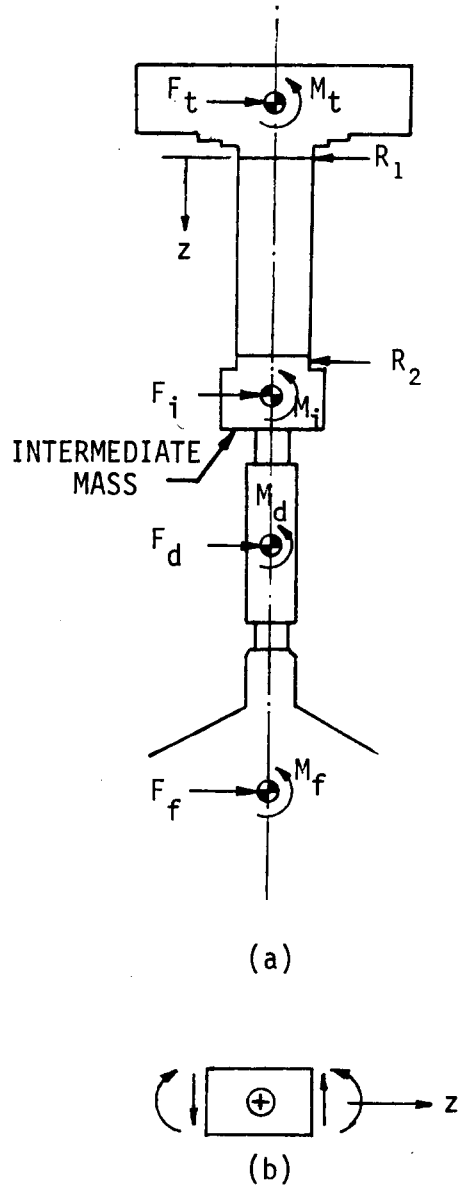

Fig. 2.2. A positive system of external forces and moments (a) and a positive shear-force and bending-moment convention (b).

2.2 Free Whirling Analysis

In the presence of gyroscopic action and in the absence of excitation and damping actions, the equations of motion of a multi-degree-of-freedom, lumped-parameter, linear dynamic system can be expressed in matrix form as*

$$[M]\{\ddot{q}\} - i[G]\{\dot{q}\} + [K]\{q\} = \{0\} \tag{2.1}$$

Here, [G], [K], and [M] are the respective gyroscopic, stiffness, and mass matrices, $i \equiv \sqrt{-1}$, and $\{q\}$ is the generalized displacement vector. For the system modeled as shown in Fig. 2.1, $\{q\}$ is

$$\{q\} = \{r_f, \phi_f, r_d, r_i, \phi_i, r_t, \phi_t\}^T \tag{2.2}$$

where r is lateral displacement, ϕ is tilt, and subscripts f, d, i, and t refer to the flywheel, damper, intermediate mass, and turbine, respectively. Note that $\phi_d = 0$ because of the details in the damper construction. The matrices [M] and [G] appearing in equation (2.1) are defined as

$$[M] = \begin{bmatrix} m_f & & & & & & \\ & I_{df} & & & 0 & & \\ & & m_d & & & & \\ & & & m_i & & & \\ & & & & I_{di} & & \\ & 0 & & & & m_t & \\ & & & & & & I_{dt} \end{bmatrix} \tag{2.3}$$

$$[G] = \begin{bmatrix} 0 & & & & & & \\ & I_{pf}\Omega & & & 0 & & \\ & & 0 & & & & \\ & & & 0 & & & \\ & & & & I_{pi}\Omega & & \\ & 0 & & & & 0 & \\ & & & & & & I_{pt}\Omega \end{bmatrix} \tag{2.4}$$

---

* See [18] for derivations of governing equations.

To obtain the stiffness matrix [K], we start with the following generalized force-generalized displacement relations expressed in compliance form (see Appendix A for details):

$$[\alpha]\begin{Bmatrix} F_f \\ M_f \\ F_d \\ M_d \\ F_i \\ M_i \\ F_t \\ M_t \end{Bmatrix} = \begin{Bmatrix} r_f \\ \phi_f \\ r_d \\ \phi_d \\ r_i \\ \phi_i \\ r_t \\ \phi_t \end{Bmatrix} \tag{2.5}$$

Inverting the equation (2.5) and setting $\phi_d = 0$, one obtains

$$\begin{Bmatrix} F_f \\ M_f \\ F_d \\ M_d \\ F_i \\ M_i \\ F_t \\ M_t \end{Bmatrix} = [\bar{K}]\begin{Bmatrix} r_f \\ \phi_f \\ r_d \\ 0 \\ r_i \\ \phi_i \\ r_t \\ \phi_t \end{Bmatrix} \tag{2.6}$$

where $[\alpha]^{-1} = [\bar{K}]$. Hence, by deleting the fourth row and fourth column in $[\bar{K}]$, one has

$$\begin{Bmatrix} F_f \\ M_f \\ F_d \\ F_i \\ M_i \\ F_t \\ M_t \end{Bmatrix} = [K] \begin{Bmatrix} r_f \\ \phi_f \\ r_d \\ r_i \\ \phi_i \\ r_t \\ \phi_t \end{Bmatrix} \tag{2.7}$$

Note that M_d is an unknown which could be calculated upon knowing $\{q\}$.

We assume the form of solution for $\{q\}$ as

$$\{q\} = \{\bar{q}\}e^{i\omega t} \tag{2.8}$$

where ω is real. Substituting the above into equation (2.1), we obtain

$$-\omega^2[M]\{\bar{q}\} + \omega[G]\{\bar{q}\} + [K]\{\bar{q}\}=\{0\} \tag{2.9}$$

Premultiplying by $[M]^{-1}$ and rearranging yield

$$\omega[M]^{-1}[G]\{\bar{q}\} + [M]^{-1}[K]\{\bar{q}\} = \omega^2\{\bar{q}\} \tag{2.10}$$

Let

$$[B_1] = [M]^{-1}[G] \quad , \quad [I] = \text{identity matrix} \ ,$$

$$[B_2] = [M]^{-1}[K] \quad , \quad [0] = \text{zero matrix} \ , \tag{2.11}$$

and

$$\{\bar{p}\} = \omega\{\bar{q}\}$$

Thus, equation (2.10) becomes

$$[B_1]\{\bar{p}\} + [B_2]\{\bar{q}\} = \omega\{\bar{p}\} \tag{2.12}$$

or

$$\left[\begin{array}{c|c} [0] & [I] \\ \hline [B_2] & [B_1] \end{array}\right] \left\{\begin{array}{c} \{\bar{q}\} \\ \hline \{\bar{p}\} \end{array}\right\} = \omega \left\{\begin{array}{c} \{\bar{q}\} \\ \hline \{\bar{p}\} \end{array}\right\} \tag{2.13}$$

which can be solved numerically by standard eigenvalue algorithms.

2.3 Stability Analysis

For the stability analysis, internal material damping (hysteretic damping) is incorporated by using complex stiffness $[K^*]$ and adding external viscous damping (in the system damper) to equation (2.1):

$$[M]\{\ddot{q}\} - i[G]\{\dot{q}\} + [C]\{\dot{q}\} + [K^*]\{q\} = \{0\} \tag{2.14}$$

where for the present system the only external damping [C] present is located at the system damper (coefficient C_d):

$$[C] = \begin{bmatrix} 0 & & & & & & \\ & 0 & & & & 0 & \\ & & C_d & & & & \\ & & & 0 & & & \\ & & & & 0 & & \\ & 0 & & & & 0 & \\ & & & & & & 0 \end{bmatrix} \tag{2.15}$$

In equation (2.14), $[K^*]$ is a complex stiffness matrix which is derived in the same way as [K] in Section 2.2 except that the moduli E and G used in the $[\alpha]$ matrix in Section 2.2 are replaced here by the corresponding <u>complex</u> moduli E^* and G^* defined by

$$E^* = (1 \pm i\gamma_s)E \quad , \quad G^* = (1 \pm i\gamma_s)G \tag{2.16}$$

A solution of the form $\{q\} = \{\bar{q}\}e^{i\omega t}$ for equation (2.14) is assumed, where $\omega = \omega_R + i\omega_I$, and ω_R and ω_I are the respective real and imaginary parts of ω. Note that the response $\{q\}$ will grow exponentially with time if $-\omega_I$ is positive. Denoting $-\omega_I$ as the growth factor, we see that a positive growth factor causes instability of the system and a negative growth factor the stability of the

system (by exponentially attenuating the disturbances). In equation (2.16) the positive sign is used when $\Omega < \omega_R$ and the negative sign when $\Omega > \omega_R$. (See Section 4.2 for a detailed discussion.) With the assumed form of solution and equation (2.14), we obtain

$$-\omega^2[M]\{\bar{q}\} + \omega[G]\{\bar{q}\} + i\omega[C]\{\bar{q}\} + [K^*]\{\bar{q}\} = \{0\} \tag{2.17}$$

Premultiplying by $[M]^{-1}$ and rearranging yield

$$[[M]^{-1}([G] + i[C])]\{\bar{q}\} + [[M]^{-1}[K^*]]\{\bar{q}\} = \omega^2\{\bar{q}\} \tag{2.18}$$

Using the definitions of $\{\bar{p}\}$, $[I]$, and $[0]$ previously defined in equations (2.11), we can rewrite equation (2.18) as

$$\left[\begin{array}{c|c} [0] & [I] \\ \hline [B_2^*] & [B_1^*] \end{array}\right] \left\{\begin{array}{c} \{\bar{q}\} \\ \hline \{\bar{p}\} \end{array}\right\} = \omega \left\{\begin{array}{c} \{\bar{q}\} \\ \hline \{\bar{p}\} \end{array}\right\} \tag{2.19}$$

where $[B_1^*] = [M]^{-1}([G] + i[C])$ and $[B_2^*] = [M]^{-1}[K^*]$.

To resolve the difficulty in using different signs for the complex stiffnesses in different regions in the ω_R - Ω plane, the above eigenvalue problem is solved twice at each rotational speed, once with the plus sign and then with the negative sign. The real component of ω is compared to the rotational speed Ω. If the relation between Ω and ω_R is not satisfied, that ω_I is discarded. Then the stability growth factor, $-\omega_I$, is plotted against rotational speed Ω to determine stability plots.

2.4 Forced Whirling Analysis

Here, the internal material damping does not come into play because the synchronous motion does not induce an alternating stress state in the shaft. Hence, with the addition of the steady-state harmonic exictation vector on the right side, the governing equation of motion is

$$[M]\{\ddot{q}\} - i[G]\{\dot{q}\} + [C]\{\dot{q}\} + [K]\{q\} = \{F\}e^{i\Omega t} \tag{2.20}$$

Here, the excitation vector can be expressed as

$$\{F\} = \begin{Bmatrix} m_f r_e \Omega^2 \\ (I_{df} - I_{pf})\phi_o \Omega^2 e^{-i\beta} \\ 0 \\ 0 \\ 0 \\ 0 \\ 0 \end{Bmatrix} \tag{2.21}$$

where r_e is the mass eccentricity, ϕ_o the initial tilt, and β the phase lag between the in-plane eccentricity r_e and initial tilt ϕ_o (see Fig. B9).

The steady-state solution is

$$\{q\} = \{\bar{q}\}e^{i\Omega t} \tag{2.22}$$

Then, equation (2.20) becomes

$$[-\Omega^2[M] + \Omega[G] + i\Omega[C] + [K]]\{\bar{q}\} = \{F\} \tag{2.23}$$

Note that $\{\bar{q}\}$ consists of the steady-state amplitudes of the seven degrees of freedom of the system, as defined in equation (2.2).

3. COMBINED (DISTRIBUTED AND LUMPED-PARAMETER) MODEL

To more accurately model the lateral dynamic behavior of rotating machinery, one can model the flexible shafts as elements having distributed elastic, damping, and mass properties. This approach has been used before for simple, single-rotor systems having a thin shaft modeled as a Bernoulli-Euler beam [8,29-30] or a thicker shaft taken to be a Timoshenko beam [31-33]. The present work is an extension of the latter work to multimass, multishaft systems and it is unique, except for some concurrent research [21], in comparing results obtained by the combined model with those of a lumped-parameter model.

3.1 Description of Model

The primary difference between this model and the strictly lumped-parameter model discussed in Section 2 is that here the turbine shaft and the quill shaft are modeled as distributed-parameter elements; see Fig. 3.1.

The assumptions on which the analysis is based are:

1. The shafts are treated as flexural systems with axisymmetrically distributed mass and stiffness.

2. The effects of rotatory inertia, transverse shear deformation, gyroscopic action, and, for the quill shaft, the pendulum-effect moment due to the dead weight of the flywheel, are included.

3. The coupling between flexural and torsional vibrations is neglected.

4. All components are assumed to be geometrically perfect.

5. The shafts are assumed to be of linearly elastic material and undergoing small deflections.

6. The flywheel and air turbine (in the spin-test configuration) are considered not as point but as rigid, finite masses, i.e., their lateral translational inertias, rotatory inertias, and gyroscopic actions are included.

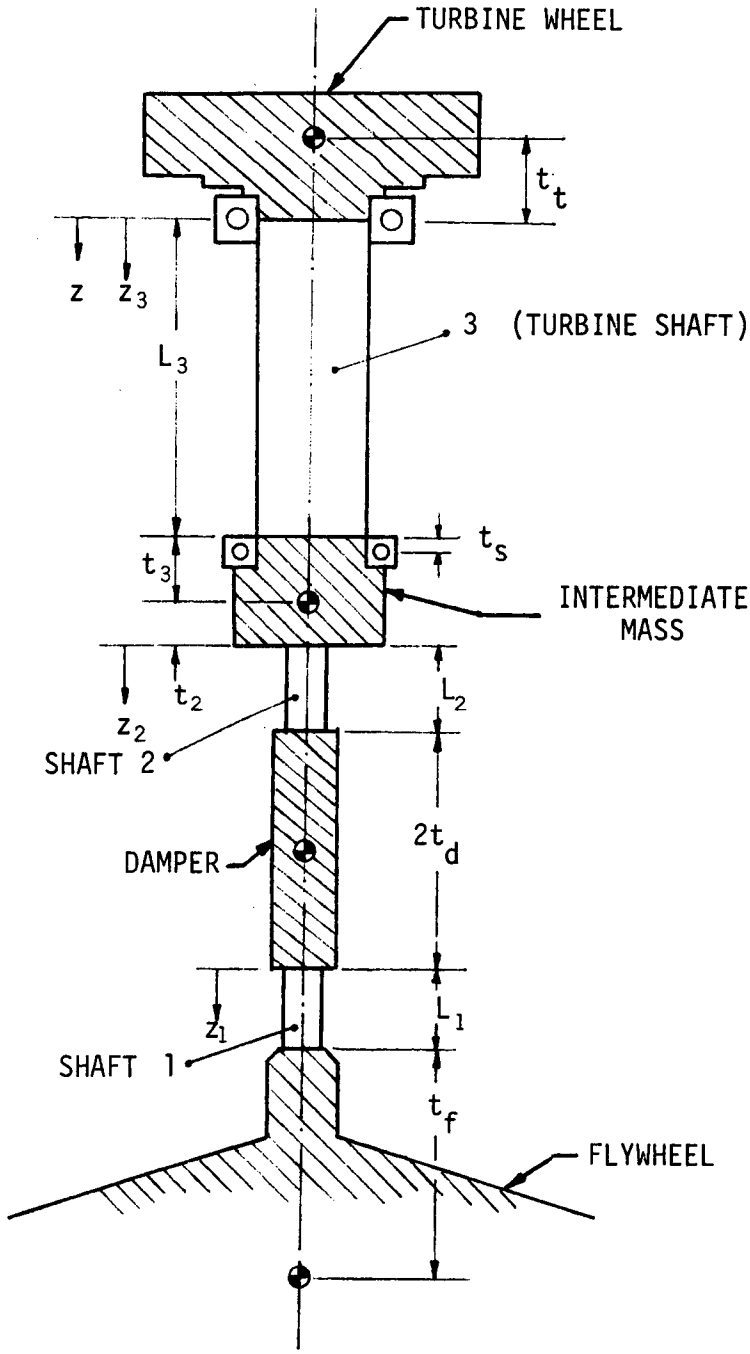

Fig. 3.1. Combined model for Oak Ridge system with pertinent dimensions. Drawing not to scale.

7. The only external damping included is a linearized oil-type damper which is assumed to provide only axisymmetric radial damping forces and is constrained from tilting. (Aerodynamic damping is neglected, since the flywheels will be expected to operate in an evacuated container.)

8. All of the support bearings are assumed to be ball bearings, approximately axisymmetric in nature, and modeled as momentless elastic supports.

3.2 Free Whirling Analysis

A single reduced differential equation governing the whirling of a shear-flexible shaft is derived (see Appendix B.2) with the shaft deflection, w, as the dependent variable. To solve the system, consisting of such a differential equation for each shaft, for the relative displacements and eigenvalues (natural whirling speeds) suitable boundary conditions and continuity conditions are written (see Appendix B.3). Note that the system is composed of three whirling shaft sections and the continuity conditions are those which connect adjacent shaft sections appropriately.

The boundary and continuity conditions are cast into a matrix form (see Appendix B.4)

$$[\bar{C}] \begin{Bmatrix} A_{11} \\ A_{12} \\ A_{13} \\ A_{14} \\ A_{21} \\ A_{22} \\ A_{23} \\ A_{24} \\ A_{31} \\ A_{32} \\ A_{33} \\ A_{34} \end{Bmatrix} = \{0\} \tag{3.1}$$

where $A_{11}, \ldots, A_{14}$ are the unknown constants in the assumed solution for shaft section 1; $A_{21}, \ldots, A_{24}$ for shaft section 2; and $A_{31}, \ldots, A_{34}$ for shaft section 3. In order to have a nonzero solution for the set of equations in the matrix equation (3.1), the determinant of $[\bar{C}]$ should be zero. From this condition the eigenvalues (natural whirling frequencies) of the system are computed.

3.3 Forced Whirling Analysis

In this analysis, the effects of mass eccentricity (r_e) and initial tilt (ϕ_o), which are shown in Fig. B9, are taken into account when formulating the boundary conditions on the shaft to which the flywheel is attached. The set of equations in equation (3.1) takes the following form (see Appendix B.5):

$$[\bar{C}] \begin{Bmatrix} A_{11} \\ A_{12} \\ A_{13} \\ A_{14} \\ A_{21} \\ A_{22} \\ A_{23} \\ A_{24} \\ A_{31} \\ A_{32} \\ A_{33} \\ A_{34} \end{Bmatrix} = \begin{Bmatrix} -m_f r_e \\ -\phi_o(I_{pf} - I_{df})e^{-i\beta} \\ 0 \\ 0 \\ 0 \\ 0 \\ 0 \\ 0 \\ 0 \\ 0 \\ 0 \\ 0 \end{Bmatrix} \tag{3.2}$$

From equation (3.2) the forced whirling responses of any point on a shaft section can be calculated.

4. NUMERICAL RESULTS FOR A BASELINE FLYWHEEL SYSTEM

In this section, we present and discuss the numerical results obtained by applying the various analyses derived in Sections 2 and 3 to a specific flywheel system, the 23-in.-diameter, 80-w-hr/kg wheel developed by Garrett AiResearch in Torrance, CA and described in detail in [34]. The air-turbine-drive data are for a four-inch Barbour Stockwell turbine as installed at the Oak Ridge Flywheel Evaluation Laboratory [15]. This flywheel/air turbine combination is used as the baseline for various parametric studies in Section 5 and is hereafter referred to as System A for brevity.

4.1 Free Whirling: Campbell Diagrams and Mode Shapes

One of the most informative ways of presenting numerical data on rotor dynamics is the Campbell diagram or "whirl map" originated in 1924 [35] in connection with turbine-disk flexural vibration. This diagram is a plot of various natural whirling frequencies of lateral vibration versus rotational speed. A Campbell diagram for System A, as predicted by the lumped-parameter analysis derived in Section 2.2, is shown in Fig. 4.1*. As is customary, in carrying out this analysis, we omitted both internal material and external viscous damping. Since this model has seven degrees of freedom, equation (2.2), it has seven natural frequencies (and a like number of associated vibration modes) at zero rotational speed Ω (see the intercepts along the vertical axis in Fig. 4.1). However, as Ω is increased, each of these frequencies (and associated mode shapes) "splits" into two distinct branches. The deviation between the two branches associated with a given zero-speed mode is caused by the gyroscopic tilting moments induced in the various masses which are free to tilt. The branches having the higher

*Complete FORTRAN computer documentation is provided in Appendix C. Of course, the program can be used to obtain Campbell diagrams for other flywheel systems in a spin-test facility of the type assumed here.

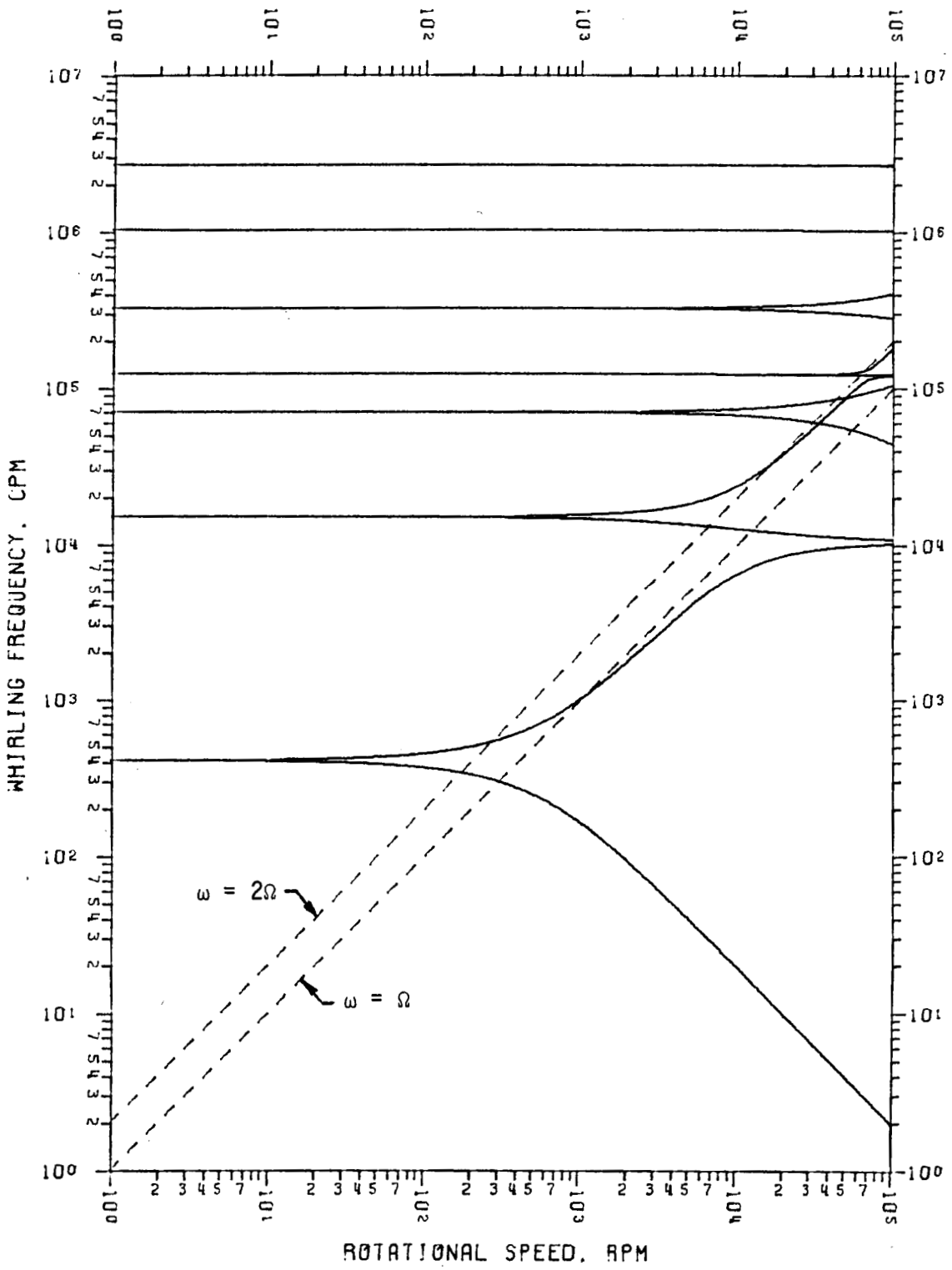

Fig. 4.1 Campbell diagram for System A (Garrett), as calculated using the lumped-parameter free-whirling analysis.

frequencies in each set are associated with forward whirling, i.e., the shaft is whirling in the same direction as the rotation. The branches with the lower frequencies in each set are associated with backward (or retrograde) whirling, i.e., the direction of whirling is opposite to the direction of rotation.

Notice that the lower modes have the most pronounced splitting deviation. In fact, within the range of the plot (rotational speeds up to 100,000 rpm*), no splitting is discernible in the two highest frequency modes. The net effect of the gyroscopic action is to stiffen the system for forward whirling and soften it in the case of retrograde whirling.

In rotating machinery, one of the most important classes of excitation is that caused by mass eccentricity and initial tilt of the principal axes of the larger rotating masses. This is still true, although to a smaller extent, even in the case of a carefully balanced system. The frequency of this sinusoidal forcing system is the same as the rotational speed. Thus, the intersections of the dotted line labeled $\omega = \Omega$ (a straight line, in Fig. 4.1 which is a log-log plot) with the various modal-frequency curves result in so-called first-order "critical speeds". Although all of these are potential resonances, experiments [7,11,36] have shown that those associated with the forward whirling branches are more severe than those associated with the retrograde branches. Furthermore, there is considerable variation in the "severity" of the various forward-whirling critical speeds (see Section 4.3). Practical experience has shown that generally the lower-speed critical speeds are much less important than the higher-speed ones.

---

*The spin-test facility is rated to only 60,000 rpm.

There are two reasons for this: first, the higher the rotational speed the higher the kinetic energy in the system and the stiffer it becomes (in forward whirling). Secondly, and perhaps more importantly, it is usually much easier to accelerate sufficiently rapidly through lower-speed critical speeds than higher-speed ones [7,10,37]. The reason for this is that typically air-turbine drives have a torque capacity that decreases as the rotational speed is increased [13], pp. 48-51.

Another important class of excitation may result from a combination of gravity force (only in the case of a horizontal or nearly horizontal axis of rotation) and nonaxisymmetric shaft cross section (due to either small errors in machining or the presence of a fatigue crack) [38]. This excitation has a frequency of exactly twice the rotational speed. Hence, the upper dotted line labeled $\omega = 2\Omega$ determines this excitation frequency, and the associated intersections with the various whirling branches give the second-order critical speeds (read from the abscissa, rotational speed) [23], pp. 247-249; [39], pp. 290-294.

All of the first- and second-order critical speeds predicted for System A up to 100,000 rpm are listed in Table 4.1.

To supplement the information provided in a Campbell diagram, experience has shown that mode shapes are very helpful. In the case of a lumped-parameter system, the mode shapes depict the relative motions* of the various rigid-body masses of the system.

The mode shapes for System A predicted by the lumped-parameter-model analysis at speeds close to the first- and second-order critical speeds

*In free whirling, as in free vibration of a nonrotating system, only relative motions, not absolute ones, can be determined.

Table 4.1 Critical Rotational Speeds, in rpm, for System A (Garrett)

Order	First ($\omega/\Omega = 1$)				Second ($\omega/\Omega = 2$)							
Mode & Branch*	1R	1F	2R	3R	1R	1F	2R	2F	3R	3F	4R	4F
Lumped Model	301	1,027	12,450	54,480	172	269	6,615	16,020	30,530	42,510	64,400	61,330
Combined Model	304	1,038	14,140	56,120	173	271	7,516	18,100	31,400	43,390	74,000	70,050
Experimental**		1,040										

*For example, 1R denotes the first (lowest) mode, retrograde branch, while 4F denotes the fourth mode, forward branch.
**Data provided by Dr. R.S. Steele, Union Carbide Corp., Nuclear Division, Oak Ridge, TN.

are shown in Figs. 4.2 and 4.3. They were plotted by computer graphics, using simple, straight lines to connect adjacent mass-center locations. The dotted lines denote flexible shaft portions, which obviously will deflect in smooth curvilinear fashion (as will be seen in Fig. 4.5). Also note that in each of the mode-shape plots the turbine wheel is at the top of the page and the flywheel is at the bottom. As would be expected at a speed (1,023 rpm) near the first-order critical speed, the most drastic mode in Fig. 4.2 is the first one (1F) and in this mode the main action is taking place in the lower end of the quill shaft, the damper and turbine being relatively unaffected.

It can be seen in Fig. 4.3, at a rotational speed of 269 rpm, that the damper is operative in the second and fourth forward modes, but not the first, third, and fifth or higher forward modes. At both 15,849 and 41,687 rpm, the damper is operative for the first, second, and fourth forward modes. In contrast, at 63,096 rpm, the damper is operative in only the first, third, and fourth modes.

Although the combined model of the system has an infinite number of forward modes, each with a forward and retrograde branch, only a relatively small number intersect the $\omega = \Omega$ and $\omega = 2\Omega$ lines in the region up to a rotational speed of 100,000 rpm. These are shown in the Campbell diagram, Fig. 4.4. The associated first- and second-order forward and retrograde critical speeds are listed in the second line of Table 4.1.

Comparison of the Campbell diagrams in Figs. 4.1 and 4.4 shows very good qualitative agreement, especially at the lower rotational speeds. The major difference between the two is that in the combined model, the critical speeds are shifted into higher regions. This is especially noticeable at

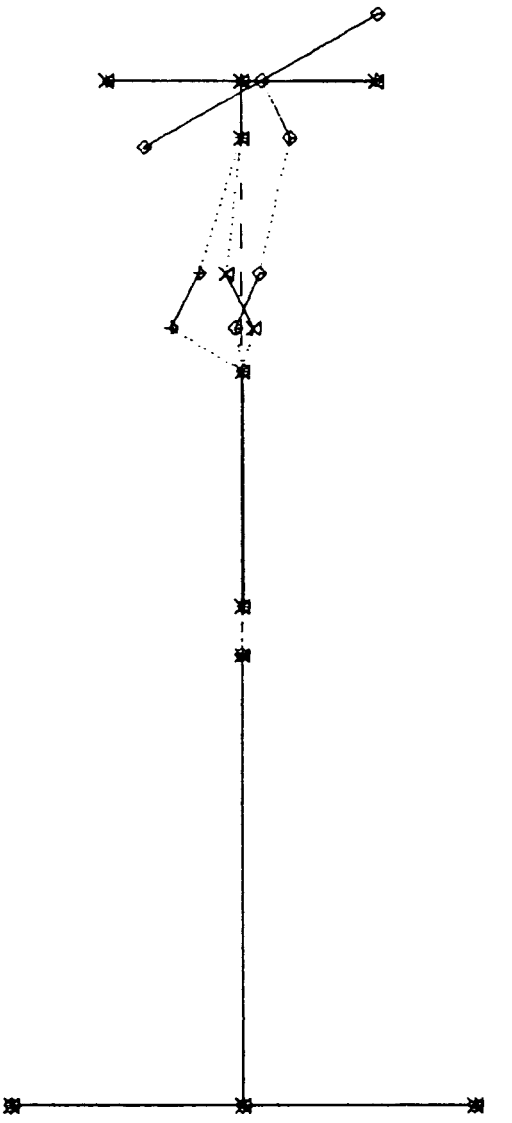

MODE IDENTIFIERS: ⊙ 1F + 3F
△ 2F × 4F

MODE IDENTIFIERS: ◇ 5F ⧖ 7F
✦ 6F

Fig. 4.2 Mode shapes of the seven forward branches at a rotational speed (1,023 rpm) near the first-order critical speed, using the lumped-parameter analysis (System A).

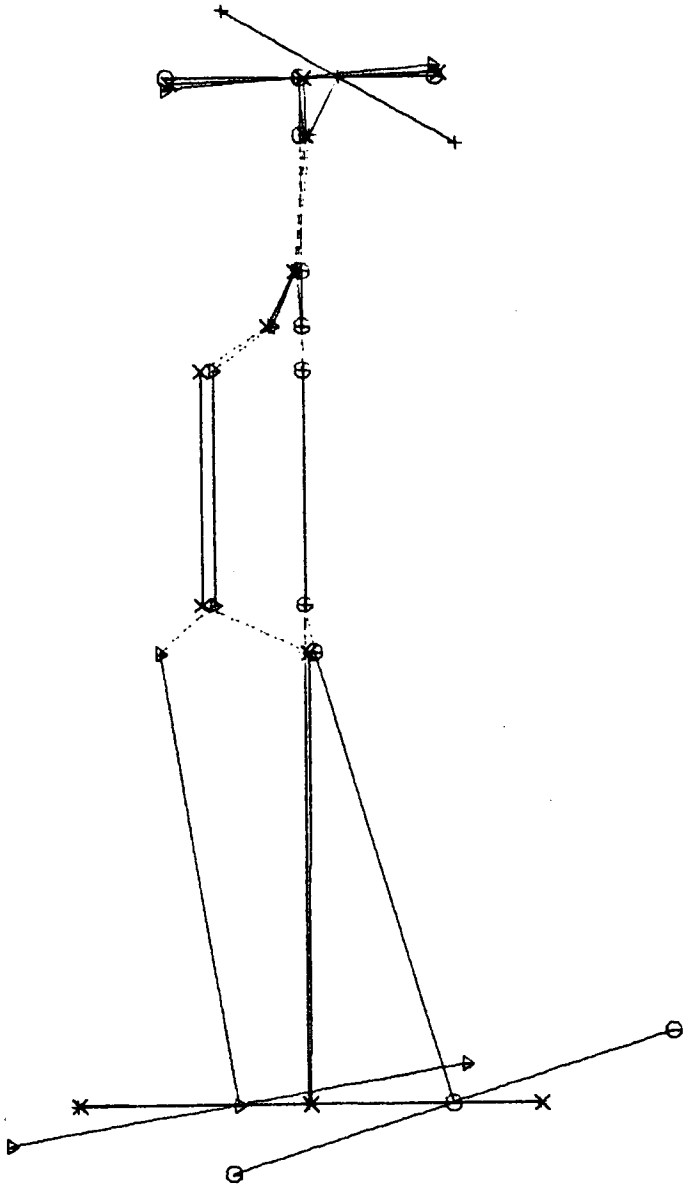

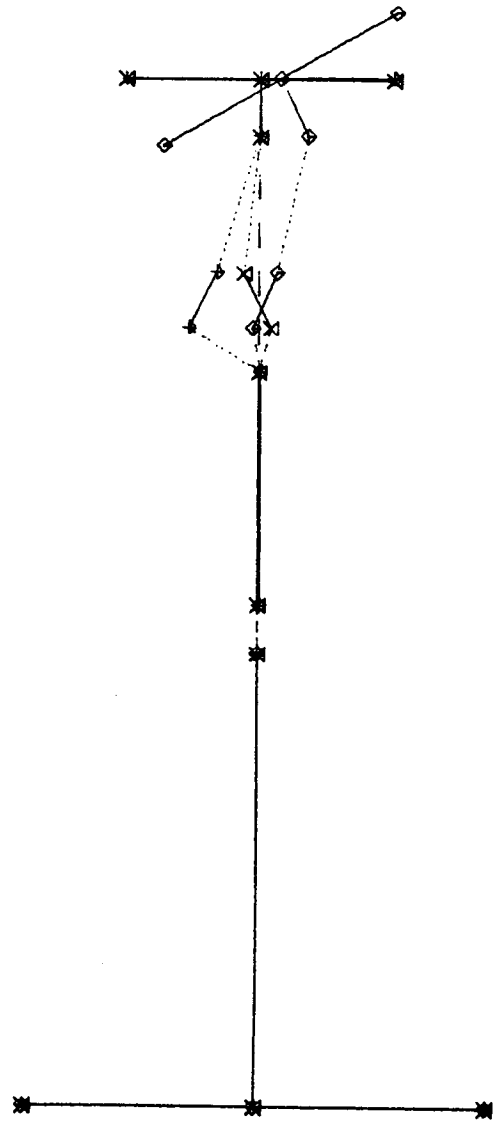

MODE IDENTIFIERS: ⊙ 1F + 3F
△ 2F × 4F

MODE IDENTIFIERS: ◇ 5F ⧖ 7F
✦ 6F

Fig. 4.3(a) Mode shapes of the forward branches of the seven modes at 269 rpm, near the first second-order critical speed, using the lumped-parameter analysis (System A).

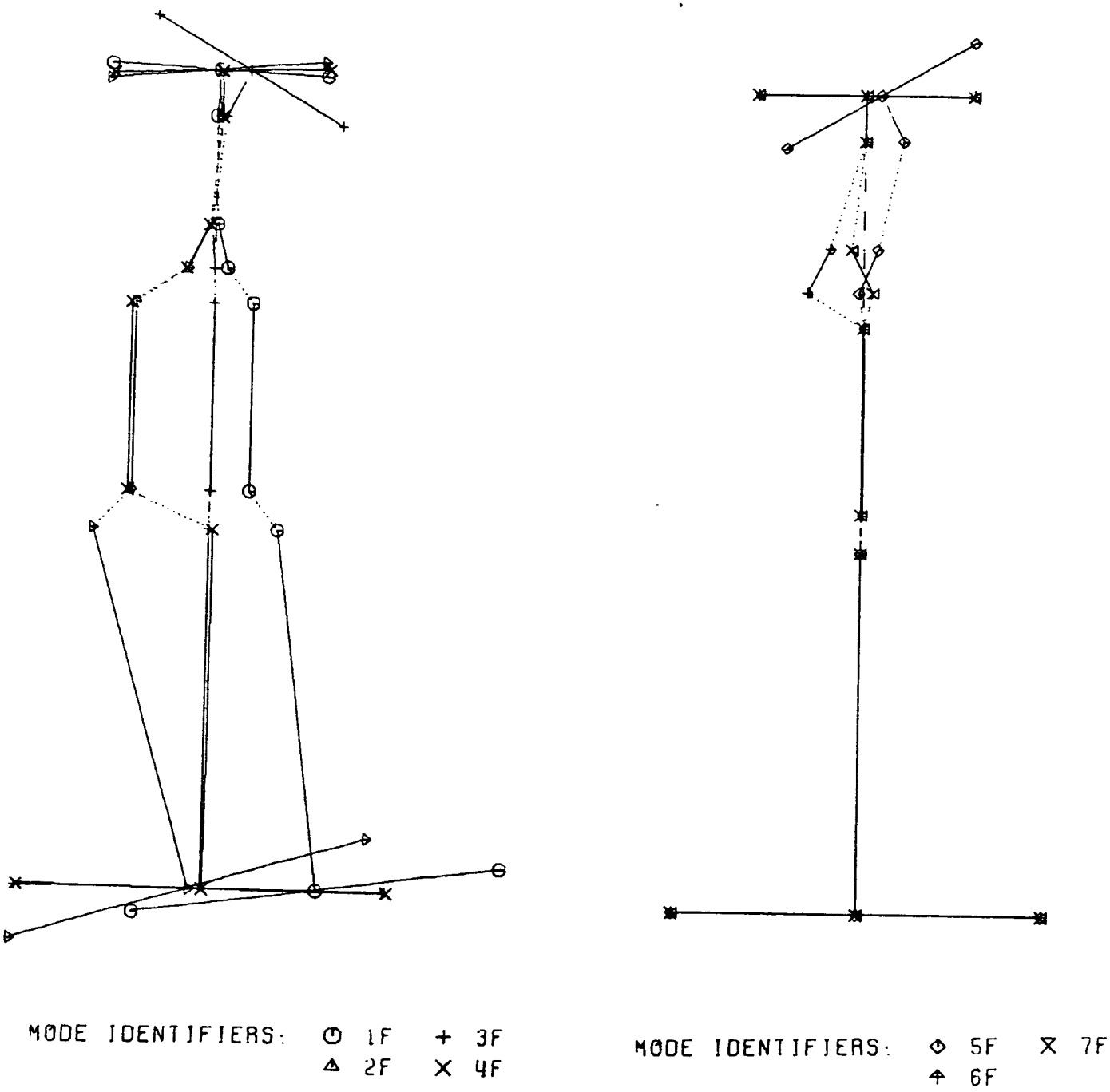

Fig. 4.3(b) Mode shapes of the forward branches of the seven modes at 15,849 rpm, near the second second-order critical speed, using the lumped-parameter analysis (System A).

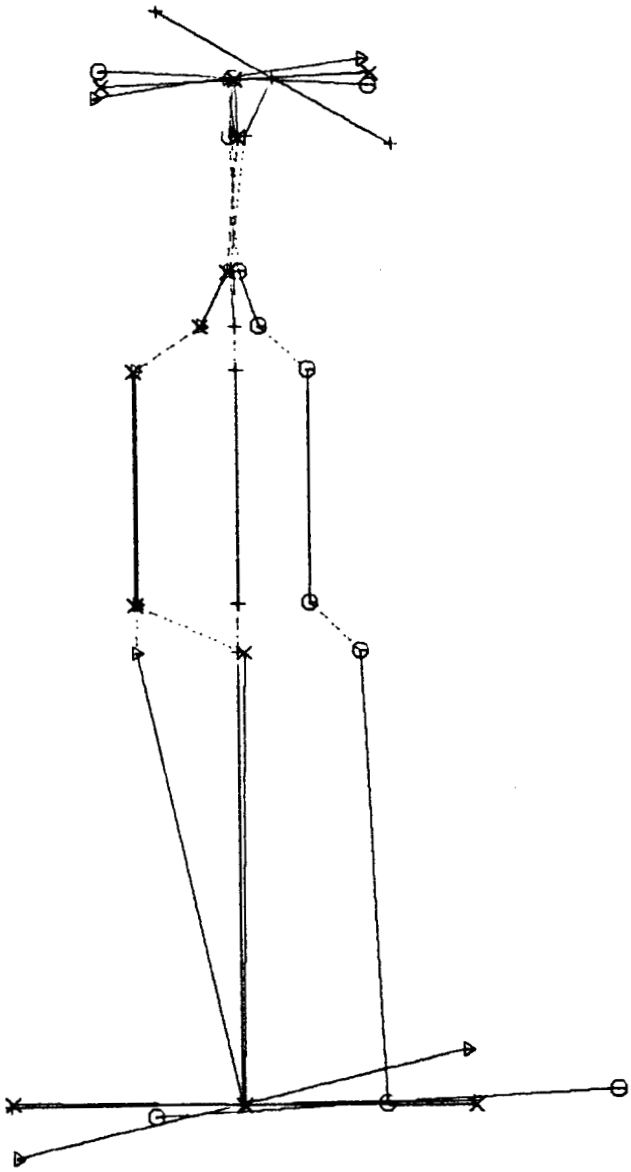

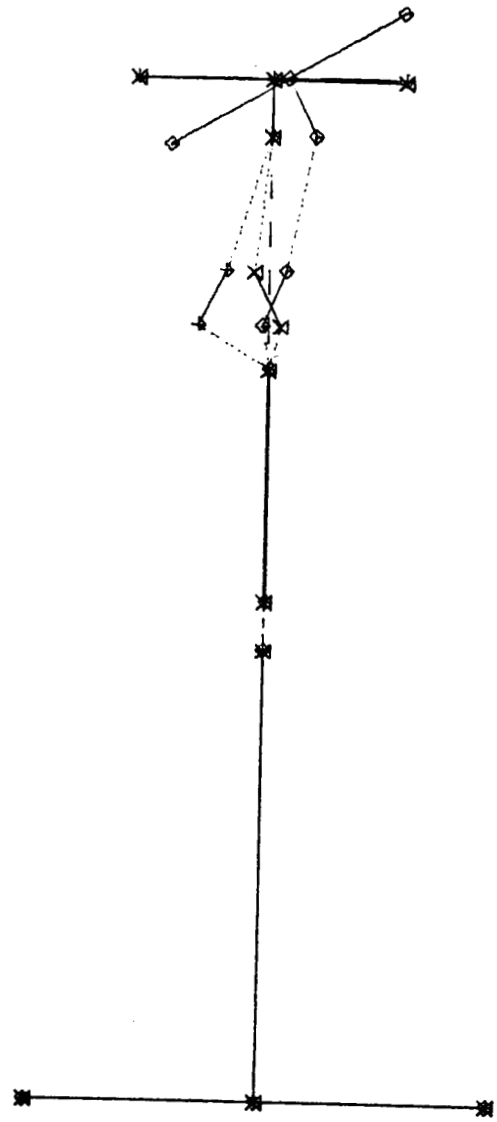

MODE IDENTIFIERS: ⊙ 1F + 3F
△ 2F × 4F

MODE IDENTIFIERS: ◇ 5F ⧖ 7F
↑ 6F

Fig. 4.3(c) Mode shapes of the forward branches of the seven modes at 41,687 rpm, near the third second-order critical speed, using the lumped-parameter analysis (System A).

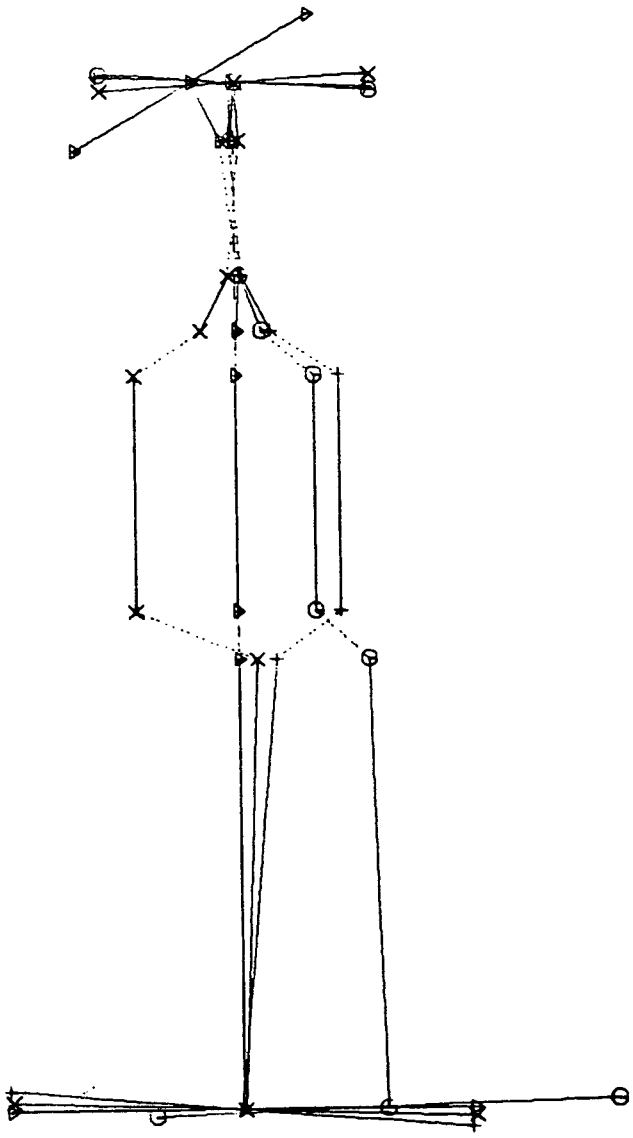

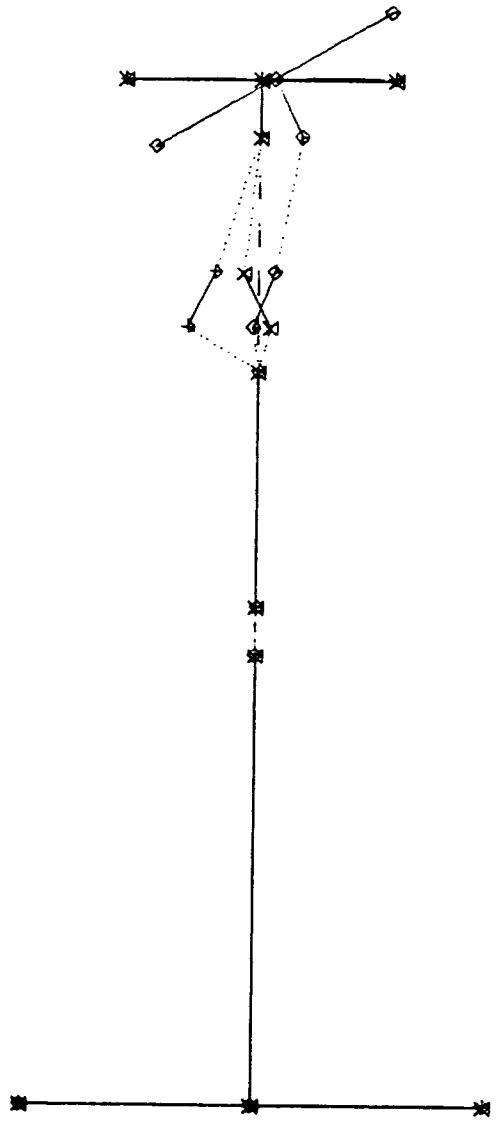

MODE IDENTIFIERS: ⊙ 1F + 3F △ 2F × 4F

MODE IDENTIFIERS: ◇ 5F ⊠ 7F ⊕ 6F

Fig. 4.3(d) Mode shapes of the forward branches of the seven modes at 63,096 rpm, near the fourth second-order critical speed, using the lumped-parameter analysis (System A).

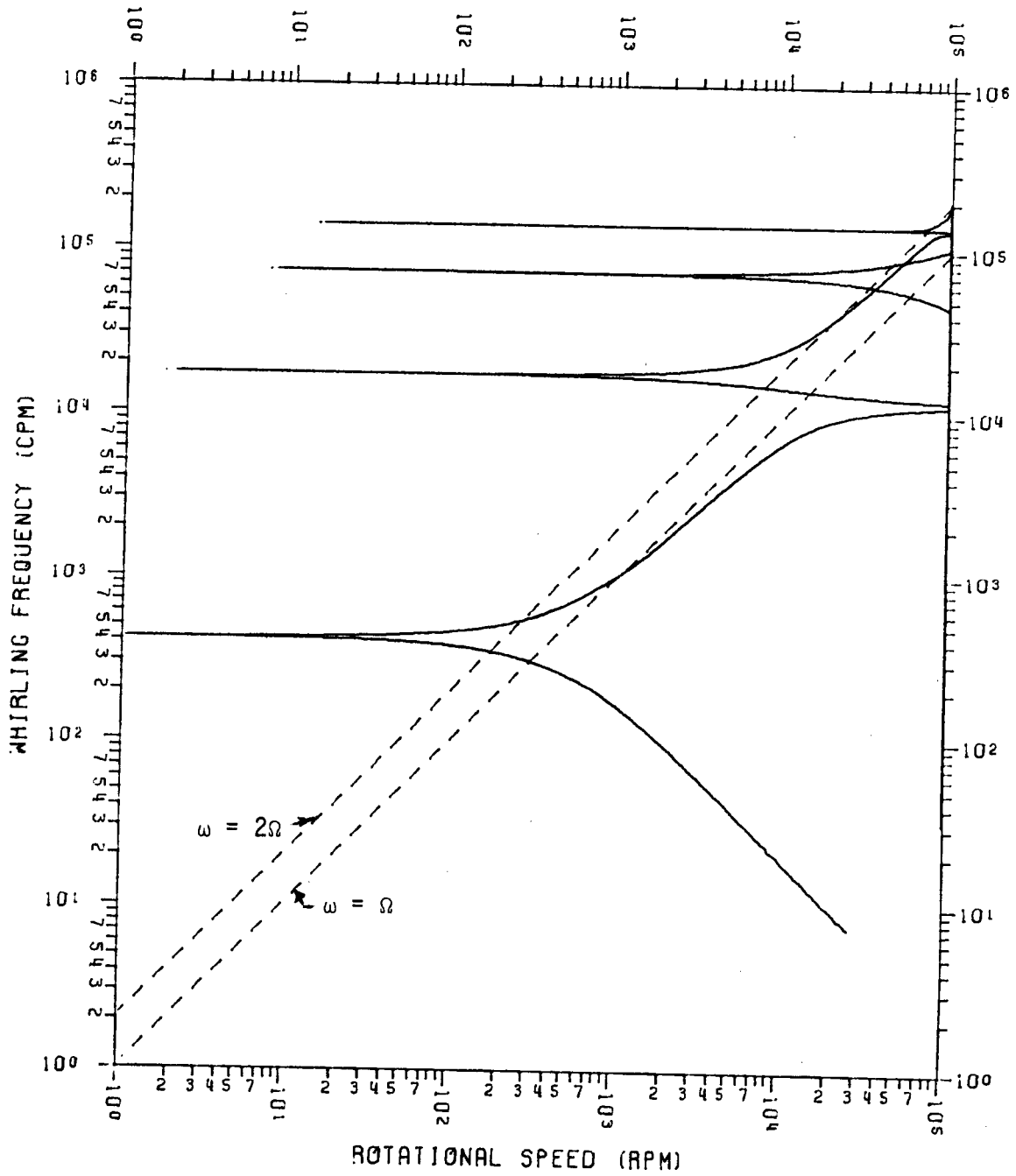

Fig. 4.4 Campbell diagram for System A, as calculated using the combined free whirling analysis.

higher rotational speeds and higher modes. This same trend is also revealed in Table 4.1. This trend suggests that the distributed shaft masses stiffen the system.

It is interesting to note that in the region covered (up to 100,000 rpm rotational speed), although this system has many second-order forward critical speeds and first-order retrograde ones, it has only one first-order forward critical speed. For this critical speed, there is good agreement among the two different models and test data obtained at Oak Ridge, as can be seen in Table 4.1.

The mode shapes associated with those forward branches that intersect the $\omega = \Omega$ and $\omega = 2\Omega$ lines (in Fig. 4.4) are plotted by computer graphics in Fig. 4.5. Again, in the mode shapes, the point of attachment of the turbine shaft to the turbine wheel is at the top of the page and the point of attachment of the flywheel to the quill shaft is at the bottom. An idea of the relative magnitudes of the tilts of the rigid masses can be obtained by observing the slopes of the shafts at the points of attachment of the respective rigid masses. It is noted that now the shafts deflect smoothly in contrast to those depicted in Figs. 4.2 and 4.3.

It is important to note the different basis for the mode shape plots in Figs. 4.2 and 4.3 on one hand and Fig. 4.5 on the other. In Figs. 4.2 and 4.3, the mode shapes associated with a fixed rotational speed are plotted, while in Fig. 4.5, those associated with a fixed order (ω/Ω ratio) are shown. Thus, the mode shapes obtained by means of the two different analyses can be compared only for the conditions listed in Table 4.2.

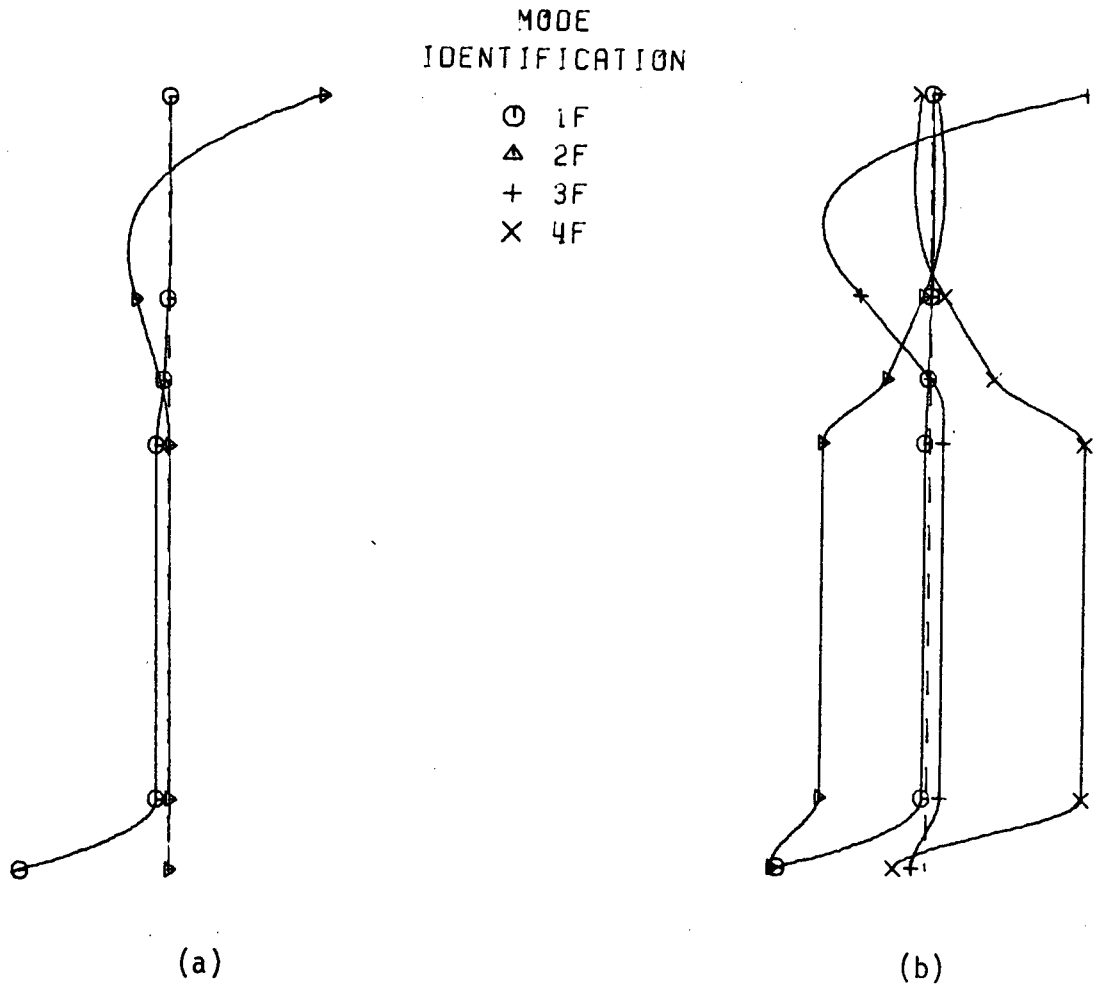

Fig. 4.5 Forward-whirling mode shapes using the combined analysis for the branches that intersect the lines (a) $\omega/\Omega = 1$ and (b) $\omega/\Omega = 2$, at speeds corresponding to their intersections. The mode shape corresponding to the second first-order forward critical speed (2F at 108,500 rpm) is also included in (a).

Table 4.2 Conditions for Comparison of Forward Mode Shapes for System A (Garrett)

Rotational Speed	Lumped-Parameter Model		Combined Model	
	Fig.	Mode & Branch	Fig.	Mode & Branch
269	4.3(a)	1F	4.5(b)	1F
1,023	4.2	1F	4.5(a)	1F
15,849	4.3(b)	2F	4.5(b)	2F
41,687	4.3(c)	3F	4.5(b)	3F
63,096	4.3(d)	4F	4.5(b)	4F

In both models, the mode shapes associated with the retrograde branches were very similar to the forward ones in the vicinity of the corresponding critical speeds and thus, for brevity, are not shown here.

4.2 Stability Growth Factor

Rotor instability due to internal material damping (hysteresis) was first reported in 1924 by Newkirk [40], who observed it experimentally. It was first explained by Kimball [41] in the same year. It has been discussed in several books [9], pp. 17-69, [23], pp. 295-299. Recently, Iwatsubo [42,43] has presented two extensive surveys of this topic.

Hysteresis in the stress-strain relation of shaft material involves a damping force which, in linear theory, is proportional to the first derivative of the strain (and, thus, of the lateral deflection of the shaft) in contrast to the restoring force which is proportional to strain (or deflection) itself. Thus, there is a 90° phase difference between the damping force ($\bar{F}_d$) and the restoring force (F_r). For forward whirling, there are three cases, depending upon the relative magnitudes of rotational speed (Ω) and whirling speed (ω_R), as shown in Fig. 4.6. The relative rotation of the shaft with respect to a frame of reference, attached to the shaft and rotating with it, is shown at

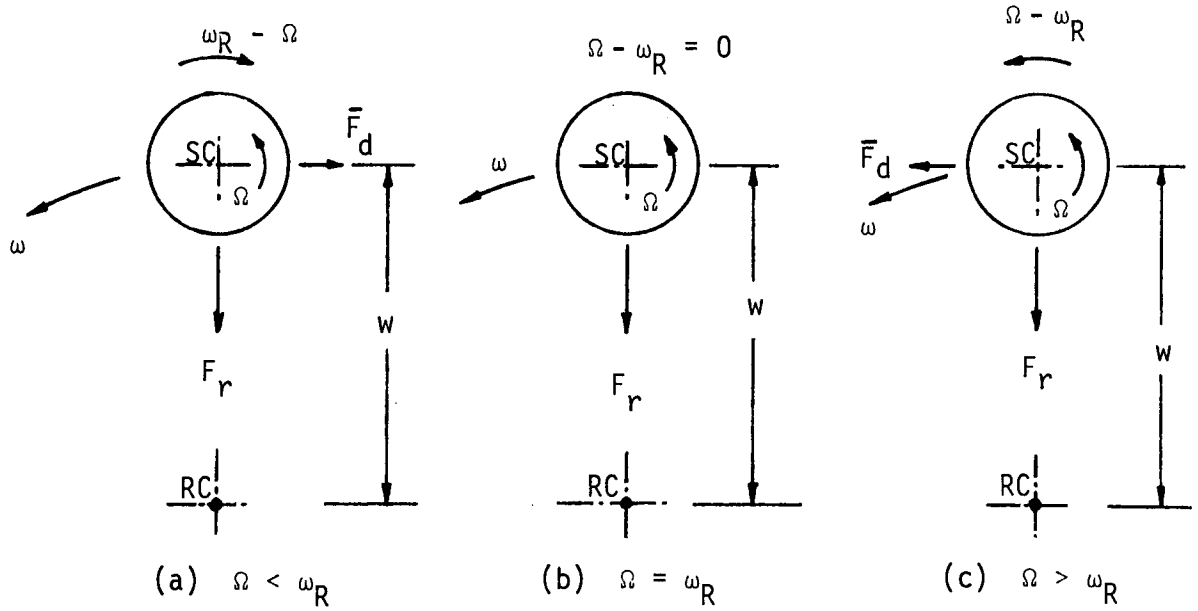

Fig. 4.6 Relationship between side force due to hysteretic damping ($\bar{F}_d$) and restoring force (F_r) due to shaft stiffness for forward whirling for (a) $\Omega < \omega_R$, (b) $\Omega = \omega_R$, (c) $\Omega > \omega_R$.

the top of the figure for each of the three cases. In each case the diagram is drawn so that the shaft center (SC) is deflected upward from the center of rotation (RC); thus, the top flexural fibers of the shaft are in tension and those at the bottom are in compression. Also, as a consequence of the upward deflection, the restoring force (F_r), due to the elastic stiffness of the shaft, acts downward.

In case (a) for running speed below the first whirling frequency (ω_R), ($\bar{F}_d$) acts in the opposite direction to the first-critical whirling motion of the shaft. Thus, the motion is damped out, even in the absence of external damping. Since $\bar{F}_d$ leads F_r by 90 degrees with respect to the rotational-speed direction, a positive sign must be used in equation (2.16) when $\Omega < \omega_R$.

In case (b), since there is no relative rotation between the shaft whirling (ω_R) and the shaft rotation (Ω), the shaft does not undergo any hysteretic cycling and hence, $\bar{F}_d = 0$.

In case (c), the side force F_d acts in the same direction as the forward whirling motion of the shaft, and unstable motion would result unless there is sufficient external damping action in the oil-type damper. Since $\bar{F}_d$ lags F_r by 90 degrees with respect to the rotational-speed direction, a negative sign must be used in equation (2.16) when $\Omega > \omega_R$.

The total force on a shaft, in general, is given by

$$\hat{F} = F_r \pm i\bar{F}_d = F_r(1 \pm i\gamma_s)$$

which is proportional to

$$(Ew)(1 \pm i\gamma_s) = E^* w$$

where $i = \sqrt{-1}$, γ_s = loss tangent ($= \bar{F}_d/F_r$), E = Young's modulus, E^* = complex modulus, and w = shaft deflection.

For retrograde whirling, the situation is as depicted in Fig. 4.7. Here, $\bar{F}_d$ is always opposed to the whirling motion and thus, the system should be stable at all rotational speeds.

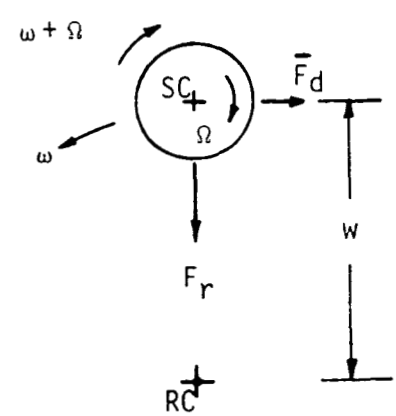

Fig. 4.7 Relationship between damping and restoring forces for retrograde whirling.

To summarize, instability due to internal damping of the shaft can occur <u>at most</u> only in forward whirling with $\Omega > \omega_R$, i.e., to the right of and below the $\omega = \Omega$ line in the Campbell diagram (Fig. 4.1). This general statement is supported by the analytical results obtained for System A by means of the

lumped-parameter stability analysis (see Section 2.3) and depicted by the plots of growth factor, $-\omega_I$, versus rotational speed in Figs. 4.8 and 4.9. Thus, all of the retrograde branches have zero or negative growth factors, i.e., $-\omega_I$ is negative. The second, third, and fifth retrograde branches are shown in Fig. 4.8. The first retrograde branch has a constant value of $-\omega_I = 0$ for all rotational speeds, while the fourth, sixth, and seventh have constant values of $-\omega_I < -200$; thus, they are not plotted.

The non-trivial stability plots for the forward branches are shown in Fig. 4.9. The sixth and seventh forward branches are not shown, since they have simply constant values of $-\omega_I < -200$. Only the first forward branch enters the region $\Omega > \omega_R$ (the region of potential instability for forward whirling) by cutting across the first-order line (dotted line $\omega = \Omega$ in Fig. 4.1) at the first-order critical speed. Thus, we expect the first forward branch to become unstable at the lowest first-order critical speed as predicted by the lumped-model free whirling analysis (1,027 rpm from Table 4.1). This is indeed the case as can be seen in Fig. 4.9(a), where the growth factor for this branch becomes positive (unstable) above 1,027 rpm. In order to show the instability regions more clearly, a considerably enlarged view of Fig. 4.9(a) is shown in Fig. 4.10. For small values of external damping in the system's oil-type damper ($C_d < 1.0$ lb-sec/in. approximately) the instability region extends indefinitely (at least up to 100,000 rpm) from 1,027 rpm upward. However, for larger values of C_d (> 2.0 lb-sec/in. approximately), the unstable region has a finite band-width which has an upper limit that decreases as C_d is increased. The situation is summarized in Table 4.3.

Unfortunately, an oil-type damper is not linear [19]; thus, it is difficult to select a proper value of linear damping coefficient.

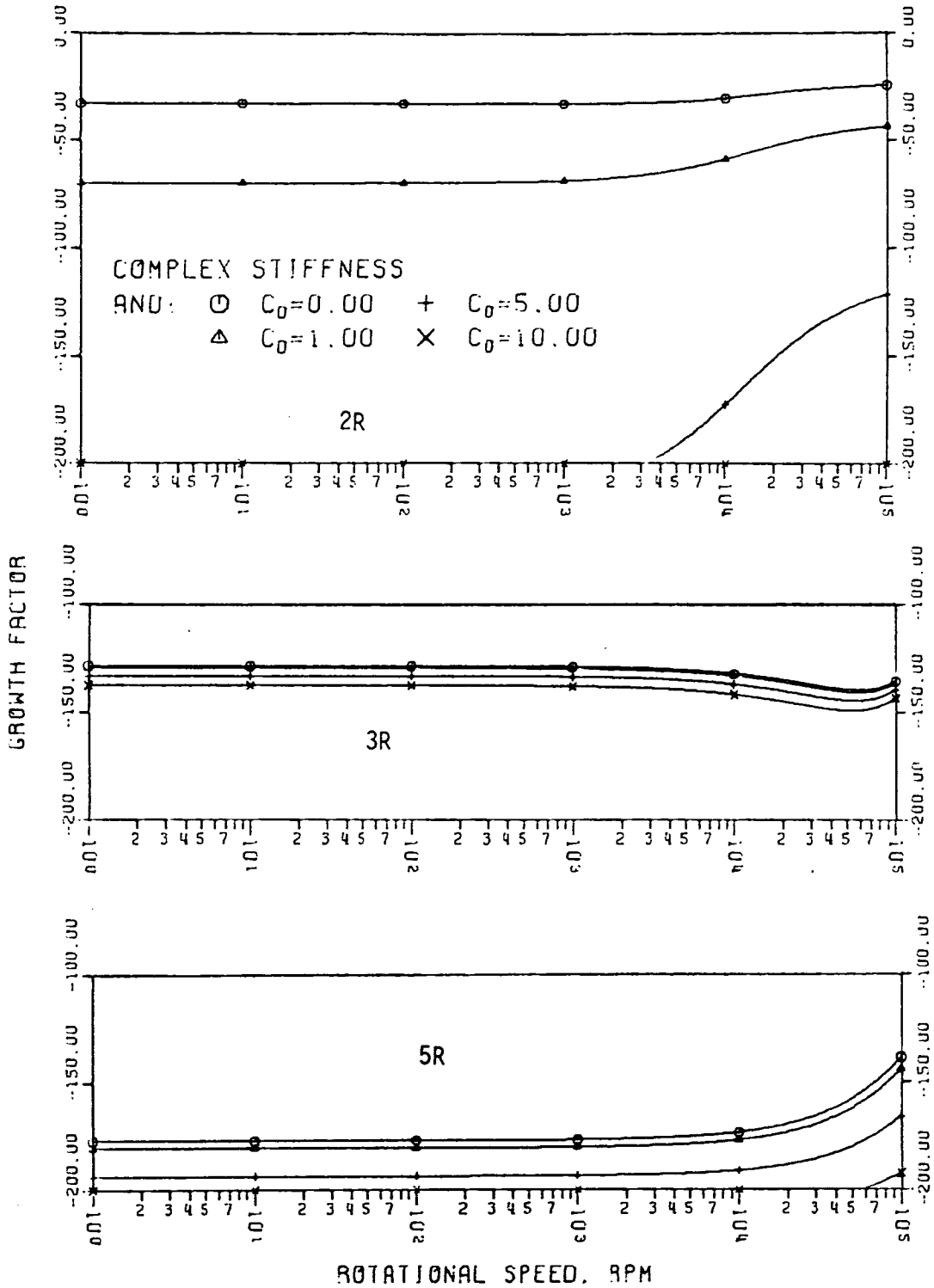

Fig. 4.8 Stability diagram: growth factor versus rotational speed for retrograde branches of modes 2, 3, and 5, with various values of external damping coefficient.

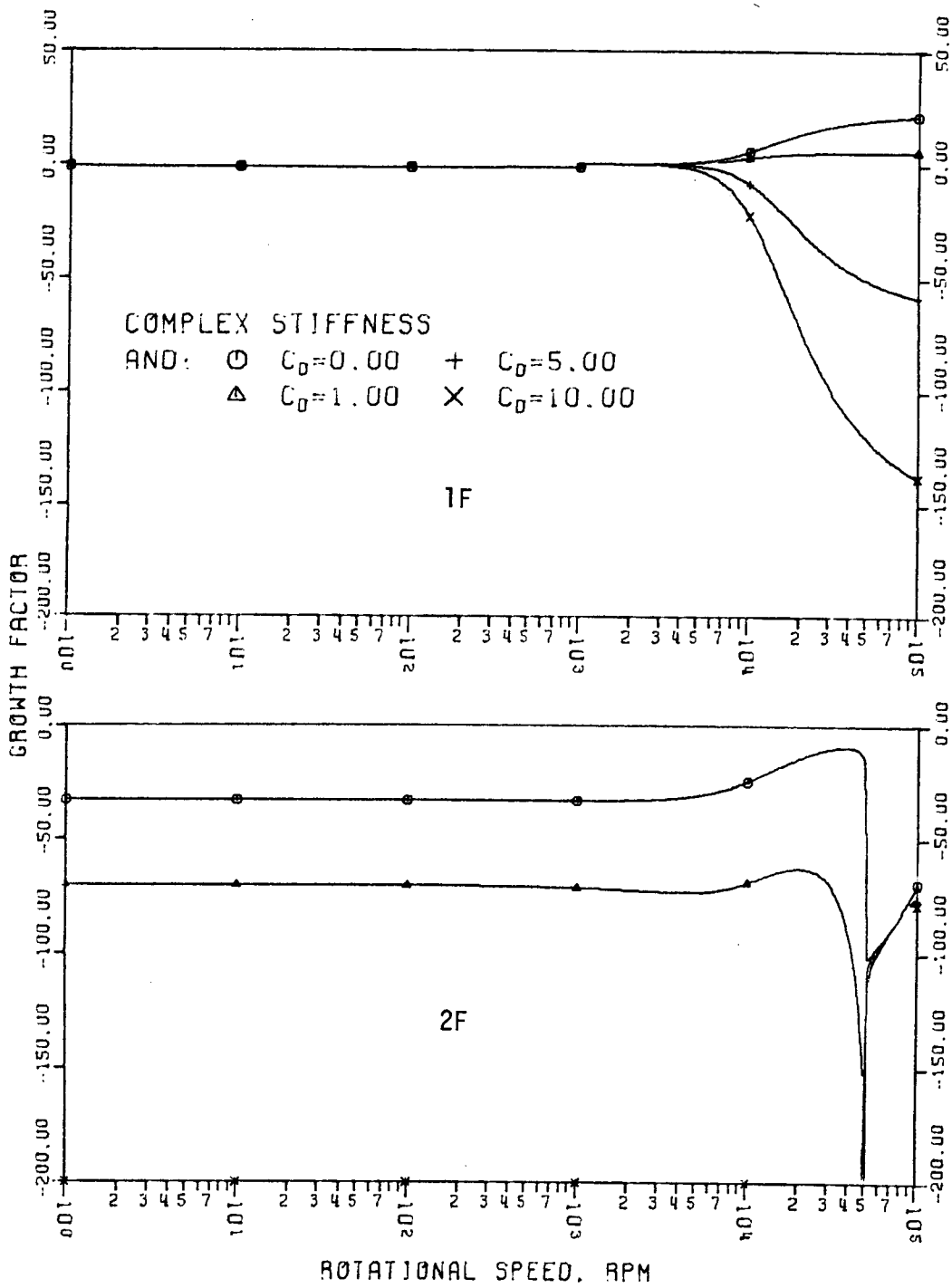

Fig. 4.9(a) Stability diagram: growth factor versus rotational speed for the forward branches of modes 1 and 2 with various values of external damping coefficient.

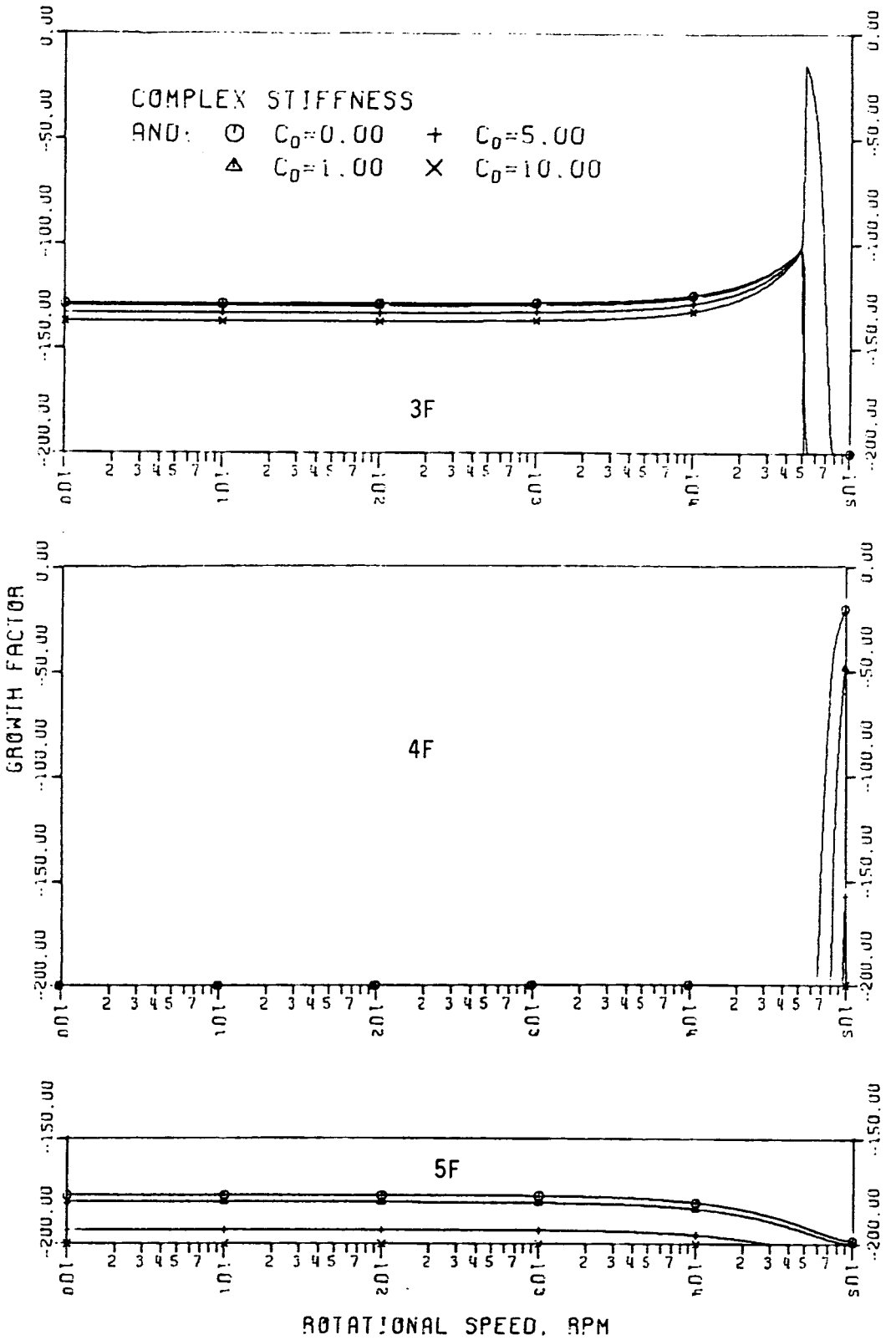

Fig. 4.9(b) Stability diagram: growth factor versus rotational speed for the forward branches of modes 3, 4, and 5 with various values of external damping coefficient.

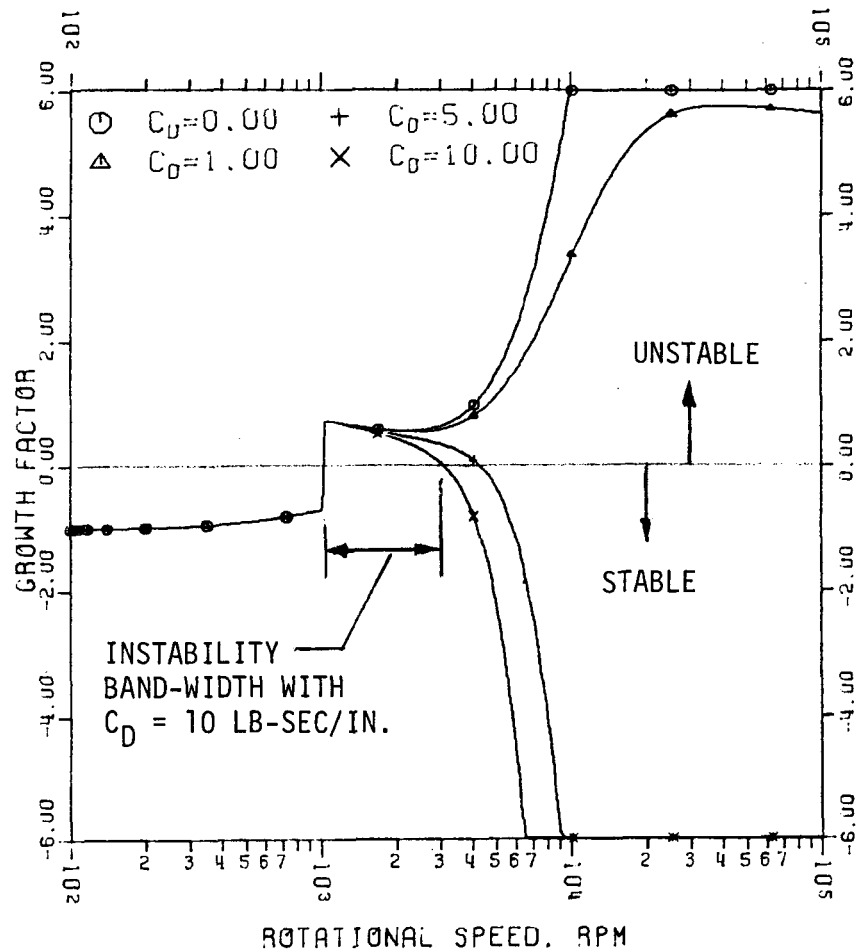

Fig. 4.10 Enlarged view of Fig. 4.9(a), which is the stability diagram for branch 1F of System A. The region (band-width) of instability, for example with C_d = 10 lb-sec/in., is shown marked.

Table 4.3 Effect of External Damping Coefficient on the Upper and Lower Limits of the Unstable Region for the First Forward Branch

Limit	External damping C_d, lb-sec/in.			
	0	1	5	10
Lower limit of instability band, rpm	1,027	1,027	1,027	1,207
Upper limit of instability band, rpm	∞	At least 100,000	5,012	3,162

4.3 Forced Whirling Response

Potentially the excitation for forced whirling can be misalignment of any masses in the rotating system. This misalignment is of two types:

1. Eccentricity, i.e., the radial distance between the mass center and the center of rotation,

2. Tilt, i.e., the smallest angle between a principal-inertia axis* and the axis of rotation.

The nature of the design of current and projected energy-storage flywheels is such that by far the largest rotating mass in the system is the flywheel itself. For example, in the system analyzed by Bert et al. [13], p. 13, the flywheel assembly comprised 76.6% of the total rotating mass. Thus, in the present analysis, the only mass eccentricity and initial tilt considered are those associated with the flywheel itself. Values believed to be typical for a flywheel system such as System A, when installed on the 4-inch Barbour Stockwell air-turbine spin-test facility, are r_e = 0.001 in. and ϕ_0 = 0.0025 radians, respectively. Thus, these values are used in the present study.

It has been found in previous studies [19,21] that the phase angle between the eccentricity and tilt (see Fig. 4.11) has an important effect on

---

*For an arbitrary rigid body, there exist three mutually perpendicular axes passing through the mass center ($\bar{x} = \bar{y} = \bar{z} = 0$) such that the mass products of inertia ($\int_V \bar{x}\bar{y}\,\rho\,dV$, $\int_V \bar{y}\bar{z}\,\rho\,dV$, $\int_V \bar{z}\bar{x}\,\rho\,dV$) are exactly zero. These axes are called the principal-inertia axes and the mass moments of inertia ($I_{m\bar{x}} = \int_V (\bar{y}^2 + \bar{z}^2)\rho\,dV$, $I_{m\bar{y}} = \int_V (\bar{z}^2 + x^2)\rho\,dV$, $I_{m\bar{z}} = \int_V (\bar{x}^2 + \bar{y}^2)\rho\,dV$) associated with them are relative minima or maxima known as principal mass moments of inertia.

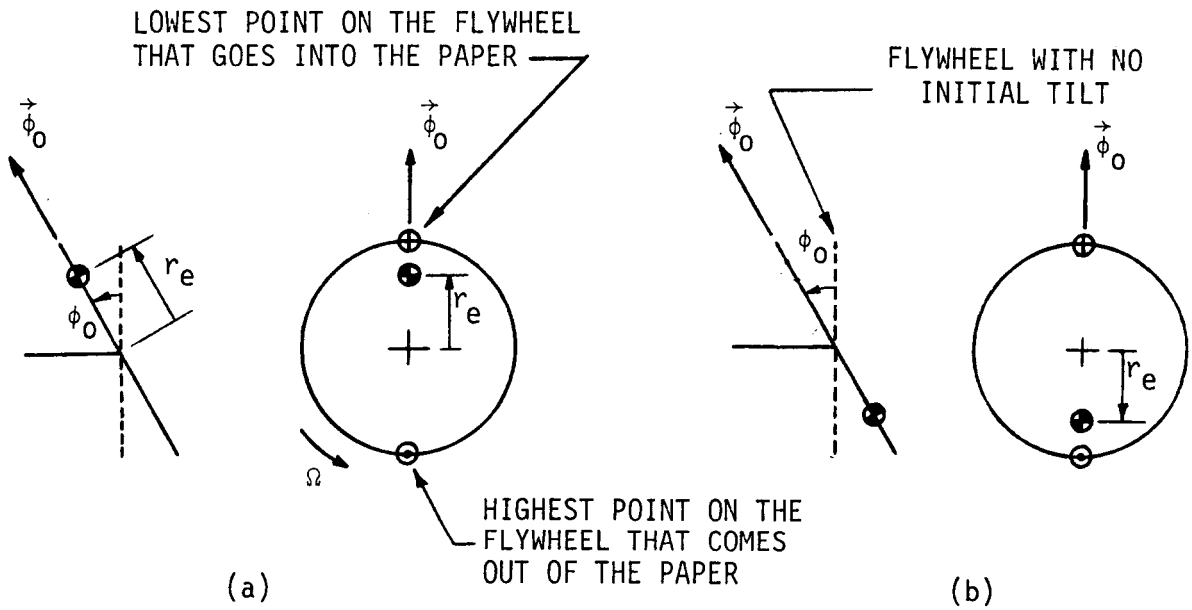

Fig. 4.11 Representation of mass eccentricity and initial tilt as vectors for convenience of defining the phase relations between them, (a) $\beta = 0$, (b) $\beta = 180$ degrees.

the forced whirling response. Probably this phase angle is a random variable in actual systems, however, there is no body of empirical data available on this parameter, especially for flywheel systems. Thus, in the present study, this angle is taken conservatively to be 180 degrees, since it has been found that this angle results in the largest response [21].

As mentioned previously in Section 2.4, the synchronous nature of forced whirling precludes internal material damping from being operative (see also Case (b) in Fig. 4.6) here. Since external damping in the oil-type damper tends to decrease the forced whirling response, the most drastic case is that of no external damping. Figure 4.12 shows the response of all seven degrees of

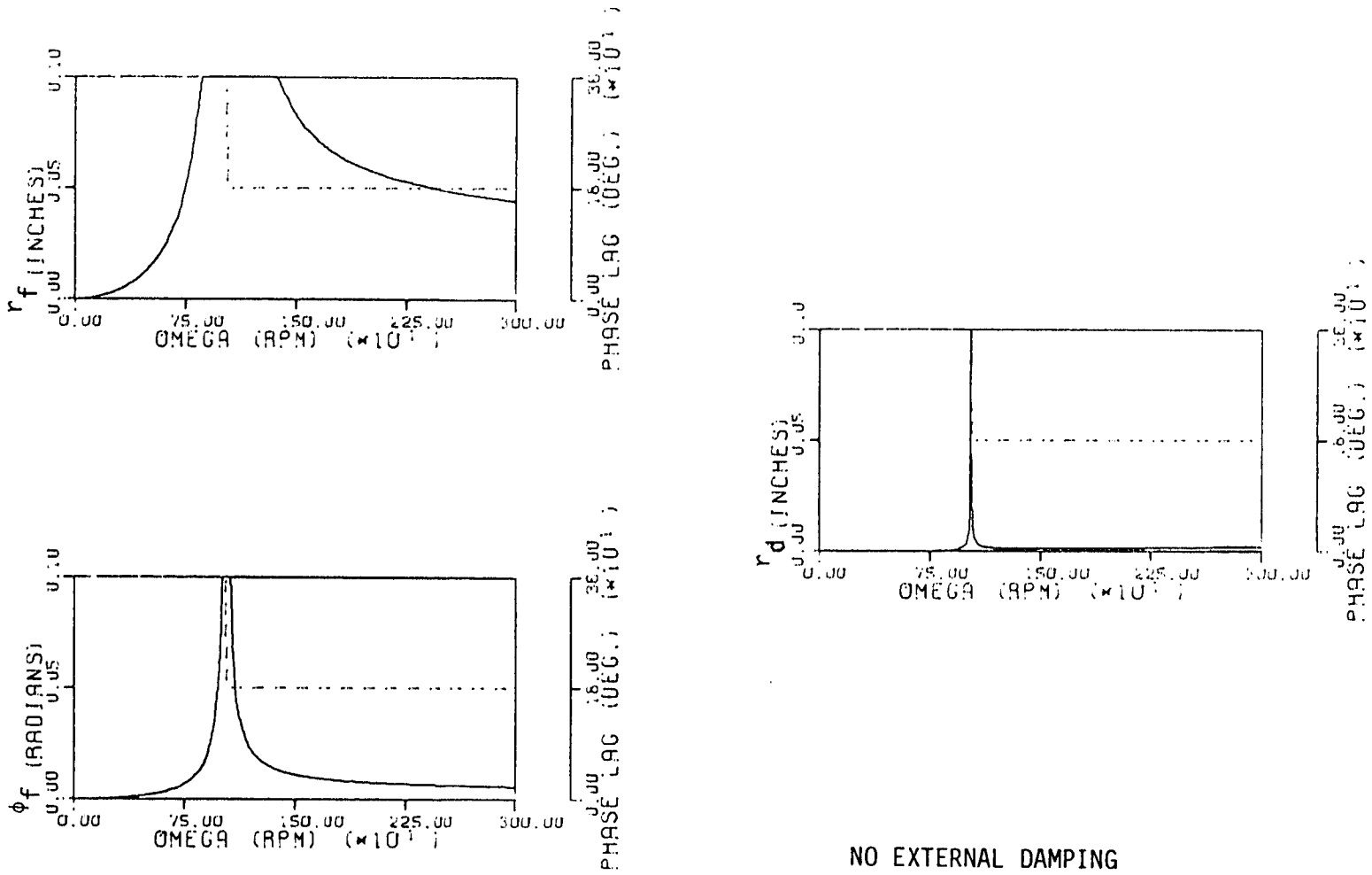

NO EXTERNAL DAMPING

Fig. 4.12(a) Forced whirling responses of three of the seven degrees of freedom in the lumped-parameter model up to 3,200 rpm (r_f and ϕ_f are the amplitudes of the flywheel displacement and tilt, respectively; r_d is the damper displacement amplitude).

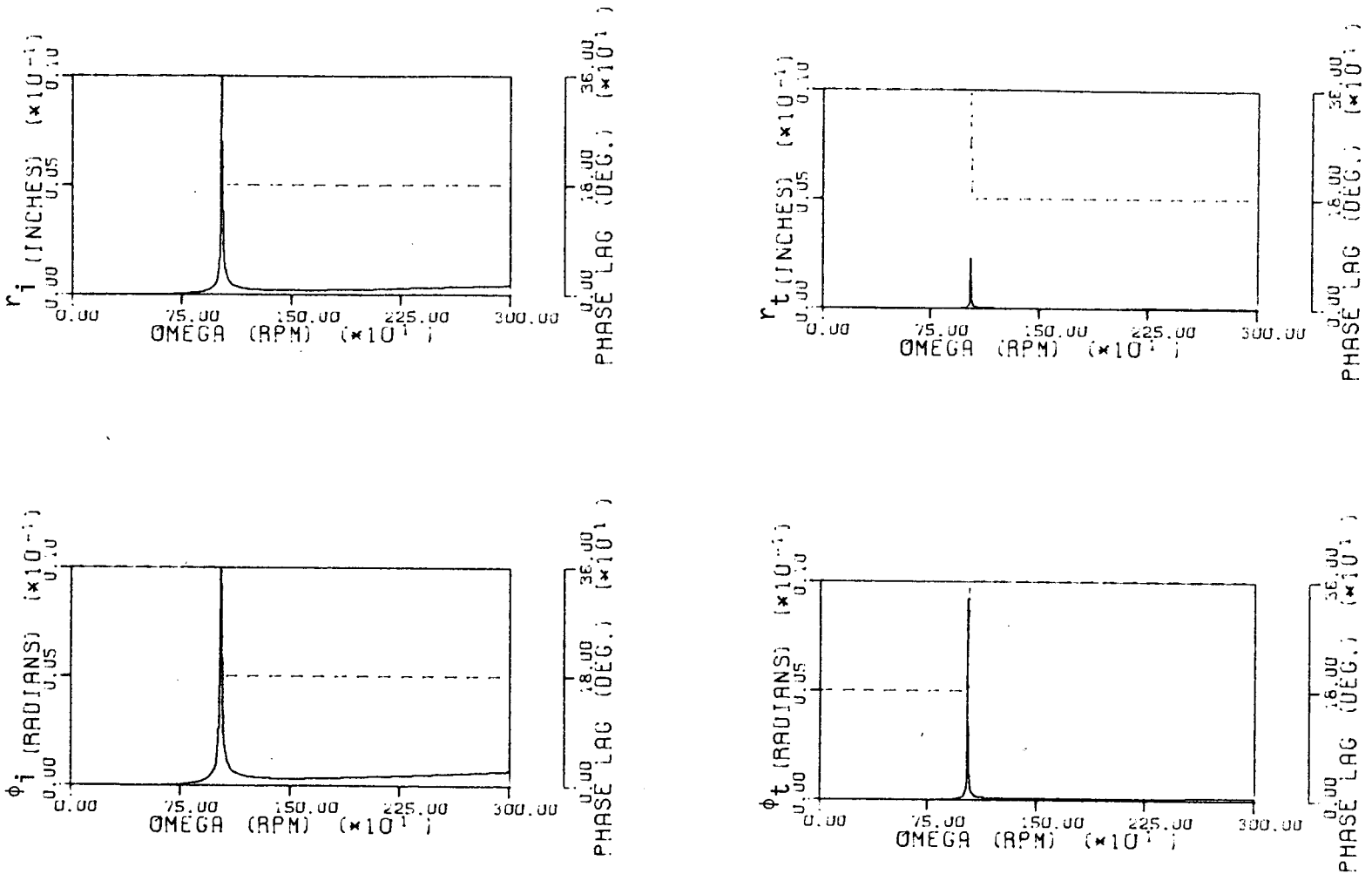

Fig. 4.12(b) Forced whirling responses of four of the seven degrees of freedom in the lumped-parameter model up to 3,200 rpm (r_i and ϕ_i are the amplitudes of the intermediate-mass displacement and tilt, respectively; r_t and ϕ_t are the amplitudes of the turbine-wheel displacement and tilt, respectively).

freedom of the lumped-parameter model with no external damping. The solid curves represent the amplitudes and the dotted curves represent the corresponding phase lags with respect to the radius (from the center of rotation) on which the flywheel mass center lies.

Let the displacements (due to whirling) of the various mass centers from their undeflected original positions be imagined as different radius vectors. Also, assume that the tilts of the various masses (induced due to whirling) are represented as line vectors such as the one depicted in Fig. 4.11 for the flywheel. Now the phase angles that are represented in all the forced whirling plots depict the lagging of these vectors with respect to the radius vector of mass eccentricity r_e in Fig. 4.11. Thus, at any specific shaft running speed, these vectors maintain their relative positions (generally not in a single plane when there is an external damping) while whirling at the shaft running speed. It is noted that in the absence of external damping, the response at resonance theoretically increases without bound. Also, the phase lag is always either 0 or 180 degrees, except at resonance for which it changes by $\pm$ 180 degrees. (Note that a 360-degree phase lag is the same as 0 degrees.)

The system's responses for a rather large external damping coefficient (C_d = 10 lb-sec/in.) were found to be essentially identical to the corresponding ones shown in Fig. 4.12. Thus, the damper is predicted to be ineffective.

Three responses, for zero external damping, as determined by the combined model, are shown in Fig. 4.13. For brevity only the flywheel responses (r_f and ϕ_f) and damper response (r_d) are shown. The close agreement between the corresponding responses presented in Figs. 4.12 and 4.13 is gratifying.

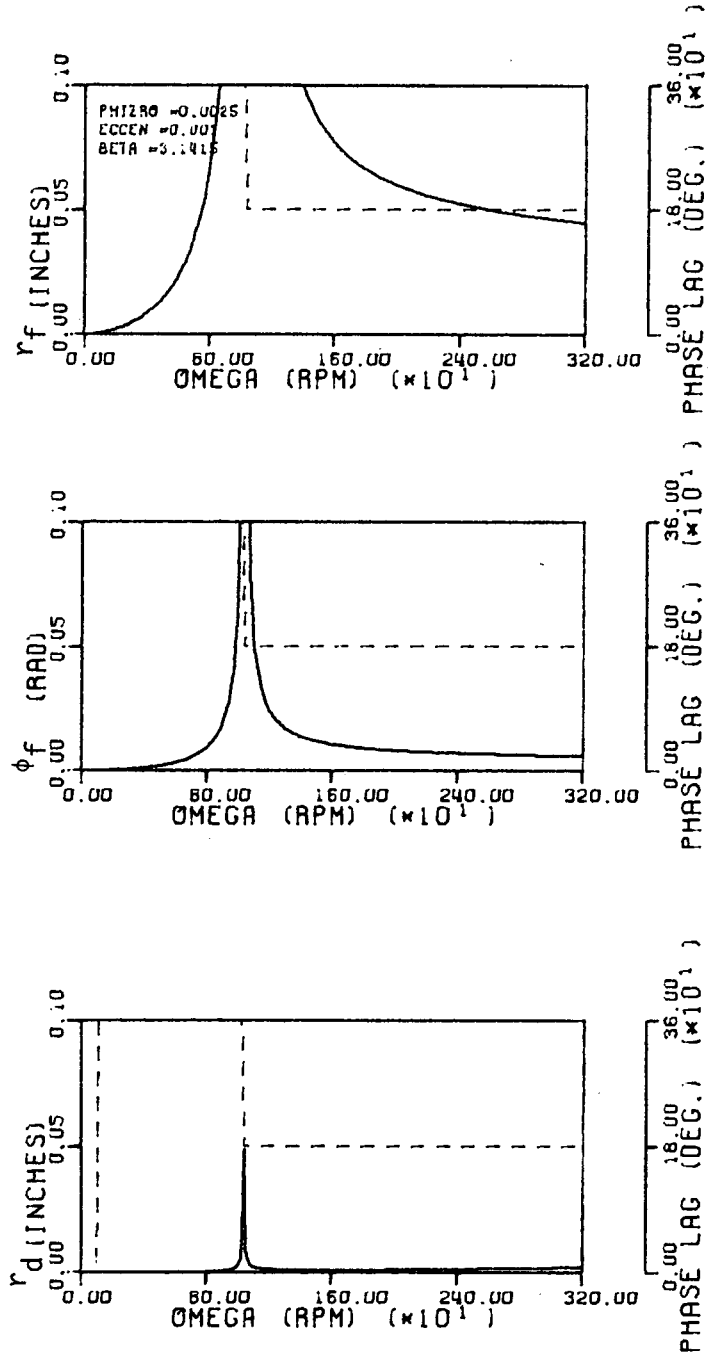

Fig. 4.13 Forced whirling response amplitudes of flywheel displacement (r_f) and tilt (ϕ_f) and damper displacement (r_d) up to 3,200 rpm, as predicted by the combined model. No external damping.

Again, when the external damping coefficient was increased to 10 lb-sec/in., there was no noticeable change in response.

The lumped model predicts a slightly larger damper displacement than the combined model. This is believed to be due to a slight difference in the technique used to obtain the computer plots. For the lumped model, the rotational speed Ω was changed in 6-rpm increments while in the combined model, 10-rpm increments were used. It so happened that one of the points plotted fell closer to the critical speed in the lumped model than in the combined model and hence the resonant response was larger.

5. PARAMETRIC STUDIES

The numerical results presented in Section 4 completely describe the free and forced whirling responses and stability characteristics of a particular flywheel system (System A) which was used as a baseline. However, to obtain data applicable to all of the existing or conceivable flywheel systems would require not only extensive computations but also a prohibitively large number of plots. Thus, in this section, the present investigators have chosen to give in tabular form the results of parametric studies in which selected parameters are varied.

In this section, two additional existing flywheel systems are studied. These are the General Electric Company's constant-thickness, alpha-ply, disk-ring-type flywheel [44] and the Lawrence Livermore National Laboratory's tapered-thickness, quasi-isotropic, composite-disk-type flywheel [45]. These are designated hereafter simply as Systems B and C, respectively.

5.1 Forward Critical Speeds

In Section 4.1, the importance of the first (lowest) forward critical speed of the first order was discussed for System A. The dynamic parameters of Systems A, B, and C are listed in Table 5.1 along with their first forward critical speeds of first order. In all three of the systems the second first-order forward critical speeds occur at 108,500 rpm. It can be seen from the mode-shape analysis in Fig. 4.5(a) of Section 4.1 that at 108,500 rpm the main action takes place at the turbine end with the flywheel remaining inactive. Further, the first and second first-order forward critical speeds are so far apart that there is no coupling between them. Thus, variations in flywheel parameters do not affect the forward critical speed related to the turbine-end action significantly.

Table 5.1 Parameters of Systems A, B, and C and Their First First-Order Forward Critical Speeds

System	m_f (lb-s²/in)	I_{pf} (lb-in-s²)	I_{df} (lb-in-s²)	t_f (in)	$I_{pf}/m_f t_f^2$	I_{df}/I_{pf}	Ω_{11} (rpm)
A	0.0951	8.517	4.830	7.05	1.802	0.5671	1,038
B	0.0576	2.036	1.648	3.45	2.970	0.8094	1,907
C	0.0336	1.645	0.823	3.15	4.934	0.5003	14,230

The effect of varying flywheel mass on the first first-order forward critical speed is summarized in Table 5.2. Here, t_f, $I_{pf}/m_f t_f^2$, and I_{df}/I_{pf} are held constant at the same values as those of System A. Notice that Ω_{11} increases as the mass is reduced, like a single-degree-of-freedom spring-mass system, with $\Omega_{11}\sqrt{m_f}$ staying constant.

Table 5.2 Effect of Flywheel Mass (m_f) on the Lowest First-Order Forward Critical Speed*

m_f (lb-s²/in)	I_{pf} (lb-in-s²)	I_{df} (lb-in-s²)	Ω_{11} (rpm)	$\Omega_{11}\sqrt{m_f}$
0.0951	8.517	4.830	1,038	320
0.08	7.165	4.063	1,133	320
0.06	5.373	3.047	1,307	320
0.05	4.478	2.539	1,432	320
0.03	2.687	1.524	1,848	320

*Fixed parameters: $I_{pf}/m_f t_f^2 = 1.802$, $I_{df}/I_{pf} = 0.5671$, $t_f = 7.05$ in.

In order to study the influence of I_{df} on the lowest first-order forward critical speed (Ω_{11}), m_f, I_{pf}, and t_f were held constant at values corresponding to those in System C, and I_{df}/I_{pf} ratio was varied. The results are presented in Table 5.3. Thus, increasing I_{df} is seen to bring down the critical speed. Flywheels used in fixed-based applications usually have an I_{df}/I_{pf} ratio ≥ 1. For flywheel systems of such ratios (with fixed parameters of System C), the second first-order critical speeds (Ω_{21}), are listed in Table 5.3. The critical

speed associated with the large motions of the intermediate mass and the turbine still remains at 108,500 rpm for all the cases discussed in this section unless otherwise stated. Further, unless mentioned otherwise, there are no second first-order critical speeds below 100,000 rpm for all of the parametric cases studied here.

Table 5.3 Effect of Flywheel Diametral Mass Moment of Inertia (I_{df}) on the Two Lowest First-Order Critical Speeds†

I_{df} (lb-in-s^2)	I_{df}/I_{pf}	Ω_{11} (rpm)	Ω_{21} (rpm)
0.823	0.5003	14,230	↑
0.987	0.6	12,400	none below 100,000 rpm
1.151	0.7	8,851	
1.316	0.8	4,018	↓
1.645	1.0	2,003	86,000
1.974	1.2	1,503	29,480

†Fixed parameters: m_f = 0.0336 lb-s^2/in, I_{pf} = 1.645 lb-in-s^2, t_f = 3.15 in.

In Table 5.4 the effect of I_{pf}, with m_f, I_{df}, and t_f held constant at their respective values as in System C, on the first first-order forward critical speed is shown. From the results we see that as I_{pf} is increased, the critical speed Ω_{11} also increases. That is, with the other parameters remaining the same, increasing I_{pf} produces a larger gyroscopic action on the system, thus stiffening the system in forward whirling.

What happens to the lowest first-order forward critical speed when the non-bending length (t_f in Fig. 3.1) of the quill shaft is increased? The answer to this question may be seen by inspecting Table 5.5. Here, all the parameters are kept the same as those of System C except t_f, which is increased. The decrease in Ω_{11} is explained as follows. Increasing length t_f increases

Table 5.4 Influence of Flywheel Polar Mass Moment of Inertia (I_{pf}) on the Lowest First-Order Critical Speed*

I_{pf} (lb-in-s^2)	$I_{pf}/m_f t_f^2$	I_{df}/I_{pf}	Ω_{11} (rpm)
1.000	3.0	0.8228	2,619
1.334	4.0	0.6171	9,358
1.645	4.934	0.5003	14,230

*Fixed parameters: m_f = 0.0336 lb-s^2/in, I_{df} = 0.823 lb-in-s^2, t_f = 3.15 in.

Table 5.5 Effect of the Distance (t_f) of the Flywheel Center of Mass from the Lower End of the Quill Shaft on the Lowest First-Order Forward Critical Speed (System C)

t_f (in)	Ω_{11} (rpm)
3.15	14,230
4.0	9,817
5.0	3,143
6.0	1,752
7.05	1,280

the moment arm at which the flywheel force is applied and thus, makes the system more flexible and reduces Ω_{11}. Note that the lengths of the flexible portions of the shaft sections have been held constant.

For purposes of comparison of the critical-speed characteristics of Systems B and C, all of the forward and retrograde critical speeds of first and second order up to 100,000 rpm are listed in Tables 5.6 and 5.7, respectively.

Although each system has three retrograde first-order critical speeds and three retrograde second-order critical speeds in the range up to 60,000

Table 5.6 First- and Second-Order Critical Rotational Speeds (rpm) for System B as Calculated by the Two Different Models

Order	First ($\omega/\Omega = 1$)				Second ($\omega/\Omega = 2$)							
Mode & Branch	1R	1F	2R	3R	1R	1F	2R	2F	3R	3F	4R	4F
Lumped Model	611	1,895	14,970	54,480	347	535	7,740	10,230	30,530	42,500	61,530	62,160
Combined Model	612	1,907	17,000	56,140	348	536	8,790	11,600	31,400	43,370	70,310	71,170

Table 5.7 Critical Rotational Speeds (rpm) for System C

Order	First ($\omega/\Omega = 1$)				Second ($\omega/\Omega = 2$)						
Mode & Branch	1R	1F	2R	3R	1R	1F	2R	2F	3R	3F	4R
Lumped Model	765	12,540	18,980	54,490	452	1,000	9,814	38,640	30,540	42,580	62,010
Combined Model	766	14,230	21,530	56,160	453	1,002	11,130	41,620	31,420	44,390	70,910

rpm, these should not cause any serious problems in spin testing*. Also, each system has three forward second-order critical speeds in the range up to 60,000 rpm. However, there should not be much excitation available to excite such critical speeds unless the systems were operated with the shafts horizontal instead of vertical. (We are assuming that the shaft out-of-round tolerances are reasonably close to ensure axisymmetric stiffness of the shafts.)

As previously mentioned on page 33, rotating machinery with a horizontal axis of rotation has a double-frequency excitation source in the form of gravity force. In pendulously supported flywheels, i.e., those supported in vertical cantilever fashion from above, gravity also has an effect, but it is a steady effect in the form of a restoring action. Thus, it is equivalent to stiffening of the flywheel shaft and tends to increase the first-order forward critical speeds. Since this gravity effect has not been treated in the literature, except for simple single-mass systems, this effect is investigated in detail in Appendix D.1.

A brief analysis which shows that the effect of steady applied torque is negligible for flywheels in spin testing is contained in Appendix D.2.

Within the constraints of the model and the actual spin test facility, two other parameters were varied independently for Systems A and B. One parameter was the flexible shaft length L_1 between the flywheel and the end of the damper nearest the flywheel (see Fig. 3.1). The other parameter was the lower turbine-bearing spring constant $K_{s\ell}$. The two lowest first-order

*See Section 5.3 for a discussion of the forced-response characteristics of retrograde modes.

critical speeds associated with these changes are presented in Tables 5.8 and 5.9, respectively.

Table 5.8 Effect of a 3.00-Inch Increase in Flexible Length L_1 on the Two Lowest First-Order Critical Speeds ($K_{s\ell}$ = 2 x 10^6 lb/in.)

System	L_1 (changed from 0.7455 in.)	Original* Ω_{11} (rpm)	With Increased L_1 Ω_{11} (rpm)	With Increased L_1 Ω_{21} (rpm)
A	3.746 in.	1,038	286	85,650
B	3.746 in.	1,907	502	85,650

*The original system had an Ω_{21} of over 100,000 rpm.

Table 5.9 Effect of Decreasing $K_{s\ell}$, the Lower Turbine-Bearing Spring Constant, to 2 x 10^2 lb/in. on the Two Lowest First-Order Critical Speeds (L_1 = 0.7455 in.)

	$K_{s\ell}$ (changed from 2 x 10^6 lb/in.)	Original* Ω_{11} (rpm)	With Decreased $K_{s\ell}$ Ω_{11} (rpm)	With Decreased $K_{s\ell}$ Ω_{21} (rpm)
System A	2 x 10^2 lb/in.	1,038	441	4,822
System B	2 x 10^2 lb/in.	1,907	653	4,720

*See footnote for Table 5.9.

In studying the effect of decreasing the lower-bearing spring constant, it was observed that the first-order critical speeds related to the turbine-end action for Systems A and B were lowered to 106,800 rpm and 104,000 rpm, respectively. Notice that the effects of increasing L_1 and decreasing $K_{s\ell}$ are to decrease the critical speeds. More discussions on these effects can be found in Section 5.3.

The following questions may arise in the reader's mind. Can the systems

(A, B, and C) we have studied so far be simplified further for easier analysis? Is there a faster way to compute the critical speeds than by the analyses presented in this report? Consider the lumped analysis presented in [11] for a pendulously supported flywheel system with two degrees of freedom (flywheel displacement and flywheel tilt). In order to apply this analysis to systems A, B, and C, one must modify these systems such that the flywheel is supported pendulously from the damper end nearest it. Thus, the flexible shaft length to be used is L_1 (see Fig. 3.1). To obtain the first-order forward critical speeds, the rotational speed is set equal to the whirling frequency and to obtain the retrograde first-order critical speeds, the whirling frequency is set equal to the negative of the rotational speed. The results are presented in Table 5.10.

Table 5.10 Comparison of Predictions on First-Order Critical Speeds (rpm) by Analysis of [11] and the More Refined Seven-Degree-of-Freedom Lumped Analysis of this Report

System	1F[11]	1F*	1R[11]	1R*	2R[11]	2R*
A	1,038	1,027	301	301	23,110	12,450
B	1,919	1,895	611	611	27,890	14,970
C	23,170	12,540	765	765	35,620	18,980

*Calculated using the seven degree-of-freedom lumped model

Notice that the agreement is very good for the first retrograde (1R) critical speeds. The numbers are reasonably close for 1F of systems A and B. The refined model predicts coupling of the flywheel motion, to a small extent (systems A and B) or to a large extent (system C), with the movements of the rest of the masses in the model. Thus, the refined model is always softer than the simplified model. As the extent of coupling increases, the difference in the critical-speed predictions can be seen to increase. Thus, when there are more than two degrees of freedom in the flywheel system, the simplified two-degree-of-freedom model of [11] should be used with caution for critical-speed predictions.

5.2 Instability Limits

For purposes of comparison, Tables 5.11 and 5.12 present the upper and lower instability limits for Systems B and C (see Table 4.3 for System A).

Table 5.11 Effect of External Damping Coefficient on the Upper and Lower Limits of the Unstable Region for the First Forward Branch* of System B

Limit	External Damping C_d, lb-sec/in.			
	0	1	5	10
Lower limit of instability band, rpm	1,895	1,895	1,895	1,895
Upper limit of instability band, rpm	∞	At least 100,000	5,830	4,575

*All other branches are stable.

Table 5.12 Effect of External Damping Coefficient on the Upper and Lower Limits of the Unstable Region for the First Forward Branch* of System C

Limit	External Damping C_d, lb-sec/in.			
	0	1	5	10
Lower limit of instability band, rpm	12,530	12,530	Stable at all speeds	
Upper limit of instability band, rpm	∞	15,540		

*All other branches are stable.

It is noted that System C is more responsive to an increase in external damping than is System A or B. However, all three systems are stable with a damping coefficient of 5 lb-sec/in. for speeds over 5,830 rpm (19.4% of a maximum operating speed of 30,000 rpm).

5.3 Forced Whirling Response of Forward Branches

The effects of increasing the lowest first-order forward critical speed to higher values on forced whirling response are shown in Figs. 5.1 to 5.3. In Figs. 5.1 and 5.2, the forced response of System C (t_f = 3.15 in.) for C_d values of 0 and 10 lb-sec/in. are presented. Note that the resonance response near 14,230 rpm is diminished by the addition of external viscous damping. Figure 5.3 is the response of System C with t_f = 7.05 in.; the resonance occurs at 1,280 rpm. It was found that adding external viscous damping (C_d = 10 lb-sec/in.) does not alter the response significantly at all. Furthermore, the mode shape at 14,230 rpm for the lowest forward branch showed a larger damper movement than that at 1,280 rpm. Comparing Figs. 5.1, 5.2, and 5.3, we see that at smaller resonance speeds the responses are sharper than those at higher resonance speeds. Thus, smaller lowest first-order critical speeds can be easily passed through, even though the damper is ineffective. At higher resonance speeds, the inability to pass through fast enough to minimize the response is usually compensated for by the increased effectiveness of the damper.

The effectiveness of a damper (in attenuating forced whirling responses and helping in stability) at a critical speed can be better understood by studying the mode shapes at that critical speed. For example, see Fig. 4.5(b) of Section 4 which shows the mode shapes at various critical speeds of the <u>second</u> order. From these mode shapes we see that the damper has relatively large movements only at the second and fourth critical speeds. Hence, all large motions in the system are likely to get dampened at these critical speeds. Thus, a damper <u>need not be effective</u> at all critical speeds.

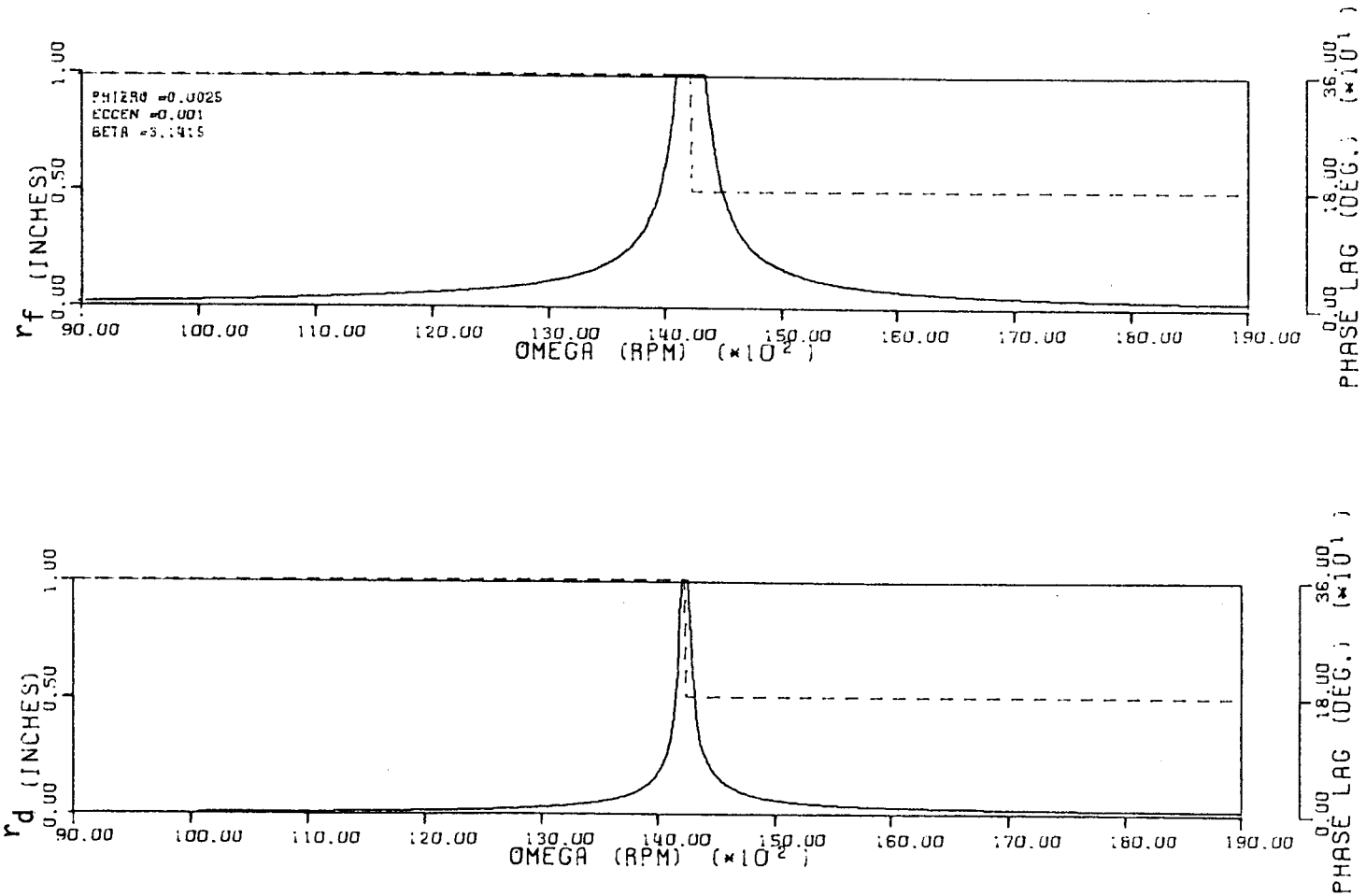

Fig. 5.1 The forced responses of the displacements, r_f and r_d, of the flywheel center of mass and the damper center of mass, respectively, of System C, with C_d = 0 lb-s/in. (r_e = 0.001 in., ϕ_o = 0.0025 rad., β = 180°).

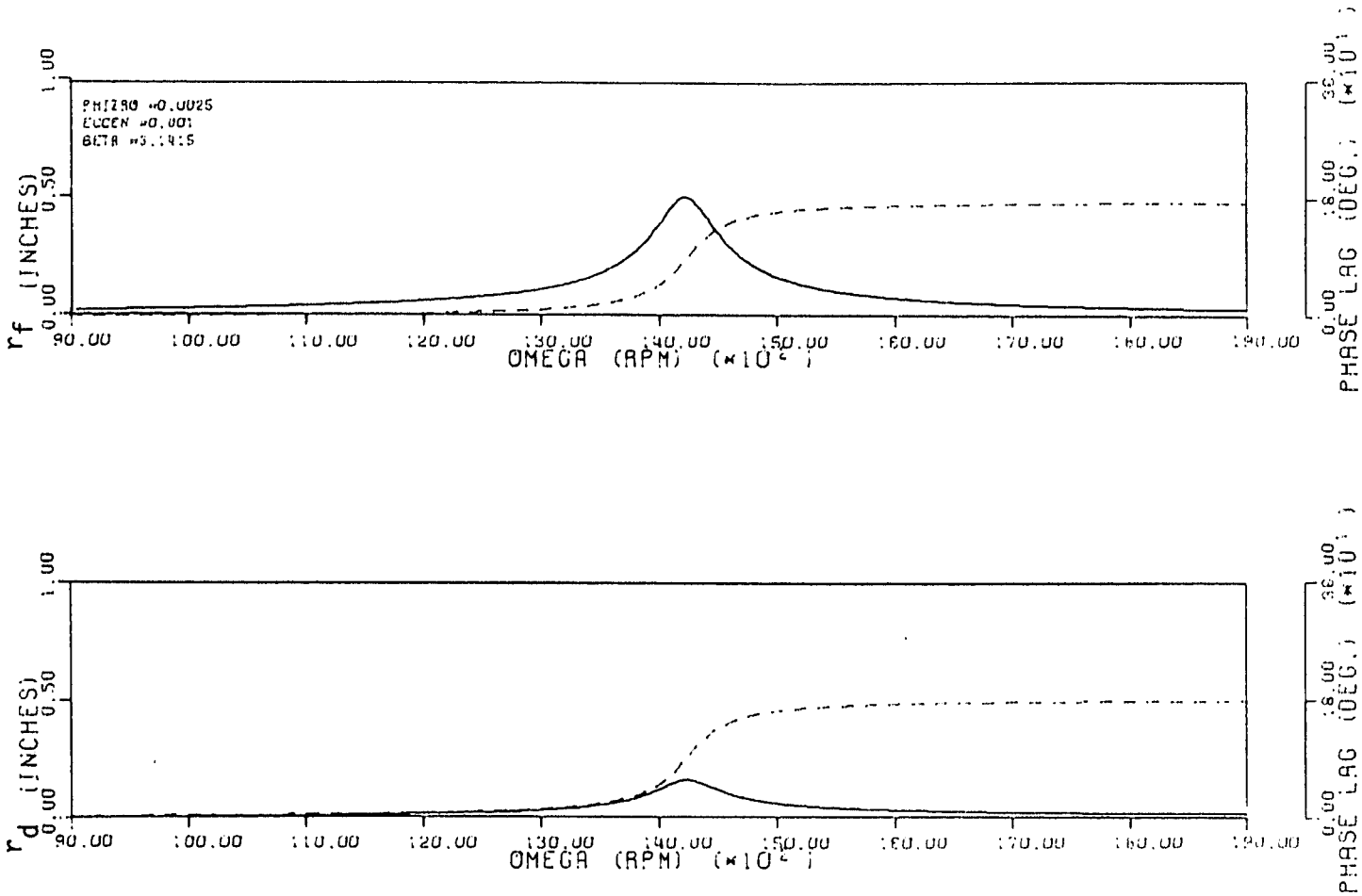

Fig. 5.2 The forced responses of the displacements, r_f and r_d, of the flywheel center of mass and the damper center of mass, respectively, of System C, with C_d = 10.0 lb-s/in. (Same r_e, ϕ_o, and β as in Fig. 5.1).

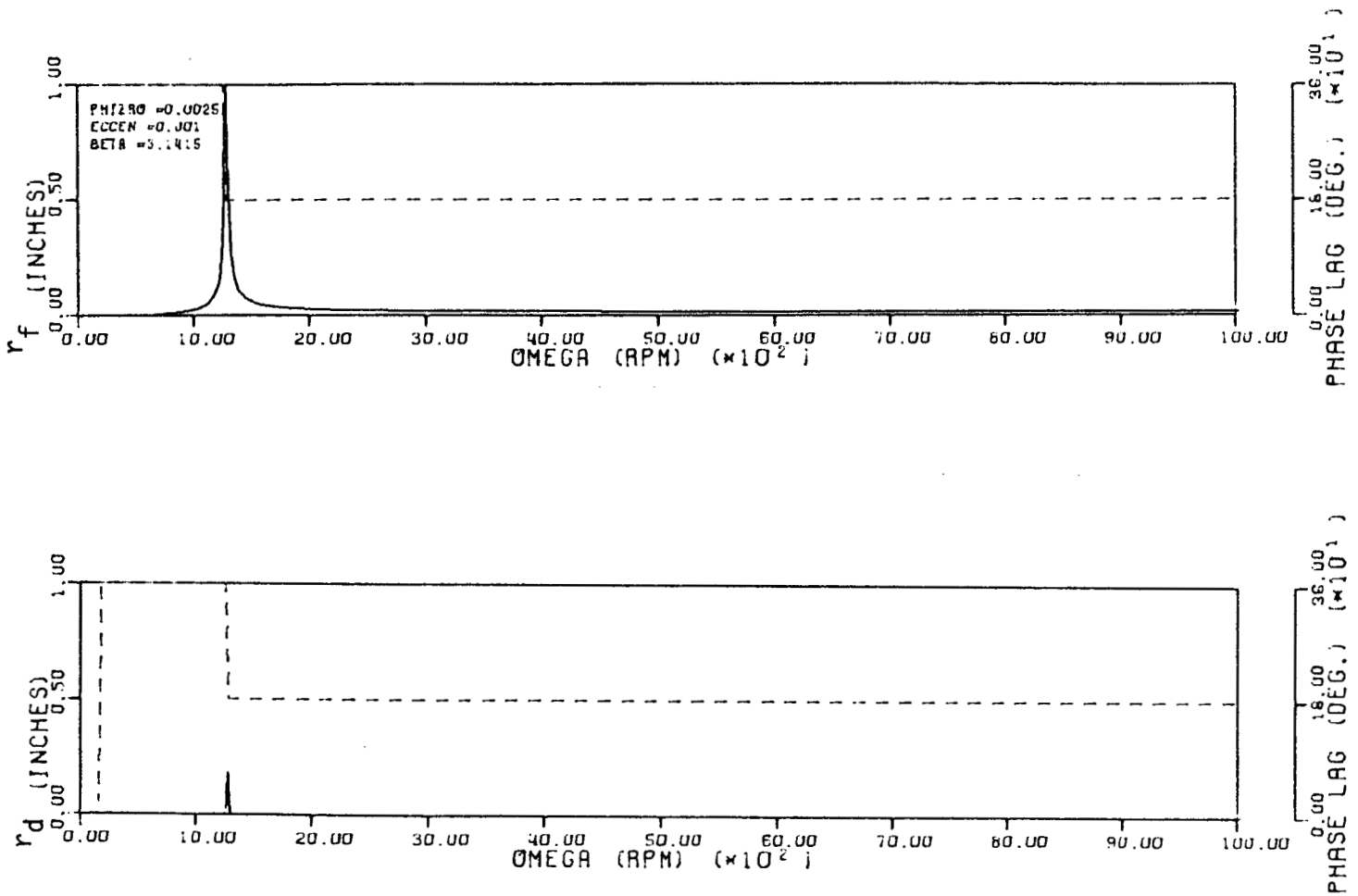

Fig. 5.3 The forced responses of the displacements, r_f and r_d, of the flywheel center of mass and the damper center of mass, respectively, of System C, modified by increasing t_f to 7.05 in., and with C_d = 0 lb-s/in. (r_e = 0.001 in., ϕ_o = 0.0025 rad., β = 180°).

Forced whirling responses were obtained for the cases when L_1 and $K_{s\ell}$ were changed independently. Increasing L_1 lowered Ω_{11} (see Table 5.8), at which only the flywheel had large displacements, and brought in a second critical speed Ω_{21} < 100,000 rpm in which the damper was the component having the most displacement. Drastically decreasing the lower turbine-bearing spring constant $K_{s\ell}$ (see Table 5.9) also brought down Ω_{11} and introduced Ω_{21} within the operating range of the system. In this particular parametric study, it was observed that there was an active participation of the damper in the first critical speed which attenuated all of the system's responses. However, it was noticed that at Ω_{21} there was a large motion of the intermediate mass and the damper was relatively inactive.

5.4 Forced Whirling Analysis of Retrograde Branches

In all of the forced vibrational analyses for steady-state response, we assumed that the response has the same frequency as the forcing function (see sections 2.4 and 3.3). Hence, a forcing function of a frequency Ω, or of the form $e^{i\Omega t}$ (due to mass eccentricity and initial tilt), alone cannot induce a retrograde response of the form $e^{-i\Omega t}$ [7,8]. There are various other forcing functions that might induce a retrograde response. These include asymmetry of the bearings and shafts, and load torque (not driving torque). The analysis presented in this report can only predict forced whirling responses for a synchronous forward whirling ($n = +1$). Note that when $n \neq +1$, the shaft undergoes stress cycling which brings in the material damping action (see section 4.2). Thus, for forced retrograde whirling, in addition to external viscous damping, we also have internal material damping which is of a helpful nature when n is negative. Thus, the forced response of a retrograde branch is very difficult to observe experimentally [7,11,36].

6. CONCLUSIONS

In this report the system analysis of the spin test facility at Oak Ridge for three different flywheel systems was described. Two linear models, a lumped-parameter model and a combined lumped- and distributed-parameter model, were used for the system analysis. The air-turbine-drive wheel and turbine shaft dynamics were included in the formulation. Free whirling and forced whirling analyses were performed using both of the models. Stability was studied using the lumped-parameter model only. It should be emphasized that all of the solutions were exact and no other approximations than suitable engineering assumptions were used.

Critical Speeds and Mode Shapes: For all the flywheel systems, the critical speeds predicted by the combined model were higher than those from the lumped model. Thus, the effect of the distributed mass, which was neglected in the lumped model, is to increase the apparent stiffness of the system. This effect is pronounced at larger rotational speeds and higher modes of vibration (only the lowest four modes were considered for comparison). The mode shapes from the combined model showed the relative motions of all points on the flexible shaft portions, whereas, in contrast the lumped model predicted only the relative motions of the lumped masses which approximate the actual system.

The simplified analysis of [11], for a pendulously supported flywheel system with two degrees of freedom for the flywheel, was applied to predict the critical speeds of Systems A, B, and C. It was shown that the results of critical speeds from the seven-degree-of-freedom model of this report and those predicted with the model of [11] differed from one another by various amounts. The extent of difference depended on the coupling of flywheel motion with the

rest of the masses in the system. In cases having coupling, the seven-degree-of-freedom model predicted lower critical speeds differing by as much as 46% (for System C) from those arrived at by [11] for the lowest forward critical speed. Thus, the analysis of [11] cannot always be used successfully to predict critical speeds in a spin-test facility.

The effects of flywheel dead weight and applied torque on Ω_{11} (the lowest first-order forward critical speed) for the pendulously supported flywheel were also studied (see Appendix D). It was shown that neglecting flywheel dead weight introduced an error of less than 1% in the calculation of Ω_{11}. Neglecting the drive torque resulted in an error of only about 40 parts in 10^9 in the determination of Ω_{11}.

Stability: It was shown that all retrograde branches are stable under hysteretic material damping of the shaft. For all the three flywheel systems, only the first (lowest) forward branch becomes unstable beyond the lowest first-order critical speed in the presence of internal material damping. With no external viscous damping the instability extends without limit. When external viscous damping is introduced, the instability extends up to a finite upper limit which decreases with increasing external damping. With suitable external viscous damping, this instability could be removed altogether.

Forced Whirling: The forced responses, due to mass eccentricity and initial tilt, predicted by both models are in close agreement. It was noticed that the damper was ineffective in Systems A and B. This is because these systems have the lowest first-order critical speeds less than 2,000 rpm, at which speed the damper movement is negligible. For System C, the lowest first-order critical speed is predicted to occur at a much higher speed, around 14,200 rpm (combined model), where the damper displacement is significant.

Thus, the damper is more effective for this system. It was also observed that responses were larger when the lowest first-order critical speed shifted into higher running-speed regions.

It was found that the best way to predict the effectiveness of the damper is to look at the mode shapes of the system at various critical speeds. The forced responses at the critical speeds which had associated mode shapes with relatively larger damper movements were attenuated effectively by the damper. It also was noted that mass eccentricity, initial tilt, or a combination of them cannot excite retrograde whirling. A retrograde whirling response excited by other means can be expected to be of a milder nature than that of forward whirling. This is explained as follows: In addition to the external viscous damping, the internal material damping participates in absorption of energy input by material stress hysteresis.

Parametric Studies: The effects of various flywheel parameters (m_f, I_{pf}, I_{df}, and t_f) on the lowest first-order forward critical speeds (Ω_{11}) were investigated. Decreasing m_f increased Ω_{11} with $\Omega_{11}\sqrt{m_f}$ remaining constant. When I_{pf} was increased, Ω_{11} increased also, due to the larger gyroscopic action of the flywheel. It was found that Ω_{11} increased with decreasing I_{df} and that increases in t_f made the system softer (Ω_{11} decreased). A four-fold increase in L_1 (the flexible length of the shaft between the flywheel and the damper end nearest it) was observed to cause a drop in critical speed Ω_{11} (72% drop for System A and 74% for System B). However, this increase in length L_1 caused a second critical speed Ω_{21} of first order (in the region of 86,000 rpm for both systems) to occur within 100,000 rpm. A ten-thousand-fold decrease in $K_{s\ell}$ (the lower turbine-bearing spring constant) also brought down Ω_{11}

(a decrease of 58% and 66% for Systems A and B, respectively) and introduced a second critical speed Ω_{21} (in the region of 4,800 rpm for both systems). Unlike the previous cases in the parametric study, a drastic reduction in $K_{s\ell}$ made the damper effective at Ω_{11} but not at Ω_{21}. The critical speed Ω_{21} for this particular case turned out to be a mode related to the intermediate mass, which is connected directly to the lower turbine-bearing spring.

ACKNOWLEDGMENTS

A special acknowledgment is due Christopher A. Kocay, who wrote the original algorithms which formed the basis for many of the computer-generated results presented here. Also, the computing time provided by the University's Merrick Computing Center is appreciated. The authors gratefully acknowledge the assistance of Dr. R.S. Steele, Jr. and E.F. Babelay, Jr. of Union Carbide Corp., Nuclear Division, Oak Ridge, TN, in providing data on the Oak Ridge Flywheel Evaluation Laboratory.

REFERENCES

1. Dann, R.T., "The Revolution in Flywheels," Machine Design, Vol. 45, No. 12, May 17, 1973, pp. 130-135.

2. Lawson, L.J., "Design and Testing of High Energy Density Flywheels for Application to Flywheel/Heat Engine Hybrid Vehicle Drives," Proceedings of the 6th Intersociety Energy Conversion Engineering Conference, 1971, pp. 1142-1150.

3. Kulkarni, S.V., "The Flywheel Rotor and Containment Technology Development Program of the U.S. Department of Energy," Proceedings of the 1980 Flywheel Technology Symposium, Scottsdale, Arizona, Oct. 26-30, 1980; U.S. Department of Energy, Publication CONF-801022 Supplement 1, pp. 5-39.

4. Rankine, W.J.McQ., "Centrifugal Whirling of Shafts," The Engineer (London), Vol. 26, Apr. 8, 1869, p. 249.

5. Stodola, A., Die Dampfturbinen, various editions, Berlin, 1903-1910.

6. Stodola, A., Steam and Gas Turbines, Vol. 2, McGraw-Hill, New York, 1927, pp. 1113-1122.

7. Biezeno, C.B. and Grammel, R., Engineering Dynamics, Vol. III: Steam Turbines, Blackie and Son, Ltd., London, 1954, Section III.

8. Dimentberg, F.M., Flexural Vibrations of Rotating Shafts, Butterworth, London, 1961.

9. Tondl, A., Some Problems of Rotor Dynamics, Chapman and Hall, London, 1965.

10. Loewy, R.G. and Piarulli, V.J., "Dynamics of Rotating Shafts," Shock and Vibration Information Center, Naval Research Laboratory, Washington, DC, Monograph SVM-4, 1969.

11. Thomson, W.T., Younger, F.C. and Gordon, H.S., "Whirl Stability of the Pendulously Supported Flywheel System," ASME Journal of Applied Mechanics, Vol. 44, No. 2, June 1977, pp. 322-328.

12. McKinnon, C.N., Jr., "Rotor Dynamic Analysis," Appendix B of "Evaluation of Selected Drive Components for a Flywheel Powered Commuter Vehicle," LMC Corp., Final Report, Contract EY-76-C-0301164, Phase I, June 30, 1977.

13. Bert, C.W., Chen, T.L.C., and Kocay, C.A., "Critical Speeds and Natural Frequencies of Rim-Type Composite-Material Flywheels," Sandia National Laboratories, Albuquerque, New Mexico, Report SAND 78-7049, Jan. 1979.

14. Rabenhorst, D.W., "Flywheel Testing Laboratory of the Johns Hopkins University Applied Physics Laboratory," APL/JHU Report, Apr. 24, 1979.

15. Steele, R.S., "Oak Ridge Flywheel Evaluation Laboratory," Proceedings of the 1979 Mechanical and Magnetic Energy Storage Contractors' Review Meeting, Washington, DC, Aug. 19-22, 1979; U.S. Department of Energy, Publication Conf-790854, Dec. 1979, pp. 416-421.

16. Miller, A.K., "Recent Spin Tests of Two Composite Wagon Wheel Flywheels," Proceedings of the 1979 Mechanical and Magnetic Energy Storage Contractors' Review Meeting, Washington, DC, Aug. 19-22, 1979; U.S. Department of Energy, Publication Conf-79-0854, Dec. 1979, pp. 348-355.

17. Bert, C.W. and Chen, T.L.C., "Lateral and Tilt Whirl Modes of Flexibly Mounted Flywheel Systems," Sandia National Laboratories, Albuquerque, New Mexico, Report SAND 78-7070, Dec. 1978; also, Shock and Vibration Bulletin 49, Part 2, Sept. 1979, pp. 35-46.

18. Chen, T.L.C. and Bert, C.W., "Whirling Response and Stability of Flexibly Mounted, Ring-Type Flywheel Systems," Sandia National Laboratories, Albuquerque, New Mexico, Report SAND 78-7073, Feb. 1979; also, ASME Journal of Mechanical Design, Vol. 102, No. 2, Apr. 1980, pp. 369-378.

19. Kocay, C.A. and Bert, C.W., "Forced Whirling Response of a Pendulously Supported Flywheel with Nonlinear Oil-Type Damping," Proceedings of the 1980 Flywheel Technology Symposium, Scottsdale, Arizona, Oct. 26-30, 1980; U.S. Department of Energy, Publication CONF-801022, pp. 225-239.

20. Millner, A.R., "A Flywheel Energy Storage and Conversion System for Photovoltaic Applications," Proceedings of the 1979 Mechanical and Magnetic Energy Storage Contractors' Review Meeting, Washington, DC, Aug. 19-22, 1979; U.S. Department of Energy, Publication Conf-790854, Dec. 1979, pp. 320-326.

21. Kocay, C.A., "Rotor Dynamic Analyses of a Pendulously Supported Flywheel with Nonlinearities," Ph.D. dissertation in preparation, University of Oklahoma, 1981.

22. Stodola, A., "New Critical Shaft Speeds as Effects of the Gyroscopic Disc-Action," Engineering, Vol. 106, Dec. 13, 1918, pp. 665-666

23. Hartog, J.P. den, Mechanical Vibrations, 4th ed., McGraw-Hill, New York, 1956, chap. 6.

24. Green, R.B., "Gyroscopic Effects on the Critical Speeds of Flexible Rotors," ASME Journal of Applied Mechanics, Vol. 15, Dec. 1948, pp. 369-376.

25. Chang, K.T., "Turbomachine Dynamics," Wright Air Development Center, WADC TR57-611, Apr. 1958, NTIS Document AD-151087.

26. Black, H.F. "Lateral Vibration of Shafts Having Radial Symmetry and Appreciable Gyro-Action," Journal of Mechanical Engineering Science, Vol. 6, Mar. 1964, pp. 53-63.

27. Kikuchi, K. and Kobayashi, S., "Stability Analysis of a Rotating Shaft System with Many Bearings and Disks," Bulletin of Japan Society of Mechanical Engineers, Vol. 20, Dec. 1977, pp. 1592-1600.

28. Finkelstein, A.R., "Myklestad's Method for Predicting Whirl Velocity as a Function of Rotational Velocity for Flexible Multimass Rotor Systems," ASME Journal of Applied Mechanics, Vol. 32, Sept. 1965, pp. 589-591.

29. Carnegie, W., "Rotary Inertia and Gyroscopic Effects in Overhung Shaft Systems," Bulletin of Mechanical Engineering Education, New Series, Vol. 3, 1964, pp. 191-199.

30. Aiba, S., "The Effects of Gyroscopic Moment and Distributed Mass on the Vibration of a Rotating Shaft with a Rotor," Bulletin of Japan Society of Mechanical Engineers, Vol. 16, Oct. 1973, pp. 1550-1561.

31. Huang, T.C. and Huang, F.C.C., "On Precession and Critical Speeds of Two-Bearing Machines with Overhung Weight," ASME Journal of Engineering for Industry, Vol. 89, Nov. 1967, pp. 713-719.

32. Dubigeon, S. and Michon, J.C., "Gyroscopic Behavior of Stressed Rotating Shafts," Journal of Sound and Vibration, Vol. 42, Oct. 8, 1975, pp. 281-293.

33. Joshi, B.B. and Dange, Y.K., "Critical Speeds of a Flexible Rotor with Combined Distributed Parameter and Lumped Mass Technique," Journal of Sound and Vibration, Vol. 45, April 18, 1976, pp. 441-449.

34. Satchwell, D.L. and Towgood, D.A., "High-Energy-Density Composite Flywheel," Sandia National Laboratories, Albuquerque, New Mexico, Report SAND 79-7019, Feb. 1980.

35. Campbell, W., "The Protection of Steam-Turbine Disk Wheels from Axial Vibration," Transactions of ASME, Vol. 46, 1924, pp. 31-160.

36. Schulte, C.A. and Riester, R.A., "Effects of Mass Distribution on Critical Speeds," Proceedings of the 2nd U.S. National Congress of Applied Mechanics, 1954, ASME, 1955, pp. 101-110.

37. Iwatsubo, T., Kanki, H., and Kawai, R., "Vibration of Asymmetric Rotor Through Critical Speed with Limited Power Supply," Journal of Mechanical Engineering Science, Vol. 14, No. 3, June 1972, pp. 184-194.

38. Bishop, R.E.D. and Parkinson, A.G., "Second Order Vibration of Flexible Shafts," Philosophical Trans., Royal Society, London, Ser. A, Vol. 259, Dec. 9, 1969, pp. 1-31.

39. Timoshenko, S. and Young, D.H., Vibration Problems in Engineering, 3rd ed., Van Nostrand, Princeton, NJ, 1955.

40. Newkirk, B.L., "Shaft Whipping," General Electric Review, Vol. 27, 1924, pp. 169-178.

41. Kimball, A.L., "Internal Friction Theory of Shaft Whirling," General Electric Review, Vol. 27, No. 4, Apr. 1924, pp. 244-251.

42. Iwatsubo, T., "Stability Problems on Rotor Systems," Shock and Vibration Digest, Vol. 11, No. 3, Mar. 1979, pp. 17-26.

43. Iwatsubo, T., "Stability Problems of Rotor Systems," Shock and Vibration Digest, Vol. 12, No. 7, July 1980, pp. 3-8.

44. Nimmer, R.P., "Laminated Flywheel Disc with Filament Wound Outer Ring," Proceedings of the 1979 Mechanical and Magnetic Energy Storage Contractors' Review Meeting, Washington, DC, Aug. 19-22, 1979; U.S. Department of Energy, Publication Conf-790854, Dec. 1979, pp. 399-406.

45. Kulkarni, S.V., "Composite-Laminate Flywheel-Rotor Development Program," Proceedings of the 1979 Mechanical and Magnetic Energy Storage Contractors' Review Meeting, Washington, DC, Aug. 19-22, 1979; U.S. Department of Energy, Publication Conf-790854, Dec. 1979, pp. 387-398.

46. Hickey, J.S., "Influence of Bearing Stiffness on Flywheel-Rotor System," Proceedings of the 1977 Flywheel Technology Symposium, San Francisco, CA, Oct. 5-7, 1977, U.S. Department of Energy, CONF-771053, Mar. 1978, pp. 435-439.

47. Pepper, J.W., "Investigation of Multi-Ring Fiber-Composite Flywheels for Energy Storage," Wm. M. Brobeck Associates, Berkeley, CA, Report EPRI EM-227 to Electric Power Research Institute, Palo Alto, CA, Sept. 1976.

48. Kung, W., "The Higher Mode Critical Speeds of Shaft Subjected to Axial Force and Torque," ASME Journal of Applied Mechanics, Vol. 42, No. 3, Sept. 1975, pp. 741-743.

49. Ziegler, H., "On the Concept of Elastic Stability," Advances in Applied Mechanics, Vol. IV, Academic Press, New York, NY, 1956, pp. 351-403.

50. Kirk, R.G. and Gunter, E.J., "Transient Response of Rotor-Bearing Systems," ASME Journal of Engineering for Industry, Vol. 96B, No. 2, May 1974, pp. 682-693.

51. Hubbard, M. and McDonald, P., "Feedback Control Systems for Flywheel Radial Instabilities," Proceedings of the 1980 Flywheel Technology Symposium, Scottsdale, Arizona, Oct. 26-30, 1980; U.S. Department of Energy, Publication CONF-801022, pp. 209-217.

52. Burrows, C.R. and Sayed-Esfahani, R., "A Comparison of Multifrequency Techniques for Measuring the Dynamics of Squeeze-Film Bearings," ASME Journal of Lubrication Technology, Vol. 103, No. 1, Jan. 1981, pp. 137-143.

APPENDIX A - DETAILED DERIVATIONS FOR LUMPED-PARAMETER MODEL

A.1 Derivation of Compliance Coefficients

The Oak Ridge National Laboratory's flywheel system is modeled as shown in Fig. 2.1. The lumped masses are shown in cross-hatched lines. The dimensions that have been used in the derivation are marked in Fig. 2.1. A positive system of generalized forces is presented in Fig. 2.2(a). The bearings are represented as springs. All eight degrees of freedom $(r_f, \phi_f, r_d, \phi_d, r_i, \phi_i, r_t, \phi_t)^T$ are assumed to be present in the following derivation. From statics,

$$R_1 = F_t\left(1 + \frac{t_t}{a_4}\right) + F_i\left(1 - \frac{a_1}{a_4}\right) + F_d\left(1 - \frac{a_2}{a_4}\right) + F_f\left(1 - \frac{a_3}{a_4}\right) - \frac{M_t + M_i + M_d + M_f}{a_4} \tag{A-1}$$

$$R_2 = -F_t\frac{t_t}{a_4} + F_i\frac{a_1}{a_4} + F_d\frac{a_2}{a_4} + F_f\frac{a_3}{a_4} + \frac{M_t + M_i + M_d + M_f}{a_4}$$

where

$$a_1 = \ell_3 + t_3$$

$$a_2 = \ell_b + t_d$$

$$a_3 = \ell_g + t_f$$

$$a_4 = \ell_3 + t_s$$

A positive system of shear forces and bending moments is shown in Fig. 2.2(b). The shear-force and bending-moment variations in the shaft (flexible) portions, from statics, are

$$V(z) = \begin{cases} F_t \dfrac{t_t}{a_4} + F_i(1 - \dfrac{a_1}{a_4}) + F_d(1 - \dfrac{a_2}{a_4}) + F_f(1 - \dfrac{a_3}{a_4}) - \dfrac{(M_t + M_i + M_d + M_f)}{a_4} & 0 \le z \le \ell_3 \\ F_d + F_f & \ell_a \le z \le \ell_b \\ F_f & \ell_c \le z \le \ell_g \end{cases} \tag{A-2}$$

$$M(z) = \begin{cases} F_t t_t(1 - \dfrac{z}{a_4}) - F_i z(1 - \dfrac{a_1}{a_4}) - F_d z(1 - \dfrac{a_2}{a_4}) - F_f z(1 - \dfrac{a_3}{a_4}) \\ \qquad + \dfrac{(M_i + M_d + M_f)}{a_4} z - M_t(1 - \dfrac{z}{a_4}) & 0 \le z \le \ell_3 \\ M_d + M_f + F_d(a_2 - z) + F_f(a_3 - z) & \ell_a \le z \le \ell_b \\ M_f + F_f(a_3 - z) & \ell_c \le z \le \ell_g \end{cases} \tag{A-3}$$

The total potential energy U of the system, including the energy in the springs, is given as follows:

$$U = \int_0^{\ell_3} \left(\frac{[M(z)]^2}{2EI_3} + \frac{[V(z)]^2}{2K_3A_3G}\right)dz + \int_{\ell_a}^{\ell_b} \left(\frac{[M(z)]^2}{2EI_2} + \frac{[V(z)]^2}{2K_2A_2G}\right)dz + \int_{\ell_c}^{\ell_g} \left(\frac{[M(z)]^2}{2EI_1} + \frac{[V(z)]^2}{2K_1A_1G}\right)dz + \frac{1}{2}\left[\frac{R_1^2}{K_{su}} + \frac{R_2^2}{K_{s\ell}}\right] \tag{A-4}$$

where K_{su} and $K_{s\ell}$ are the upper and lower bearing spring constants. By Castigliano's least work theorem

$$r_j = \frac{\partial U}{\partial F_j} \qquad \text{where } j = f,d,i,t \tag{A-5}$$

$$\phi_j = \frac{\partial U}{\partial M_j}$$

For example,

$$r_f = \frac{\partial U}{\partial F_f} = \alpha_{11}F_f + \alpha_{12}M_f + \alpha_{13}F_d + \alpha_{14}M_d + \alpha_{15}F_i + \alpha_{16}M_i + \alpha_{17}F_t + \alpha_{18}M_t \tag{A-6}$$

etc. Therefore, using equations (A-1) - (A-5), we derive the following compliances:

$$\alpha_{11} = \overline{AA}\left(1 - \frac{a_3}{a_4}\right)^2 + \left(\frac{\ell_b - \ell_a}{K_2A_2G}\right) + \frac{a_3}{EI_2}\left\{(\ell_b - \ell_a)(a_3 - \ell_b - \ell_a) + \frac{\ell_b^3 - \ell_a^3}{3}\right\}$$
$$+ \left(\frac{\ell_g - \ell_c}{K_1A_1G}\right) + \frac{a_3}{EI_1}\left\{(\ell_g - \ell_c)(a_3 - \ell_g - \ell_c) + \frac{\ell_g^3 - \ell_c^3}{3}\right\}$$
$$+ \frac{1}{K_{su}}\left(1 - \frac{a_3}{a_4}\right)^2 + \frac{1}{K_{s\ell}}\left(\frac{a_3}{a_4}\right)^2$$

$$\alpha_{12} = -\frac{1}{a_4}\left(1 - \frac{a_3}{a_4}\right)\overline{AA} + \frac{\ell_b - \ell_a}{EI_2}\left(a_3 - \frac{\ell_b + \ell_a}{2}\right) + \frac{\ell_g - \ell_c}{EI_1}\left(a_3 - \frac{\ell_g + \ell_c}{2}\right)$$
$$- \frac{1}{K_{su}a_4}\left(1 - \frac{a_3}{a_4}\right) + \frac{1}{K_{s\ell}}\frac{a_3}{a_4^2}$$

$$\alpha_{13} = \left(1 - \frac{a_3}{a_4}\right)\left(1 - \frac{a_2}{a_4}\right)\overline{AA} + \frac{\ell_b - \ell_a}{K_2A_2G} + \frac{1}{EI_2}\left\{a_2a_3(\ell_b - \ell_a) - \left(\frac{\ell_b^2 - \ell_a^2}{2}\right)(a_2 + a_3)\right.$$
$$\left. + \frac{\ell_b^3 - \ell_a^3}{3}\right\} + \frac{1}{K_{su}}\left(1 - \frac{a_2}{a_4}\right)\left(1 - \frac{a_3}{a_4}\right) + \frac{1}{K_{s\ell}}\frac{a_2a_3}{a_4^2}$$

$$\alpha_{14} = -\frac{1}{a_4}\left(1 - \frac{a_3}{a_4}\right)\overline{AA} + \frac{(\ell_b - \ell_a)}{EI_2}\left(a_3 - \frac{\ell_b + \ell_a}{2}\right) - \frac{1}{K_{su}a_4}\left(1 - \frac{a_3}{a_4}\right) + \frac{1}{K_{s\ell}}\frac{a_3}{a_4^2}$$

$$\alpha_{15} = \left(1 - \frac{a_3}{a_4}\right)\left(1 - \frac{a_1}{a_4}\right)\overline{AA} + \frac{1}{K_{su}}\left(1 - \frac{a_1}{a_4}\right)\left(1 - \frac{a_3}{a_4}\right) + \frac{1}{K_{s\ell}}\frac{a_1a_3}{a_4^2}$$

$$\alpha_{16} = -\frac{1}{a_4}\left(1 - \frac{a_3}{a_4}\right)\overline{AA} - \frac{1}{K_{su}}\left(1 - \frac{a_3}{a_4}\right) + \frac{1}{K_{s\ell}}\frac{a_3}{a_4^2}$$

$$\alpha_{17} = \frac{t_t}{a_4}\left(1-\frac{a_3}{a_4}\right)\overline{AA} - \frac{t_t}{EI_3}\left(1-\frac{a_3}{a_4}\right)\frac{\ell_3^2}{2} + \frac{1}{K_{su}}\left(1+\frac{t_t}{a_4}\right)\left(1-\frac{a_3}{a_4}\right) - \frac{1}{K_{s\ell}}\frac{t_t a_3}{a_4^2}$$

$$\alpha_{18} = -\frac{1}{a_4}\left(1-\frac{a_3}{a_4}\right)\overline{AA} + \frac{1}{EI_3}\left(1-\frac{a_3}{a_4}\right)\frac{\ell_3^2}{2} - \frac{1}{K_{su}a_4}\left(1-\frac{a_3}{a_4}\right) + \frac{1}{K_{s\ell}}\frac{a_3}{a_4^2}$$

$$\alpha_{22} = \frac{1}{a_4^2}\overline{AA} + \frac{\ell_b-\ell_a}{EI_2} + \frac{\ell_g-\ell_c}{EI_1} + \frac{1}{K_{su}a_4^2} + \frac{1}{K_{s\ell}a_4^2}$$

$$\alpha_{23} = -\frac{1}{a_4}\left(1-\frac{a_2}{a_4}\right)\overline{AA} + \frac{(\ell_b-\ell_a)}{EI_2}\left(a_2-\frac{\ell_b+\ell_a}{2}\right) - \frac{1}{K_{su}a_4}\left(1-\frac{a_2}{a_4}\right) + \frac{1}{K_{s\ell}}\frac{a_2}{a_4^2}$$

$$\alpha_{24} = \frac{1}{a_4^2}\overline{AA} + \frac{\ell_b-\ell_a}{EI_2} + \frac{1}{K_{su}a_4^2} + \frac{1}{K_{s\ell}a_4^2}$$

$$\alpha_{25} = -\frac{1}{a_4}\left(1-\frac{a_1}{a_4}\right)\overline{AA} - \frac{1}{K_{su}a_4}\left(1-\frac{a_1}{a_4}\right) + \frac{1}{K_{s\ell}}\frac{a_1}{a_4^2}$$

$$\alpha_{26} = \frac{1}{a_4^2}\overline{AA} + \frac{1}{K_{su}a_4^2} + \frac{1}{K_{s\ell}a_4^2}$$

$$\alpha_{27} = -\frac{t_t}{a_4^2}\overline{AA} + \frac{t_t}{a_4EI_3}\frac{\ell_3^2}{2} - \frac{1}{K_{su}a_4}\left(1+\frac{t_t}{a_4}\right) - \frac{1}{K_{s\ell}}\frac{t_t}{a_4^2}$$

$$\alpha_{28} = \frac{1}{a_4^2}\overline{AA} - \frac{1}{a_4EI_3}\frac{\ell_3^2}{2} + \frac{1}{K_{su}a_4^2} + \frac{1}{K_{s\ell}a_4^2}$$

$$\alpha_{33} = \left(1-\frac{a_2}{a_4}\right)^2\overline{AA} + \frac{\ell_b-\ell_a}{K_2A_2G} + \frac{a_2(\ell_b-\ell_a)}{EI_2}\left(a_2-\ell_b-\ell_a+\frac{\ell_b^3-\ell_a^3}{3}\right)$$

$$+ \frac{1}{K_{su}}\left(1-\frac{a_2}{a_4}\right)^2 + \frac{1}{K_2}\left(\frac{a_2}{a_4}\right)^2$$

$$\alpha_{34} = \alpha_{23}$$

$$\alpha_{35} = (1 - \frac{a_2}{a_4})(1 - \frac{a_1}{a_4})\ \overline{AA} + \frac{1}{K_{su}}\ (1 - \frac{a_2}{a_4})(1 - \frac{a_1}{a_4}) + \frac{1}{K_{s\ell}}\ \frac{a_1 a_2}{a_4^2}$$

$$\alpha_{36} = -\ \frac{1}{a_4}\ (1 - \frac{a_2}{a_4})\ \overline{AA} - \frac{1}{K_{su} a_4}\ (1 - \frac{a_2}{a_4}) + \frac{1}{K_{s\ell}}\ \frac{a_2}{a_4^2}$$

$$\alpha_{37} = \frac{t_t}{a_4}\ (1 - \frac{a_2}{a_4})\ \overline{AA} - \frac{t_t}{EI_3}\ (1 - \frac{a_2}{a_4})\ \frac{\ell_3^2}{2} + \frac{1}{K_{su}}\ (1 - \frac{a_2}{a_4})(1 + \frac{t_t}{a_4}) - \frac{1}{K_{s\ell}}\ \frac{t_t a_2}{a_4^2}$$

$$\alpha_{38} = -\ \frac{1}{a_4}\ (1 - \frac{a_2}{a_4})\ \overline{AA} + \frac{1}{EI_3}\ (1 - \frac{a_2}{a_4})\ \frac{\ell_3^2}{2} - \frac{1}{K_{su} a_4}\ (1 - \frac{a_2}{a_4}) + \frac{1}{K_{s\ell}}\ \frac{a_2}{a_4^2}$$

$$\alpha_{44} = \frac{1}{a_4^2}\ \overline{AA} + \frac{\ell_b - \ell_a}{EI_2} + \frac{1}{K_{su} a_4^2} + \frac{1}{K_{s\ell} a_4^2}$$

$$\alpha_{45} = \alpha_{25}$$

$$\alpha_{46} = \alpha_{26}$$

$$\alpha_{47} = \alpha_{27}$$

$$\alpha_{48} = \alpha_{28}$$

$$\alpha_{55} = (1 - \frac{a_1}{a_4})^2\ \overline{AA} + \frac{1}{K_{su}}\ (1 - \frac{a_1}{a_4})^2 + \frac{1}{K_{s\ell}}\ (\frac{a_1}{a_4})^2$$

$$\alpha_{56} = -\ \frac{1}{a_4}\ (1 - \frac{a_1}{a_4})\ \overline{AA} - \frac{1}{K_{su} a_4}\ (1 - \frac{a_1}{a_4}) + \frac{1}{K_{s\ell}}\ \frac{a_1}{a_4^2}$$

$$\alpha_{57} = \frac{t_t}{a_4}\ (1 - \frac{a_1}{a_4})\ \overline{AA} - \frac{t_t}{EI_3}\ (1 - \frac{a_1}{a_4})\ \frac{\ell_3^2}{2} + \frac{1}{K_{su}}\ (1 - \frac{a_1}{a_4})(1 + \frac{t_t}{a_4}) - \frac{1}{K_{s\ell}}\ \frac{t_t a_1}{a_4^2}$$

$$\alpha_{58} = -\ \frac{1}{a_4}\ (1 - \frac{a_1}{a_4})\ \overline{AA} + \frac{1}{EI_3}\ (1 - \frac{a_1}{a_4})\ \frac{\ell_3^2}{2} - \frac{1}{K_{su} a_4}\ (1 - \frac{a_1}{a_4}) + \frac{1}{K_{s\ell}}\ \frac{a_1}{a_4^2}$$

$$\alpha_{66} = \alpha_{26}$$

$$\alpha_{67} = \alpha_{27}$$

$$\alpha_{68} = \alpha_{28}$$

$$\alpha_{77} = -\frac{t_t^2}{a_4^2}\overline{AA} + \frac{t_t^2 \ell_3}{EI_3}\left(1 - \frac{\ell_3}{a_4}\right) + \frac{1}{K_{su}}\left(1 + \frac{t_t}{a_4}\right)^2 + \frac{1}{K_{s\ell}}\left(\frac{t_t}{a_4}\right)^2$$

$$\alpha_{78} = -\frac{t_t}{a_4^2}\overline{AA} + \frac{t_t \ell_3}{EI_3}\left(\frac{\ell_3}{a_4} - 1\right) - \frac{1}{K_{su} a_4}\left(1 + \frac{t_t}{a_4}\right) - \frac{1}{K_{s\ell}}\frac{t_t}{a_4^2}$$

$$\alpha_{88} = \frac{1}{a_4^2}\overline{AA} + \frac{\ell_3}{EI_3}\left(1 - \frac{\ell_3}{a_4}\right) + \frac{1}{K_{su} a_4^2} + \frac{1}{K_{s\ell} a_4^2} \qquad \text{(A-7)}$$

where

$$\overline{AA} = \left(\frac{\ell_3}{K_3 A_3 G} + \frac{\ell_3^3}{3EI_3}\right)$$

Further, the compliance matrix is symmetric.

A.2 Derivation of an Equivalent Shaft for the Stepped Turbine Shaft

The forces and moment acting on the turbine and its shaft are as shown in Fig. A1. The turbine shaft is assumed to be pinned at the locations marked by x. From statics,

$$R_1 = \frac{F_o(t_t + \ell_3) - M_o}{\ell_3}$$

$$V(z) = (M_o - F_o\, t_t)/\ell_3 \qquad \text{(A-8)}$$

$$M(z) = (M_o - F_o\, t_t)\left(1 - \frac{z}{\ell_3}\right)$$

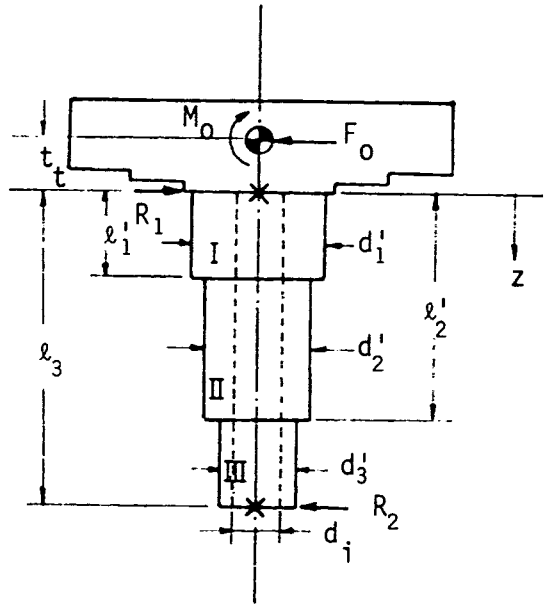

Fig. A1. Dimensioned stepped turbine shaft for which an equivalent shaft with a uniform outside diameter is determined (see Fig. B1(b)).

The strain energy U^* is given by

$$U^* = \int_0^{\ell_3} \left[\frac{M^2(z)}{2EI(z)} + \frac{V^2(z)}{2K(z)A(z)G}\right]dz \tag{A-9}$$

Let r_o denote the deflection of turbine center of mass; then

$$r_o = \frac{\partial U^*}{\partial F_o} = \int_0^{\ell_3} \left[\frac{M(z)\,\frac{\partial M}{\partial F_o}}{EI(z)} + \frac{V(z)\,\frac{\partial V}{\partial F_o}}{K(z)A(z)G}\right]dz \tag{A-10}$$

Substituting equations (A-8) into equation (A-10) and carrying the integrations over the three shaft portions I, II, and III, one obtains

$$r_o = \alpha_{11}' F_o + \alpha_{12}' M_o \tag{A-11}$$

where

$$\alpha'_{11} = t_t^2[(\frac{\ell_3}{3EI'_3} + \frac{1}{K'_3A'_3G\ell_3}) + \{\ell'_1 + \frac{(\ell'_1)^3}{3\ell_3^2} - \frac{(\ell'_1)^2}{\ell_3}\}(\frac{1}{EI'_1} - \frac{1}{EI'_2})$$

$$+ \frac{\ell'_1}{G\ell_3^2}(\frac{1}{A'_1K'_1} - \frac{1}{A'_2K'_2}) + \{\ell'_2 + \frac{(\ell'_2)^3}{3\ell_3^2} - \frac{(\ell'_2)^2}{\ell_3}\}(\frac{1}{EI'_2} - \frac{1}{EI'_3})$$

$$+ \frac{\ell'_2}{G\ell_3^2}(\frac{1}{A'_2K'_2} - \frac{1}{A'_3K'_3})] = t_t^2\,\theta$$

$$\alpha'_{12} = -\,t_t\,\theta \tag{A-12}$$

Let $\bar{\phi}_o$ be the rotation of the turbine wheel. Then,

$$\bar{\phi}_o = \frac{\partial U^*}{\partial M_o} = \int_0^{\ell_3} [\frac{M(z)\,\frac{\partial M}{\partial M_o}}{EI(z)} + \frac{V(z)\,\frac{\partial V}{\partial M_o}}{K(z)A(z)G}]dz \tag{A-13}$$

Using equations (A-8), one obtains

$$\bar{\phi}_o = \alpha'_{12}F_o + \alpha'_{22}M_o \tag{A-14}$$

where $\alpha'_{22} = \theta$.

The equivalent uniform shaft is defined so that the same generalized displacements are produced by the same force and moment system as in the actual shaft. Let A_3, I_3, and K_3 be the cross-sectional area, area moment of inertia of the cross section, and shear factor, respectively, of the equivalent uniform shaft. Then

$$r_o = \alpha^*_{11}F_o + \alpha^*_{12}M_o \quad ; \quad \bar{\phi}_o = \alpha^*_{12}F_o + \alpha^*_{22}M_o \tag{A-15}$$

where

$$\alpha^*_{11} = t_t^2[\frac{\ell_3}{3EI_3} + \frac{1}{K_3A_3G\ell_3}] = t_t^2\,\theta^* \quad ; \quad \alpha^*_{12} = -\,t_t\,\theta^* \quad ; \quad \alpha^*_{22} = \theta^* \tag{A-16}$$

Hence,

$$\theta^* = \theta \tag{A-17}$$

From scaled drawing, the dimensions d_1', d_2', d_3', ℓ_1', ℓ_2', and ℓ_3' (Fig. A1) were determined. The shear factors were determined for each stepped-shaft portion from the following formula

$$K = \frac{6(1+\nu)(1+m^2)^2}{(7+6\nu)(1+m^2)^2 + (20+12\nu)m^2} \tag{A-18}$$

where ν is the Poisson's ratio for the material and m is the ratio of the inner diameter to outer diameter.

From calculations,

$$\theta = 1.9146 \times 10^{-6} \text{ radians/in-lb}$$

Assuming that the inner diameter d_i is the same for the equivalent shaft and that

$$I_3 = (\pi/64)(d_o^4 - d_i^4) \quad ; \quad A_3 = (\pi/4)(d_o^2 - d_i^2)$$

$$K_3 = \frac{6(1+\nu)(1+\bar{m}^2)^2}{(7+6\nu)(1+\bar{m}^2)^2 + (20+12\nu)\bar{m}^2}$$

where d_o is the outer diameter of the equivalent shaft and $\bar{m} = d_i/d_o$, we arrive at the following equation, which is derived from equation (A-17)

$$\left[\frac{52.7657}{(\bar{m}^4 - 1)} + \frac{0.4712}{(\bar{m}^4 - 1)(\bar{m}^2 + 1)}\{1.1299(1+\bar{m}^2)^2 + 3.0396\,\bar{m}^2\}\right] = 1.9146$$

By trial and error, $\bar{m} = 2.3599$. Since $d_i = 0.3175$ in., $d_o = 0.7493$ in.

A.3 Summary of Data Used in Lumped-Parameter Model

Table A-1. Data Used for Lumped-Parameter Model of the Oak Ridge System (see Fig. 2.1)

Lengths ℓ_a	2.978 in.
ℓ_b	3.658 in.
ℓ_c	7.324 in.
ℓ_g	8.070 in.
ℓ_3	2.127 in.
L_{ac} (see Fig. B1)	3.597 in.
t_t	0.894 in.
t_3	0.435 in.
t_s	0.243 in.
t_d	1.833 in.
t_f: System A 7.05 in.; System B 3.45 in.; System C 3.15 in.	
a_1	2.562 in.
a_2	5.491 in.
a_3	15.120 in.
a_4	2.37 in.
Diameter of shaft 1	0.3125 in.
Diameter of shaft 2	0.3125 in.
Equivalent uniform outer diameter of turbine shaft (d_o)	0.7493 in.
Inner diameter of turbine shaft (d_i)	0.3175 in.
Young's modulus of shaft material (E)	29.5×10^6 psi
Shear modulus of shaft material (G)	11.5×10^6 psi
Specific weight of shaft material	0.283 lb/in.^{3}
Loss tangent of shaft material (γ_s)	0.005
Shear correction factor for shaft 1 (K_1) and shaft 2 (K_2)	0.885
Shear correction factor for the equivalent turbine shaft (K_t)	0.657

Table A-1 (Cont'd)

Shear correction factor for the equivalent quill shaft within the turbine shaft (K_{eq})	0.885
Mass of turbine wheel (m_t)	0.00479 lb-s^2/in.
Diametral mass moment of inertia of turbine wheel (I_{dt})	0.00340 lb-in-s^2
Polar mass moment of inertia of turbine wheel (I_{pt})	0.00628 lb-in-s^2
Mass of intermediate mass (m_i)	0.000202 lb-s^2/in.
Diametral mass moment of inertia of intermediate mass (I_{di})	1.798×10^{-5} lb-in-s^2
Polar mass moment of inertia of intermediate mass (I_{pi})	1.15×10^{-5} lb-in-s^2
Mass of damper (m_d)	0.00300 lb-s^2/in.
Mass of flywheel (m_f):	
System A	0.0951 lb-s^2/in.
System B	0.0576 lb-s^2/in.
System C	0.0336 lb-s^2/in.
Diametral mass moment of inertia of flywheel (I_{df}):	
System A	4.83 lb-in-s^2
System B	1.648 lb-in-s^2
System C	0.823 lb-in-s^2
Polar mass moment of inertia of flywheel (I_{pf}):	
System A	8.517 lb-in-s^2
System B	2.036 lb-in-s^2
System C	1.645 lb-in-s^2
Upper and lower bearing spring constants* (K_{su}, $K_{s\ell}$)	2×10^6 lb/in. each
External viscous damping coefficient (C_d), values used	0,1,5, and 10 lb-s/in.

*Since the experimental values of the ball-bearing stiffnesses were not available, they were assumed, based on [46].

APPENDIX B - DERIVATIONS RELATED TO THE COMBINED MODEL

B.1 Turbine and Flywheel Shaft Modeling

The experimental set-up is simplified to the system shown in Fig. 3.1. Note that there are three shaft portions between discontinuities. The cross-hatched portions are assumed to be rigid masses. The damper is assumed not to tilt because of constructional details and narrow clearances. Also, notice that the turbine shaft end is clamped over a portion of the flywheel shaft. Furthermore, the actual turbine-flywheel shaft connection, Fig. B1(a), has been modified, Fig. B1(b), by suitable transformation of flywheel shaft dimensions within the turbine shaft. It is assumed that the transformed flywheel shaft within the turbine shaft and the turbine shaft itself act as some equivalent single shaft. This transformation reduces the number of shaft portions from four to three, thereby saving computational time and any appreciable error from this modification is assumed to enter only at very high rotational speeds.

B.2 Governing Differential Equation for a Whirling Shaft and the Solution Form

In the analysis, forces, moments, displacements and small rotations are positive if they point along the positive coordinate axis when treated as vectors.

Consider a shaft element of length 'dz' as shown in Fig. B2. Here, $x_o y_o z_o$ is an inertial reference frame, and xyz is a reference frame attached to the shaft center such that it tilts with the shaft as it deflects (as shown) but does not change its orientation as the shaft rotates.

The projections of the shaft element on $x_o z_o$ and $y_o z_o$ planes with forces and moments acting on it are shown in Figs. B3 and B4.

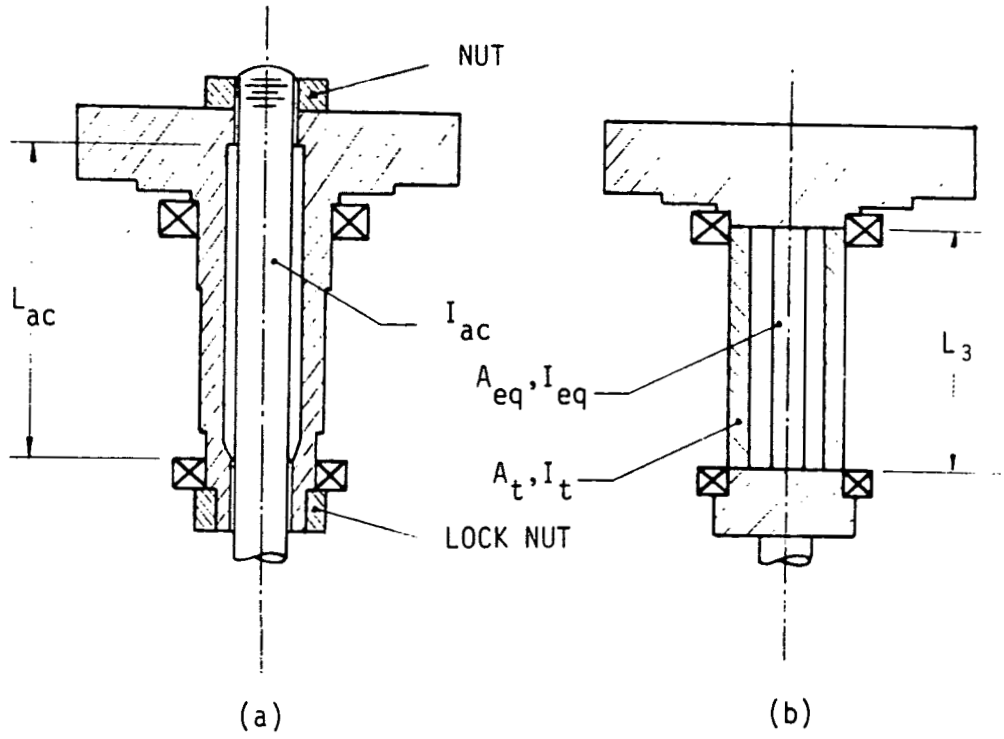

Fig. B1. Modeling of turbine wheel, turbine shaft, and flywheel shaft within the turbine shaft: (a) actual system (b) assumed model. See Appendix A.2 for derivation of the outer diameter of an equivalent shaft for the stepped turbine shaft. To determine the equivalent flywheel shaft (which is inside the turbine shaft) diameter the relation $EI_{ac}/L_{ac}^4 = EI_{eq}/L_3^4$ is used.

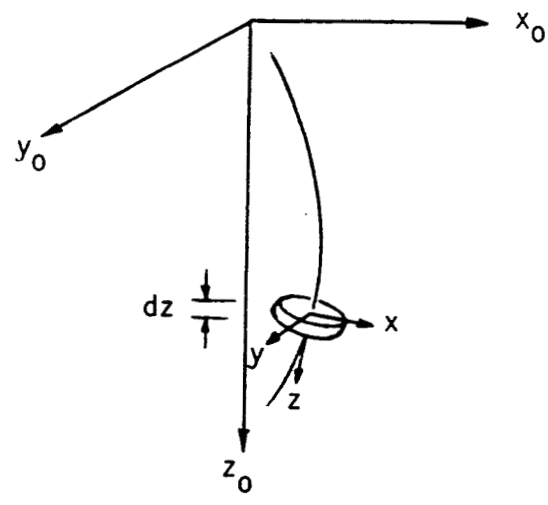

Fig. B2. A typical whirling shaft element.

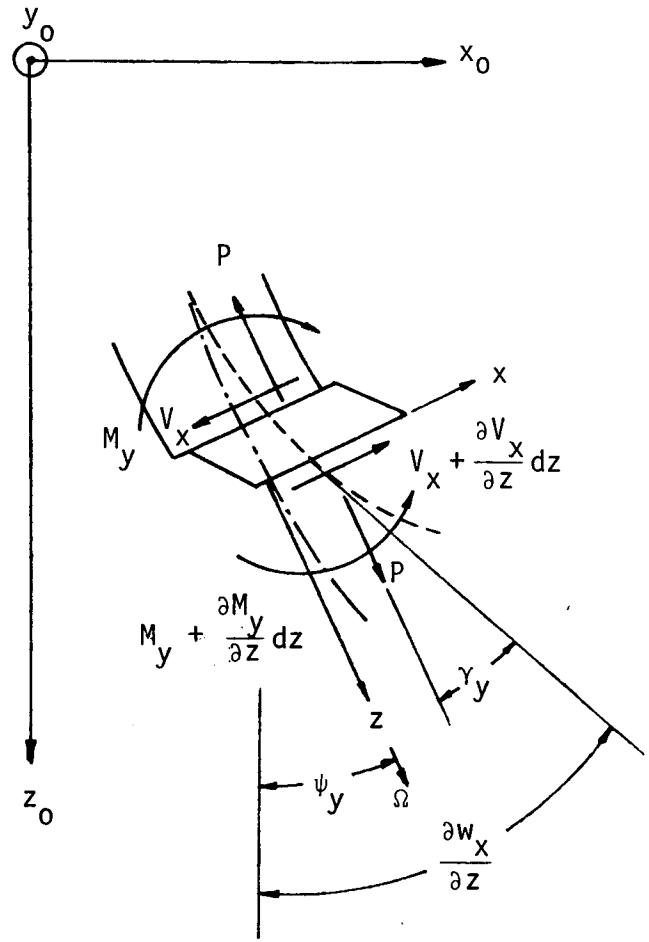

------ slope of shaft center line with shear deformation

—·—·— slope with bending only (shear deformation neglected)

Fig. B3. Projection onto the $x_o z_o$ plane of a deformed shaft element with its system of generalized forces.

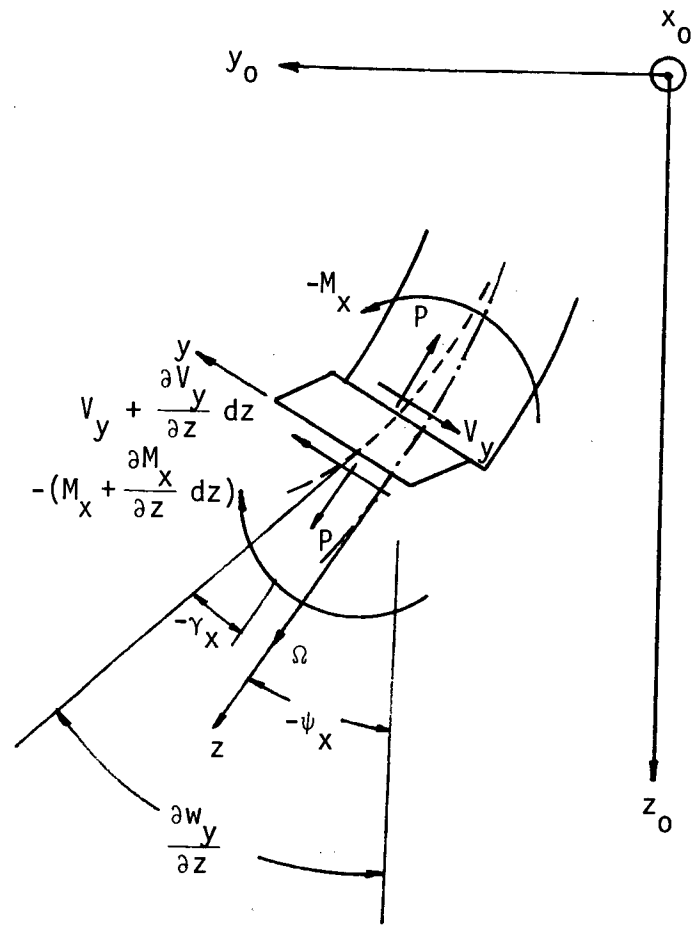

------ slope of shaft center line with shear deformation

—·—·— slope with bending only (shear deformation neglected)

Fig. B4. Projection onto the $y_o z_o$ plane of a deformed shaft element with its system of generalized forces.

In Fig. B4, γ_x and ψ_x are marked negative, since when they are measured from the positive z_o axis, they point in the negative x_o direction. Further, the moments are shown negative since this system of moments causes negative rotation of the shaft elements.

The constitutive relations between bending moments and bending slopes are as follows:

$$M_x = EI \frac{\partial \psi_x}{\partial z} \quad , \quad M_y = EI \frac{\partial \psi_y}{\partial z} \tag{B-1}$$

Let

$$\psi = \psi_y - i\psi_x \quad , \quad M = M_y - iM_x \tag{B-2}$$

Hence,

$$M = EI \frac{\partial \psi}{\partial z} \tag{B-3}$$

Further,

$$\frac{\partial w_x}{\partial z} = \psi_y + \gamma_y \quad , \quad \frac{\partial w_y}{\partial z} = - \psi_x - \gamma_x \tag{B-4}$$

If

$$w = w_x + iw_y \quad , \quad \gamma = \gamma_y - i\gamma_x \tag{B-5}$$

Then,

$$\frac{\partial w}{\partial z} = \psi + \gamma \tag{B-6}$$

Shear force V and shear strain γ are related by

$$V = K\hat{A}G\gamma \tag{B-7}$$

where

$$V = V_x + iV_y \tag{B-8}$$

Writing the force equation for the element, we obtain:

$$\frac{\partial V_y}{\partial z} dz = \rho \hat{A}\, dz \frac{\partial^2 w_y}{\partial t^2} \tag{B-9}$$

$$\frac{\partial V_x}{\partial z} dz = \rho \hat{A}\, dz \frac{\partial^2 w_x}{\partial t^2} \tag{B-10}$$

Note that all forces in the section are resolved into components parallel and perpendicular to the face of the element. In view of equation (B-8), equations (B-9) and (B-10) can be combined to give

$$\frac{\partial V}{\partial z} = \rho \hat{A} \frac{\partial^2 w}{\partial t^2} \tag{B-11}$$

Considering the rotational equation of motion of the element about the y and x axes respectively, we have the following equations of motion:

$$\begin{aligned} \frac{\partial M_y}{\partial z} dz + V_x\, dz &= \frac{\partial}{\partial t} \left(I_d \frac{\partial \psi_y}{\partial t} - I_p \Omega\, \psi_x\right) \\ \frac{\partial M_x}{\partial z} dz - V_y\, dz &= \frac{\partial}{\partial t} \left(I_d \frac{\partial \psi_x}{\partial t} + I_p \Omega\, \psi_y\right) \end{aligned} \tag{B-12}$$

Since

$$I_d = \frac{\rho \hat{A} dz (R_o^2 + R_i^2)}{4} \quad , \quad I_p = \frac{\rho \hat{A} dz (R_o^2 + R_i^2)}{2} \tag{B-13}$$

we get

$$\begin{aligned} \frac{\partial M_y}{\partial z} + V_x &= \frac{\rho \hat{A}(R_o^2 + R_i^2)}{4} \left(\frac{\partial^2 \psi_y}{\partial t^2} - 2\Omega \frac{\partial \psi_x}{\partial t}\right) \\ -\frac{\partial M_x}{\partial z} + V_y &= \frac{\rho \hat{A}(R_o^2 + R_i^2)}{4} \left(-\frac{\partial^2 \psi_x}{\partial t^2} - 2\Omega \frac{\partial \psi_y}{\partial t}\right) \end{aligned} \tag{B-14}$$

Hence,

$$\frac{\partial M}{\partial z} + V = \frac{\rho \hat{A}(R_o^2 + R_i^2)}{4} \left(\frac{\partial^2 \psi}{\partial t^2} - 2i\Omega \frac{\partial \psi}{\partial t}\right) \tag{B-15}$$

Combining equations (B-7) and (B-11), we obtain

$$K\hat{A}G \frac{\partial \gamma}{\partial z} = \rho \hat{A} \frac{\partial^2 w}{\partial t^2} \tag{B-16}$$

Now substituting equation (B-6) into equation (B-16), we get

$$\frac{\partial^2 w}{\partial z^2} - \frac{\partial \psi}{\partial z} = \frac{\rho}{KG}\frac{\partial^2 w}{\partial t^2} \tag{B-17}$$

Taking the derivative of both sides of equation (B-15), we get

$$\frac{\partial^2 M}{\partial z^2} + \frac{\partial V}{\partial z} = \frac{\rho\hat{A}(R_o^2 + R_i^2)}{4}\left(\frac{\partial^3 \psi}{\partial z \partial t^2} - 2i\Omega\frac{\partial^2 \psi}{\partial z \partial t}\right) \tag{B-18}$$

Substituting equations (B-1) and (B-11) into equation (B-18) yields

$$EI\frac{\partial^3 \psi}{\partial z^3} + \rho\hat{A}\frac{\partial^2 w}{\partial t^2} = \frac{\rho\hat{A}(R_o^2 + R_i^2)}{4}\left(\frac{\partial^3 \psi}{\partial z \partial t^2} - 2i\Omega\frac{\partial^2 \psi}{\partial z \partial t}\right) \tag{B-19}$$

From equations (B-17) and (B-19), we have

$$EI\left(\frac{\partial^4 w}{\partial z^4} - \frac{\rho}{KG}\frac{\partial^4 w}{\partial z^2 \partial t^2}\right) + \rho\hat{A}\frac{\partial^2 w}{\partial t^2} = \frac{\rho\hat{A}(R_o^2 + R_i^2)}{4}\left\{\left(\frac{\partial^4 w}{\partial z^2 \partial t^2} - \frac{\rho}{KG}\frac{\partial^4 w}{\partial t^4}\right) - 2i\Omega\left(\frac{\partial^3 w}{\partial z^2 \partial t} - \frac{\rho}{KG}\frac{\partial^3 w}{\partial t^3}\right)\right\} \tag{B-20}$$

or

$$\frac{\partial^4 w}{\partial z^4} - \left[\frac{\rho}{KG} + \frac{\rho\hat{A}(R_o^2 + R_i^2)}{4EI}\right]\frac{\partial^4 w}{\partial z^2 \partial t^2} + \frac{\rho\hat{A}(R_o^2 + R_i^2)}{4EI}2i\Omega\frac{\partial^3 w}{\partial z^2 \partial t} + \frac{\rho\hat{A}}{EI}\frac{\partial^2 w}{\partial t^2} - 2i\Omega\frac{\rho}{KG}\frac{\rho\hat{A}(R_o^2 + R_i^2)}{4EI}\frac{\partial^3 w}{\partial t^3} + \frac{\rho^2\hat{A}(R_o^2 + R_i^2)}{4KGEI}\frac{\partial^4 w}{\partial t^4} = 0 \tag{B-21}$$

Using equations (B-3), (B-6), (B-11), and (B-15), we similarly obtain

$$\frac{\partial^4 \psi}{\partial z^4} - \left[\frac{\rho}{KG} + \frac{\rho\hat{A}(R_o^2 + R_i^2)}{4EI}\right]\frac{\partial^4 \psi}{\partial z^2 \partial t^2} + \frac{\rho\hat{A}(R_o^2 + R_i^2)}{4EI}2i\Omega\frac{\partial^3 \psi}{\partial z^2 \partial t} + \frac{\rho\hat{A}}{EI}\frac{\partial^2 \psi}{\partial t^2} - 2i\Omega\frac{\rho}{KG}\frac{\rho\hat{A}(R_o^2 + R_i^2)}{4EI}\frac{\partial^3 \psi}{\partial t^3} + \frac{\rho^2\hat{A}(R_o^2 + R_i^2)}{4KGEI}\frac{\partial^4 \psi}{\partial t^4} = 0 \tag{B-22}$$

Note that equation (B-22) is identical in form to equation (B-21), except that ψ replaces w. Thus, the general solutions of the two equations are of the same functional form, i.e.,

$$w = Ae^{\bar{\alpha}z + i\omega t} \quad , \quad \psi = Be^{\bar{\alpha}z + i\omega t} \tag{B-23}$$

and substituting into equation (B-21) or (B-22), we obtain the following characteristic equation:

$$\bar{\alpha}^4 + [\frac{\rho}{KG} + \frac{\rho\hat{A}(R_o^2 + R_i^2)}{4EI}]\omega^2\bar{\alpha}^2 - \frac{\rho\hat{A}(R_o^2 + R_i^2)}{2EI}\omega\Omega\bar{\alpha}^2 - \frac{\rho\hat{A}}{EI}\omega^2$$

$$- \frac{\rho^2\hat{A}(R_o^2 + R_i^2)}{2KGEI}\Omega\omega^3 + \frac{\rho^2\hat{A}(R_o^2 + R_i^2)}{4KGEI}\omega^4 = 0$$

or

$$\bar{\alpha}^4 + \rho\omega[\frac{\omega}{KG} + \frac{\hat{A}(R_o^2 + R_i^2)}{4EI}(\omega - 2\Omega)]\bar{\alpha}^2 + \frac{\rho\hat{A}\omega^2}{EI}[\frac{\rho(R_o^2 + R_i^2)}{4KG}\omega(\omega - 2\Omega) - 1] = 0 \qquad \text{(B-24)}$$

Equation (B-24) yields four roots for $\bar{\alpha}$ and hence the closed-form solutions of equations (B-21) and (B-22) are (in any portion of the system between discontinuities)

$$w = \sum_{j=1}^{4} \bar{A}_j e^{\bar{\alpha}_j z + i\omega t} \quad , \quad \psi = \sum_{j=1}^{4} B_j e^{\bar{\alpha}_j z + i\omega t} \qquad \text{(B-25)}$$

From equations (B-11), (B-15), and (B-25), we get two relations between $\bar{A}_j$'s and B_j's. The simpler one, given below, alone will be used in later calculations

$$B_j = \bar{A}_j(\bar{\alpha}_j + \frac{\rho}{KG}\frac{\omega^2}{\bar{\alpha}_j}) \qquad \text{(B-26)}$$

Thus, for each of the three shaft sections 1, 2, 3, (see Fig. 3.1), we have

$$w_p = \sum_{j=1}^{4} A_{pj} e^{\bar{\alpha}_{pj} z_p + i\omega t}$$

$$\psi_p = \sum_{j=1}^{4} B_{pj} e^{\bar{\alpha}_{pj} z_p + i\omega t} \qquad p = 1,2,3 \qquad \text{(B-27)}$$

Here, $\bar{\alpha}_{pj}$, p = 1,2,3 and j = 1,2,3,4 are obtained when the characteristic equation is applied to the three shaft sections 1, 2, and 3. Also, it is

assumed that $\omega = n\Omega$. Hence, n is to be specified to solve equation (B-24). Symbols z_1, z_2, and z_3 denote the local coordinates of the shaft sections 1, 2, and 3, respectively.

B.3 Derivation of Boundary and Continuity Conditions

In the various boundary conditions discussed in the following, all of the numerical subscripts to variables denote that they are associated with that shaft portion having the same number.

Boundary Conditions on the Shaft Attached to the Flywheel:

Forces and moments acting on the flywheel are shown in Fig. B5. Variables subscripted as 1 are to be evaluated at $z_1 = L_1$.

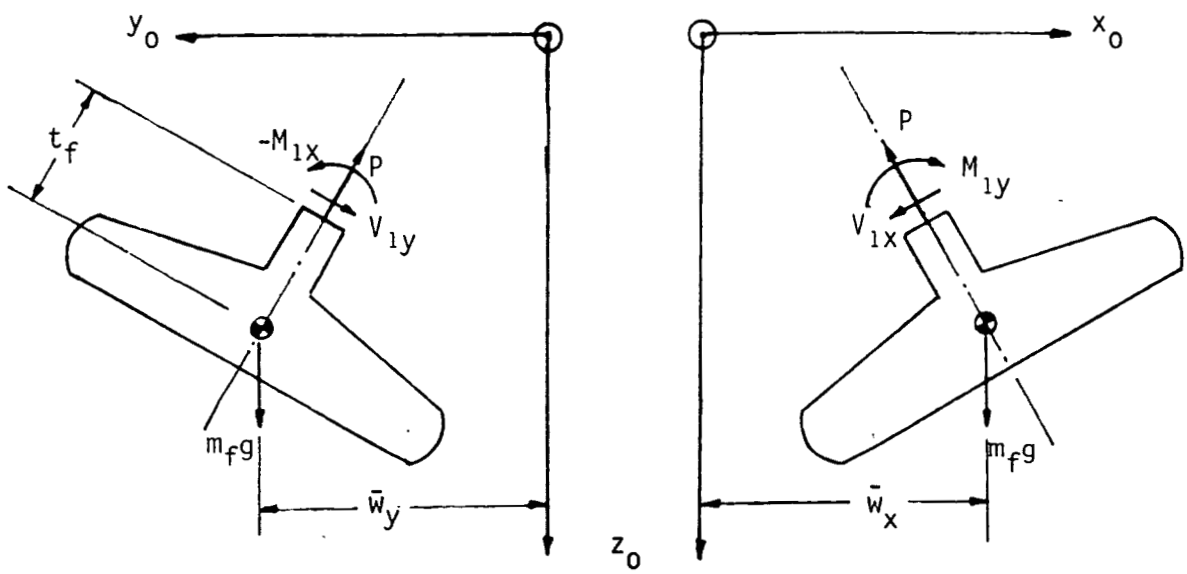

Fig. B5. System of forces and moment acting on the flywheel.

Force equations of motion:

$$- V_{1y} - m_f g \frac{\partial w_{1y}}{\partial z_1} = m_f \frac{\partial^2 \bar{w}_y}{\partial t^2}$$

$$- V_{1x} - m_f g \frac{\partial w_{1x}}{\partial z_1} = m_f \frac{\partial^2 \bar{w}_x}{\partial t^2} \qquad \text{(B-28)}$$

i.e.,

$$V_1 + m_f g \frac{\partial w_1}{\partial z_1} + m_f \frac{\partial^2 \bar{w}}{\partial t^2} = 0 \qquad \text{(B-29)}$$

Since $\bar{w} = w_1 + t_f \frac{\partial w_1}{\partial z_1}$, the preceding equation becomes

$$K_1 A_1 G\left(\frac{\partial w_1}{\partial z_1} - \psi_1\right) + m_f g \frac{\partial w_1}{\partial z_1} + m_f \frac{\partial^2}{\partial t^2}\left(w_1 + t_f \frac{\partial w_1}{\partial z_1}\right) = 0 \tag{B-30}$$

Rotational equations of motion about the center of mass of flywheel:

$$\begin{aligned} - M_{1y} + V_{1x} t_f &= I_{df} \frac{\partial^3 w_{1x}}{\partial z_1 \partial t^2} + I_{pf}\Omega \frac{\partial^2 w_{1y}}{\partial z_1 \partial t} \\ - M_{1x} - V_{1y} t_f &= - I_{df} \frac{\partial^3 w_{1y}}{\partial z_1 \partial t^2} + I_{pf}\Omega \frac{\partial^2 w_{1x}}{\partial x_1 \partial t} \end{aligned} \tag{B-31}$$

Combining the last two equations, we obtain

$$- M_1 + V_1 t_f = I_{df} \frac{\partial^3 w_1}{\partial z_1 \partial t^2} - i I_{pf}\Omega \frac{\partial^2 w_1}{\partial z_1 \partial t} \tag{B-32}$$

or

$$- EI_1 \frac{\partial \psi_1}{\partial z_1} + t_f K_1 A_1 G\left(\frac{\partial w_1}{\partial z_1} - \psi_1\right) - \left(I_{df} \frac{\partial^3 w_1}{\partial z_1 \partial t^2} - i I_{pf}\Omega \frac{\partial^2 w_1}{\partial z_1 \partial t}\right) = 0 \tag{B-33}$$

Continuity Conditions Across the Damper:

Variables subscripted as 1 are evaluated at $z_1 = 0$ and those subscripted as 2 are evaluated at $z_2 = L_2$. Since the damper is assumed not to tilt

$$w_1 = w_2 \tag{B-34}$$

$$\frac{\partial w_1}{\partial z_1} = 0 \tag{B-35}$$

$$\frac{\partial w_2}{\partial z_2} = 0 \tag{B-36}$$

The forces and moments acting on the damper are shown in Fig. B6. Note that there is an additional external moment on the damper which

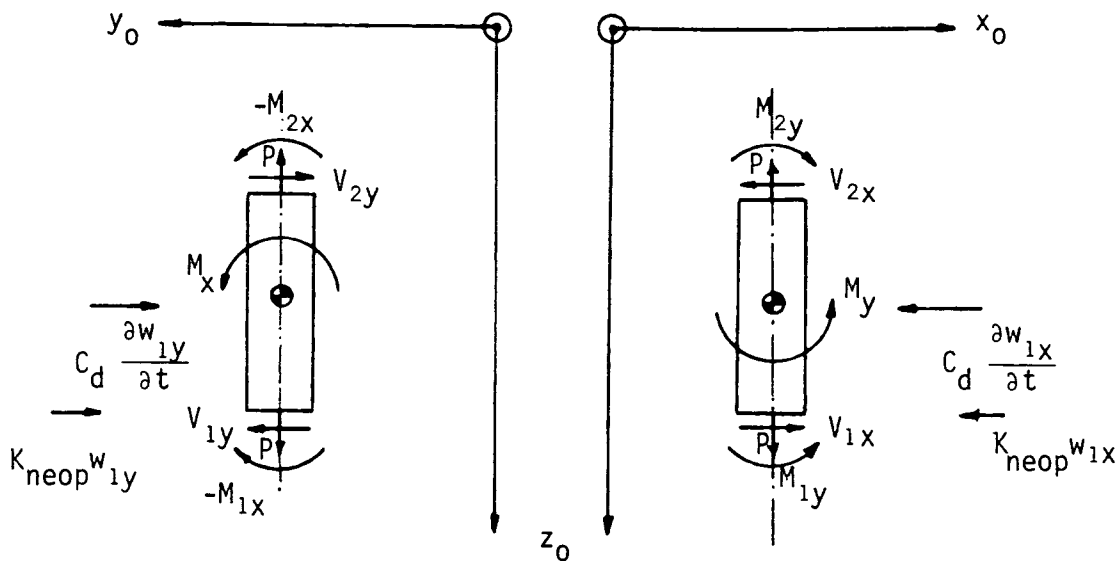

Fig. B6. Damper forces and moments. Note that damper weight has been neglected.

prevents the tilting. Considering the force equation of the damper:

$$- V_{2y} + V_{1y} - K_{neop} w_{1y} - C_d \frac{\partial w_{1y}}{\partial t} = m_d \frac{\partial^2 w_{1y}}{\partial t^2}$$
$$- V_{2x} + V_{1x} - K_{neop} w_{1x} - C_d \frac{\partial w_{1x}}{\partial t} = m_d \frac{\partial^2 w_{1x}}{\partial t^2} \qquad \text{(B-37)}$$

Combining the above two equations,

$$- V_2 + V_1 - K_{neop} w_1 - C_d \frac{\partial w_1}{\partial t} - m_d \frac{\partial^2 w_1}{\partial t^2} = 0 \qquad \text{(B-38)}$$

or

$$K_2 A_2 G\left(\frac{\partial w_2}{\partial z_2} - \psi_2\right) - K_1 A_1 G\left(\frac{\partial w_1}{\partial z_1} - \psi_1\right) + K_{neop} w_1 + C_d \frac{\partial w_1}{\partial t} + m_d \frac{\partial^2 w_1}{\partial t^2} = 0 \qquad \text{(B-39)}$$

Continuity Conditions Across the Intermediate Mass:

The free-body diagram of the intermediate mass is drawn in Fig. B7. Note that the center of mass and the bearing center (where the spring

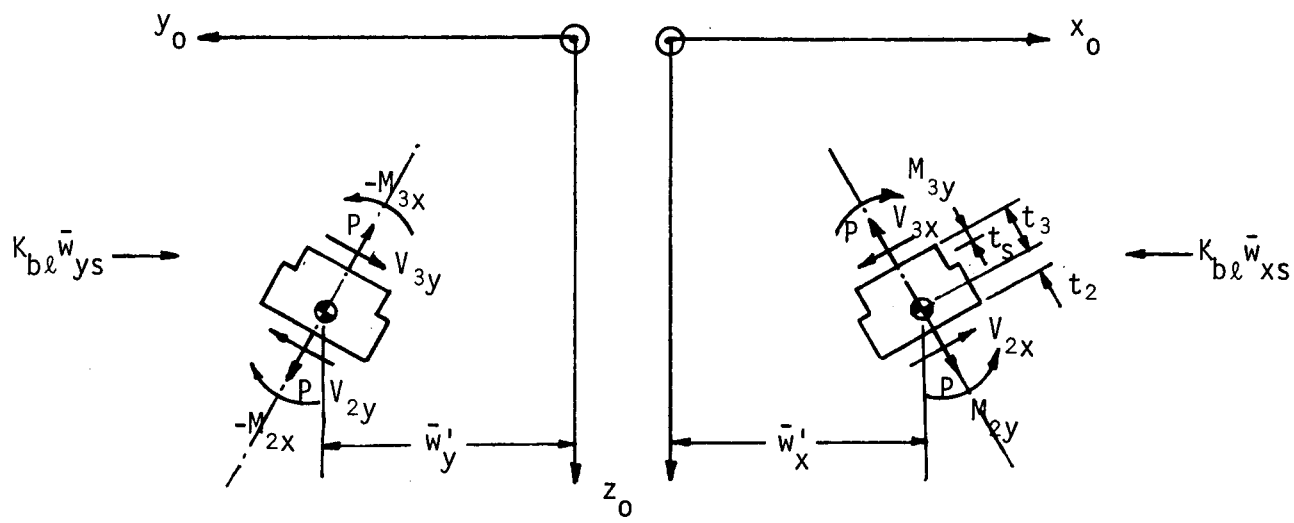

Fig. B7. Intermediate mass and its system of generalized forces. Weight of the intermediate mass is neglected.

approximating the bearing is assumed to act) do not coincide. Variables subscripted as 3 are evaluated at $z_3 = L_3$ and those subscripted as 2 at $z_2 = 0$. From kinematics,

$$\frac{\partial w_3}{\partial z_3} = \frac{\partial w_2}{\partial z_2} \tag{B-40}$$

$$w_2 = w_3 + (t_2 + t_3)\frac{\partial w_2}{\partial z_2} \tag{B-41}$$

The translational equations of motion of the intermediate mass are:

$$\begin{aligned} V_{2y} - V_{3y} - K_{s\ell}\,\bar{w}_{ys} &= m_i\,\frac{\partial^2 \bar{w}'_y}{\partial t^2} \\ V_{2x} - V_{3x} - K_{s\ell}\,\bar{w}_{xs} &= m_i\,\frac{\partial^2 \bar{w}'_x}{\partial t^2} \end{aligned} \tag{B-42}$$

Combining the above two, we obtain

$$V_2 - V_3 - K_{s\ell}\,\bar{w}_s = m_i\,\frac{\partial^2 \bar{w}'}{\partial t^2} \tag{B-43}$$

Since

$$\bar{w}' = w_2 - t_2 \frac{\partial w_2}{\partial z_2}$$

and (B-44)

$$\bar{w}_s = w_2 - (t_2 + t_3 - t_s) \frac{\partial w_2}{\partial z_2}$$

equation (B-43) becomes

$$K_2A_2G(\frac{\partial w_2}{\partial z_2} - \psi_2) - K_3A_3G(\frac{\partial w_3}{\partial z_3} - \psi_3) - K_{s\ell}[w_2 - (t_2 + t_3 - t_s) \frac{\partial w_2}{\partial z_2}]$$

$$- m_i \frac{\partial^2}{\partial t^2} (w_2 - t_2 \frac{\partial w_2}{\partial z_2}) = 0 \qquad \text{(B-45)}$$

Note that $A_3 = A_t + A_{eq}$ and $K_3 = \frac{K_{eq}A_{eq} + K_tA_t}{A_{eq} + A_t}$ (see Fig. B1). Considering the rotational equations of motion about the center of mass,

$$M_{2x} - M_{3x} - V_{2y}t_2 - V_{3y}t_3 - K_{s\ell}(t_3 - t_s)\bar{w}_{ys} = (- I_{di} \frac{\partial^3 w_{2y}}{\partial z_2 \partial t^2} + I_{pi}\, \Omega \frac{\partial^2 w_{2x}}{\partial z_2 \partial t})$$

$$M_{2y} - M_{3y} + V_{2x}t_2 + V_{3x}t_3 + K_{s\ell}(t_3 - t_s)\bar{w}_{xs} = (I_{di} \frac{\partial^3 w_{2x}}{\partial z_2 \partial t^2} + I_{pi}\, \Omega \frac{\partial^2 w_{2y}}{\partial z_2 \partial t}) \qquad \text{(B-46)}$$

From the above two equations, we get

$$M_2 - M_3 + V_2t_2 + V_3t_3 + K_{s\ell}(t_3 - t_s)[w_2 - (t_2 + t_3 - t_s) \frac{\partial w_2}{\partial z_2}]$$

$$- (I_{di} \frac{\partial^3 w_2}{\partial z_2 \partial t^2} - iI_{pi}\, \Omega \frac{\partial^2 w_2}{\partial z_2 \partial t}) = 0 \qquad \text{(B-47)}$$

or

$$EI_2 \frac{\partial \psi_2}{\partial z_2} - EI_3 \frac{\partial \psi_3}{\partial z_3} + K_2A_2Gt_2(\frac{\partial w_2}{\partial z_2} - \psi_2) + K_3A_3Gt_3(\frac{\partial w_3}{\partial z_3} - \psi_3)$$

$$+ K_{s\ell}(t_3 - t_s)[w_2 - (t_2 + t_3 - t_s) \frac{\partial w_2}{\partial z_2}] - (I_{di} \frac{\partial^3 w_2}{\partial z_2 \partial t^2} - iI_{pi}\, \Omega \frac{\partial^2 w_2}{\partial z_2 \partial t}) = 0 \qquad \text{(B-48)}$$

Note: $I_3 = I_t + I_{eq}$ (see Fig. B1).

Boundary Conditions on the Shaft Attached to the Turbine:

Here, all the variables are evaluated at $z_3 = 0$. The forces and moments acting on the turbine are shown in Fig. B8.

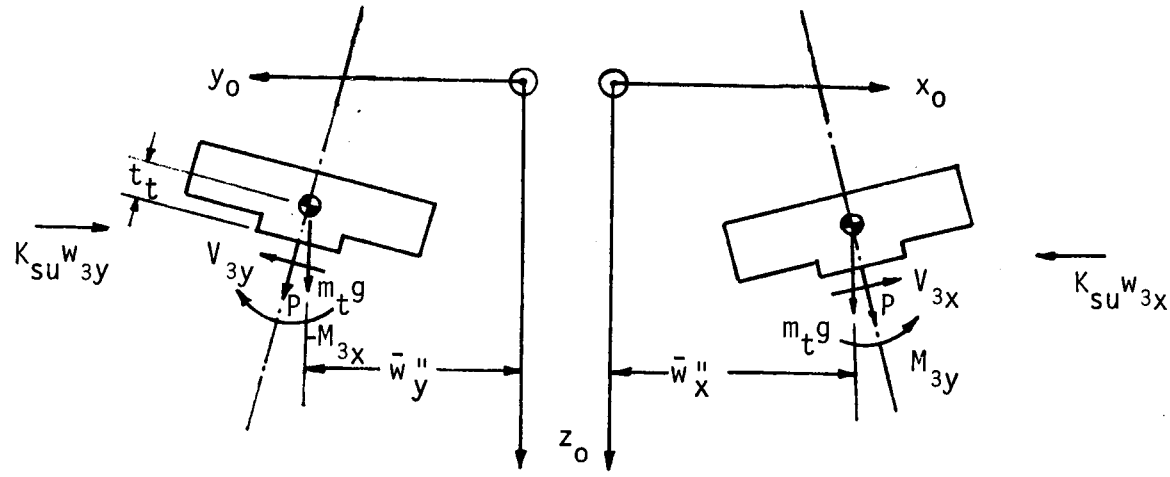

Fig. B8. Turbine wheel forces and moments.

Translational equations of motion give

$$V_{3x} - K_{su}w_{3x} - m_t g \frac{\partial w_{3x}}{\partial z_3} = m_t \frac{\partial^2 \bar{w}''_x}{\partial t^2}$$

$$V_{3y} - K_{su}w_{3y} - m_t g \frac{\partial w_{3y}}{\partial z_3} = m_t \frac{\partial^2 \bar{w}''_y}{\partial t^2} \qquad \text{(B-49)}$$

which combine as

$$V_3 - K_{su}w_3 - m_t g \frac{\partial w_3}{\partial z_3} - m_t \frac{\partial^2 \bar{w}''}{\partial t^2} = 0 \qquad \text{(B-50)}$$

Since

$$\bar{w}'' = w_3 - t_t \frac{\partial w_3}{\partial z_3}$$

the above equation becomes

$$K_3 A_3 G\left(\frac{\partial w_3}{\partial z_3} - \psi_3\right) - K_{su}w_3 - m_t g \frac{\partial w_3}{\partial z_3} - m_t \frac{\partial^2}{\partial t^2}\left(w_3 - t_t \frac{\partial w_3}{\partial z_3}\right) = 0 \qquad \text{(B-51)}$$

The moment equations about the center of mass are:

$$M_{3x} - t_t V_{3y} + K_{su} w_{3y} t_t = (- I_{dt} \frac{\partial^3 w_{3y}}{\partial z_3 \partial t^2} + I_{pt}\Omega \frac{\partial^2 w_{3x}}{\partial z_3 \partial t})$$

$$M_{3y} + t_t V_{3x} - K_{su} w_{3x} t_t = (I_{dt} \frac{\partial^3 w_{3x}}{\partial z_3 \partial t^2} + I_{pt}\Omega \frac{\partial^2 w_{3y}}{\partial z_3 \partial t}) \tag{B-52}$$

When combined, they give

$$M_3 + t_t V_3 - K_{su} t_t w_3 - (I_{dt} \frac{\partial^3 w_3}{\partial z_3 \partial t^2} - i I_{pt}\Omega \frac{\partial^2 w_3}{\partial z_3 \partial t}) = 0 \tag{B-53}$$

or

$$EI_3 \frac{\partial \psi_3}{\partial z_3} + K_3 A_3 G\, t_t (\frac{\partial w_3}{\partial z_3} - \psi_3) - K_{su} t_t w_3 - (I_{dt} \frac{\partial^3 w_3}{\partial z_3 \partial t^2} - i I_{pt}\Omega \frac{\partial^2 w_3}{\partial z_3 \partial t}) = 0 \tag{B-54}$$

The equations (B-30), (B-33)-(B-36), (B-39)-(B-41), (B-45), (B-48), (B-51) and (B-54) are cast into the following form (see Appendix B.4):

$$[\bar{C}] \begin{Bmatrix} A_{11} \\ A_{12} \\ A_{13} \\ A_{14} \\ A_{21} \\ A_{22} \\ A_{23} \\ A_{24} \\ A_{31} \\ A_{32} \\ A_{33} \\ A_{34} \end{Bmatrix} = [0] \tag{B-55}$$

Here, $\{A_{pj}\}$($p = 1,2,3$ and $j = 1,2,3,4$) is the unknown column vector which determines the deflections of the three shaft portions [equation (B-27)]. The matrix $[\bar{C}]$ has elements which are functions of $\bar{\alpha}_{pj}$ ($j = 1,2,3,4$), ω and Ω. Note that, since each shaft portion has four boundary conditions (two on each end) and each shaft, $p(p = 1,2,3)$ has four unknown coefficients A_{pj} ($j = 1,2,3,4$), $[\bar{C}]$ is a 12×12 matrix. Now, for a chosen n such that $\omega = n\Omega$, any Ω that makes det $[\bar{C}] = 0$ is a critical running speed for that n.

B.4 Transformation of Boundary/Continuity Conditions for Computer Implementation

Equation (B-27) is substituted into equation (B-30) to obtain the following result:

$$\sum_{j=1}^{4} [K_1 A_1 G(A_{1j}\bar{\alpha}_{1j} - B_{1j}) + m_f g A_{1j}\bar{\alpha}_{1j} + m_f(-\omega^2 A_{1j} - t_f A_{1j}\bar{\alpha}_{1j}\omega^2)]e^{\bar{\alpha}_{1j}L_1} = 0$$

Using equation (B-26) and dividing by $-\omega^2$, we reduce the preceding equation to the following:

$$\sum_{j=1}^{4} [\frac{\rho A_1}{\bar{\alpha}_{1j}} - \frac{m_f g\bar{\alpha}_{1j}}{\omega^2} + m_f(1 + t_f\bar{\alpha}_{1j})]A_{1j}e^{\bar{\alpha}_{1j}L_1} = 0 \qquad \text{(B-56)}$$

Similarly, substitution into equation (B-33) gives

$$\sum_{j=1}^{4} [-EI_1\bar{\alpha}_{1j}B_{1j} + K_1 A_1 G_1 t_f(\bar{\alpha}_{1j}A_{1j} - B_{1j}) - (-I_{df}A_{1j}\bar{\alpha}_{1j}\omega^2 + I_{pf}\Omega A_{1j}\bar{\alpha}_{1j}\omega)]e^{\bar{\alpha}_{1j}L_1} = 0$$

Using equation (B-26) and dividing by $-\omega^2$, we get

$$\sum_{j=1}^{4} [EI_1(\frac{\bar{\alpha}_{1j}^2}{\omega^2} + \frac{\rho}{K_1 g}) + t_f \frac{\rho A_1}{\bar{\alpha}_{1j}} - \bar{\alpha}_{1j}(I_{df} - \frac{\Omega}{\omega} I_{pf})]A_{1j}e^{\bar{\alpha}_{1j}L_1} = 0 \qquad \text{(B-57)}$$

In similar fashion, substitution into equations (B-34)-(B-36) gives

$$\sum_{j=1}^{4} [A_{1j} - A_{2j}e^{\bar{\alpha}_{2j}L_2}] = 0 \qquad \text{(B-58)}$$

$$\sum_{j=1}^{4} A_{1j}\bar{\alpha}_{1j} = 0 \qquad \text{(B-59)}$$

$$\sum_{j=1}^{4} A_{2j}\bar{\alpha}_{2j}e^{\bar{\alpha}_{2j}L_2} = 0 \qquad \text{(B-60)}$$

Substitution into equation (B-39) yields

$$\sum_{j=1}^{4} [K_2A_2G(A_{2j}\bar{\alpha}_{2j} - B_{2j})e^{\bar{\alpha}_{2j}L_2} - K_1A_1G(\bar{\alpha}_{1j}A_{1j} - B_{1j}) + K_{neop}A_{1j} + i\omega C_dA_{1j} - m_d\omega^2A_{1j}] = 0$$

which can be reduced, using equation (B-26), to:

$$\sum_{j=1}^{4} [(\frac{\rho A_1}{\bar{\alpha}_{1j}} + \frac{K_{neop}}{\omega^2} + \frac{iC_d}{\omega} - m_d)A_{1j} - \frac{\rho A_2}{\bar{\alpha}_{2j}} e^{\bar{\alpha}_{2j}L_2} A_{2j}] = 0 \qquad \text{(B-61)}$$

Similarly equations (B-40), (B-41), and (B-45) give

$$\sum_{j=1}^{4} [-\bar{\alpha}_{2j}A_{2j} + \bar{\alpha}_{3j}A_{3j}e^{\bar{\alpha}_{3j}L_3}] = 0 \qquad \text{(B-62)}$$

$$\sum_{j=1}^{4} [A_{2j}\{1 - (t_2 + t_3)\bar{\alpha}_{2j}\} - A_{3j}e^{\bar{\alpha}_{3j}L_3}] = 0 \qquad \text{(B-63)}$$

$$\sum_{j=1}^{4} [K_2A_2G(A_{2j}\bar{\alpha}_{2j} - B_{2j}) - K_3A_3G(A_{3j}\bar{\alpha}_{3j} - B_{3j})e^{\bar{\alpha}_{3j}L_3} - K_{s\ell}\{A_{2j} - A_{2j}\bar{\alpha}_{2j}(t_2 + t_3 - t_s)\} - m_i\ (-A_{2j}\omega^2 + A_{2j}\omega^2\bar{\alpha}_{2j}t_2)] = 0$$

which can be reduced to

$$\sum_{j=1}^{4} [A_{2j}\{- \frac{\rho A_2}{\bar{\alpha}_{2j}} - \frac{K_{s\ell}}{\omega^2} (1 - (t_2 + t_3 - t_s)\bar{\alpha}_{2j}) + m_i\ (1 - \bar{\alpha}_{2j}t_2)\} + A_{3j} \frac{\rho A_3}{\bar{\alpha}_{3j}} e^{\bar{\alpha}_{3j}L_3}] = 0 \qquad \text{(B-64)}$$

Equation (B-48) becomes

$$\sum_{j=1}^{4} [EI_2B_{2j}\bar{\alpha}_{2j} - EI_3B_{3j}\bar{\alpha}_{3j}e^{\bar{\alpha}_{3j}L_3} + K_2A_2Gt_2(A_{2j}\bar{\alpha}_{2j} - B_{2j}) + K_3A_3Gt_3(A_{3j}\bar{\alpha}_{3j} - B_{3j})e^{\bar{\alpha}_{3j}L_3}$$

$$+ K_{s\ell}(t_3 - t_s)\{A_{2j} - (t_2 + t_3 - t_s)\bar{\alpha}_{2j}A_{2j}\} - (-I_{di}\ \bar{\alpha}_{2j}\omega^2A_{2j} + I_{pi}\ \Omega\omega A_{2j}\bar{\alpha}_{2j})] = 0$$

or

$$\sum_{j=1}^{4} [A_{2j}\{EI_2 (\frac{\bar{\alpha}_{2j}^2}{\omega^2}+\frac{\rho}{K_2G}) - \frac{t_2\rho A_2}{\bar{\alpha}_{2j}} + \frac{K_{s\ell}}{\omega^2} (t_3 - t_s)(1 - (t_2 + t_3 - t_s)\bar{\alpha}_{2j})$$

$$+ \bar{\alpha}_{2j}(I_{di} - \frac{\Omega}{\omega} I_{pi})\} + A_{3j}\{-EI_3 (\frac{\bar{\alpha}_{3j}^2}{\omega^2} + \frac{\rho}{K_3G}) - \frac{t_3\rho A_3}{\bar{\alpha}_{3j}}\}e^{\bar{\alpha}_{3j}L_3}] = 0 \qquad \text{(B-65)}$$

Equation (B-51) yields

$$\sum_{j=1}^{4} [K_3A_3G(A_{3j}\bar{\alpha}_{3j} - B_{3j}) - K_{su}A_{3j} - m_f g\bar{\alpha}_{3j}A_{3j} - m_t(-\omega^2A_{3j} + t_t\omega^2\bar{\alpha}_{3j}A_{3j})] = 0$$

which can be reduced to

$$\sum_{j=1}^{4} [- \frac{\rho A_3}{\bar{\alpha}_{3j}} - \frac{K_{su}}{\omega^2} - m_t\{\frac{g\bar{\alpha}_{3j}}{\omega^2} - (1 - t_t\bar{\alpha}_{3j})\}]A_{3j} = 0 \qquad \text{(B-66)}$$

Equation (B-54) can be rewritten as

$$\sum_{j=1}^{4} [EI_3\bar{\alpha}_{3j}B_{3j} + K_3A_3G\, t_t (A_{3j}\bar{\alpha}_{3j} - B_{3j}) - K_{su}\, t_t A_{3j}$$

$$- (-I_{dt}\omega^3\bar{\alpha}_{3j}A_{3j} + I_{pt}\Omega\omega\bar{\alpha}_{3j}A_{3j})] = 0$$

or

$$\sum_{j=1}^{4} [EI_3(\frac{\bar{\alpha}_{3j}^2}{\omega^2}+\frac{\rho}{K_3G}) - \frac{t_t\rho A_3}{\bar{\alpha}_{3j}} - \frac{K_{su}\, t_t}{\omega^2} + \bar{\alpha}_{3j}(I_{dt} - I_{pt}\frac{\Omega}{\omega})]A_{3j} = 0 \qquad \text{(B-67)}$$

The above twelve conditions, (B-56)-(B-67), can be expressed in the matrix form of equations (3.1) for free whirling analysis.

B.5 Derivations Relating to Forced Whirling Analysis

Mass eccentricity (r_e) and initial tilt (ϕ_o) are illustrated in Fig. B9. The modifications in the boundary conditions on the shaft attaching to the flywheel is explained in the following equations.

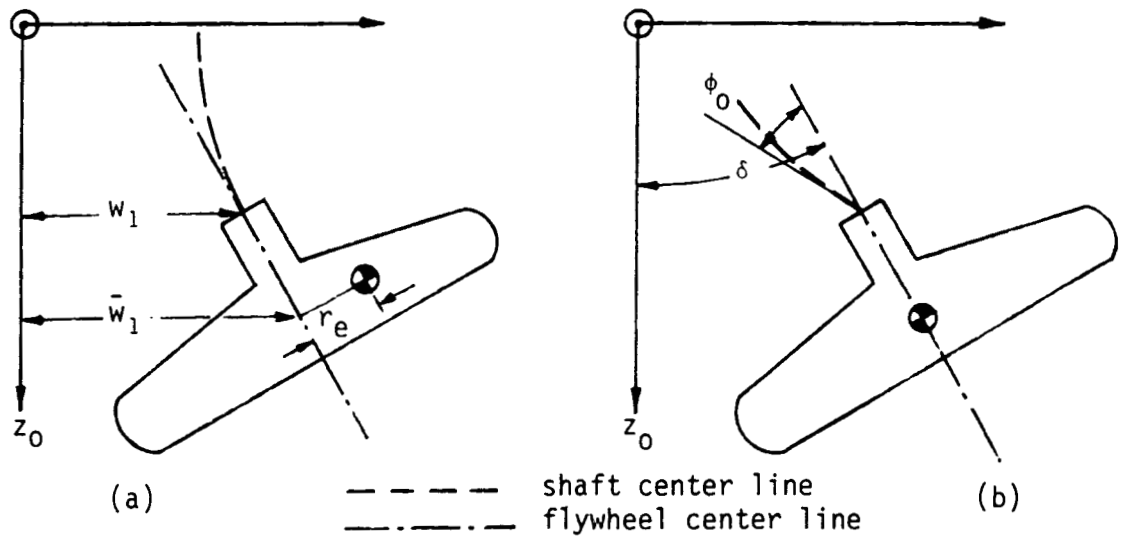

Fig. B9. Exaggerated (a) mass eccentricity and (b) initial tilt in the flywheel.

$$\bar{w} = \bar{w}_1 + r_e e^{i\Omega t} \tag{B-68}$$

$$= w_1 + t_f \frac{\partial w_1}{\partial z_1} + r_e e^{i\Omega t}$$

where $\bar{w}$ is the displacement of the flywheel mass center. Hence, from equation (B-29), we obtain

$$V_1 + m_f g \frac{\partial w_1}{\partial z_1} + m_f \frac{\partial^2}{\partial t^2} (w_1 + t_f \frac{\partial w_1}{\partial z_1} + r_e e^{i\Omega t}) = 0 \tag{B-69}$$

which reduces to

$$K_1 A_1 G(\frac{\partial w_1}{\partial z_1} - \psi_1) + m_f g \frac{\partial w_1}{\partial z_1} + m_f \frac{\partial^2}{\partial t^2} (w_1 + t_f \frac{\partial w_1}{\partial z_1}) = m_f \Omega^2 r_e e^{i\Omega t} \tag{B-70}$$

The above equation is similar to equation (B-30) except that here there is a forcing term on the right. Similarly, equation (B-32) is modified to

$$- M_1 + V_1 t_f = I_{df} \frac{\partial^2 \delta}{\partial t^2} - i I_{pf} \Omega \frac{\partial \delta}{\partial t} \tag{B-71}$$

where

$$\delta = \frac{\partial w_1}{\partial z_1} + \phi_o e^{i(\Omega t - \beta)} \tag{B-72}$$

and ϕ_o is the initial tilt and β the phase lag of initial tilt relative to the mass eccentricity. Hence,

$$- EI_1 \frac{\partial \psi_1}{\partial z_1} + t_f K_1 A_1 G\left(\frac{\partial w_1}{\partial z_1} - \psi_1\right) - \left(I_{df} \frac{\partial^3 w_1}{\partial z_1 \partial t^2} - i I_{pf} \Omega \frac{\partial^2 w_1}{\partial z_1 \partial t}\right) =$$

$$\phi_o \Omega^2 (I_{pf} - I_{df}) e^{i(\Omega t - \beta)} \tag{B-73}$$

The above equation is similar to equation (B-33) with the exception that here there is a forcing term on the right. Hence, in the computer implementation, we have the following form:

$$[\bar{C}] \begin{Bmatrix} A_{11} \\ A_{12} \\ A_{13} \\ A_{14} \\ A_{21} \\ A_{22} \\ A_{23} \\ A_{24} \\ A_{31} \\ A_{32} \\ A_{33} \\ A_{34} \end{Bmatrix} = \begin{Bmatrix} - m_f r_e \\ -\phi_o (I_{pf} - I_{df}) e^{-i\beta} \\ 0 \\ 0 \\ 0 \\ 0 \\ 0 \\ 0 \\ 0 \\ 0 \\ 0 \\ 0 \end{Bmatrix} \tag{B-74}$$

Note that in this synchronous forced whirling due to mass and tilt unbalances, $\omega = \Omega$ with $n = 1$. Further, any steady-state response at a point $z_p = z^*$, $p = 1,2,3$ for a running speed Ω^* can be obtained from equation (B-27) after solving equation (B-74) for A_{pj} ($p = 1,2,3$; $j = 1,2,3,4$).

B.6 Summary of Data Used in Combined Model

Table B-1. Data Used for Combined Model of the Oak Ridge System (see Fig. 3.1)

Lengths L_1	0.746 in.
L_2	0.670 in.
L_3	2.127 in.
L_{ac} (see Fig. B1)	3.597 in.
t_f:	
System A 7.05 in.	
System B 3.45 in.	
System C 3.15 in.	
t_d	1.833 in.
t_s	0.243 in.
t_2	0.416 in.
t_3	0.435 in.
t_t	0.894 in.
Diameter of shaft 1	0.3125 in.
Diameter of shaft 2	0.3125 in.
Equivalent uniform outer diameter of turbine shaft (d_o)	0.7493 in.
Inner diameter of turbine shaft (d_i)	0.3175 in.
Young's modulus of shaft material (E)	29.5×10^6 psi
Shear modulus of shaft material (G)	11.5×10^6 psi
Specific weight of shaft material	0.283 lb/in.^{3}
Shear correction factor for shaft 1 (K_1) and shaft 2 (K_2)	0.885
Shear correction factor for the equivalent turbine shaft (K_t)	0.6569
Shear correction factor for the equivalent quill shaft within the turbine shaft (K_{eq})	0.885
Mass of turbine wheel (m_t)	0.00479 lb-s^2/in.
Diametral mass moment of inertia of turbine wheel (I_{dt})	0.00340 lb-in-s^2

Table B-1 (Cont'd)

Polar mass moment of inertia of turbine wheel (I_{pt})	0.00628 lb-in-s^2
Mass of intermediate mass (m_i)	0.000202 lb-s^2/in.
Diametral mass moment of inertia of intermediate mass (I_{di})	1.798×10^{-5} lb-in-s^2
Polar mass moment of inertia of intermediate mass (I_{pi})	1.15×10^{-5} lb-in-s^2
Mass of damper (m_d)	0.00300 lb-s^2/in.
Mass of flywheel (m_f)	
System A	0.0951 lb-s^2/in.
System B	0.0576 lb-s^2/in.
System C	0.0336 lb-s^2/in.
Diametral mass moment of inertia of flywheel (I_{df}):	
System A	4.83 lb-in-s^2
System B	1.648 lb-in-s^2
System C	0.823 lb-in-s^2
Polar mass moment of inertia of flywheel (I_{pf}):	
System A	8.517 lb-in-s^2
System B	2.036 lb-in-s^2
System C	1.645 lb-in-s^2
Upper and lower bearing spring constants* (K_{su}, $K_{s\ell}$)	2×10^6 lb/in. each
Neoprene pad spring constant (K_{neop})	0 lb/in.
External viscous damping coefficient (C_d) values used	0 and 10 lb-s/in.

*See footnote in Table A-1.

APPENDIX C - COMPUTER CODES, FLOW CHARTS, AND NOTES FOR PROGRAM USERS

The programs presented here were written in FORTRAN IV for the IBM System 370, Model 158J with graphical outputs on a COMPLOT DP-853 plotter.

C.1 Free Whirling and Stability Using the Lumped Model

The same program is used for both the free whirling (including mode shapes) and stability analyses. However, for the sake of clarity, separate flow charts are presented for free whirling and for stability.

The use of the subroutine CRITCL for determining the approximate locations of first- and second-order critical speeds on a logarithmic Campbell diagram (log of natural frequency ω versus log of rotational speed Ω) is explained in Fig. C1. The flow chart for free whirling analysis is shown in Fig. C2, and the computation takes approximately 7 minutes of CPU time. All of the input data related to the Oak Ridge spin-test facility and the three flywheel systems investigated are listed in Table A-1.

For stability analysis, subroutine CRITCL is used to compute the rotational speeds associated with the respective beginning and end limits of the unstable region. The flow chart for stability analysis is shown in Fig. C3, and the computation takes approximately 25 minutes of CPU time.

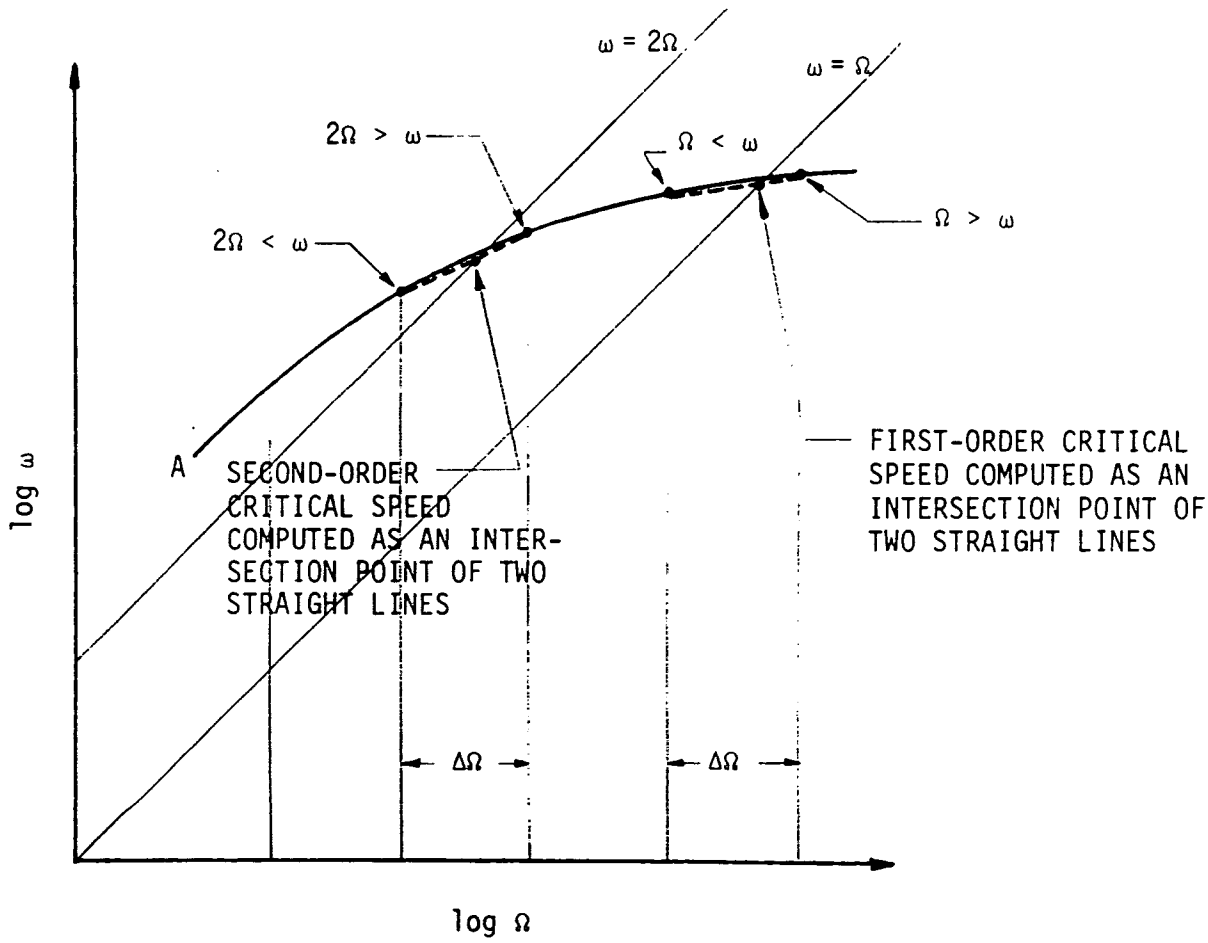

Fig. C1. Approximate determination of first- and second-order critical speeds on a forward branch (A), using subroutine CRITCL.

Fig. C2. Flow chart for free whirling analysis (including mode shapes) using the lumped model.

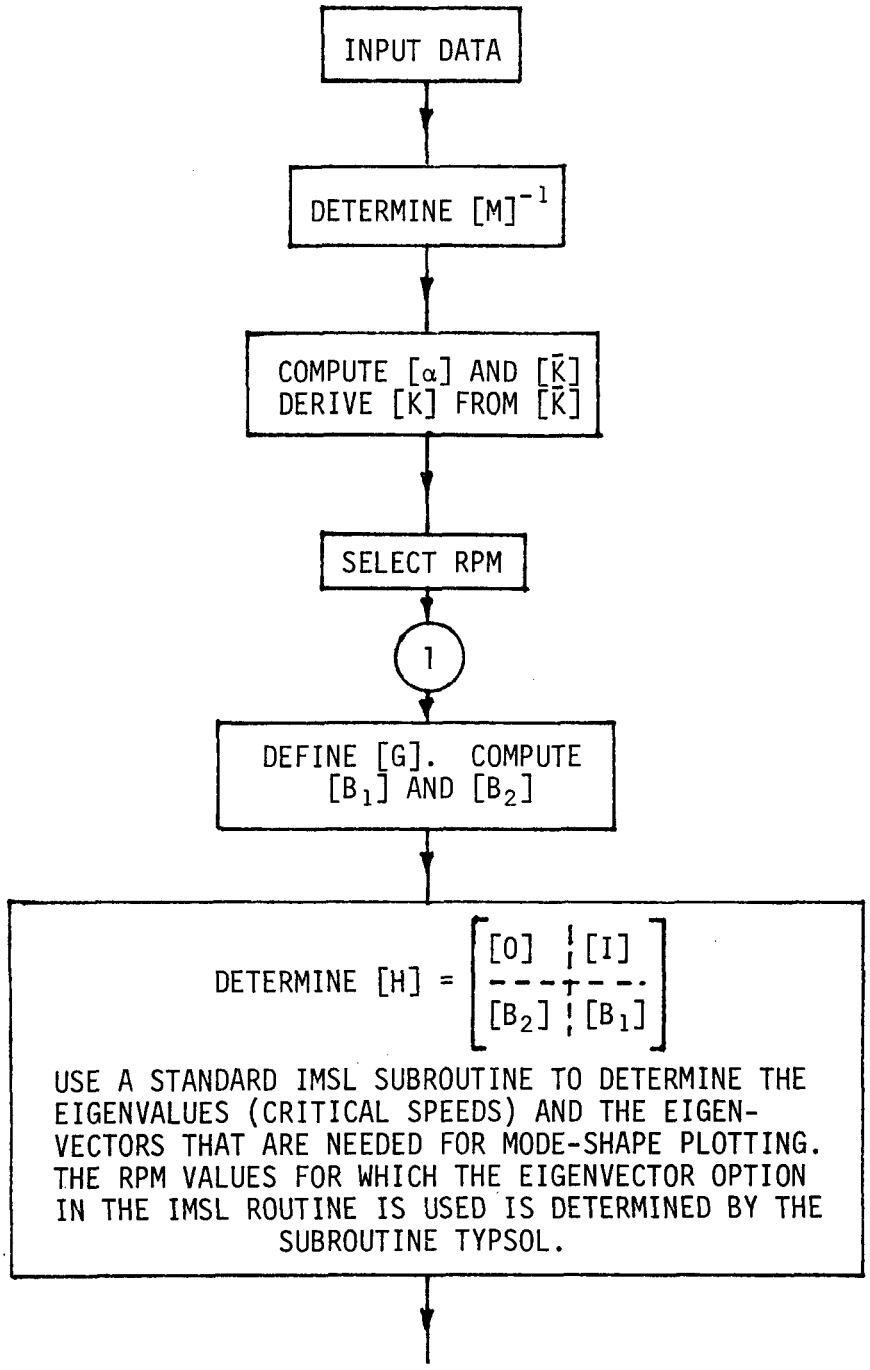

Continued on next page

Fig. C2 (continued)

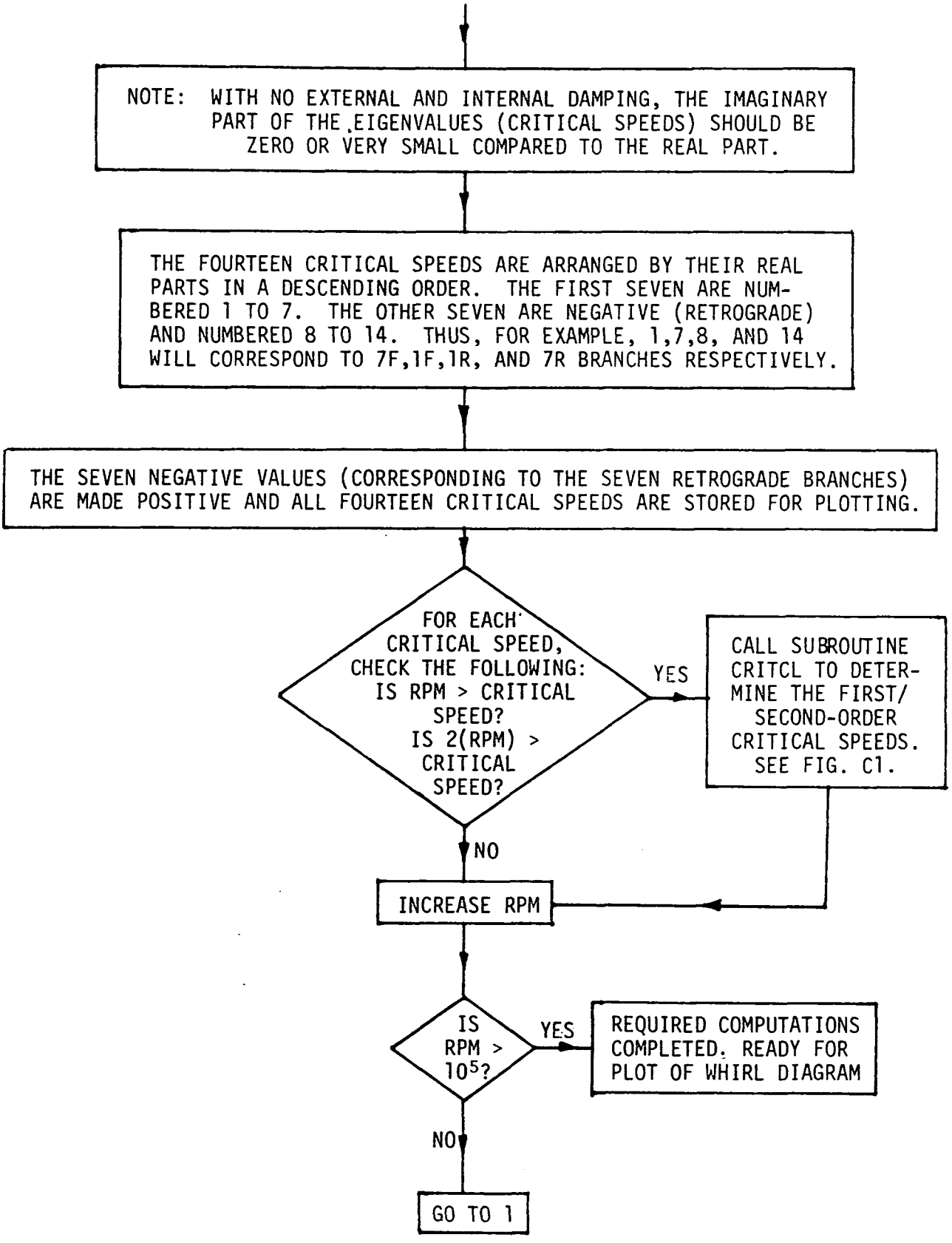

Fig. C3. Flow chart for stability analysis using the lumped model.

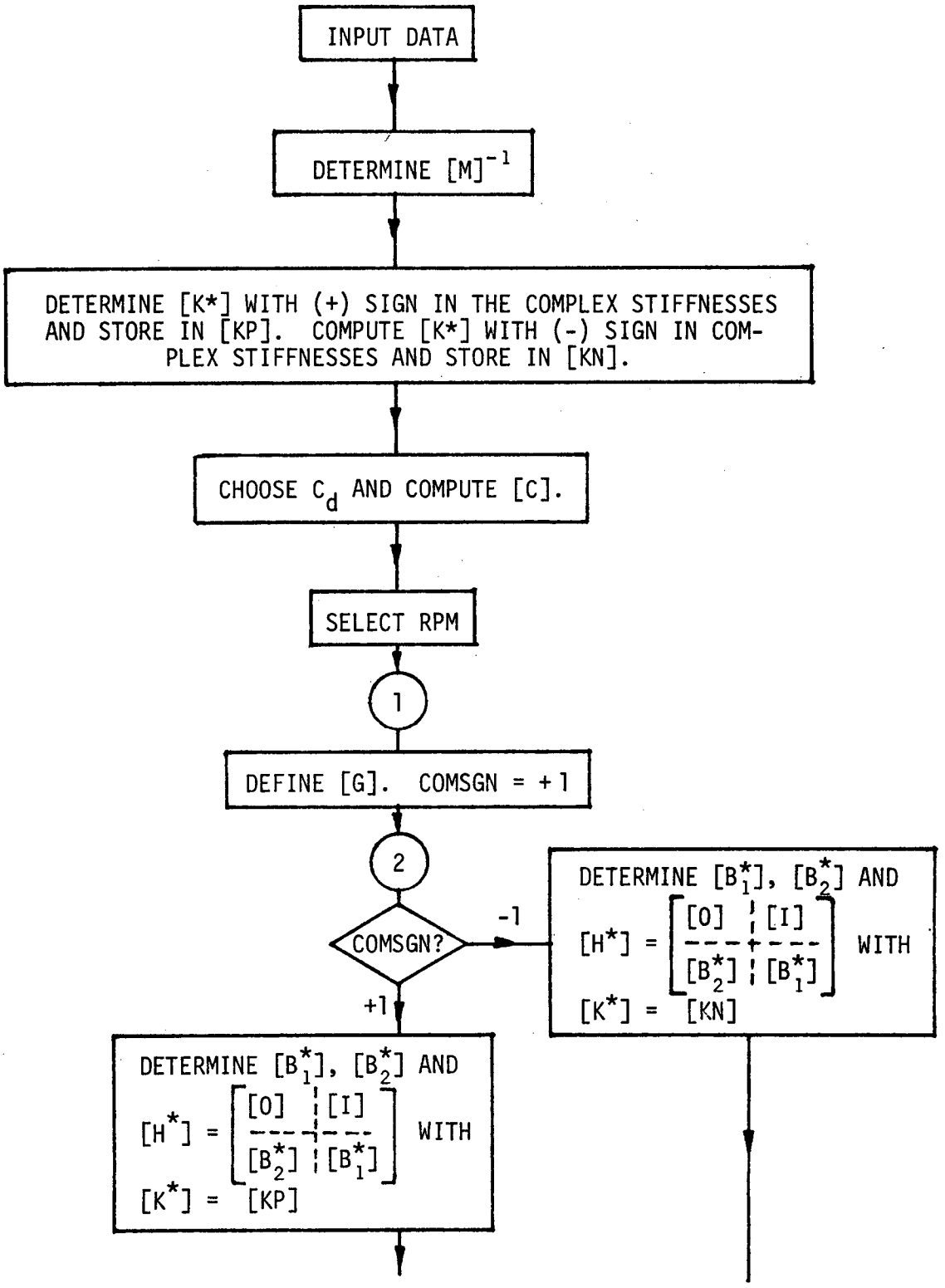

Continued on next page

Fig. C3 (continued)

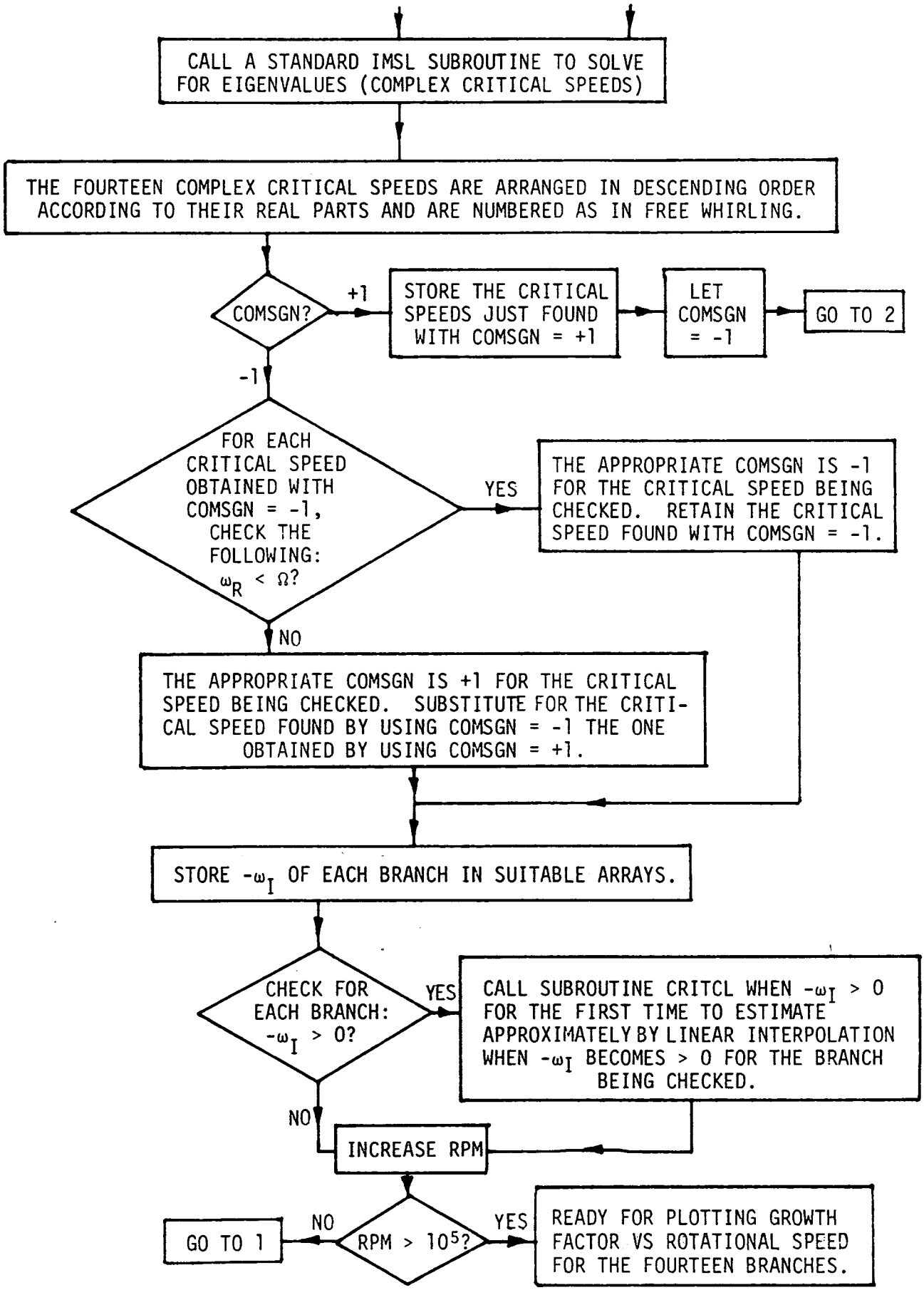

```
C
C        F R E E   V I B R A T I O N   $   S T A B I L I T Y
C                    ( L U M P E D   M O D E L )
C
C  NOTE: THE COMPONENTS OF THE Q VECTOR ARE:
C        (RF,PHIF,RD, RI,PHII,RT,PHIT)
C
C
      IMPLICIT REAL*8(A-H,O-Z)
      REAL*4 RCPM(7016),UM(7016),Y1,Y2,EV(7)
      REAL*4 ICPMA1(7014),ICPMA2(7014),ICPMA3(7014),ICPMA4(7014)
      REAL*4 AL2,AL3,S12,S11,ALEN,PI,XFB
      REAL*4 ICPM1(7016),ICPM2(7016),ICPM3(7016),ICPM4(7016)
      REAL*4 BN,BNP(14)
      REAL*4 CDS,RPDIVS,CDSV(4)
      REAL*8 LB,LG,L3
      REAL*8 MD,MF,MIN,MT
      REAL*8 IDF,IPF,IDIN,IPIN,IDT,IPT
      COMPLEX*16 ALPH(8,8),KN(7,7),KP(7,7),KZ(7,7),STIF(8,8)
      COMPLEX*16 CPMT(14),ZT(7,14)
      COMPLEX*16 WA1(80),WA2(8)
      COMPLEX*16 MI(7,7),G(7,7),CE(7,7),K(7,7)
      COMPLEX*16 B1(7,7),B2(7,7),H(14,14),W(14),Z(14,14)
      COMPLEX*16 ZMAX,SE(7)
      COMPLEX*16 A1(7,7),A2(7,7),CPM(14),INUM,S,SI
      DIMENSION R(14),RPMUNS(14),CRITS1(14),CRITS2(14),WK1(420)
      DIMENSION UPLUNS(14)
      DIMENSION MMV(14),JSTART(4),JEND(4)
C
C   THE FLYWHEEL DATA IN THIS PROGRAM ARE FOR THE LLNL FLYWHEEL
C
C
C   TF: FLYWHEEL CG DISTANCE FROM END OF QUILL SHAFT. TD: DAMPER
C   CG DISTANCE FROM DAMPER EDGE.  TT1: TURBINE CG DISTANCE FROM
C   ONE END OF TURBINE.  SEE FIG.B1.  TT1 IS THE SAME AS TT IN FIG.
C
C   LB,LG,L3: LENGTHS DEFINED IN APPENDIX A1
C
C   MF,MD,MT: MASS OF FLYWHEEL,DAMPER AND TURBINE
C
C   IDF,IPF: FLYWHEEL DIAMETRAL AND POLAR MASS MOMENTS OF INERTIA
C
C   IDT,IPT: TURBINE DIAMETRAL AND POLAR MASS MOMENTS OF INERTIA
C
C   MIN: MASS OF THE INTERMEDIATE MASS
C
C   IDIN,IPIN: DIAMETRAL AND POLAR MASS MOMENTS OF INERTIA OF THE
C   INTERMEDIATE MASS
C
C   THE VARIABLES IN THE COMMON BLOCK MODLM3 ARE RELATED TO MODE SHAPE
C   PLOTTING
```

```
      COMMON/MAIN1/TD,TF,TT1
      COMMON/MAIN2/LB,LG,L3
      COMMON/MODLM3/AL2,AL3,S12,S11,ALEN,PI,XFB
C
C   * * * DATA INPUT: SOME OF THE DATA CAN BE SEEN IN SUBROUTINE COMPLI,
C         SUBROUTINE MODLUM AND IN 'BLOCK DATA' * * *
C
C
C   THE FOLLOWING THREE DATA STATEMENTS ARE RELATED TO MODE SHAPE PLOTS
      DATA MMV/7,6,5,4,3,2,1,8,9,10,11,12,13,14/
      DATA JSTART/4,8,1,12/
      DATA JEND/7,11,3,14/
      DATA MF,MD,MT/0.0336D0,0.002998D0,0.00479D0/
      DATA IDF,IPF/0.823D0,1.645D0/
      DATA IDT,IPT/0.003402D0,0.00628D0/
      DATA MIN/0.000202D0/
      DATA IDIN,IPIN/1.798D-05,1.15D-05/
C
C
C
C  IPLOT INDICATES WHICH PLOT IS DESIRED:
C        IPLOT=0 . . . FOR FREE WHIRLING MAPS (COMBINED POS. AND NEG.
C                      BRANCHES,JUST NEG. BRANCHES,JUST POS. BRANCHES);
C                      AND MODE SHAPES IF ANY
C        IPLOT=1 . . . FOR PLOTS OF MINUS THE IMAGINARY PART OF THE
C                      WHIRLING SPEED(GROWTH FACTOR) VS. ROTATIONAL SPEED
C        IDAMP=0 . . . CAUSES THE STATEMENT 'NO MATERIAL DAMPING' TO
C                      BE DRAWN IN GROWTH FACTOR PLOTS
C        IDAMP=2 . . . CAUSES THE STATEMENT 'COMPLEX STIFFNESS' TO BE
C                      DRAWN IN GROWTH FACTOR PLOTS.SEE SUBROUTINE LEGND5
C
      IPLOT=0
      IDAMP=0
C
C  THE FOLLOWING REAL*4 VARIABLES ARE REQUIRED BY SUEROUTINE MODLUM
C  WHICH PLOTS THE MODE SHAPES.AXIAL LENGTHS HAVE BEEN SCALED TO 1/3
C  ACTUAL SIZE
C
      AL2=2.0*TD/3.0
      AL3=TF/3.0
      S12=(LB+TT1)/3.0
      S11=(L3+TT1)/3.0
      XFB=(LG+TT1)/3.0
      ALEN=(LG+TT1+TF)/3.0
      PII=2.0D0*DARSIN(1.0D0)
      PI=PII
      INUM=(0.0D0,1.0D0)
      DO 100 IM=1,7
      DO 100 IN=1,7
      MI(IM,IN)=(0.0D0,0.0D0)
      G(IM,IN)=(0.0D0,0.0D0)
      CE(IM,IN)=(0.0D0,0.0D0)
  100 K(IM,IN)=(0.0D0,0.0D0)
C
C   INVERSE OF MASS MATRIX DEFINED.SEE CHAPTER 2
```

```
      MI(1,1)=1.0D0/MF
      MI(2,2)=1.0D0/IDF
      MI(3,3)=1.0D0/MD
      MI(4,4)=1.0D0/MIN
      MI(5,5)=1.0D0/IDIN
      MI(6,6)=1.0D0/MT
      MI(7,7)=1.0D0/IDT
      DO 110 I=1,8
      DO 110 J=1,8
  110 ALPH(I,J)=(0.0D0,0.0D0)
C
C   COMSGN: SIGN IN COMPLEX MODULUS.COMSGN=0 FOR FREE WHIRLING.
C   COMSGN=+1,-1 FOR STABILITY ANALYSIS
C
      IF(IPLOT.EQ.0) COMSGN=0.0D0
      IF(IPLOT.EQ.1) COMSGN=1.0D0
  112 CONTINUE
C
C   SUBROUTINE COMPLI COMPUTES THE 8X8 COMPLIANCE MATRIX
C
      CALL COMPLI(ALPH,COMSGN)
      DO 114 I=1,8
      DO 114 J=1,8
      STIF(I,J)=(0.0D0,0.0D0)
      IF(I.EQ.J) STIF(I,J)=(1.0D0,0.0D0)
  114 CONTINUE
      INT=0
C
C   LEQ2C: IMSL SUBROUTINE FOR MATRIX INVERSION
C
      CALL LEQ2C(ALPH,8,8,STIF,8,8,INT,WA1,WA2,IER)
C
C   DETERMINATION OF THE 7X7 STIFFNESS MATRIX OF THE SYSTEM
C
      DO 115 I=1,7
      II=I
      IF(I.GT.3) II=I+1
      DO 115 J=1,7
      JJ=J
      IF(J.GT.3) JJ=J+1
      IF(COMSGN.EQ.0.0D0) KZ(I,J)=STIF(II,JJ)
      IF(COMSGN.EQ. 1.0D0) KP(I,J)=STIF(II,JJ)
      IF(COMSGN.EQ.-1.0D0) KN(I,J)=STIF(II,JJ)
  115 CONTINUE
      IF(COMSGN.NE.1.0D0) GO TO 120
      COMSGN=-1.0D0
      GO TO 112
  120 CONTINUE
      CALL SETMSG(47,'PLEASE SET THE STEPSIZE TO .005 INCHES. THANKS.')
      CALL PLOT(0.0,-40.0,-3)
      CALL PLOT(1.0,10.0,-3)
      IXSTP=1
      IF(IPLOT.EQ.0) IXSTP=3
      DO 960 IX=1,4,IXSTP
```

```
      DO 145 I=1,14
      UPLUNS(I)=99999.9
      RPMUNS(I)=99999.9
      CRITS1(I)=99999.9
  145 CRITS2(I)=99999.9
C
C   UPLUNS(I): UPPER LIMIT OF UNSTABLE REGION IN GROWTH FACTOR VS. RPM
C   PLOT.RPMUNS(I): BEGINNING OF INSTABILITY IN GROWTH FACTOR VS. RPM
C   PLOT.CRITS1(I): ARRAY OF FIRST ORDER CRITICAL SPEEDS.CRITS2(I): ARRAY
C   OF SECOND ORDER CRITICAL SPEEDS
C
      IF (IX.EQ.1) CD=0.0D0
      IF (IX.EQ.2) CD=1.0D0
      IF (IX.EQ.3) CD=5.0D0
      IF (IX.EQ.4) CD=10.0D0
      CDS=CD
      CDSV(IX)=CD
C
C   THE ONLY NON-ZERO ELEMENT OF THE DAMPING MATRIX IS DEFINED
C
      CE(3,3)=DCMPLX(CD,0.0D0)
      RPM=1.0D0
      DO 800 I=1,501
      IKT=I-1
      IPTST=MOD(IKT,100)
      RAD=RPM*PII/30.0D0
C
C   COMPUTATION OF NON-ZERO ELEMENTS OF THE GYROSCOPIC MATRIX
C
      G(2,2)=IPF*RAD
      G(5,5)=IPIN*RAD
      G(7,7)=IPT*RAD
      DO 240 IM=1,7
      DO 240 IN=1,7
      A1(IM,IN)=G(IM,IN)+INUM* CE(IM,IN)
  240 CONTINUE
      IF(IPLOT.EQ.0) GO TO 180
      COMSGN=1.0D0
      GO TO 180
  175 COMSGN=-1.0D0
  180 CONTINUE
      DO 245 IM=1,7
      DO 245 IN=1,7
      IF(IPLOT.EQ.0) A2(IM,IN)=KZ(IM,IN)
      IF(COMSGN.EQ.1.0D0) A2(IM,IN)=KP(IM,IN)
      IF(COMSGN.EQ.-1.0D0) A2(IM,IN)=KN(IM,IN)
  245 CONTINUE
C
C   MULTYC: SUBROUTINE THAT PERFORMS MATRIX MULTIPLICATIONS
C
      CALL MULTYC(MI,A1,B1,7)
      CALL MULTYC(MI,A2,B2,7)
      DO 250 KD=1,7
```

```
      DO 250 KE=1,14
  250 H(KD,KE)=(0.D0,0.D0)
      DO 260 KD=1,7
      KDD=KD+7
  260 H(KD,KDD)=(1.D0,0.D0)
      DO 270 KD=1,7
      KDD=KD+7
      DO 270 KE=1,7
  270 H(KDD,KE)= B2(KD,KE)
      DO 280 KD=1,7
      KDD=KD+7
      DO 280 KE=1,7
      KEE=KE+7
  280 H(KDD,KEE)= B1(KD,KE)
      IJOB=0
C
C  SEE SUBROUTINE TYPSOL FOR AN EXPLANATION OF THE VARIABLE JEVST.
      JEVST=0
C
C  THE FOLLOWING CALL TO SUBROUTINE TYPSOL WILL CAUSE E-VECTORS TO BE
C  COMPUTED AT VARIOUS SPEEDS.THE SPEEDS CHOSEN ARE OBTAINED FROM AN
C  INITIAL RUN WITHOUT THIS CALL INCLUDED.THE SPEEDS INDICATED BY TYPSOL
C  ARE CONSERVATIVE,I.E. LOW,ESTIMATES OF THE ACTUAL CRITICAL SPEEDS
C  CORRESPONDING TO THE MATHEMATICAL MODEL OF THE PROBLEM
C
      CALL TYPSOL(I,IJOB,JEVST,IPLOT,IDAMP)
C
C   EIGCC: IMSL SUBROUTINE FOR COMPLEX VALUED EIGENVALUES/VECTORS.H IS
C   THE MATRIX FOR WHICH EIGENVALUES ARE TO BE DETERMINED
C
      CALL EIGCC(H,14,14,IJOB,W,Z,14,WK1,IER)
      DO 290 IP=1,14
  290 CPM(IP)=W(IP)*30.0D0/PII
C
C  THE FOLLOWING LOOP ORDERS THE COMPUTED EIGENVALUES SUCH THAT R(1)>R(2) ,
C  . . >R(14), WHERE R(1) IS THE REAL PART OF CPM(1). IN ADDITION, THE
C  E-VECTORS ARE ALSO CORRESPONDINGLY ORDERED
C
      SI=(0.0D0,0.0D0)
      DO 320 JJ=1,13
      S=SI
      DO 310 J=1,13
      R(J)=DREAL(CPM(J))
      R(J+1)=DREAL(CPM(J+1))
      IF (R(J).GE.R(J+1)) GO TO 310
      S=CPM(J)
      CPM(J)=CPM(J+1)
      CPM(J+1)=S
      IF(IJOB.EQ.0) GO TO 310
      DO 300 JK=1,7
      SE(JK)=Z(JK,J)
      Z(JK,J)=Z(JK,J+1)
      Z(JK,J+1)=SE(JK)
  300 CONTINUE
```

```
  310 CONTINUE
      SR=DREAL(S)
      IF (SR.EQ.0.0) GO TO 325
  320 CONTINUE
  325 IF(IPLOT.EQ.0) GO TO 380
      IF(COMSGN.LT.0.0D0) GO TO 350
C
C  IF COMSGN IS POSITIVE THE E-VALUES AND E-VECTORS ARE PLACED IN
C  TEMPORARY STORAGE
C
      DO 340 IN=1,14
      CPMT(IN)=CPM(IN)
      IF(IJOB.EQ.0) GO TO 340
      DO 330 IM=1,7
  330 ZT(IM,IN)=Z(IM,IN)
  340 CONTINUE
      GO TO 175
C
C  IN THE FOLLOWING LOOP, CPM(IN) AND Z(IM,IN) CORRESPOND TO COMSGN=-1.0.
C  IF RPM IS NOT > DREAL(CPM(IN)),THE VALUES OBTAINED FOR COMSGN=+1.0
C  ARE SUBSTITUTED FOR CPM(IN) AND Z(IM,IN)
C
  350 DO 370 IN=1,14
      IF(RPM.GT.DREAL(CPM(IN))) GO TO 370
      CPM(IN)=CPMT(IN)
      IF(IJOB.EQ.0) GO TO 370
      DO 360 IM=1,7
  360 Z(IM,IN)=ZT(IM,IN)
  370 CONTINUE
  380 IF (IJOB.EQ.0) GO TO 710
C
C  THE FOLLOWING LOOP NORMALIZES EACH E-VECTOR.
C
      DO 410 J=1,14
      ZMAX=(0.0D0,0.0D0)
      DO 390 JK=1,7
      DZMAX=CDABS(ZMAX)
      IF(CDABS(Z(JK,J)).LE.DZMAX) GO TO 390
      ZMAX=Z(JK,J)
  390 CONTINUE
      DO 400 JK=1,7
  400 Z(JK,J)=Z(JK,J)/ZMAX
  410 CONTINUE
      PRINT 420,RPM,CD
  420 FORMAT('1',14X,'AT',D14.6,' RPM',10X,'*****   CD =',F6.2,'   *****'
     *,//)
      PRINT 440
  440 FORMAT(2X,2(13X,'EIGENVECTOR',3X,'CORRESPONDING TO',3X,'EIGENVALUE
     *',8X),/)
      DO 500 LV=1,14,2
C
C  ONLY THE FIRST SEVEN ELEMENTS OF EACH E-VECTOR CORRESPOND TO THE
C  GENERALIZED DISPLACEMENT Q-VECTOR
```

```
      DO 480 KV=1,7
      IF (KV.EQ.1) PRINT 450,Z(KV,LV),CPM(LV),Z(KV,LV+1),CPM(LV+1)
      IF (KV.NE.1) PRINT 460,Z(KV,LV),Z(KV,LV+1)
  450 FORMAT(5X,2(2X,2D13.4,2X,2D17.8))
  460 FORMAT(5X,2(2X,2D13.4,36X))
  480 CONTINUE
      PRINT 490
  490 FORMAT(//)
  500 CONTINUE
      PRINT 510
  510 FORMAT(////)
  540 IF(CD.GT.0.0D0) GO TO 710
      IF(IPLOT.EQ.1.OR.IDAMP.NE.0) GO TO 710
      CALL PLOT(0.0,6.75,-3)
C
C  THE FOLLOWING LOOP PLOTS THE MODE SHAPES FOR ROTATIONAL SPEEDS
C  INDICATED BY THE SUBROUTINE TYPSCL
C
      DO 700 JX=1,4
      IF(JX.EQ.2.OR.JX.EQ.4) CALL PLOT(0.0,-4.75,-3)
      IF(JX.EQ.3) CALL PLOT(8.00,4.75,-3)
      JST=JSTART(JX)
      JND=JEND(JX)
      DO 670 J=JST,JND
      DO 650 JK=1,7
  650 EV(JK)=DREAL(Z(JK,J))
      IAXIS=0
      IF(J.EQ.JND) IAXIS=1
      MM=MMV(J)
      CALL MODLUM(EV,MM,IAXIS)
      IF(J.EQ.7) CALL LEGND1
      IF(J.EQ.11) CALL LEGND2
      IF(J.EQ.3) CALL LEGND3
      IF(J.EQ.14) CALL LEGND4
      IF(J.EQ.JND) CALL LEGND7(RPM)
  670 CONTINUE
  700 CONTINUE
      CALL PLOT(10.0,-2.00,-3)
  710 CONTINUE
      RPM2=2.0D0*RPM
C
C  RCPM, ICPM, AND OM ARE REAL*4 VECTORS REQUIRED FOR THE PLOTTING
C  ROUTINES
C
      DO 750 M=1,14
      IDAT=I+(M-1)*501
      IDATP=IDAT-1
      A=DREAL(CPM(M))
      IF (M.GT.7) A=-A
      IF (A.LT.1.0) A=1.0
      RCPM(IDAT)=A
      OM(IDAT)=RPM
C
C   FIRST ORDER CRITICAL SPEEDS CALCULATED USING SUBROUTINE CRITCL
```

```
      IF (A.LE.RPM .AND.CRITS1(M).GT.99999.0) CALL CRITCL(OM(IDATP),OM(
     *IDAT),RCPM(IDATP),RCPM(IDAT),1.0,CRITS1(M))
C
C   DETERMINATION OF SECOND ORDER CRITICAL SPEEDS USING CRITCL
C
      IF (A.LE.RPM2.AND.CRITS2(M).GT.99999.0) CALL CRITCL(OM(IDATP),OM(
     *IDAT),RCPM(IDATP),RCPM(IDAT),2.0,CRITS2(M))
      B=DIMAG(CPM(M))
      BN=-B
      IF(ABS(BN).LT.1.0E-10) BN=0.0
C
C   CALCULATION OF BEGINNING OF INSTABILITY BY CRITCL
C
      IF(BN.GT.0.0.AND.RPMUNS(M).GT.99999.0) CALL CRITCL(OM(IDATP),OM(ID
     *AT),BNP(M),BN,0.0,RPMUNS(M))
C
C   UPPER INSTABILITY LIMIT IS FOUND BY USING SUBROUTINE CRITCL
C
      IF(BN.GT.0.0) UPLUNS(M)=88888.8
      IF(BN.LT.0.0.AND.UPLUNS(M).EQ.88888.8)  CALL CRITCL(OM(IDATP),OM(
     *IDAT),BNP(M),BN,0.0,UPLUNS(M))
      BNP(M)=BN
      IF(IX.EQ.1) ICPMA1(IDAT)=BN
      IF(IX.EQ.2) ICPMA2(IDAT)=BN
      IF(IX.EQ.3) ICPMA3(IDAT)=BN
      IF(IX.EQ.4) ICPMA4(IDAT)=BN
      IF (BN.GT.200.0) BN=200.0
      IF (BN.LT.-200.0) BN=-200.0
      IF (IX.EQ.1) ICPM1(IDAT)=BN
      IF (IX.EQ.2) ICPM2(IDAT)=BN
      IF (IX.EQ.3) ICPM3(IDAT)=BN
      IF (IX.EQ.4) ICPM4(IDAT)=BN
      IF (BN.GT.0.0.AND.RPMUNS(M).EQ.99999.9) RPMUNS(M)=RPM
  750 CONTINUE
      RPM=10.0**(I*0.01)
  800 CONTINUE
      PRINT 910,CD
  910 FORMAT('1',61X,'CD =',F6.2,//)
      PRINT 912
  912 FORMAT(11X,'RPM AT ONSET OF UNSTABLE MOTION',12X,'FIRST ORDER CRIT
     *ICAL SPEEDS',14X,'SECOND ORDER CRITICAL SPEEDS',/)
      PRINT 915
  915 FORMAT(1X,3(10X,'BRANCH    RETROGRADE    FORWARD'))
      DO 940 M=1,7
      PRINT 930,M,RPMUNS(M+7),RPMUNS(8-M),M,CRITS1(M+7),CRITS1(8-M),M,
     *CRITS2(M+7),CRITS2(8-M)
  930 FORMAT(1X,3(13X,I1,7X,F7.1,6X,F7.1))
  940 CONTINUE
      PRINT 941
  941 FORMAT(//,11X,'UPPER LIMIT ON UNSTABLE MOTION(RPM)')
      PRINT 942
  942 FORMAT(/,11X,'BRANCH     RETROGRADE     FORWARD')
      DO 944 M=1,7
      PRINT 943,M,UPLUNS(M+7),UPLUNS(8-M)
  943 FORMAT(14X,I1,7X,F7.1,6X,F7.1)
  944 CONTINUE
```

```
      PRINT 945
  945 FORMAT(//,11X,'NOTE:  IF 99999.9 APPEARS IN ABOVE TABLE, NO INSTAB
     *ILITY OR CRITICAL',/,18X,'SPEED WAS ENCOUNTERED WITHIN SPEED RANGE
     * 0.0 TO 100000.0 RPM.',/,18X,'88888.8 IMPLIES THAT INSTABILITY UPP
     *ER LIMIT IS AT LEAST UPTO 100000.0 RPM.')
C
C   BEGINNING OF WHIRL DIAGRAM PLOTS
C
      OM(7015)=1.0
      OM(7016)=1.5
      RCPM(7015)=1.0
      RCPM(7016)=1.5
      CALL FACTOR(1.30)
      IF(IPLOT.EQ.1) GO TO 960
      DO 955 I=1,3
      ISTART=6514
      ISTOP=0
      IF (I.EQ.2) ISTOP=3507
      IF (I.EQ.3) ISTART=3007
      CALL LAXIS(0.0,0.0,'WHIRLING FREQUENCY, CPM',23,10.5,90.0,RCPM(701
     *5),RCPM(7016))
      CALL LAXIS(0.0,0.0,'ROTATIONAL SPEED, RPM',-21,7.5,0.0,OM(7015),OM
     *(7016))
      KK=ISTART
  950 DOM1=OM(KK+501)
      DOM2=OM(KK+502)
      DRC1=RCPM(KK+501)
      DRC2=RCPM(KK+502)
      OM(KK+501)=OM(7015)
      OM(KK+502)=OM(7016)
      RCPM(KK+501)=RCPM(7015)
      RCPM(KK+502)=RCPM(7016)
      CALL LINE(OM(KK),RCPM(KK),501,1,0,0,3)
      OM(KK+501)=DOM1
      OM(KK+502)=DOM2
      RCPM(KK+501)=DRC1
      RCPM(KK+502)=DRC2
      KK=KK-501
      IF (KK.GT.ISTOP) GO TO 950
      CALL LAXIS(0.0,10.5,' ',1,-7.5,0.0,OM(7015),OM(7016))
      CALL LAXIS(7.5,0.0,' ',-1,-10.5,90.0,RCPM(7015),RCPM(7016))
      CALL PLOT(0.0,0.0,3)
      CALL DASH(7.5,7.5,4)
      Y1=DLOG10(2.0D0)*1.5
      Y2=Y1+7.5
      CALL PLOT(0.0,Y1,3)
      CALL DASH(7.5,Y2,4)
      CALL SYMBOL(2.90,-1.70,0.16,'C D =',0.0,5)
      CALL NUMBER(999.,-1.70,0.16,CDS,0.0,2)
      CALL LEGND5(RPOIVS,4.80,-1.70,IDAMP)
      IF (I.EQ.2) CALL SYMBOL(2.20,11.30,.20,'NEGATIVE BRANCHES',0.,17)
      IF (I.EQ.3) CALL SYMBOL(2.20,11.30,.20,'POSITIVE BRANCHES',0.,17)
      CALL PLOT(13.0,0.0,-3)
  955 CONTINUE
```

```
C  THE FOLLOWING CARDS THROUGH 960 WILL CAUSE A SMALL PORTION OF THE
C  FORWARD WHIRLING MAP TO BE ENLARGED AND PLOTTED SEPARATELY.
C
      OM(7015)=8.0E3
      OM(7016)=6.0
      RCPM(7015)=2.0E4
      RCPM(7016)=6.0
      ISTART=2506
      ISTOP=0
      DO 956 I=1,3006
      IF(RCPM(I).LT.2.0E4) RCPM(I)=2.0E4
      IF(RCPM(I).GT.2.0E5) RCPM(I)=2.0E5
      IF(OM(I).LT.8.0E3) OM(I)=8.0E3
  956 IF(OM(I).GT.8.0E4) OM(I)=8.0E4
      CALL LAXIS(0.0,0.0,'WHIRLING FREQUENCY, CPM',23,6.0,90.0,RCPM(7015
     *),RCPM(7016))
      CALL LAXIS(0.0,0.0,'ROTATIONAL SPEED, RPM',-21,6.0,0.0,OM(7015),OM
     *(7016))
      KK=ISTART
  958 OM(KK+501)=OM(7015)
      OM(KK+502)=OM(7016)
      RCPM(KK+501)=RCPM(7015)
      RCPM(KK+502)=RCPM(7016)
      CALL LINE(OM(KK),RCPM(KK),501,1,0,0,3)
      KK=KK-501
      IF (KK.GT.ISTOP) GO TO 958
      CALL LAXIS(0.0,6.0,' ',1,-6.0,0.0,OM(7015),OM(7016))
      CALL LAXIS(6.0,0.0,' ',-1,-6.0,90.0,RCPM(7015),RCPM(7016))
      CALL SYMBOL(1.90,-1.70,0.16,'C D =',0.0,5)
      CALL NUMBER(999.,-1.70,0.16,CDS,0.0,2)
      CALL LEGND5(RPDIVS,3.80,-1.70,IDAMP)
      CALL PLOT(12.0,0.0,-3)
      IF(IX.EQ.1.OR.IX.EQ.3) CALL PLOT(-51.0,20.0,-3)
      IF(IX.EQ.2) CALL PLOT(3.0,-20.0,-3)
  960 CONTINUE
      IF (IPLOT.EQ.0) GO TO 990
      DO 975 M=5,7
      IF(M.EQ.1) PRINT 961
      IF(M.EQ.2) PRINT 962
      IF(M.EQ.3) PRINT 963
      IF(M.EQ.4) PRINT 964
      IF(M.EQ.5) PRINT 965
      IF(M.EQ.6) PRINT 966
      IF(M.EQ.7) PRINT 967
  961 FORMAT('1',1X,'****  7TH FORWARD BRANCH:  GROWTH FACTORS (IN CPM)'
     *,//)
  962 FORMAT('1',1X,'****  6TH FORWARD BRANCH:  GROWTH FACTORS (IN CPM)'
     *,//)
  963 FORMAT('1',1X,'****  5TH FORWARD BRANCH:  GROWTH FACTORS (IN CPM)'
     *,//)
  964 FORMAT('1',1X,'****  4TH FORWARD BRANCH:  GROWTH FACTORS (IN CPM)'
     *,//)
  965 FORMAT('1',1X,'****  3TH FORWARD BRANCH:  GROWTH FACTORS (IN CPM)'
     *,//)
  966 FORMAT('1',1X,'****  2TH FORWARD BRANCH:  GROWTH FACTORS (IN CPM)'
     *,//)
```

```
  967 FORMAT('1',1X,'****  1TH FORWARD BRANCH:  GROWTH FACTORS (IN CPM)'
     *,//)
      PRINT 970,(CDSV(IX),IX=1,4)
  970 FORMAT(13X,'RPM',4X,4(11X,'CD =',F5.2),/)
      DO 975 I=1,501,10
      IDAT=I+(M-1)*501
      PRINT 974,OM(IDAT),ICPMA1(IDAT),ICPMA2(IDAT),ICPMA3(IDAT),ICPMA4(I
     *DAT)
  974 FORMAT(1X,5E20.5)
  975 CONTINUE
C
C   BEGINNING OF GROWTH FACTOR PLOTS
C
      RCPM(7015)=10.0
      ICPM1(7015)=-200.0
      ICPM2(7015)=-200.0
      ICPM3(7015)=-200.0
      ICPM4(7015)=-200.0
      ICPM1(7016)=50.0
      ICPM2(7016)=50.0
      ICPM3(7016)=50.0
      ICPM4(7016)=50.0
C
C  TO HAVE ALL GROWTH FACTOR PLOTS SET ISTART=6514, ISTOP=0.  IF ONLY THE
C  FIRST THREE FORWARD BRANCHES ARE DESIRED,SET ISTART=3007,ISTOP=2004
C
      ISTART=6514
      ISTOP=0
      KK=ISTART
      I=1
  980 OM(KK+501)=OM(7015)
      OM(KK+502)=OM(7016)
      ICPM1(KK+501)=ICPM1(7015)
      ICPM2(KK+501)=ICPM2(7015)
      ICPM3(KK+501)=ICPM3(7015)
      ICPM4(KK+501)=ICPM4(7015)
      ICPM1(KK+502)=ICPM1(7016)
      ICPM2(KK+502)=ICPM2(7016)
      ICPM3(KK+502)=ICPM3(7016)
      ICPM4(KK+502)=ICPM4(7016)
      CALL AXIS(0.,0.,'       GROWTH FACTOR',19,8.,90.,ICPM1(7015),ICPM1(
     *7016))
      CALL LAXIS(0.0,0.0,'ROTATIONAL SPEED, RPM',-21,7.5,0.0,OM(7015),OM
     *(7016))
      CALL LINE(OM(KK),ICPM1(KK),501,1,100,1,2)
      CALL LINE(OM(KK),ICPM2(KK),501,1,100,2,2)
      CALL LINE(OM(KK),ICPM3(KK),501,1,100,3,2)
      CALL LINE(OM(KK),ICPM4(KK),501,1,100,4,2)
      CALL AXIS(7.5,0.0,' ',-1,8.00,90.0,ICPM1(7015),ICPM1(7016))
      CALL LAXIS(0.0,8.0,' ',1,-7.5,0.0,OM(7015),OM(7016))
      CALL LEGND5(RPDIVS,0.45,7.20,IDAMP)
      CALL LEGND6(0.45,6.88,0.16,CDSV,KK)
      CALL PLOT(0.0,8.0,-3)
```

```
      J=MOD(I,2)
      IF (J.EQ.0) GO TO 982
      CALL PLOT(0.0,7.0,-3)
      GO TO 985
  982 CALL PLOT(15.0,-23.0,-3)
      I=0
  985 KK=KK-501
      I=I+1
      IF(KK.GT.ISTOP) GO TO 980
  990 CALL PLOT(0.0,0.0,999)
      STOP
      END



      SUBROUTINE COMPLI(ALPH,COMSGN)
      IMPLICIT REAL*8(A-H,O-Z)
      REAL*8 IA(3),K(3),KEQ
      REAL*8 IEQ,LAC,L3,LA,LB,LC,LG
      REAL*8 KB,KSL,KSU
      COMPLEX*16 ALPH(8,8),EI(3),E,G,KAG(3),INUM
      COMPLEX*16 FAC1,FAC2
      DIMENSION AREA(3),DIN(3),DOUT(3)
C
C   ER,GR: REAL PARTS OF THE COMPLEX YOUNG'S AND SHEAR MODULI
C
C   DOUT AND DIN ARE SHAFT OUTER AND INNER DIAMETER DATA RESPECTIVELY
C   DOUT(3) AND DIN(3) ARE THOSE OF THE TURBINE SHAFT
C
C   K(1),K(2),K(3): SHEAR CORRECTION FACTORS.K(3) IS THAT OF THE
C   TURBINE SHAFT
C   KEQ:  SHEAR CORRECTION FACTOR OF THE EQUIVALENT QUILL SHAFT
C   INSIDE THE TURBINE SHAFT
C
C   LAC: ACTUAL LENGTH OF QUILL SHAFT INSIDE TURBINE SHAFT
C
C   L3,LA,LB,LC,LG,A1,A2,A3,A4: LENGTHS DEFINED IN APPENDIX A1
C
C   T3,TS: DIMENSIONS ON THE INTERMEDIATE MASS.SEE FIG.A1
C
C
C   GAMAS: LOSS TANGENT FOR STEEL
C
C  L3  . . . DIST. FROM THE CENTER OF UPPER BEARING TO BEGINNING OF
C  LOWER BEARING
C   LA . . . DIST. FROM THE UPPER BARING CENTER (UBC) TO END OF INTER-
C  MEDIATE MASS
C  LB . . . DIST. FROM UBC TO THE BEGINNING OF DAMPER
C  LC . . . DIST. FROM UBC TO DAMPER END
C  LG . . . DIST. FROM UBC TO FLYWHEEL SHAFT END
C  A1 . . . DIST. FROM UBC TO INTERMEDIATE MASS CG
C  A2 . . . DIST. FROM UBC TO DAMPER  CG
C  A3 . . . DIST. FROM UBC TO FLYWHEEL CG
C  A4 . . . SEPARATION OF THE TWO BEARING CENTERS
```

```
      COMMON/MAIN1/TD,TF,TT1
      CCMMON/MAIN2/LB,LG,L3
C
C
      DATA ER,GR/29.5D06,11.5D06/
      DATA DOUT/0.3125D0,0.3125D0,0.7493D0/
      DATA DIN/2*0.0D0,0.3175D0/
      DATA K,KEQ/2*0.885D0,0.6569D0,0.885D0/
      DATA LAC,LA,LC/3.5969D0,2.9784D0,7.324D0/
      DATA T3,TS/0.4352D0,0.2431D0/
      DATA KSU,KSL/2*2.0D06/
      DATA A1,A2,A3,A4/2.5621D0,5.4908D0,11.2195D0,2.37D0/
      DATA GAMAS/0.005D0/
C
C
C
      PII=2.0*DARSIN(1.0D0)
      INUM=(0.0D0,1.0D0)
      E=(1.0D0+COMSGN*INUM*GAMAS)*ER
      G=(1.0D0+COMSGN*INUM*GAMAS)*GR
C
C   AREAS AND MOMENTS OF INERTIA OF SHAFT SECTIONS 1 & 2 AND
C   THAT OF TURBINE SHAFT ARE CALCULATED
C
      DO 30 J=1,3
      AREA(J)=PII*(DOUT(J)**2-DIN(J)**2)/4.0
      IA(J)=  PII*(DOUT(J)**4-DIN(J)**4)/64.0
   30 CONTINUE
C
C   CALCULATION OF DIAMETER AND AREA OF EQUIVALENT QUILL SHAFT
C   INSIDE TURBINE SHAFT
C
      IEQ=IA(2)*(L3/LAC)**4
      DEQ=(64.0*IEQ/PII)**0.25
      AEQ=PII*DEQ**2/4.0
C
C   K(3),AREA(3),IA(3) ARE  NEWLY DEFINED FOR THE EQUIVALENT SECTION
C   CONTAINING BOTH THE TURBINE SHAFT AND FLYWHEEL SHAFT
C
      K(3)=(KEQ*AEQ+K(3)*AREA(3))/(AEQ+AREA(3))
      AREA(3)=AREA(3)+AEQ
      IA(3)=IA(3)+IEQ
      DO 40 I=1,3
   40 KAG(I)=K(I)*AREA(I)*G
      DO 45 I=1,3
   45 EI(I)=E*IA(I)
      A1A4=1.0-A1/A4
      A2A4=1.0-A2/A4
      A3A4=1.0-A3/A4
      TTA4=1.0+TT1/A4
      A4S=A4**2
      FAC1=1.0/KAG(3)+L3**2/(3.0*EI(3))
      FAC2=1.0/(KAG(3)*A4)-L3*(0.5-L3/(3.0*A4))/EI(3)
      FAC3=A3/(A4S*KSL)-A3A4/(KSU*A4)
```

```
      FAC4=(1.0/KSU+1.0/KSL)/A4S
      FAC5=A2/(A4S*KSL)-A2A4/(A4*KSU)
      FAC6=A1/(A4S*KSL)-A1A4/(A4*KSU)
C
C   COMPUTATION OF COMPLIANCE MATRIX
C
      ALPH(1,1)=L3*A3A4**2*FAC1+(LB-LA)/KAG(2)+(A3*(LB-LA)*(A3-LE-LA)+(L
     *B**3-LA**3)/3.0)/EI(2)+(LG-LC)/KAG(1)+(A3*(LG-LC)*(A3-LG-LC)+(LG**
     *3-LC**3)/3.0)/EI(1)+A3A4**2/KSL+(A3/A4)**2/KSL
      ALPH(1,2)=-L3*A3A4/A4*FAC1+(LB-LA)*(A3-(LB+LA)/2.0)/EI(2)+(LG-LC)*
     *(A3-(LG+LC)/2.0)/EI(1)+FAC3
      ALPH(1,3)=L3*A3A4*A2A4*FAC1+(LB-LA)/KAG(2)+((LE-LA)*(A2*A3-(LB+LA)
     */2.0*(A2+A3))+(LB**3-LA**3)/3.0)/EI(2)+A2A4*A3A4/KSU+A2*A3/(KSL*
     *A4S)
      ALPH(1,4)=-L3*A3A4/A4*FAC1+(LB-LA)*(A3-(LB+LA)/2.0)/EI(2)+FAC3
      ALPH(1,5)=L3*A3A4*A1A4*FAC1+A1A4*A3A4/KSU+A1*A3/(KSL*A4S)
      ALPH(1,6)=-L3*A3A4/A4*FAC1+FAC3
      ALPH(1,7)=L3*A3A4*TT1*FAC2+TTA4*A3A4/KSU-TT1*A3/(KSL*A4S)
      ALPH(1,8)=-L3*A3A4*FAC2+FAC3
      ALPH(2,2)=L3/A4**2*FAC1+(LB-LA)/EI(2)+(LG-LC)/EI(1)+FAC4
      ALPH(2,3)=-L3*A2A4/A4*FAC1+(LB-LA)*(A2-(LB+LA)/2.0)/EI(2)-A2A4/(
     *A4*KSU)+A2/(KSL*A4S)
      ALPH(2,4)=L3/A4**2*FAC1+(LB-LA)/EI(2)+FAC4
      ALPH(2,5)=-L3*A1A4/A4*FAC1-A1A4/(KSU*A4)+A1/(KSL*A4S)
      ALPH(2,6)=L3/A4**2*FAC1+FAC4
      ALPH(2,7)=-L3*TT1/A4*FAC2-TTA4/(KSU*A4)-TT1/(A4S*KSL)
      ALPH(2,8)=L3/A4*FAC2+FAC4
      ALPH(3,3)=L3*A2A4**2*FAC1+(LB-LA)/KAG(2)+(A2*(LB-LA)*(A2-LE-LA)+(L
     *B**3-LA**3)/3.0)/EI(2)+A2A4**2/KSU+(A2/A4)**2/KSL
      ALPH(3,4)=ALPH(2,3)
      ALPH(3,5)=L3*A2A4*A1A4*FAC1+A1A4*A2A4/KSU+A1*A2/(A4S*KSL)
      ALPH(3,6)=-L3*A2A4/A4*FAC1+FAC5
      ALPH(3,7)=L3*A2A4*TT1*FAC2+A2A4*TTA4/KSU-A2*TT1/(A4S*KSL)
      ALPH(3,8)=-L3*A2A4*FAC2+FAC5
      ALPH(4,4)=L3/A4**2*FAC1+(LB-LA)/EI(2)+FAC4
      ALPH(4,5)=ALPH(2,5)
      ALPH(4,6)=ALPH(2,6)
      ALPH(4,7)=ALPH(2,7)
      ALPH(4,8)=ALPH(2,8)
      ALPH(5,5)=L3*A1A4**2*FAC1+A1A4**2/KSU+(A1/A4)**2/KSL
      ALPH(5,6)=-L3*A1A4/A4*FAC1+FAC6
      ALPH(5,7)=L3*TT1*A1A4*FAC2+A1A4*TTA4/KSU-TT1*A1/(A4S*KSL)
      ALPH(5,8)=-L3*A1A4*FAC2+FAC6
      ALPH(6,6)=ALPH(2,6)
      ALPH(6,7)=ALPH(2,7)
      ALPH(6,8)=ALPH(2,8)
      ALPH(7,7)=TT1**2*L3*(FAC2/A4+(1.0-L3/(2.0*A4))/EI(3))+TTA4**2/KSU+
     *(TT1/A4)**2/KSL
      ALPH(7,8)=-TT1*L3*(FAC2/A4+(1.0-L3/(2.0*A4))/EI(3))-TTA4/(A4*KSU)-
     *TT1/(A4S*KSL)
      ALPH(8,8)=L3*(FAC2/A4+(1.0-L3/(2.0*A4))/EI(3))+FAC4
      DO 80 J=1,8
      DO 80 M=J,8
      ALPH(M,J)=ALPH(J,M)
   80 CONTINUE
      RETURN
      END
```

```
      SUBROUTINE MULTYC(A,B,C,N)
      COMPLEX*16 A(N,N),B(N,N),C(N,N)
      DO 5 I=1,N
      DO 5 J=1,N
      C(I,J)=(0.D0,0.D0)
      DO 5 K=1,N
    5 C(I,J)=C(I,J)+A(I,K)*B(K,J)
      RETURN
      END



      SUBROUTINE CRITCL(X1,X2,Y1,Y2,ORDER,CRVALU)
C
C  THIS SUBROUTINE COMPUTES THE X-COORDINATE OF THE INTERSECTION OF TWO
C  STRAIGHT LINES. THE FIRST STAIGHT LINE IS THAT CONNECTING THE POINTS
C  X1,Y1 TO X2,Y2. THE SECOND STRAIGHT LINE IS Y = ORDER * X.
C
      IMPLICIT REAL*4(A-H,O-Z)
      SLOPE=(Y2-Y1)/(X2-X1)
      CRVALU=(Y1-SLOPE*X1)/(ORDER-SLOPE)
      RETURN
      END



      SUBROUTINE TYPSOL(I,IJOB,JEVST,IPLOT,IDAMP)
C
C  THE VARIABLE JEVST INDICATES WHICH CRITICAL SPEED IS CURRENTLY BEING
C  CONSIDERED.  FIRST ORDER FORWARD CRITICALS FOR 7F THRU 1F HAVE JEVST
C  1 THRU 7 RESPECTIVELY.  THAT IS, JEVST CORRESPONDS TO THE ORDERING OF
C  CRITICALS FROM HIGHEST TO LOWEST.  THUS, FIRST ORDER RETROGRADE
C  CRITICALS FOR 1R THRU 7R HAVE JEVST 8 THRU 14 RESPECTIVELY.(RECALL
C  THAT RETROGRADE CRITICALS ARE NEGATIVE).FOR SECOND ORDER CRITICALS,
C  ADD 14 TO THE ABOVE JEVST VALUES
C
C  OBVIOUSLY A RUN MUST BE ACCOMPLISHED WITH IJOB=0 TO OBTAIN THE CRITICAL
C  SPEEDS REFERRED TO BY THE VARIABLE I.
C
      IMPLICIT REAL*4(A-H,O-Z)
      JEVST=0
      IF(I.EQ.302) JEVST=7
C
C  SINCE MODE SHAPES ARE PLOTTED ONLY FOR IPLOT=0 AND IDAMP=0, E-VECTORS
C  FOR SECOND ORDER CRITICAL SPEEDS ARE NOT EVEN COMPUTED UNLESS MODE
C  SHAPES ARE TO BE PLOTTED
C
      IF(IPLOT.EQ.1.OR.IDAMP.NE.0) GO TO 20
      IF(I.EQ.244) JEVST=21
      IF(I.EQ.421) JEVST=20
      IF(I.EQ.463) JEVST=19
      IF(I.EQ.481) JEVST=18
```

```
   20 IF(JEVST.NE.0) IJCB=1
C
C  NOTE:  THIS SUBROUTINE DOES NOT ALLOW FOR THE POSSIBILITY THAT TWO (OR
C  MORE) CRITICAL SPEEDS MAY OCCUR AT THE SAME ROTATIONAL SPEED.IF THIS
C  WERE  TO OCCUR,CHOOSE HIGHER OR LOWER VALUES OF THE VARIABLE'I' SO
C  THAT NO TWO VALUES OF 'I' ABOVE ARE EQUAL.THIS WILL ONLY AFFECT THE
C  MODE SHAPE AND THE DIFFERENCE SHOULD BE SLIGHT
C
      RETURN
      END



      SUBROUTINE MODLUM(EV,MM,IAXIS)
      IMPLICIT REAL*4(A-H,O-Z)
      DIMENSION EV(7),XV(5),YV(5)
C
C   T2: DIMENSION ON INTERMEDIATE MASS.SEE FIG.A1
C   SOME OF THE VARIABLES USED IN THIS SUBROUTINE ARE DEFINED AS:
C      R1 . . . RADIUS OF TURBINE (NOT TO SCALE)
C      R4 . . . RADIUS OF FLYWHEEL RIM (NOT TO SCALE)
C      AL2. . . AXIAL LENGTH OF DAMPER (=2.0*TD/3.0)
C      AL3. . . AXIAL LENGTH FROM END OF FLYWHEEL SHAFT TO FLYWHEEL CG
C      (=TF/3.0)
C      S12. . . AXIAL LENGTH FROM TURBINE C.G. TO UPPER END OF DAMPER
C      ALEN . . AXIAL LENGTH FROM TURBINE C.G. TO FLYWHEEL CG WHERE
C        ABOVE AXIAL LENGTHS HAVE BEEN SCALED TO 1/3 ACTUAL SIZE
C      EV(J). . THE EIGENVECTOR REPRESENTING THE MODE SHAPE TO BE DRAWN
C      ORIGIN,STEP . . ARE REQUIRED BY THE LIBRARY SUBROUTINE LINE
C      XV(J),YV(J) . . COORDINATES OF POINTS TO BE PLOTTED
C
C
C
      COMMON/MODLM1/R1,R4
      COMMON/MODLM2/ORIGIN,STEP
      COMMON/MODLM3/AL2,AL3,S12,S11,ALEN,PI,XFB
C
C
      DATA TT1,T2,T3/0.8942,0.4163,0.4352/
C
C
C
      CALL FACTOR(2.00)
C
C  THE FOLLOWING MULTIPLIER CAUSES MAXIMUM DISPLACEMENTS TO APPEAR
C  IN THE PLOT AS 3/4 INCHES
C
      DSCALE=0.75
      DO 10 J=1,7
   10 EV(J)=EV(J)*DSCALE
C
C  DUE TO THE 1/3 SCALING, TILTING ANGLES MUST BE MULTIPLIED BY 3 TO BE
C  CONSISTENT.
```

```
      EV(2)=EV(2)*3.0
      EV(5)=EV(5)*3.0
      EV(7)=EV(7)*3.0
C
C  THE FOLLOWING CARDS (THROUGH 20) INSURE THAT THE MAXIMUM TILTING
C  ANGLE WILL BE PI/6 RADIANS OR LESS
C
      EVM2=ABS(EV(2))
      EVM5=ABS(EV(5))
      EVM7=ABS(EV(7))
      PHIMAX=AMAX1(EVM2,EVM5,EVM7)
      IF(PHIMAX.LT.PI/6.0) GO TO 30
      DO 20 J=1,7
   20 EV(J)=EV(J)*PI/(6.0*PHIMAX)
C
C  IT IS POSSIBLE THAT THE HUB-FLYWHEEL SHAFT ATTACHMENTPOINT WILL HAVE
C  THE MAX.DISPLACEMENT. THE FOLLOWING STATEMENTS (THROUGH 40) LIMIT
C  THIS HUB DISPLACEMENT TO APPROXIMATELY 3/4 INCHES
C
   30 AHFA=ABS(EV(1)-AL3*SIN(EV(2)))
      IF(AHFA.LT.0.75) GO TO 50
      DO 40 J=1,7
   40 EV(J)=EV(J)*0.75/AHFA
C
C  THE FOLLOWING CARDS (THROUGH 90) CAUSE THE MODE SHAPES OF ODD-NUMBERED
C  BRANCHES TO BE PLOTTED PRIMARILY IN THE UPPER HALF-PLANE AND THOSE OF
C  EVEN-NUMBERED BRANCHES IN THE LOWER HALF-PLANE
C
   50 IMM=MOD(MM,2)
      IF(MM.GT.7) GO TO 70
      IF(IMM.NE.0) GO TO 90
      DO 60 J=1,7
   60 EV(J)=-EV(J)
      GO TO 90
C
C  NOTE THAT RETROGRADE BRANCHES 1 THRU 7 ARE ASSOCIATED WITH MM VALUES OF
C  8 THRU 14 RESPECTIVELY
C
   70 IF(IMM.EQ.0) GO TO 90
      DO 80 J=1,7
   80 EV(J)=-EV(J)
   90 CONTINUE
      XV(4)=ORIGIN
      YV(4)=ORIGIN
      XV(5)=STEP
      YV(5)=STEP
C
C  COMPUTE POINTS DEPICTING THE DISPLACED TURBINE
C
      XV(1)=-R1*SIN(EV(7))
      YV(1)=R1*COS(EV(7))+EV(6)
      XV(2)=0.0
      YV(2)=EV(6)
      XV(3)=-XV(1)
```

```
      YV(3)=-R1*COS(EV(7))+EV(6)
      CALL LINE(XV,YV,3,1,1,MM)
      CALL PLOT(XV(2),YV(2),3)
      TT=TT1/3.0
      TTY=TT*SIN(EV(7))+EV(6)
      CALL PLOT(TT,TTY,2)
      CALL SYMBOL(TT,TTY,0.08,MM,0.0,-1)
      CALL PLOT(TT,TTY,3)
      XV(3)=ORIGIN
      YV(3)=ORIGIN
      XV(4)=STEP
      YV(4)=STEP
C
C  COMPUTE POINTS TO PLOT INTERMEDIATE MASS
C
      AXLIN=(T2+T3)/3.0
      XV(1)=S11
      YV(1)=EV(4)-T3/3.0*SIN(EV(5))
      XV(2)=S11+AXLIN
      YV(2)=EV(4)+T2/3.0*SIN(EV(5))
      CALL DASH(XV(1),YV(1),12)
      CALL LINE(XV,YV,2,1,1,MM)
      CALL PLOT(XV(2),YV(2),3)
C
C  COMPUTE POINTS DEPICTING THE DISPLACED DAMPER
C
      XV(1)=S12
      YV(1)=EV(3)
      XV(2)=XV(1)+AL2
      YV(2)=YV(1)
      CALL DASH(XV(1),YV(1),12)
      CALL LINE(XV,YV,2,1,1,MM)
      CALL PLOT(XV(2),YV(2),3)
      XV(4)=ORIGIN
      YV(4)=ORIGIN
      XV(5)=STEP
      YV(5)=STEP
C
C  COMPUTE POINTS DEPICTING THE DISPLACED FLYWHEEL
C
      YFB=EV(1)-AL3*SIN(EV(2))
      CALL DASH(XFB,YFB,12)
      CALL SYMBOL(XFB,YFB,0.08,MM,0.0,-1)
      CALL PLOT(XFB,YFB,3)
      XV(1)=ALEN-R4*SIN(EV(2))
      YV(1)=EV(1)+R4*COS(EV(2))
      XV(2)=ALEN
      YV(2)=EV(1)
      XV(3)=ALEN+R4*SIN(EV(2))
      YV(3)=EV(1)-R4*COS(EV(2))
      CALL PLOT(XV(2),YV(2),2)
      CALL LINE(XV,YV,3,1,1,MM)
      CALL PLOT(0.0,0.0,3)
```

```
      IF(IAXIS.EQ.0) GO TO 100
      CALL DASH(ALEN,0.0,4)
      CALL PLOT(0.0,0.0,3)
  100 RETURN
      END



      SUBROUTINE LEGND1
      IMPLICIT REAL*8(A-H,O-Z)
C
C  THIS SUBROUTINE PROVIDES CAPTIONS FOR BRANCHES 1F THROUGH 4F.
C
      CALL FACTOR(2.00)
      CALL SYMBOL(0.0,1.35,.10,'MODE IDENTIFIERS:',0.0,17)
      CALL SYMBOL(1.95,1.40,.10,1,0.0,-1)
      CALL SYMBOL(2.17,1.35,.10,'1F',0.0,2)
      CALL SYMBOL(2.67,1.40,.10,3,0.0,-1)
      CALL SYMBOL(2.89,1.35,.10,'3F',0.0,2)
      CALL SYMBOL(1.95,1.20,.10,2,0.0,-1)
      CALL SYMBOL(2.17,1.15,.10,'2F',0.0,2)
      CALL SYMBOL(2.67,1.20,.10,4,0.0,-1)
      CALL SYMBOL(2.89,1.15,.10,'4F',0.0,2)
      RETURN
      END



      SUBROUTINE LEGND2
      IMPLICIT REAL*8(A-H,O-Z)
C
C  THIS SUBROUTINE PROVIDES CAPTIONS FOR BRANCHES 1R THROUGH 4R.
C
      CALL FACTOR(2.00)
      CALL SYMBOL(0.0,1.35,.10,'MODE IDENTIFIERS:',0.0,17)
      CALL SYMBOL(1.95,1.40,.10,8,0.0,-1)
      CALL SYMBOL(2.17,1.35,.10,'1R',0.0,2)
      CALL SYMBOL(2.67,1.40,.10,10,0.0,-1)
      CALL SYMBOL(2.89,1.35,.10,'3R',0.0,2)
      CALL SYMBOL(1.95,1.20,.10,9,0.0,-1)
      CALL SYMBOL(2.17,1.15,.10,'2R',0.0,2)
      CALL SYMBOL(2.67,1.20,.10,11,0.0,-1)
      CALL SYMBOL(2.89,1.15,.10,'4R',0.0,2)
      RETURN
      END



      SUBROUTINE LEGND3
      IMPLICIT REAL*8(A-H,O-Z)
C
C  THIS SUBROUTINE PROVIDES CAPTIONS FOR BRANCHES 5F THROUGH 7F.
```

```
      CALL FACTOR(2.00)
      CALL SYMBOL(0.0,1.35,.10,'MODE IDENTIFIERS:',0.0,17)
      CALL SYMBOL(1.95,1.40,.10,5,0.0,-1)
      CALL SYMBOL(2.17,1.35,.10,'5F',0.0,2)
      CALL SYMBOL(2.67,1.40,.10,7,0.0,-1)
      CALL SYMBOL(2.89,1.35,.10,'7F',0.0,2)
      CALL SYMBOL(1.95,1.20,.10,6,0.0,-1)
      CALL SYMBOL(2.17,1.15,.10,'6F',0.0,2)
      RETURN
      END



      SUBROUTINE LEGND4
      IMPLICIT REAL*8(A-H,O-Z)
C
C  THIS SUBROUTINE PROVIDES CAPTIONS FOR BRANCHES 5R THROUGH 7R.
C
      CALL FACTOR(2.00)
      CALL SYMBOL(0.0,1.35,.10,'MODE IDENTIFIERS:',0.0,17)
      CALL SYMBOL(1.95,1.40,.10,12,0.0,-1)
      CALL SYMBOL(2.17,1.35,.10,'5R',0.0,2)
      CALL SYMBOL(2.67,1.40,.10,14,0.0,-1)
      CALL SYMBOL(2.89,1.35,.10,'7R',0.0,2)
      CALL SYMBOL(1.95,1.20,.10,13,0.0,-1)
      CALL SYMBOL(2.17,1.15,.10,'6R',0.0,2)
      RETURN
      END



      SUBROUTINE LEGND7(RPM)
      IMPLICIT REAL*8(A-H,O-Z)
      REAL*4 RS
      RS=RPM
C
C  SINCE A CAPITAL OMEGA IS NOT AN AVAILABLE CHARACTER, SPACE IS LEFT FOR
C  MANUAL INSERTION.
C
      CALL SYMBOL(1.77,-1.35,.12,'= ',0.0,2)
      CALL NUMBER(999.,-1.35,.12,RS,0.0,2)
      CALL SYMBOL(999.,-1.35,.12,' RPM',0.0,4)
      CALL PLOT(0.0,0.0,3)
      RETURN
      END



      SUBROUTINE LEGND5(RPDIVS,XCOOR,YCOOR,IDAMP)
      IMPLICIT REAL*4(A-H,O-Z)
```

```
      YPLUS=YCOOR+0.24
      XPLUS=XCOOR+0.48
      IF(IDAMP-1) 10,20,30
   10 CALL SYMBOL(XCOOR,YCOOR,0.16,'NO MATERIAL DAMPING',0.0,19)
      GO TO 40
   20 CALL SYMBOL(XCOOR,YPLUS,0.16,'VISCOUS INTERNAL DAMPING',0.0,24)
      CALL SYMBOL(XPLUS,YCOOR,0.16,'WITH     =',0.0,9)
      CALL NUMBER(999.,YCOOR,0.16,RPDIVS,0.0,-1)
      CALL SYMBOL(999.,YCOOR,0.16,' RPM',0.0,4)
      GO TO 40
   30 CALL SYMBOL(XCOOR,YCOOR,0.16,'COMPLEX STIFFNESS',0.0,17)
   40 RETURN
      END



      SUBROUTINE LEGND6(XCOOR,YCOOR,HGHT,CDSV,KK)
      IMPLICIT REAL*4(A-H,C-Z)
      DIMENSION CDSV(4)
      IF (KK.EQ.6514) CALL SYMBOL(3.53, 9.10,0.16,'7-R',0.0,3)
      IF (KK.EQ.6013) CALL SYMBOL(3.53, 9.10,0.16,'6-R',0.0,3)
      IF (KK.EQ.5512) CALL SYMBOL(3.53, 9.10,0.16,'5-R',0.0,3)
      IF (KK.EQ.5011) CALL SYMBOL(3.53, 9.10,0.16,'4-R',0.0,3)
      IF (KK.EQ.4510) CALL SYMBOL(3.53, 9.10,0.16,'3-R',0.0,3)
      IF (KK.EQ.4009) CALL SYMBOL(3.53, 9.10,0.16,'2-R',0.0,3)
      IF (KK.EQ.3508) CALL SYMBOL(3.53, 9.10,0.16,'1-R',0.0,3)
      IF (KK.EQ.3007) CALL SYMBOL(3.53, 9.10,0.16,'1-F',0.0,3)
      IF (KK.EQ.2506) CALL SYMBOL(3.53, 9.10,0.16,'2-F',0.0,3)
      IF (KK.EQ.2005) CALL SYMBOL(3.53, 9.10,0.16,'3-F',0.0,3)
      IF (KK.EQ.1504) CALL SYMBOL(3.53, 9.10,0.16,'4-F',0.0,3)
      IF (KK.EQ.1003) CALL SYMBOL(3.53, 9.10,0.16,'5-F',0.0,3)
      IF (KK.EQ.502) CALL SYMBOL(3.53, 9.10,0.16,'6-F',0.0,3)
      IF (KK.EQ.1) CALL SYMBOL(3.53, 9.10,0.16,'7-F',0.0,3)
      X1=XCOOR
      Y1=YCOOR
      X2=X1+6.0*HGHT
      X3=X2+12.0*HGHT
      Y2=Y1-2.0*HGHT
      YS1=Y1+HGHT/2.0
      YS2=Y2+HGHT/2.0
      IF(CDSV(1).GT.9.9.OR.CDSV(2).GT.9.9) X3=X3+HGHT
      IF(CDSV(1).GT.99.9.OR.CDSV(2).GT.99.9) X3=X3+HGHT
      CALL SYMBOL(X1,Y1,HGHT,'AND:',0.0,4)
      CALL SYMBOL(X2,YS1,HGHT,1,0.0,-1)
      CALL SYMBOL(999.,Y1,HGHT,' C D =',0.0,6)
      CALL NUMBER(999.,Y1,HGHT,CDSV(1),0.0,2)
      CALL SYMBOL(X3,YS1,HGHT,3,0.0,-1)
      CALL SYMBOL(999.,Y1,HGHT,' C D =',0.0,6)
      CALL NUMBER(999.,Y1,HGHT,CDSV(3),0.0,2)
      CALL SYMBOL(X2,YS2,HGHT,2,0.0,-1)
      CALL SYMBOL(999.,Y2,HGHT,' C D =',0.0,6)
      CALL NUMBER(999.,Y2,HGHT,CDSV(2),0.0,2)
```

```
CALL SYMBOL(X3,YS2,HGHT,4,0.0,-1)
CALL SYMBOL(999.,Y2,HGHT,' C D =',0.0,6)
CALL NUMBER(999.,Y2,HGHT,CDSV(4),0.0,2)
CALL PLOT(0.0,0.0,3)
RETURN
END
```

```
BLOCK DATA
IMPLICIT REAL*8(A-H,O-Z)
REAL*4 R1,R4,ORIGIN,STEP
REAL*8 LB,LG,L3
COMMON/MAIN1/TD,TF,TT1
COMMON/MAIN2/LB,LG,L3
COMMON/MODLM1/R1,R4
COMMON/MODLM2/ORIGIN,STEP
DATA TD,TF,TT1/1.8332D0,3.15D0,0.8942D0/
DATA LB,LG,L3/3.6576D0,8.0695D0,2.1269D0/
DATA R1,R4/0.70,1.20/
DATA ORIGIN,STEP/0.0,1.0/
END
```

C.2 Forced Whirling Using the Lumped Model

The purpose of this computation is to obtain plots of the amplitudes of the various deflections and slopes versus rotational speed, with flywheel mass eccentricity, initial tilt, and the phase angle between them as parameters. The flow chart is shown in Fig. C4, and the CPU time required is only 40 seconds, approximately.

Fig. C4. Flow chart for forced whirling using lumped model.

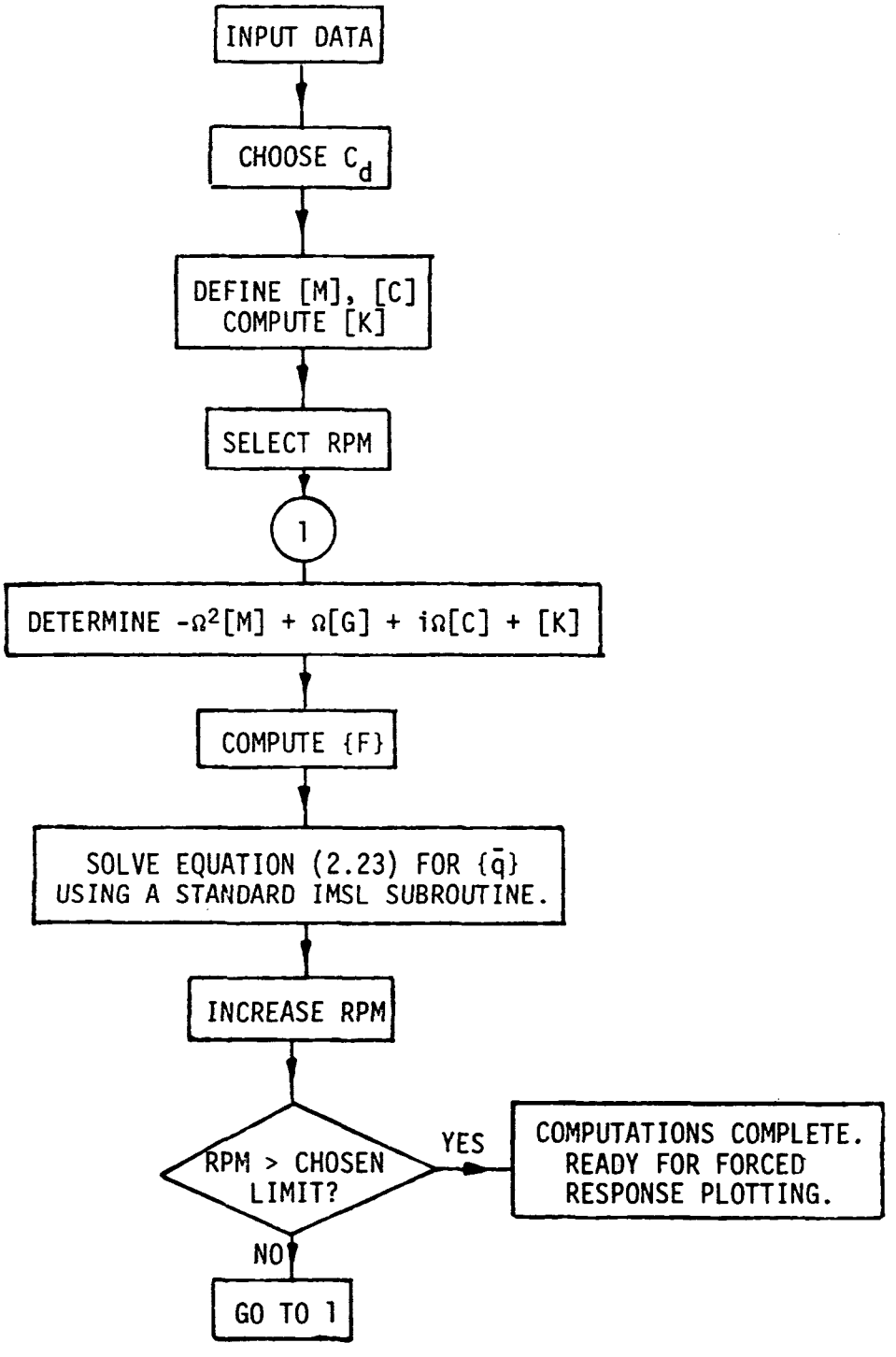

```
C
C        F O R C E D     V I B R A T I O N
C              ( L U M P E D   M O D E L )
C
C  NOTE: THE COMPONENTS OF THE Q VECTOR ARE:
C        (RF,PHIF,RD,RIN,PHIN,RT,PHIT)
C
      IMPLICIT REAL*8(A-H,O-Z)
      DIMENSION AMP(7),ANG(7),YM(7,500),ZM(7,500)
      REAL*4 BETA,ECCEN,PHIZRO,CDP,YVMAX
      REAL*4 XV(502),YV(502),ZV(502)
      REAL*8 MD,MF, MIN,MT,IDF,IPF,IDIN,IPIN,IDT,IPT
      COMPLEX*16 INUM,THETA,ALPH(8,8),F(7),K(7,7),STIF(8,8),S(7,7)
      COMPLEX*16 WA1(80),WA2(8),WA3(63),WA4(7)
C
C   NDEG: NO. OF DEGREES OF FREEDOM OF THE SYSTEM
C
C   BETA: PHASE LAG OF INITIAL TILT FROM MASS ECCENTRICITY
C
C   ECCEN: MASS ECCENTRICITY
C
C   PHIZRO: INITIAL TILT
C
C   REFER TO 'FREE WHIRLING AND STABILITY (LUMPED MODEL)' PROGRAM
C   FOR OTHER DEFINITIONS OF VARIABLES IN THE DATA
C
C   FLYWHEEL DATA IN THIS PROGRAM ARE THOSE OF GARRET
C
C
C
C
      DATA NDEG/7/
      DATA MF,IDF,IPF/0.0951D0,4.83D0,8.517D0/
      DATA MD/0.002998D0/
      DATA MIN,IDIN,IPIN/0.000202D0,1.798D-05,1.15D-05/
      DATA MT,IDT,IPT/0.00479D0,0.003402D0,0.00628D0/
      DATA BETA,ECCEN,PHIZRO/3.1415,0.001,0.0025/
C
C
C
      PII=2.0*DARSIN(1.0D0)
      INUM=(0.0D0,1.0D0)
      COMSGN=0.0
C
C   COMPLI: SUBROUTINE TO CALCULATE THE 8X8 COMPLIANCE MATRIX OF
C   THE SYSTEM
C
      CALL COMPLI(ALPH,COMSGN)
      DO 50 I=1,8
      DO 50 J=1,8
      STIF(I,J)=(0.0D0,0.0D0)
      IF(I.EQ.J) STIF(I,J)=(1.0D0,0.0D0)
   50 CONTINUE
```

```
      INT=0
C
C   LEQ2C: IMSL SUBROUTINE
C
      CALL LEQ2C(ALPH,8,8,STIF,8,8,INT,WA1,WA2,IER)
C
C   COMPUTATION OF THE 7X7 SIFFNESS MATRIX OF THE SYSTEM
C
      DO 60 I=1,7
      II=I
      IF(I.GT.3) II=I+1
      DO 60 J=1,7
      JJ=J
      IF(J.GT.3) JJ=J+1
      S(I,J)=STIF(II,JJ)
   60 CONTINUE
      PRINT 300
  300 FORMAT(5X,'RF(INCHES)',5X,'PHIF(DEG.)',5X,'RD(INCHES)',5X,'RIN(INC
     *HES)',5X,'PHIN(DEG.)',5X,'RT(INCHES)',5X,'PHIT(DEG.)',5X,'RPM',//)
      CD=10.0
      CDP=CD
      RPM=0.0D0
      DO 900 I=1,500
      RPM=RPM+6.0D0
      RAD=RPM*PII/30.
      DO 350 IF=1,NDEG
      F(IF)=(0.D0,0.D0)
  350 CONTINUE
      THETA=INUM*BETA
C
C   COMPUTATION OF THE NON-ZERO TERMS OF FORCING VECTOR
C
      F(1)=ECCEN*MF*RAD**2
      F(2)=PHIZRO*(IDF-IPF)*RAD**2*CDEXP(-THETA)
      DO 360 IX=1,7
      DO 360 IY=1,7
  360 K(IX,IY)=S(IX,IY)
C
C   INCLUSION OF MASS,GYROSCOPIC AND DAMPING MATRICES.CHAPTER 2
C
      K(1,1)=K(1,1)-MF*RAD**2
      K(2,2)=K(2,2)-(IDF-IPF)*RAD**2
      K(3,3)=K(3,3)-MD*RAD**2+INUM*CD*RAD
      K(4,4)=K(4,4)-MIN*RAD**2
      K(5,5)=K(5,5)-(IDIN-IPIN)*RAD**2
      K(6,6)=K(6,6)-MT*RAD**2
      K(7,7)=K(7,7)-(IDT-IPT)*RAD**2
C
C         CALL LEQ2C TO SOLVE LINEAR SIMULTANEOUS EQS.
C
      CALL LEQ2C(K,NDEG,NDEG,F,1,NDEG,0,WA3,WA4,IR)
      DO 400 IP=1,NDEG
      AMP(IP)=CDABS(F(IP))
      YM(IP,I)=AMP(IP)
```

```
      ANG(IP)=0.0
      FIMAG=DIMAG(F(IP))
      FREAL=DREAL(F(IP))
      IF (FIMAG.EQ.0.0.AND.FREAL.EQ.0.0) GO TO 370
      ANG(IP)=-DATAN2(FIMAG,FREAL)*180.0/PII
  370 IF (ANG(IP).LT.0.0) ANG(IP)=ANG(IP)+360.0
      IF (ANG(IP).GT.360.0) ANG(IP)=ANG(IP)-360.0
  400 ZM(IP,I)=ANG(IP)
      PRINT 500,(AMP(L),L=1,NDEG),RPM
  500 FORMAT(4X,8(D11.4,4X),/)
      XV(I)=RPM
  900 CONTINUE
C
C  ALL OF THE FOLLOWING STATEMENTS ARE FOR PLOTTING THE COMPUTED RESULTS.
C
      XV(501)=0.0
      XV(502)=750.0
      YV(501)=0.0
      ZV(501)=0.0
      ZV(502)=180.0
      CALL SETMSG(39,'PLEASE SET THE STEPSIZE TO .005 INCHES.')
      CALL FACTOR(1.3)
      CALL PLOT(0.0,-40.0,-3)
      CALL PLOT(4.0,4.0,-3)
      DO 950 IP=1,NDEG
      IF(IP.EQ.1) CALL PLOT(0.0,16.0,-3)
      IF(IP.EQ.4) CALL PLOT(8.0,9.0,-3)
      IF(IP.NE.1.AND.IP.NE.4) CALL PLOT(0.0,-4.5,-3)
      YV(502)=0.05
      IF(IP.GT.3) YV(502)=0.005
      IF(IP.EQ.1) CALL AXIS(0.0,0.0,'RF (INCHES)',11,2.0,90.0,YV(501),
     *YV(502))
      IF(IP.EQ.2) CALL AXIS(0.0,0.0,'PHIF (RADIANS)',14,2.0,90.0,YV(501)
     *,YV(502))
      IF(IP.EQ.3) CALL AXIS(0.0,0.0,'RD (INCHES)',11,2.0,90.0,YV(501),
     *YV(502))
      IF(IP.EQ.4) CALL AXIS(0.0,0.0,'RIN (INCHES)',12,2.0,90.0,YV(501),
     *YV(502))
      IF(IP.EQ.5) CALL AXIS(0.0,0.0,'PHIN (RADIANS)',14,2.0,90.0,YV(501)
     *,YV(502))
      IF(IP.EQ.6) CALL AXIS(0.0,0.0,'RT (INCHES)',11,2.0,90.0,YV(501),
     *YV(502))
      IF(IP.EQ.7) CALL AXIS(0.0,0.0,'PHIT (RADIANS)',14,2.0,90.0,YV(501)
     *,YV(502))
      CALL AXIS(0.0,0.0,'OMEGA (RPM)',-11,4.0,0.0,XV(501),XV(502))
      YVMAX=2.0*YV(502)
      DO 935 I=1,500
      ZV(I)=ZM(IP,I)
      YV(I)=YM(IP,I)
      IF (YV(I).GT.YVMAX) YV(I)=YVMAX
  935 CONTINUE
      CALL LINE(XV,YV,500,1,0,0)
      CALL DLINE(XV,ZV,500,1,5)
      CALL AXIS(4.5,0.0,'PHASE LAG (DEG.)',-16,2.0,90.0,ZV(501),ZV(502))
```

```
      CALL PLOT(4.0,0.0,3)
      CALL PLOT(4.0,2.0,2)
      CALL PLOT(0.0,2.0,2)
  950 CONTINUE
      CALL PLOT(-8.0,2.0,-3)
      CALL SYMBOL(0.0,0.0,0.125,'OAKRIDGE SYSTEM',0.0,15)
       CALL SYMBOL(0.0,-0.5,0.08,'BETA=',0.0,5)
      CALL NUMBER(999.0,-0.5,0.08,BETA,0.0,4)
      CALL SYMBOL(0.0,-0.7,0.08,'ECCEN=',0.0,6)
      CALL NUMBER(999.0,-0.7,0.08,ECCEN,0.0,4)
       CALL SYMBOL(0.0,-0.9,0.08,'PHIZRO=',0.0,7)
      CALL NUMBER(999.0,-0.9,0.08,PHIZRO,0.0,4)
      CALL SYMBOL(0.0,-1.1,0.08,'CD (LB-SEC/IN)=',0.0,15)
      CALL NUMBER(999.0,-1.1,0.08,CDP,0.0,2)
      CALL PLOT(0.0,0.0,999)
      STOP
      END



      SUBROUTINE COMPLI(ALPH,COMSGN)
      IMPLICIT REAL*8(A-H,O-Z)
      REAL*8 IA(3),K(3),KEQ
      REAL*8 IEQ,LAC,L3,LA,LB,LC,LG
      REAL*8 KB,KSL,KSU
      COMPLEX*16 ALPH(8,8),EI(3),E,G,KAG(3),INUM
      COMPLEX*16 FAC1,FAC2
      DIMENSION AREA(3),DIN(3),DOUT(3)
C
C
      DATA ER,GR/29.5D06,11.5D06/
      DATA DOUT/0.3125D0,0.3125D0,0.7493D0/
      DATA DIN/2*0.0D0,0.3175D0/
      DATA K,KEQ/2*0.885D0,0.6569D0,0.885D0/
      DATA TD,TF,TT1/1.8332D0,7.05D0,0.8942D0/
      DATA LB,LG,L3/3.6576D0,8.0695D0,2.1269D0/
      DATA LAC,LA,LC/3.5969D0,2.9784D0,7.324D0/
      DATA T3,TS/0.4352D0,0.2431D0/
      DATA KSU,KSL/2*2.0D06/
      DATA A1,A2,A3,A4/2.5621D0,5.4908D0,15.1195D0,2.37D0/
      DATA GAMAS/0.005D0/
C
C
      PII=2.0*DARSIN(1.0D0)
      INUM=(0.0D0,1.0D0)
      E=(1.0D0+COMSGN*INUM*GAMAS)*ER
      G=(1.0D0+COMSGN*INUM*GAMAS)*GR
      DO 30 J=1,3
      AREA(J)=PII*(DOUT(J)**2-DIN(J)**2)/4.0
      IA(J)=  PII*(DOUT(J)**4-DIN(J)**4)/64.0
   30 CONTINUE
      IEQ=IA(2)*(L3/LAC)**4
      DEQ=(64.0*IEQ/PII)**0.25
      AEQ=PII*DEQ**2/4.0
```

```
      K(3)=(KEQ*AEQ+K(3)*AREA(3))/(AEQ+AREA(3))
      AREA(3)=AREA(3)+AEQ
      IA(3)=IA(3)+IEQ
      DO 40 I=1,3
40    KAG(I)=K(I)*AREA(I)*G
      DO 45 I=1,3
45    EI(I)=E*IA(I)
      A1A4=1.0-A1/A4
      A2A4=1.0-A2/A4
      A3A4=1.0-A3/A4
      TTA4=1.0+TT1/A4
      A4S=A4**2
      FAC1=1.0/KAG(3)+L3**2/(3.0*EI(3))
      FAC2=1.0/(KAG(3)*A4)-L3*(0.5-L3/(3.0*A4))/EI(3)
      FAC3=A3/(A4S*KSL)-A3A4/(KSU*A4)
      FAC4=(1.0/KSU+1.0/KSL)/A4S
      FAC5=A2/(A4S*KSL)-A2A4/(A4*KSU)
      FAC6=A1/(A4S*KSL)-A1A4/(A4*KSU)
      ALPH(1,1)=L3*A3A4**2*FAC1+(LB-LA)/KAG(2)+(A3*(LB-LA)*(A3-LB-LA)+(L
     *B**3-LA**3)/3.0)/EI(2)+(LG-LC)/KAG(1)+(A3*(LG-LC)*(A3-LG-LC)+(LG**
     *3-LC**3)/3.0)/EI(1)+A3A4**2/KSU+(A3/A4)**2/KSL
      ALPH(1,2)=-L3*A3A4/A4*FAC1+(LB-LA)*(A3-(LB+LA)/2.0)/EI(2)+(LG-LC)*
     *(A3-(LG+LC)/2.0)/EI(1)+FAC3
      ALPH(1,3)=L3*A3A4*A2A4*FAC1+(LB-LA)/KAG(2)+((LB-LA)*(A2*A3-(LB+LA)
     */2.0*(A2+A3))+(LB**3-LA**3)/3.0)/EI(2)+A2A4*A3A4/KSU+A2*A3/(KSL*
     *A4S)
      ALPH(1,4)=-L3*A3A4/A4*FAC1+(LB-LA)*(A3-(LB+LA)/2.0)/EI(2)+FAC3
      ALPH(1,5)=L3*A3A4*A1A4*FAC1+A1A4*A3A4/KSU+A1*A3/(KSL*A4S)
      ALPH(1,6)=-L3*A3A4/A4*FAC1+FAC3
      ALPH(1,7)=L3*A3A4*TT1*FAC2+TTA4*A3A4/KSU-TT1*A3/(KSL*A4S)
      ALPH(1,8)=-L3*A3A4*FAC2+FAC3
      ALPH(2,2)=L3/A4**2*FAC1+(LB-LA)/EI(2)+(LG-LC)/EI(1)+FAC4
      ALPH(2,3)=-L3*A2A4/A4*FAC1+(LB-LA)*(A2-(LB+LA)/2.0)/EI(2)-A2A4/(
     *A4*KSU)+A2/(KSL*A4S)
      ALPH(2,4)=L3/A4**2*FAC1+(LB-LA)/EI(2)+FAC4
      ALPH(2,5)=-L3*A1A4/A4*FAC1-A1A4/(KSU*A4)+A1/(KSL*A4S)
      ALPH(2,6)=L3/A4**2*FAC1+FAC4
      ALPH(2,7)=-L3*TT1/A4*FAC2-TTA4/(KSU*A4)-TT1/(A4S*KSL)
      ALPH(2,8)=L3/A4*FAC2+FAC4
      ALPH(3,3)=L3*A2A4**2*FAC1+(LB-LA)/KAG(2)+(A2*(LB-LA)*(A2-LB-LA)+(L
     *B**3-LA**3)/3.0)/EI(2)+A2A4**2/KSU+(A2/A4)**2/KSL
      ALPH(3,4)=ALPH(2,3)
      ALPH(3,5)=L3*A2A4*A1A4*FAC1+A1A4*A2A4/KSU+A1*A2/(A4S*KSL)
      ALPH(3,6)=-L3*A2A4/A4*FAC1+FAC5
      ALPH(3,7)=L3*A2A4*TT1*FAC2+A2A4*TTA4/KSU-A2*TT1/(A4S*KSL)
      ALPH(3,8)=-L3*A2A4*FAC2+FAC5
      ALPH(4,4)=L3/A4**2*FAC1+(LB-LA)/EI(2)+FAC4
      ALPH(4,5)=ALPH(2,5)
      ALPH(4,6)=ALPH(2,6)
      ALPH(4,7)=ALPH(2,7)
      ALPH(4,8)=ALPH(2,8)
      ALPH(5,5)=L3*A1A4**2*FAC1+A1A4**2/KSU+(A1/A4)**2/KSL
      ALPH(5,6)=-L3*A1A4/A4*FAC1+FAC6
      ALPH(5,7)=L3*TT1*A1A4*FAC2+A1A4*TTA4/KSU-TT1*A1/(A4S*KSL)
```

```
      ALPH(5,8)=-L3*A1A4*FAC2+FAC6
      ALPH(6,6)=ALPH(2,6)
      ALPH(6,7)=ALPH(2,7)
      ALPH(6,8)=ALPH(2,8)
      ALPH(7,7)=TT1**2*L3*(FAC2/A4+(1.0-L3/(2.0*A4))/EI(3))+TTA4**2/KSU+
     *(TT1/A4)**2/KSL
      ALPH(7,8)=-TT1*L3*(FAC2/A4+(1.0-L3/(2.0*A4))/EI(3))-TTA4/(A4*KSU)-
     *TT1/(A4S*KSL)
      ALPH(8,8)=L3*(FAC2/A4+(1.0-L3/(2.0*A4))/EI(3))+FAC4
      DO 80 J=1,8
      DO 80 M=J,8
      ALPH(M,J)=ALPH(J,M)
80    CONTINUE
      RETURN
      END
```

C.3 Free Whirling Analysis Using the Combined Model

Notes:

1) The relation $\omega = n\Omega$ defines the order of the whirling critical speeds. Positive n denotes forward whirling speeds and negative n denotes retrograde whirling speeds. For example, n = 1 denotes a first-order forward whirling speed, n = -2 denotes a second-order retrograde whirling speed.

2) In the program there are in total 200 n-lines, beginning at $n = 10^4$ and ending with $n = 10^{-3.56}$. The same 200 lines are used for both forward and retrograde branches.

3) Initially, the $n = 10^4$ line is chosen. Rotational speed Ω(RPM) is varied from some initial value in steps of $\Delta\Omega(\Delta RPM)$. Each time, the complex determinant value of $[\bar{C}]$ is found. By some initial runs the values of the complex determinant of $[\bar{C}]$ should be determined to see which of the real and imaginary parts is the most significant number. Any sign change in the significant part of the determinant while changing Ω(RPM) in steps, signals that the det $[\bar{C}]$ will become zero between the values of Ω(RPM) which produced the sign changes. Using this technique and narrowing down $\Delta\Omega(\Delta RPM)$ to required accuracy, the critical speeds corresponding to the required number of forward branches are found for $n = 10^4$. Now n is changed to -10^4. Assuming the same initial value for Ω(RPM) and $\Delta\Omega(\Delta RPM)$, the corresponding retrograde-branch critical speeds are determined.

4) From numerous previous investigations [8,18,19], it is known that the forward whirling speeds increase and the retrograde ones decrease as the shaft running speed is increased. This knowledge is utilized in determining critical speeds of the forward and retrograde branches on an n-line when the critical speeds of the corresponding branches on a previous n-line are known as explained in Figs. C5 and C6.

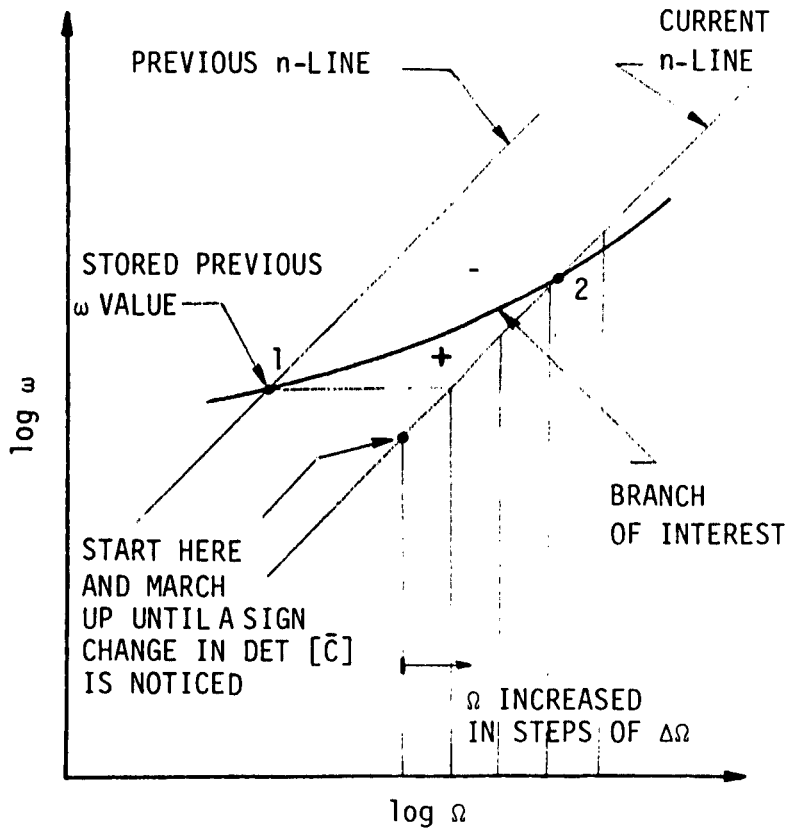

Fig. C5. Determination of the critical speed on a forward branch (point 2) along an n-line when the critical speed on a previous n-line (point 1) for the same branch is known. Positive and negative signs denote the signs of det [C̄]. These are arbitrary and are shown only to emphasize the idea of a sign change across a branch.

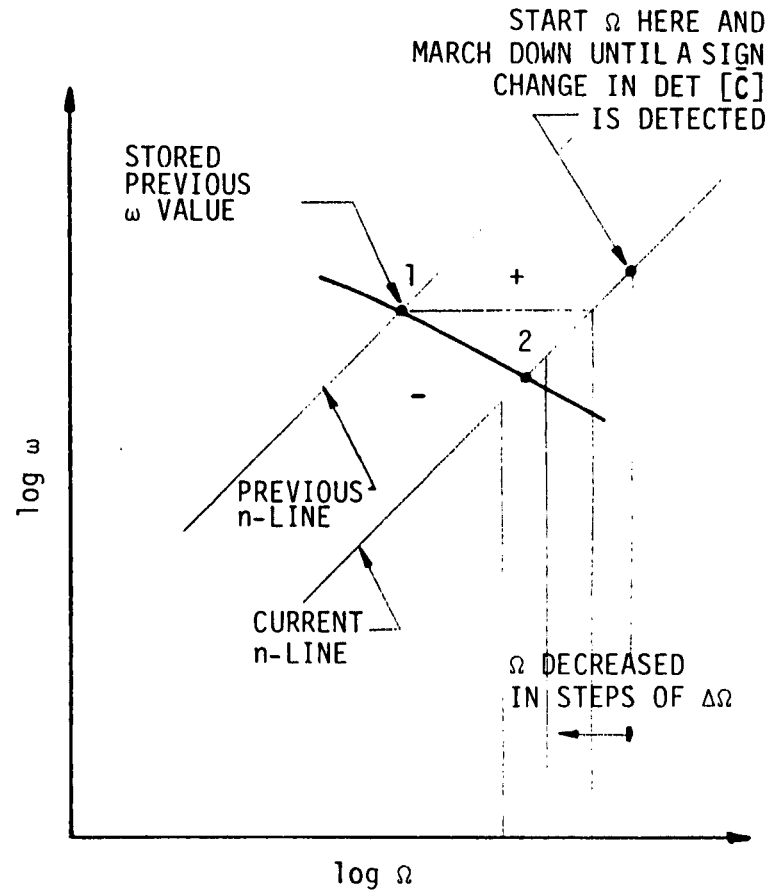

Fig. C6. Determination of the critical speed on a retrograde branch (point 2) along an n-line when the critical speed on a previous n-line (point 1) for the same branch is known. Positive and negative signs denote the signs of det [C̄]. These are arbitrary and are shown only to emphasize the idea of a sign change across a branch.

5) Thus, having obtained the critical speeds at $n = \pm 10^4$, one generates the whole whirling plot by decreasing n to $\pm 10^{-3.56}$ in steps and repeatedly applying the ideas in item 4, above. The plotter performs plotting essentially by joining the adjacent points by straight lines.

6) The program calculates the critical speeds corresponding to the lowest four forward and retrograde branches. The forward branches from the lowest to the highest are numbered from 1 to 4 and the retrograde branches from the lowest to the highest from 5 to 8.

7) Since the ideas expressed in Figs. C5 and C6 are used in locating critical speeds on a branch, a problem arises (close to the point of intersection) when two consecutive branches approach each other for intersection. This is shown in an exaggerated sense in Figs. C7 and C8. An arbitrary set of sign changes across the branches is shown in the figures. Note that while marching up, from point 1 or 2, a sign change in $\det[\bar{C}]$ is detected only once. Thus, the actual intersection point is shifted to point 3. For ease of computation and plotting, a switch in branch names is carried out after an intersection of two consecutive forward branches (see Fig. C8). Imagine points 5 and 6 to be lying on the $n = 1$ line ($\omega = \Omega$ line). Let branch A (before intersection) represent the branch corresponding to the second forward mode and branch B (before intersection) that of the third forward mode. When a flywheel is run through a spin test, the critical speed corresponding to point 5 will be observed before that of point 6 despite the fact that point 5 belongs to a third-mode motion of the system. Notice that, by experiment, point 5 will be called the second first-order forward critical speed. Once point 5 has been determined, the starting place for point 6 lies beyond that

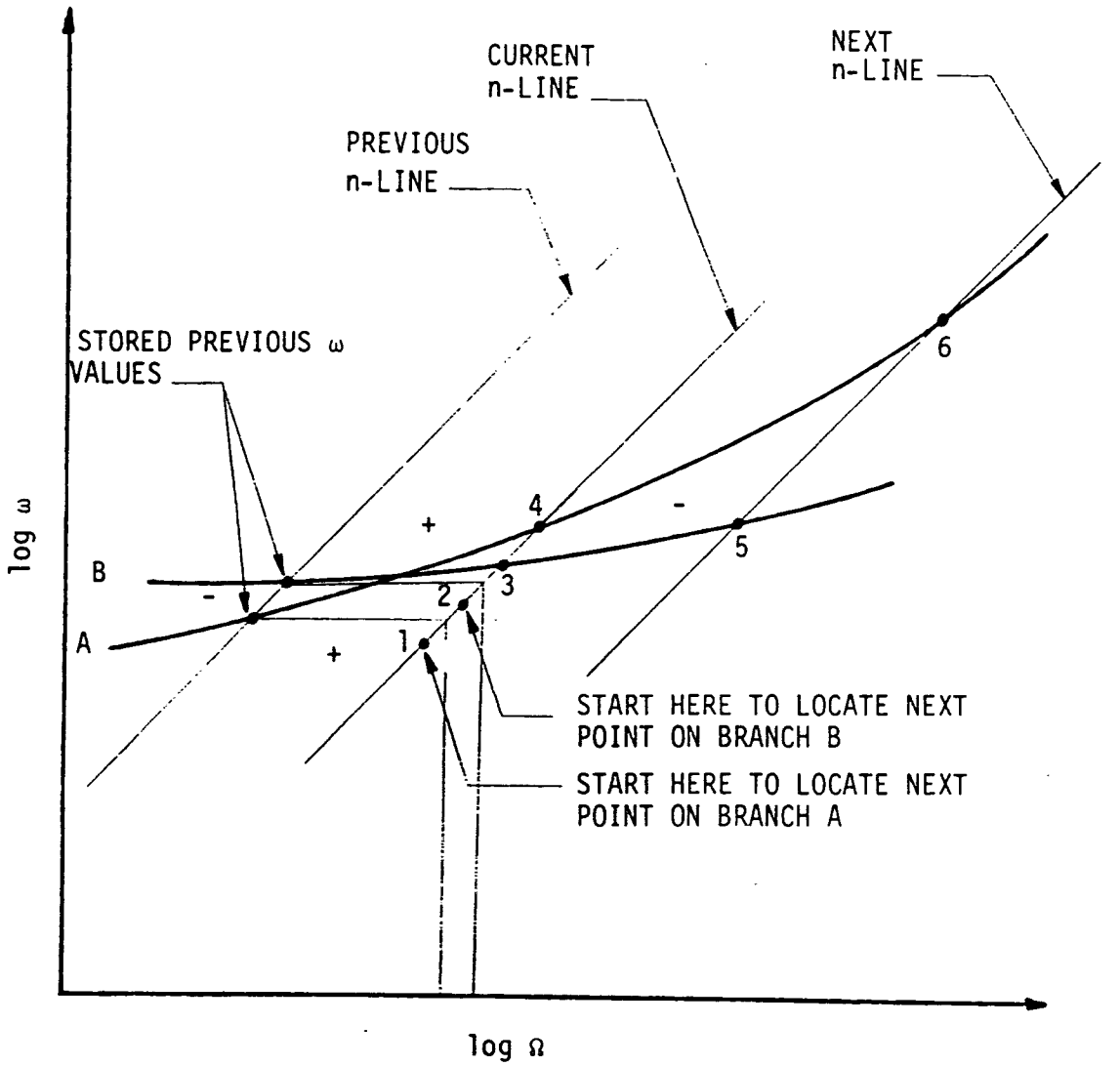

Fig. C7. A true magnified picture of what happens near the point of intersection of two forward branches. Points 1 and 2 are the starting points for branches A and B, respectively. The points to be located are 3 and 4 on the current n-line and 5 and 6 on the next n-line.

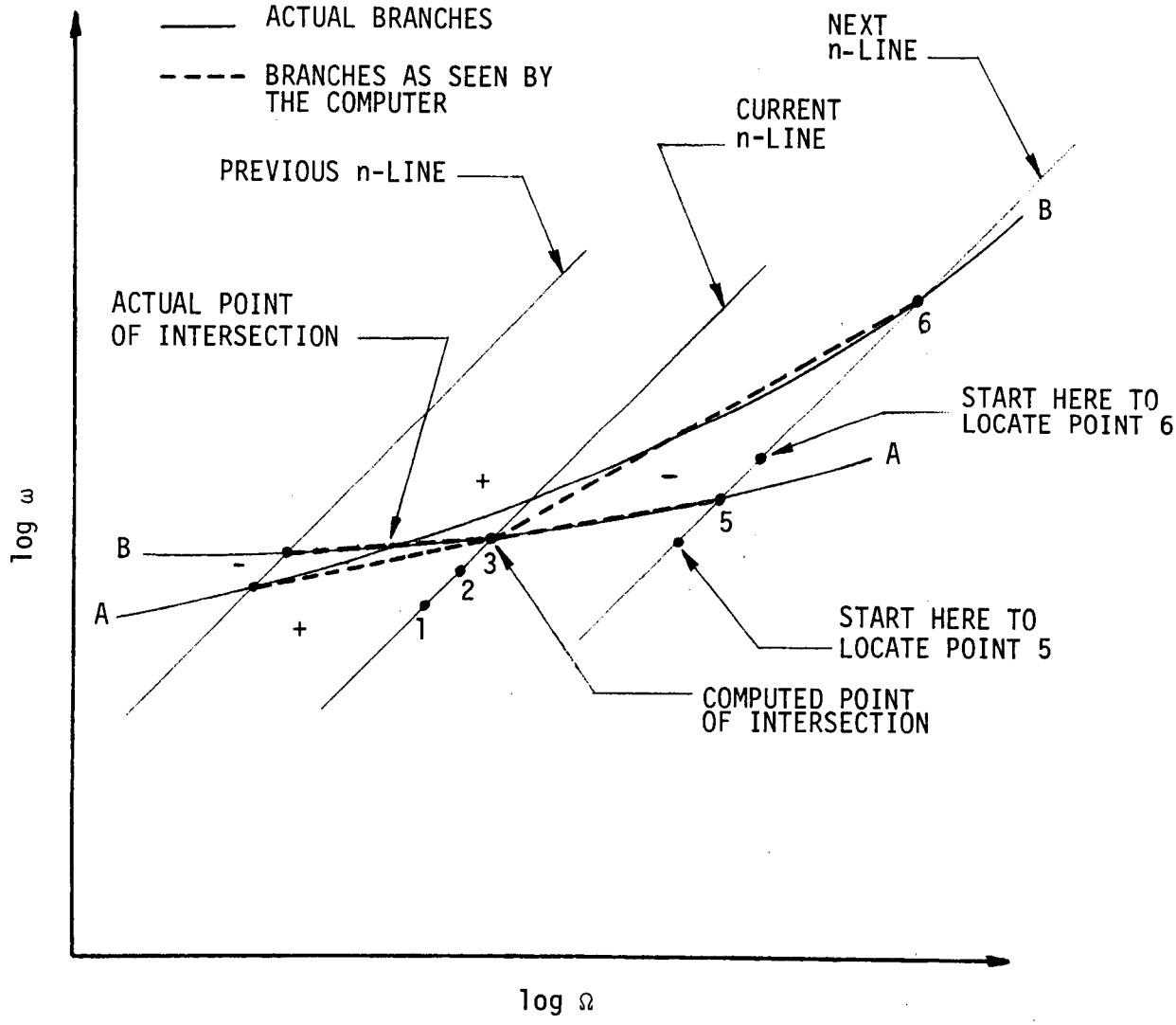

Fig. C8. Diagram showing the actual branch intersection and the computed branch intersection. Immediately after intersection, point 5 is located by the usual way as explained in Fig. C5. But point 6 is located by using a higher value from that of point 5.

of point 5 as shown in Fig. C8. Thus, when the computer senses that two consecutive branches have the same critical-speed value, the above changes automatically come into play in the actual program.

8) The logic of the program is explained in a flow chart shown in Fig. C9. For clarity, in this flow chart, it is assumed that no two consecutive forward branches intersect.

9) It is possible that one of the forward branches may become parallel to one of the n-lines. What is actually drawn in such a case is explained in Fig. C10.

10) This program requires about 62 minutes of CPU time.

11) The input data used for the Oak Ridge system in the analysis by the combined model are presented in Table B-1.

Fig. C9. Flow chart for free whirling analysis by the combined model.

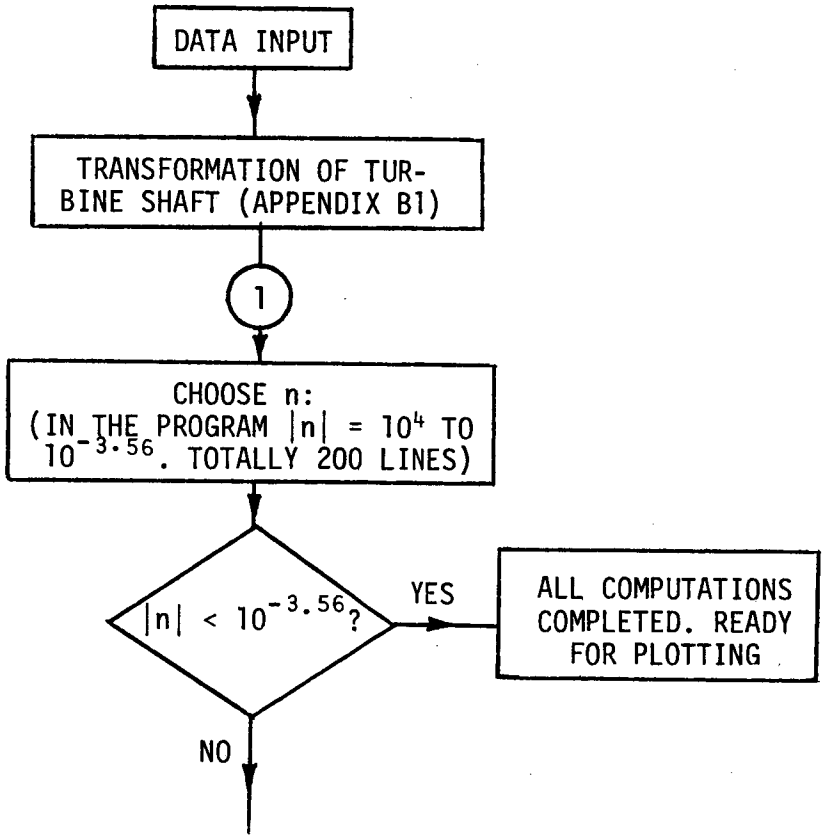

Continued on next page

Fig. C9 (continued)

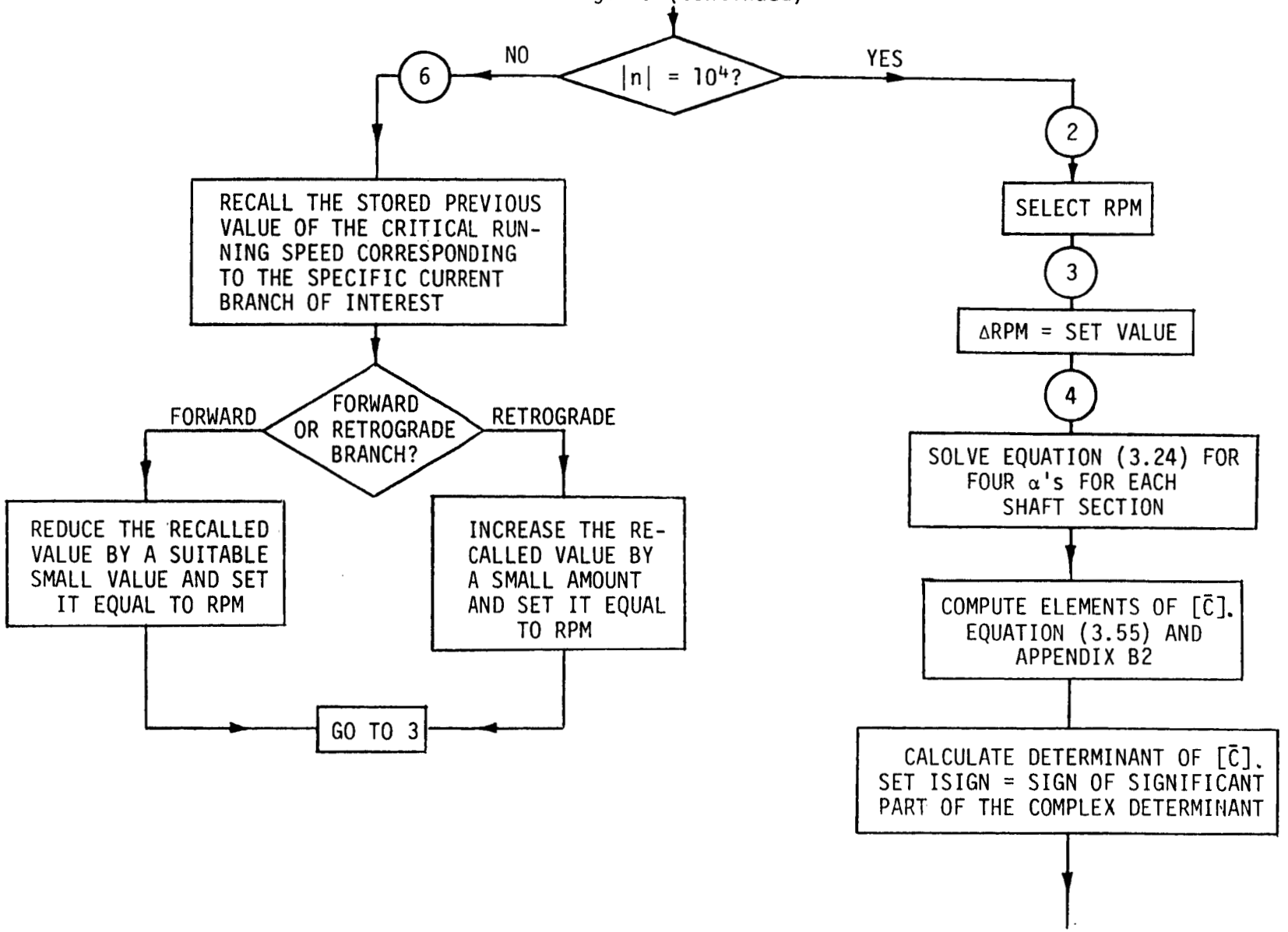

Continued on next page

Fig. C9 (continued)

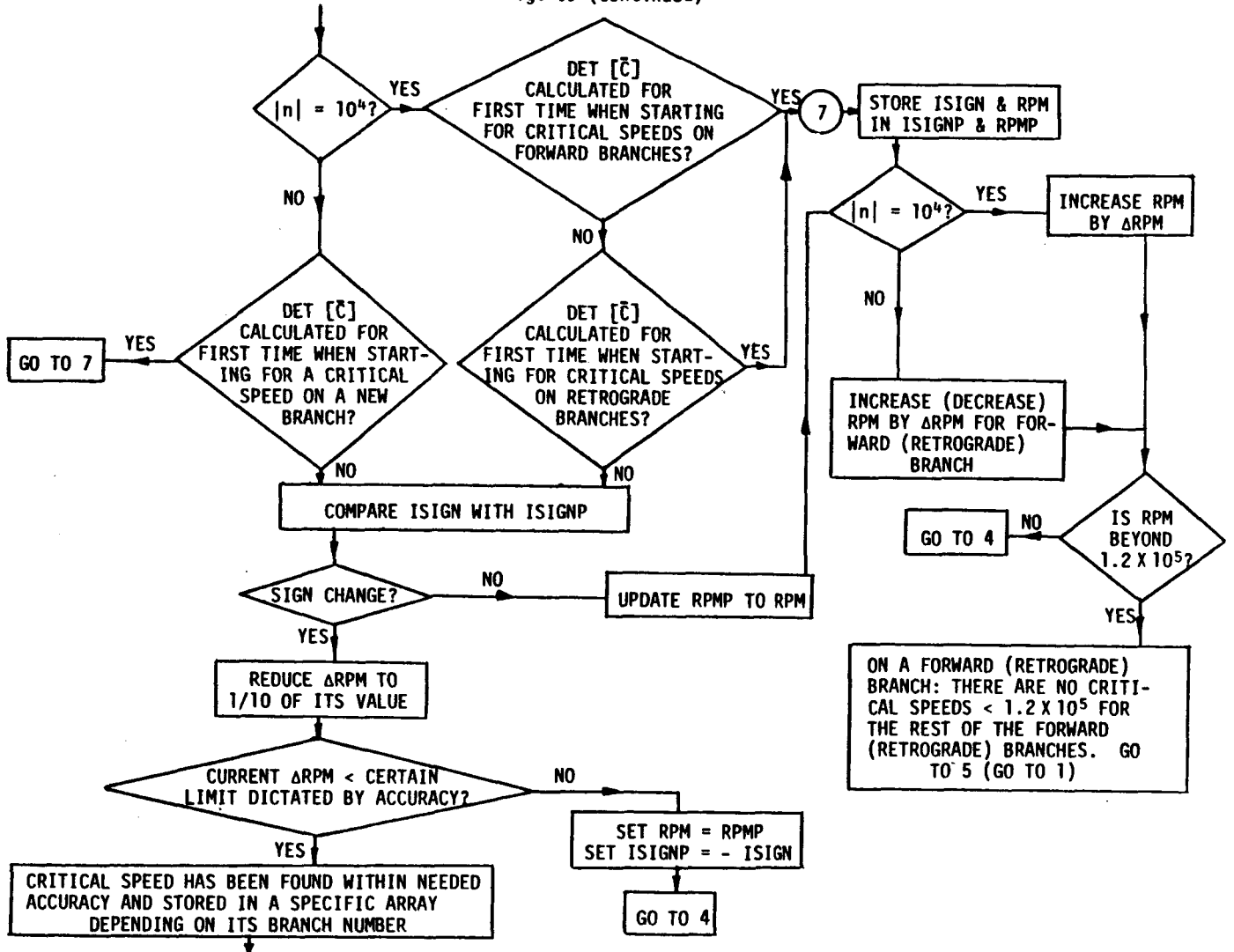

Continued on next page

Fig. C9 (continued)

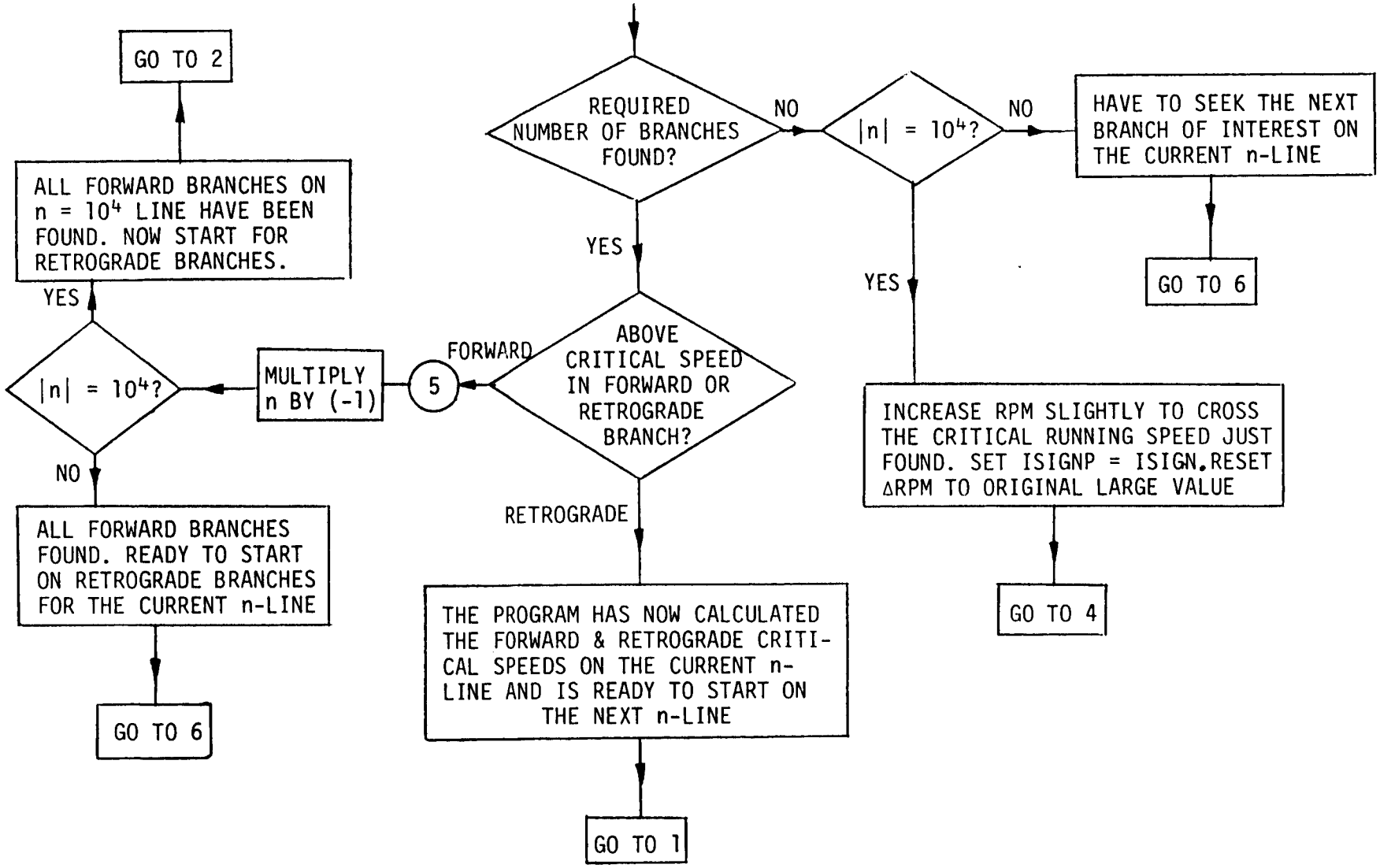

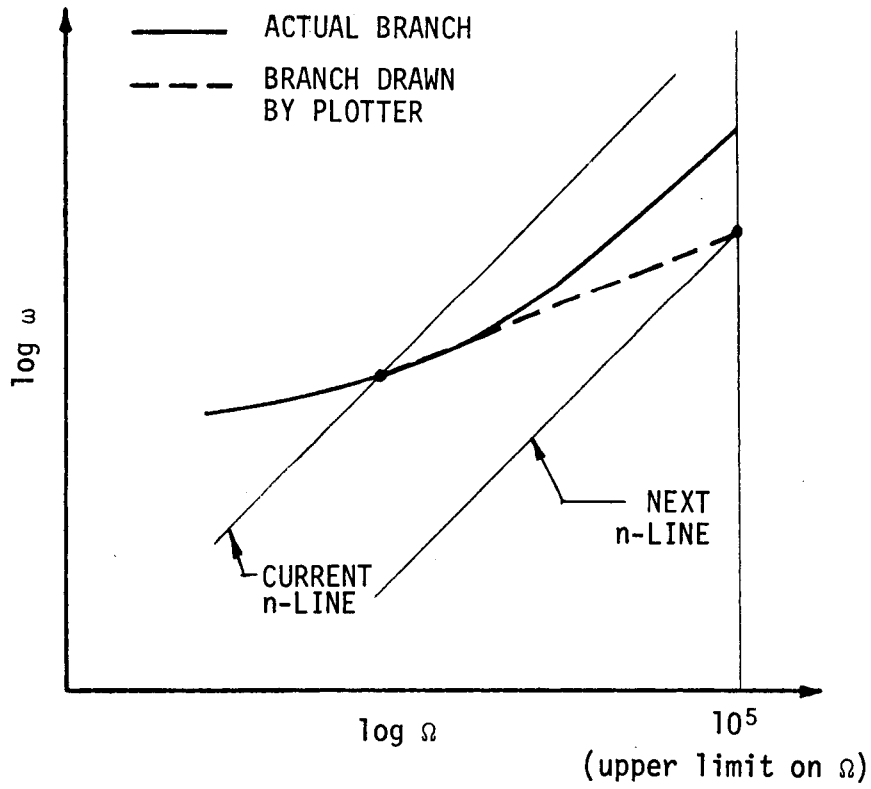

Fig. C10. Diagram explaining the case of one forward branch becoming parallel to an n-line.

```
C              F R E E   W H I R L I N G   A N A L Y S I S   B Y
C              C O M B I N E D   M O D E L :   W H I R L
C              D I A G R A M S   A N D   M O D E   S H A P E   P L O T S
C
      IMPLICIT REAL*8(A-H,O-Z)
      REAL*8 N,IA(3),K(3),L(3),KSU,KSL,NOMSQ,NABS
      REAL*8 MF,MD,MT
      REAL*8 IDF,IPF,IDD,IPD,IDT,IPT
      REAL*8 ISIGN,ISIGNP,NTRPM
      REAL*8 IDMOD,IPMOD,MMOD
      REAL*8 IEQ,KEQ,KNEOP,LAC
      REAL*4 OM(1602),RCPM(1602),Y1,Y2
      REAL*4 ALEN
      COMPLEX*16 CDESIN,RADIN,DSOUT1,DSOUT2,ALP(12),C(12,12),B(12,12)
      COMPLEX*16 DET,A(12),CR(11,11),AR(11)
      COMPLEX*16 UNITIM
      COMPLEX*16 WA(143),WK(11)
      COMPLEX*16 W10,W1L,W20
      DIMENSION DOUT(3),DIN(3),AREA(3),ANUM(3),BB(3),C1(3),C2(3),WB(12)
      DIMENSION Z1(101),Z2(101),Z3(101)
C
C   THE FLYWHEEL DATA IN THIS PROGRAM ARE FOR THE LLNL FLYWHEEL
C
C
C   TF: FLYWHEEL CG DISTANCE FROM END OF QUILL SHAFT. TD: DAMPER
C   CG DISTANCE FROM DAMPER EDGE.  TT1: TURBINE CG DISTANCE FROM
C   ONE END OF TURBINE.  SEE FIG.B1.  TT1 IS THE SAME AS TT IN FIG.
C
C   L(1),L(2),L(3) ARE LENGTHS OF THE THREE FLEXIBLE PORTIONS OF
C   THE SHAFT
C
C   TMOD2,TMOD3: SAME DIMENSIONS AS T2,T3 IN FIG.B1
C   ALEN: TOTAL LENGTH FROM TURBINEWHEEL-TURBINE SHAFT ATTAHMENT
C   TO FLYWHEEL-QUILL SHAFT ATTACHMENT
C
C   E,G,WL: SHAFT MATERIAL PROPERTIES
C
C   DOUT AND DIN ARE SHAFT OUTER AND INNER DIAMETER DATA RESPECTIVELY
C   DOUT(3) AND DIN(3) ARE THOSE OF THE TURBINE SHAFT
C
C   K(1),K(2),K(3): SHEAR CORRECTION FACTORS.K(3) IS THAT OF THE
C   TURBINE SHAFT
C
C   MF,MD,MT: MASS OF FLYWHEEL,DAMPER AND TURBINE
C
C   IDF,IPF: FLYWHEEL DIAMETRAL AND POLAR MASS MOMENTS OF INERTIA
C
C   IDT,IPT: TURBINE DIAMETRAL AND POLAR MASS MOMENTS OF INERTIA
C
C   KSU,KSL: BEARING SPRING CONSTANTS
C
```

```
C    KEQ:  SHEAR CORRECTION FACTOR OF THE EQUIVALENT QUILL SHAFT
C    INSIDE THE TURBINE SHAFT
C    LAC: ACTUAL LENGTH OF QUILL SHAFT INSIDE TURBINE SHAFT
C    MMOD: INTERMEDIATE MASS
C
C    IPMOD,IDMOD: POLAR AND DIAMETRAL MASS MOMENTS OF INERTIA OF THE
C    INTERMEDIATE MASS
C
C    TSP: DISTANCE OF LOWER BEARING SPRING FROM ONE EDGE OF THE
C    INTERMEDIATE MASS.SEE FIG.B1
C
C    KNEOP: SPRING CONSTANT OF NEOPRENE PAD IN DAMPER
C
C    CD: EXTERNAL VISCOUS DAMPING COEFFICIENT
C
C
C
      COMMON/MAIN1/TF,TD,TT1
      COMMON/MAIN2/L
      COMMON/MODES1/TMOD2,TMOD3,ALEN
      COMMON/MODES2/Z1,Z2,Z3
C
C    * * * DATA INPUT: SOME OF THE DATA CAN BE SEEN IN 'BLOCK DATA'.
C                      TMOD2,TMOD3 ARE DEFINED IN THE BODY OF THE MAIN
C                      PROGRAM * * *
C
C
      DATA E,G,WL/29.5D6,11.5D6,0.283D0/
      DATA DOUT/0.3125D0,0.3125D0,0.7493D0/
      DATA DIN/0.0D0,0.0D0,0.3175D0/
      DATA K/0.885D0,0.885D0,0.6569D0/
      DATA MF,MD,MT/0.0336D0,0.002998D0,0.00479D0/
      DATA IDF,IPF/0.823D0,1.645D0/
      DATA IDT,IPT/0.003402D0,0.00628D0/
      DATA KSU,KSL/2.0D6,2.0D6/
      DATA KEQ,LAC,MMOD/0.885D0,3.5969D0,0.000202D0/
      DATA IPMOD,IDMOD/1.15D-05,1.798D-05/
      DATA TSP/0.2431D0/
      DATA KNEOP/0.0D0/
      DATA CD/0.0D0/
C
C
C  THE FOLLOWING CARDS THROUGH LOOP 20 ARE REQUIRED BY THE SUBROUTINE
C  MODSHP
C
      NUMPT=101
      WMAXP=0.8
      TMOD2=0.4163D0
      TMOD3=0.4352D0
      ALEN=(L(1)+L(2)+L(3)+2.0*TD+TMOD2+TMOD3)/2.0
      NUM=NUMPT-1
C
C    THE LENGTHS L(1),L(2),AND L(3) ARE EACH DIVIDED INTO  100 EQUAL
C    PARTS
```

```
      DO 20 J=1,NUMPT
      Z1(J)=(J-1)*L(1)/NUM
      Z2(J)=(J-1)*L(2)/NUM
      Z3(J)=(J-1)*L(3)/NUM
   20 CONTINUE
      PII=2.0*DARSIN(1.0D0)
C
C   TO NEGLECT THE RESTCRING EFFECT OF GRAVITY ON THE MOTION OF THE
C  DISKS, SET GR=0.0.OTHERWISE SET GR=386.0
C
      GR=0.0
      RHO=WL/386.0
      UNITIM=(0.0D0,1.0D0)
C
C   AREAS AND MOMENTS OF INERTIA OF SHAFT SECTIONS 1 & 2 AND
C   THAT OF TURBINE SHAFT ARE CALCULATED
C
      DO 30 J=1,3
      AREA(J)=PII*(COUT(J)**2-DIN(J)**2)/4.0
      IA(J)=PII*(DOUT(J)**4-DIN(J)**4)/64.0
      ANUM(J)=E*IA(J)
   30 CONTINUE
C
C   CALCULATION OF DIAMETER AND AREA OF EQUIVALENT QUILL SHAFT
C   INSIDE TURBINE SHAFT
C
      IEQ=IA(2)*(L(3)/LAC)**4
      DEQ=(64.0*IEQ/PII)**0.25
      AEQ=PII*DEQ**2/4.0
C
C   K(3),AREA(3),IA(3) ARE  NEWLY DEFINED FOR THE EQUIVALENT SECTION
C   CONTAINING BOTH THE TURBINE SHAFT AND FLYWHEEL SHAFT
C
      K(3)=(KEQ*AEQ+K( 3)*AREA(3))/(AEQ+AREA(3))
      AREA(3)=AREA(3)+AEQ
      IA(3)=IA(3)+IEQ
      ANUM(3)=E*IA(3)
      CALL SETMSG(47,'PLEASE SET THE STEPSIZE TO .005 INCHES. THANKS.')
      CALL FACTOR(2.00)
      CALL PLOT(0.0,-40.0,-3)
      CALL PLOT(0.0,10.0,-3)
      CALL LEGEND
      CALL PLOT(0.00,-4.50,-3)
C
C   DO-LOOP FOR THE 200 'N' LINES
C
      DO 800 IN=1,200
      IPRINT=1
C
C   MM REPRESENTS THE BRANCH WE ARE CURRENTLY IN. 1 THROUGH 4
C   STAND FOR THE FIRST THROUGH FOURTH FORWARD MODES. 5 THROUGH 8
C   REPRESENT THE FIRST THROUGH FOURTH RETROGRADES
C
      MM=1
```

```
      EX=4.0D0-(IN-1)*0.04D0
      IF(IN.GT.91) EX=EX+(IN-91)*0.02D0
      IF(IN.GT.111) EX=EX-(IN-111)*0.02D0
      N=10.0D0**EX
      IF(IN.EQ.96) N=2.00D0
      IF(DABS(N-1.0D04).LT.1.0D-6) IPRINT=0
      IF(DABS(N-10.0D0).LT.1.0D-6) IPRINT=0
      IF(DABS(N-2.00D0).LT.1.0D-6) IPRINT=0
      IF(DABS(N-1.00D0).LT.1.0D-6) IPRINT=0
      NABS=N
      RPMST=100.0/N
C
C   RPMINX IS THE RPM INCREMENT STEPS
C
      RPMINX=10.0/N
      ARPMNX=RPMINX
      IF(IN.EQ.1) RPMINX=100.0/N
      GO TO 40
   35 N=-N
      IF(IN.GT.1) RPMINX=-RPMINX
   40 DO 50 J=1,3
      BB(J)=RHO*IA(J)*N*(N*E/(K(J)*G)+N-2.0)
      C1(J)=(RHO**2)*IA(J)*(N**3)*(N-2.0)/(K(J)*G)
      C2(J)=RHO*AREA(J)*N**2
   50 CONTINUE
   55 IRETEQ=0
      INDTB=IN-1+(MM-1)*200
      IF(IN.EQ.1) GO TO 65
      IF(OM(INDTB).LT.1.20E5) GO TO 60
   56 DO 58  IM=MM,8
      RCPM(IN+(IM-1)*200)=NABS*1.2E5
      OM(IN+(IM-1)*200)=1.2E5
   58 CONTINUE
      IF(MM.GT.4) GO TO 780
      MM=5
      GO TO 35
   60 RPMST=RCPM(INDTB)/NABS
   61 RPMST=RPMST-1.0D0*RPMINX
C
C   THE ABOVE TWO STATEMENTS DETERMINE THE RPM STARTING VALUE
C   FOR EACH BRANCH ON A 'N' LINE,EXCEPT FOR THE STARTING 'N' LINE
C
      IF(MM.EQ.1.OR.MM.EQ.8) GO TO 65
      IF(MM.GE.5.AND.MM.LT.8) GO TO 62
      INDPB=INDTB-200
C
C   THE FOLLOWING STATEMENT COMPARES THE CRITICAL RUNNING SPEEDS OF
C   THE CURRENT BRANCH AND THE PREVIOUS BRANCH .IF THEY ARE VERY CLOSE
C   THEN THE RPM START VALUE FOR THE CURRENT BRANCH  IS MODIFIED AS
C   EXPLAINED IN THE NOTES PERTAINING TO THIS PROGRAM
C
      IF (ABS(OM(INDTB)-OM(INDPB)).LE.1.0E-1*ARPMNX) RPMST=OM(INDPB+1)
     *+0.10*RPMINX
      GO TO 65
```

```
   62 INDNB=INDTB+200
      IF(ABS(OM(INDTB)-OM(INDNB)).LE.1.0E-1*ARPMNX) IRETEQ=1
      GO TO 65
   64 IRETEQ=0
   65 ISIGNP=0.0
      IF(IPRINT.NE.0) GO TO 100
      IF(MM.NE.1.AND.MM.NE.5) GO TO 100
      PRINT 70,N
   70 FORMAT('1',2X,'**********  N = ',F14.6,'  **********',//)
C
C   THE FOLLOWING LOOP  INCREASES RPM IN STEPS FROM 'RPM START' TO
C   LOCATE A SIGN CHANGE IN THE DETERMINANT  IN ORDER TO FIND A
C   CRITICAL SPEED
C
  100 DO 750 I=1,100000
      IDET=MOD(I-1,10)
      IF(IN.GT.1) IDET=1
      RPMINC=RPMINX
      RPM=RPMST+(I-1)*RPMINX
      IF(IN.EQ.1) GO TO 170
      IF(MM.LE.4) GO TO 170
      IF(RPM.LT.OM(INDTB)-2.0*ARPMNX) GO TO 61
  170 IF(RPM-1.19D5) 210,210,56
  200 RPM=RPM+RPMINC
  210 OMEGA=RPM*PII/30.0
      NOMSQ=N**2*OMEGA**2
C
C   DETERMINATION OF THE ALPHAS
C
      DO 300 J=1,3
      M=4*(J-1)
      DESIN=BB(J)**2-4.0*ANUM(J)*(C1(J)-C2(J)/(OMEGA**2))
      CDESIN=DCMPLX(DESIN,0.0D0)
      RADIN=CDSQRT(CDESIN)
      DSOUT1=(-BB(J)+RADIN)/(2.0*ANUM(J))
      DSOUT2=(-BB(J)-RADIN)/(2.0*ANUM(J))
      ALP(M+1)=OMEGA*CDSQRT(DSOUT1)
      ALP(M+2)=-ALP(M+1)
      ALP(M+3)=OMEGA*CDSQRT(DSOUT2)
      ALP(M+4)=-ALP(M+3)
  300 CONTINUE
      DO 350 J=1,12
      DO 350 M=1,12
      B(J,M)=(0.0D0,0.0D0)
  350 C(J,M)=(0.0D0,0.0D0)
C
C   DEFINING CBAR MATRIX.SEE CHAPTER 3
C
      DO 400 J=1,4
      C(1,J)=(RHO*AREA(1)/ALP(J)+MF*(1.0+ALP(J)*(TF-GR/NOMSQ)))*CDEXP(AL
     *P(J)*L(1))
      C(2,J)=(E*IA(1)*(ALP(J)**2/NOMSQ+RHO/(K(1)*G))+RHO*AREA(1)*TF/ALP(
     *J)-(IDF-IPF/N)*ALP(J))*CDEXP(ALP(J)*L(1))
```

```
      C(3,J)=(1.0D0,0.0D0)
      C(3,J+4)=-CDEXP(ALP(J+4)*L(2))
      C(4,J)=ALP(J)
      C(5,J)= RHO*AREA(1)/ALP(J)+KNEOP/NOMSQ+UNITIM*CD/(N*OMEGA)-MD
      C(5,J+4)=-RHO*AREA(2)/ALP(J+4)*CDEXP(ALP(J+4)*L(2))
      C(6,J+4)=ALP(J+4)*CDEXP(ALP(J+4)*L(2))
      C(7,J+4)=-ALP(J+4)
      C(7,J+8) =ALP(J+8)*CDEXP(ALP(J+8)*L(3))
      C(8,J+4)=1.0-(TMOD2+TMOD3)*ALP(J+4)
      C(8,J+8)=-CDEXP(ALP(J+8)*L(3))
      C(9,J+4)=-RHO*AREA(2)/ALP(J+4)-KSL/NOMSQ*(1.0-(TMOD2+TMOD3-TSP)*AL
     *P(J+4))+MMOD*(1.0-TMOD2*ALP(J+4))
      C(9,J+8)=RHO*AREA(3)/ALP(J+8)*CDEXP(ALP(J+8)*L(3))
      C(10,J+4)=E*IA(2)*(ALP(J+4)**2/NOMSQ+RHO/(K(2)*G))-TMOD2*RHO*AREA(
     *2)/ALP(J+4)+ALP(J+4)*(IDMOD-IPMOD/N)+KSL/NOMSQ*(TMOD3-TSP)*(1.0-(T
     *MOD3+TMOD2-TSP)*ALP(J+4))
      C(10,J+8)=(-E*IA(3)*(ALP(J+8)**2/NOMSQ+RHO/(K(3)*G))-TMOD3*RHO*ARE
     *A(3)/ALP(J+8))*CDEXP(ALP(J+8)*L(3))
      C(11,J+8)=-(RHO*AREA(3)/ALP(J+8)+MT*(GR*ALP(J+8)/NOMSQ-1.0+TT1*ALP
     *(J+8))+KSL/NOMSQ)
      C(12,J+8)=E*IA(3)*(ALP(J+8)**2/NOMSQ+RHO/(K(3)*G))-TT1*RHO*AREA(3)
     */ALP(J+8)-KSL*TT1/NOMSQ+ALP(J+8)*(IDT-IPT/N)
  400 CONTINUE
      DO 420 JR=1,11
      AR(JR)=-C(JR,1)
      DO 420 JC=1,11
      CR(JC,JR)=C(JC,JR+1)
  420 CONTINUE
      IJOB=1
      JN=12
C
C   LEQT1C IS AN IMSL SUBROUTINE
C
      CALL LEQT1C(C,JN,JN,B,JN,JN,IJOB,WB,IER)
C
C   CALCULATION OF THE DETERMINANT OF CBAR MATRIX FOLLOWING
C   THE PROCEDURE GIVEN IN THE IMSL ROUTINE LEQT1C.
C
      DET=(1.0D0,0.0D0)
      DO 450 JQ=1,JN
      IPVT=WB(JQ)
      IF(IPVT.NE.JQ) DET=-DET
      DET=DET*C(JQ,JQ)
  450 CONTINUE
      ARPMNC=DABS(RPMINC)
      IF(ARPMNC.GT.ARPMNX/1.00D3) GO TO 650                                  1.00D3
C
C   THE ACCURACY OF THE CRITICAL SPEEDS CALCULATED IS DECIDED IN THE
C   ABOVE STATEMENT
C
      NTRPM=NABS*RPM
      IF(IRETEQ.EQ.0) GO TO 455
      RPMST=RPM+0.10*RPMINX
      GO TO 64
```

```
  455 RCPM(IN+(MM-1)*200)=NTRPM
      OM(IN+(MM-1)*200)=RPM
C
C   THE ABOVE TWO STATEMENTS STORE THE CRITICAL SPEED AND THE
C   CORRESPONDING RUNNING SPEED  FOR THE CURRENT BRANCH
      IF(IPRINT.NE.0) GO TO 645
C
C   THE FOLLOWING CARDS UPTO 640 ARE RELATED TO MODE SHAPE PLOTTING
C
      IJOB=0
      JM=11
      M=1
C
C   LEQ2C IS AN IMSL SUBROUTINE
C
      CALL LEQ2C(CR,JM,JM,AR,M,JM,IJOB,WA,WK,IER)
      A(1)=(1.0D0,0.0D0)
      DO 460 J=1,11
      A(J+1)=AR(J)
  460 CONTINUE
      CALL MODSHP(A,ALP,NUMPT,WMAXP,N,MM)
      PRINT 490
  490 FORMAT(/,2X,130('*'))
      PRINT 500,A(1),ALP(1)
  500 FORMAT(/,2X,'MODE SHAPE COEFFICIENTS CORRESPONDING TO THE FOLLOWIN
     *G CRITICAL:  A 1 =',2D12.3,4X,'ALP 1 =',2D12.3)
      DO 550 J=1,11
      JI=J+1
      PRINT 540,JI,A(JI),JI,ALP(JI)
  540 FORMAT(68X,'A',I2,' =',2D12.3,4X,'ALP',I2,' =',2D12.3)
  550 CONTINUE
      PRINT 630
  630 FORMAT(7X,'ROT. SPEED (RPM)',4X,'NAT. FREQ. (CPM)',11X,'COMPLEX DE
     *TERMINANT')
      PRINT 640,RPM,NTRPM,DET
  640 FORMAT(2X,'****',2X,F13.6,8X,F10.2,6X,2D17.8,2X,49('*'),/)
  645 MM=MM+1
      IF(MM.EQ.5) GO TO 35
C
C   IF MM.EQ.5,THE CRITICAL SPEEDS OF ALL THE FOUR FORWARD BRANCHES
C   HAVE BEEN COMPUTED FOR A 'N' LINE. THE 'GO TO 35' STATEMENT
C   STARTS THE PROCESS FOR DETERMINATION OF RETROGRADE BRANCHES
C
      IF(MM.EQ.9 ) GO TO 780
C
C   IF MM.EQ.9,CRITICAL SPEEDS OF THE FOUR FORWARD AND RETROGRADE
C   BRANCHES HAVE BEEN COMPUTED
C
      IF(IN.GT.1) GO TO 55
      ISIGNP=-ISIGNP
      RPMP=RPM+RPMINX/100.0
      GO TO 750
  650 DETIP=DIMAG(DET)
      ISIGN=DETIP/DABS(DETIP)
```

```
C    THE FOLLOWING STATEMENT CHECKS THE SIGN CHANGE IN THE DETERMINANT
C
      IF(DABS(ISIGN+ISIGNP).GT.0.0D0) GO TO 670
C    RPM INCREMENT IS REDUCED BECAUSE OF SIGN CHANGE
C
      RPMINC=RPMINC/10.0
      RPM=RPMP
      GO TO 200
  670 IF(IDET.NE.0) GO TO 700
      PRINT 690,RPM,DET
  690 FORMAT(8X,F13.6,24X,2D17.8,/)
  700 ISIGNP=ISIGN
      RPMP=RPM
      IF(RPMINC.NE.RPMINX) GO TO 200
  750 CONTINUE
  780 PRINT 790,IN,(RCPM(IN+(MK-1)*200),MK=1,8)
  790 FORMAT(2X,'IN=',I3,8E15.5)
  800 CONTINUE
C
C   SET LIMITS ON THE VALUES TO BE PLOTTED
C
      DO 850 J=1,1600
      IF(OM(J).LT.1.0E0) OM(J)=1.0E0
      IF(OM(J).GT.1.0E5) OM(J)=1.0E5
      IF(RCPM(J).LT.1.0E0) RCPM(J)=1.0E0
      IF(RCPM(J).GT.1.0E6) RCPM(J)=1.0E6
  850 CONTINUE
C
C   ALL OF THE FOLLOWING STATEMENTS CAUSE WHIRLING DIAGRAMS (I.E. NATURAL
C   FREQUENCY VS. ROTATIONAL SPEED) TO BE GENERATED ON THE COMPUTER
C   SYSTEM'S DIGITAL PLOTTER
C
      OM(1601)=1.0
      OM(1602)=1.5
      RCPM(1601)=1.0
      RCPM(1602)=1.5
      CALL FACTOR(1.3)
      CALL PLOT(0.0,-40.0,-3)
      CALL PLOT(16.0,6.0,-3)
      DO 958 I=1,3
      ISTART=1401
      ISTOP=0
      IF (I.EQ.2) ISTOP=800
      IF (I.EQ.3) ISTART= 601
      CALL LAXIS(0.0,0.0,'WHIRLING FREQUENCY (CPM)',24,9.0,90.0,RCPM(160
     *1),RCPM(1602))
      CALL LAXIS(0.0,0.0,'ROTATICNAL SPEED (RPM)',-22,7.5,0.0,OM(1601),O
     *M(1602))
      KK=ISTART
  950 DOM1=OM(KK+200)
      DOM2=OM(KK+201)
      DRC1=RCPM(KK+200)
      DRC2=RCPM(KK+201)
      OM(KK+200)=OM(1601)
```

```
      OM(KK+201)=OM(1602)
      RCPM(KK+200)=RCPM(1601)
      RCPM(KK+201)=RCPM(1602)
      CALL LINE(OM(KK),RCPM(KK),200,1,0,0,3)
      OM(KK+200)=DOM1
      OM(KK+201)=DOM2
      RCPM(KK+200)=DRC1
      RCPM(KK+201)=DRC2
      KK=KK-200
      IF (KK.GT.ISTOP) GO TO 950
      CALL LAXIS(0.0,9.0,' ',1,-7.5,0.0,OM(1601),OM(1602))
      CALL LAXIS(7.5,0.0,' ',-1,-9.0,90.0,RCPM(1601),RCPM(1602))
      CALL PLOT(0.0,0.0,3)
      CALL DASH(7.5,7.5,4)
      Y1=DLOG10(2.0D0)*1.5
      Y2=Y1+7.5
      CALL PLOT(0.0,Y1,3)
      CALL DASH(7.5,Y2,4)
      IF (I.EQ.2) CALL SYMBOL(2.20,10.30,.20,'NEGATIVE BRANCHES',0.,17)
      IF (I.EQ.3) CALL SYMBOL(2.20,10.30,.20,'POSITIVE BRANCHES',0.,17)
      CALL PLOT(13.0,0.0,-3)
  958 CONTINUE
      CALL PLOT(0.0,0.0,999)
      STOP
      END


      SUBROUTINE MODSHP(A,ALP,NUMPT,WMAXP,N,MM)
      IMPLICIT REAL*8(A-H,O-Z)
      REAL*8 L(3),N
      REAL*4 BGDAMP,BGMOD,ENDMOD,ENDAMP
      REAL*4 WBMOD,WEMOD,WBDAMP,WEDAMP
      REAL*4 ZV(305),WV(305),ALEN,NS
      COMPLEX*16 A(12),ALP(12)
      COMPLEX*16 W1(101),W2(101),W3(101)
      DIMENSION Z1(101),Z2(101),Z3(101)
      COMMON/MAIN1/TF,TD,TT1
      COMMON/MAIN2/L
      COMMON/MODES1/TMOD2,TMOD3,ALEN
      COMMON/MODES2/Z1,Z2,Z3
      NS=N
      IF(MM.NE.1) GO TO 10
      CALL PLOT(7.50,4.50,-3)
      CALL DASH(ALEN,0.0,4)
      CALL SYMBOL(1.06,-1.75,.12,'FORWARD WHIRLING MODES',0.0,22)
      CALL SYMBOL(1.66,-1.95,.12,'N = ',0.0,4)
      CALL NUMBER(999.,-1.95,.12,NS,0.0,4)
   10 IF(MM.NE.5) GO TO 20
      CALL PLOT(0.00,-4.50,-3)
      CALL DASH(ALEN,0.0,4)
      CALL SYMBOL(0.88,-1.75,.12,'RETROGRADE WHIRLING MODES',0.0,25)
      CALL SYMBOL(1.66,-1.95,.12,'N = ',0.0,4)
      CALL NUMBER(999.,-1.95,.12,NS,0.0,4)
```

```
   20 WMAX=0.0
C
C    CALCULATION OF RELATIVE DISPLACEMENTS OF VARIOUS POINTS ON
C    EACH SHAFT SECTION
      DO 60 IZ=1,NUMPT
      W1(IZ)=(0.0D0,0.0D0)
      W2(IZ)=(0.0D0,0.0D0)
      W3(IZ)=(0.0D0,0.0D0)
      DO 50 JZ=1,4
      W1(IZ)=W1(IZ)+A(JZ)*CDEXP(ALP(JZ)*Z1(IZ))
      W2(IZ)=W2(IZ)+A(JZ+4)*CDEXP(ALP(JZ+4)*Z2(IZ))
      W3(IZ)=W3(IZ)+A(JZ+8)*CDEXP(ALP(JZ+8)*Z3(IZ))
   50 CONTINUE
      W1ABS=CDABS(W1(IZ))
      W2ABS=CDABS(W2(IZ))
      W3ABS=CDABS(W3(IZ))
      IF(W1ABS.GT.WMAX) WMAX=W1ABS
      IF(W2ABS.GT.WMAX) WMAX=W2ABS
      IF(W3ABS.GT.WMAX) WMAX=W3ABS
   60 CONTINUE
C
C    NOTE THAT  THE DIPLACEMENT VECTOR IS NORMALIZED BY  WMAX
C
      DO 100 IZ=1,NUMPT
      ZV(IZ)=Z3(IZ)
      ZV(IZ+NUMPT)=L(3)+TMOD2+TMOD3+Z2(IZ)
      ZV(IZ+2*NUMPT)=L(3)+TMOD2+TMOD3+L(2)+2.0*TD+Z1(IZ)
      WV(IZ)=DREAL(W3(IZ))*WMAXP/WMAX
      WV(IZ+NUMPT)=DREAL(W2(IZ))*WMAXP/WMAX
      WV(IZ+2*NUMPT)=DREAL(W1(IZ))*WMAXP/WMAX
  100 CONTINUE
      NPPT=3*NUMPT
      NP1=NPPT+1
      NP2=NPPT+2
      ZV(NP1)=0.0
      ZV(NP2)=2.0
      WV(NP1)=0.0
      WV(NP2)=1.0
      CALL LINE(ZV,WV,NPPT,1,100,MM)
      ENDMOD=ZV(NUMPT+1)/2.0
      WEMOD=WV(NUMPT +1)
      CALL SYMBOL(ENDMOD,WEMOD,0.08,MM,0.0,-1)
      ENDAMP=ZV(2*NUMPT+1)/2.0
      WEDAMP=WV(2*NUMPT+1)
      CALL SYMBOL(ENDAMP,WEDAMP,0.08,MM,0.0,-1)
      RETURN
      END



      SUBROUTINE LEGEND
      CALL SYMBOL(0.02,0.40,.10,'MODE',0.0,4)
      CALL SYMBOL(-0.48,0.20,.10,'IDENTIFICATION',0.0,14)
      CALL SYMBOL(0.00,-0.05,.10,1,0.0,-1)
```

```
CALL SYMBOL(0.22,-0.10,.10,'1F',0.0,2)
CALL SYMBOL(0.00,-0.25,.10,2,0.0,-1)
CALL SYMBOL(0.22,-0.30,.10,'2F',0.0,2)
CALL SYMBOL(0.00,-0.45,.10,3,0.0,-1)
CALL SYMBOL(0.22,-0.50,.10,'3F',0.0,2)
CALL SYMBOL(0.00,-0.65,.10,4,0.0,-1)
CALL SYMBOL(0.22,-0.70,.10,'4F',0.0,2)
CALL SYMBOL(0.00,-0.85,.10,5,0.0,-1)
CALL SYMBOL(0.22,-0.90,.10,'5F',0.0,2)
CALL SYMBOL(0.00,-1.15,.10,6,0.0,-1)
CALL SYMBOL(0.22,-1.20,.10,'1R',0.0,2)
CALL SYMBOL(0.00,-1.35,.10,7,0.0,-1)
CALL SYMBOL(0.22,-1.40,.10,'2R',0.0,2)
CALL SYMBOL(0.00,-1.55,.10,8,0.0,-1)
CALL SYMBOL(0.22,-1.60,.10,'3R',0.0,2)
CALL SYMBOL(0.00,-1.75,.10,9,0.0,-1)
CALL SYMBOL(0.22,-1.80,.10,'4R',0.0,2)
CALL SYMBOL(0.00,-1.95,.10,10,0.0,-1)
CALL SYMBOL(0.22,-2.00,.10,'5R',0.0,2)
RETURN
END


BLOCK DATA
IMPLICIT REAL*8(A-H,O-Z)
REAL*8 L(3)
COMMON/MAIN1/TF,TD,TT1
COMMON/MAIN2/L
DATA TF,TD,TT1/3.15D0,1.8332D0,0.8942D0/
DATA L/0.7455D0,0.6792D0,2.1269D0/
END
```

C.4 Simplified Program for Critical Speeds Using the Combined Model

1. This program, which gives the critical speeds (forward and retrograde) on a single n-line, is a simplified version of the program listed in Appendix C.3.

2. The relative displacements and rotations of the four rigid masses, at the critical speeds computed, can also be obtained by this program by setting IPRINT = 0.

3. Note that for $n = 1$, $\Delta\Omega = 100$ rpm and for $n = 2$, $\Delta\Omega = 50$ rpm. Checking back on the Campbell diagram in Fig. 4.1, we see that on the $n = 2$ line there are many crossings of the branches. Hence, if it is necessary, the step size $\Delta\Omega$ should be decreased further so that two branches (either forward or retrograde) which are very close together will not be missed altogether.

4. With $\Delta\Omega = 100$ rpm, the program takes about 3 minutes and 30 seconds of CPU time on the IBM 370 Model 158J. It should be noted that the CPU time increases when the rpm step size is reduced.

```
      IMPLICIT REAL*8(A-H,C-Z)
      REAL*8 N,IA(3),K(3),L(3),KSU,KSL,NOMSC,NABS
      REAL*8 MF,MD,MT
      REAL*8 IDF,IPF,IDC,IFD,IDT,IPT
      REAL*8 ISIGN,ISIGNP,NTRPM
      REAL*8 IDMCD,IFMCD,MMCD
      REAL*8 IEQ,KEQ,KNECP,LAC
      COMPLEX*16 CDESIN,RADIN,DSOUT1,DSOUT2,ALP(12),C(12,12),B(12,12)
      COMPLEX*16 DET,A(12),CR(11,11),AR(11),DINTE,DTLRBE
      COMPLEX*16 UNITIM,YY(7)
      COMPLEX*16 WA(143),WK(11)
      COMPLEX*16 W10,W1L,W20,WFSEND,FACTR
      DIMENSION DOUT(3),DIN(3),AREA(3),ANUM(3),BB(3),C1(3),C2(3),WB(12)
C
C  SEE SECTION C.3 FOR DETAILS RELATING TO INPUT DATA
C
      DATA E,G,WL/29.5D6,11.5D6,0.283D0/
      DATA DOUT/0.3125D0,0.3125D0,0.7493D0/
      DATA DIN/0.0D0,0.0D0,0.3175D0/
      DATA K/0.885D0,0.885D0,0.6569D0/
      DATA MD,MT/0.002998D0,0.00479D0/
      DATA MF,IPF,IDF/0.0951D0,8.517D0,4.83D0/
      DATA IDT,IPT/0.003402D0,0.00628D0/
      DATA KSU,KSL/2.0D6,2.0D6/
      DATA KEQ,LAC,MMCD/0.885D0,3.5969D0,0.000202D0/
      DATA IPMOD,IDMCD/1.15D-05,1.798D-05/
      DATA TSP/0.2431D0/
      DATA KNECP/0.0D0/
      DATA CD/0.0D0/
      DATA TMOD2,TMOD3/0.4163D0,0.4352D0/
      DATA TF,TD,TT1/7.05D0,1.8332D0,0.8942D0/
      DATA L/0.7455D0,0.6792D0,2.1269D0/

C
C
      PII=2.0*DARSIN(1.0D0)
C
C   TO NEGLECT THE RESTORING EFFECT OF GRAVITY ON THE MOTION OF THE DISKS,
C   SET GR = 0.0.
C
      GR=0.0
      RHO=WL/386.0
      UNITIM=(0.0D0,1.0D0)
      DO 30 J=1,3
      AREA(J)=PII*(DOUT(J)**2-DIN(J)**2)/4.0
      IA(J)=PII*(DOUT(J)**4-DIN(J)**4)/64.0
      ANUM(J)=E*IA(J)
   30 CONTINUE
      IEQ=IA(2)*(L(3)/LAC)**4
      DEQ=(64.0*IEQ/PII)**0.25
      AEQ=PII*DEQ**2/4.0
C
C   K(3),AREA(3),IA(3) ARE  NEWLY DEFINED FOR THE EQUIVALENT SECTION
C   CONTAINING BOTH THE TURBINE SHAFT AND FLYWHEEL SHAFT
```

```
      K(3)=(KEQ*AEQ+K( 3)*AREA(3))/(AEQ+AREA(3))
      AREA(3)=AREA(3)+AEQ
      IA(3)=IA(3)+IEQ
      ANUM(3)=E*IA(3)
      IPRINT=0
      MM=1
C
C  SELECTING N-LINE OF INTEREST
C
      N=1.0D0
      NABS=N
C
C  CHOOSING RPM BEGINNING AND RPM STEPS
C
      RPMST=100.0/N
      RPMINX=100.0/N
C
      ARPMNX=RPMINX
      GO TO 40
   35 N=-N
   40 DO 50 J=1,3
      BB(J)=RHO*IA(J)*N*(N*E/(K(J)*G)+N-2.0)
      C1(J)=(RHO**2)*IA(J)*(N**3)*(N-2.0)/(K(J)*G)
      C2(J)=RHO*AREA(J)*N**2
   50 CONTINUE
      GO TO 65
   55 CONTINUE
      PRINT 60
   60 FORMAT(/,2X,10('$'),'NO MORE FORWARD CRITICAL SPEEDS<120.000
     *RPM',10('$'),/)
      IF(MM.GT.4) GO TO 800
      MM=5
      GO TO 35
   65 ISIGNP=0.0
      IF(MM.NE.1.AND.MM.NE.5) GO TO 100
      PRINT 70,N
   70 FORMAT('1',2X,'**********  N = ',F14.6,'  **********',//)
  100 DO 750 I=1,100000
      IDET=MOD(I-1,100)
      RPMINC=RPMINX
      RPM=RPMST+(I-1)*RPMINX
      IF(RPM-1.19D5) 210,210,55
  200 RPM=RPM+RPMINC
  210 OMEGA=RPM*PII/30.0
      NOMSQ=N**2*OMEGA**2
C
C  CALCULATION OF ALPHAS
C
      DO 300 J=1,3
      M=4*(J-1)
      DESIN=BB(J)**2-4.0*ANUM(J)*(C1(J)-C2(J)/(OMEGA**2))
      CDESIN=DCMPLX(DESIN,0.0D0)
      RADIN=CDSQRT(CDESIN)
      DSCUT1=(-BB(J)+RADIN)/(2.0*ANUM(J))
```

```
      DSOUT2=(-BB(J)-RADIN)/(2.0*ANUM(J))
      ALP(M+1)=OMEGA*CDSQRT(DSOUT1)
      ALP(M+2)=-ALP(M+1)
      ALP(M+3)=OMEGA*CDSQRT(DSOUT2)
      ALP(M+4)=-ALP(M+3)
  300 CONTINUE
      DO 350 J=1,12
      DO 350 M=1,12
      B(J,M)=(0.0D0,0.0D0)
  350 C(J,M)=(0.0D0,0.0D0)
C
C  DEFINING CBAR MATRIX
C
      DO 400 J=1,4
      C(1,J)=(RHO*AREA(1)/ALP(J)+MF*(1.0+ALP(J)*(TF-GR/NOMSQ)))*CDEXP(AL
     *P(J)*L(1))
      C(2,J)=(E*IA(1)*(ALP(J)**2/NOMSQ+RHO/(K(1)*G))+RHO*AREA(1)*TF/ALP(
     *J)-(IDF-IPF/N)*ALP(J))*CDEXP(ALP(J)*L(1))
      C(3,J)=(1.0D0,0.0D0)
      C(3,J+4)=-CDEXP(ALP(J+4)*L(2))
      C(4,J)=ALP(J)
      C(5,J)= RHO*AREA(1)/ALP(J)+KNECP/NOMSQ+UNITIM*CD/(N*OMEGA)-MD
      C(5,J+4)=-RHO*AREA(2)/ALP(J+4)*CDEXP(ALP(J+4)*L(2))
      C(6,J+4)=ALP(J+4)*CDEXP(ALP(J+4)*L(2))
      C(7,J+4)=-ALP(J+4)
      C(7,J+8) =ALP(J+8)*CDEXP(ALP(J+8)*L(3))
      C(8,J+4)=1.0-(TMOD2+TMOD3)*ALP(J+4)
      C(8,J+8)=-CDEXP(ALP(J+8)*L(3))
      C(9,J+4)=-RHO*AREA(2)/ALP(J+4)-KSL/NOMSQ*(1.0-(TMOD2+TMOD3-TSP)*AL
     *P(J+4))+MMCD*(1.0-TMOD2*ALP(J+4))
      C(9,J+8)=RHO*AREA(3)/ALP(J+8)*CDEXP(ALP(J+8)*L(3))
      C(10,J+4)=E*IA(2)*(ALP(J+4)**2/NOMSQ+RHO/(K(2)*G))-TMOD2*RHO*AREA(
     *2)/ALP(J+4)+ALP(J+4)*(IDMCD-IPMCD/N)+KSL/NOMSQ*(TMOD3-TSP)*(1.0-(T
     *MOD3+TMOD2-TSP)*ALP(J+4))
      C(10,J+8)=(-E*IA(3)*(ALP(J+8)**2/NOMSQ+RHO/(K(3)*G))-TMOD3*RHO*ARE
     *A(3)/ALP(J+8))*CDEXP(ALP(J+8)*L(3))
      C(11,J+8)=-(RHO*AREA(3)/ALP(J+8)+MT*(GR*ALP(J+8)/NOMSQ-1.0+TT1*ALP
     *(J+8))+KSL/NOMSQ)
      C(12,J+8)=E*IA(3)*(ALP(J+8)**2/NOMSQ+RHO/(K(3)*G))-TT1*RHO*AREA(3)
     */ALP(J+8)-KSL*TT1/NOMSQ+ALP(J+8)*(IDT-IPT/N)

  400 CONTINUE
      DO 420 JR=1,11
      AR(JR)=-C(JR,1)
      DO 420 JC=1,11
      CR(JC,JR)=C(JC,JR+1)
  420 CONTINUE
```

```
C  CALCULATION OF DETERMINANT OF CBAR
C
      IJCB=1
      JN=12
      CALL LEQT1C(C,JN,JN,B,JN,JN,IJCB,WB,IER)
      DET=(1.0D0,0.0D0)
      DO 450 JQ=1,JN
      IPVT=WB(JQ)
      IF(IPVT.NE.JQ) DET=-DET
      DET=DET*C(JQ,JQ)
  450 CONTINUE
      ARPMNC=DABS(RPMINC)
      IF(ARPMNC.GT.ARPMNX/1.00D3) GO TO 650                              1.00D3
      NTRPM=NABS*RPM
C
C  ESTIMATING THE MODE SHAPE COEFFICIENTS,A(J) J=1,.....,12
C
      IJCB=0
      JM=11
      M=1
      CALL LEQ2C(CR,JM,JM,AR,M,JM,IJCB,WA,WK,IER)
      A(1)=(1.0D0,0.0D0)
      DO 460 J=1,11
      A(J+1)=AR(J)
  460 CONTINUE
C
C
C  RELATIVE DISPLACEMENTS AND ROTATIONS ARE CALCULATED FOR
C  THE FLYWHEEL,DAMPER,INTERMEDIATE MASS AND TURBINE.THESE ARE
C  STORED IN ORDER (FLYWHEEL DISP.,FLYWHEEL ROT.,DAMPER DISP.,
C  INT.MASS DISP.,INT.MASS ROT.,TURE.DISP.,AND TURB.ROT.)
C  IN VECTOR YY(1),.....,YY(7)
C
      YY(3)=(0.0D0,0.0D0)
      DO 495 J=1,4
      YY(3)=YY(3)+A(J)
  495 CONTINUE
      WFSEND=(0.0D0,0.0D0)
      YY(2)=(0.0D0,0.0D0)
      DO 500 J=1,4
      FACTR=A(J)*CDEXP(ALP(J)*L(1))
      WFSEND=WFSEND+FACTR
      YY(2)=YY(2)+ALP(J)*FACTR
  500 CONTINUE
      YY(1)=WFSEND+TF*YY(2)
      DINTE=(0.0D0,0.0D0)
      YY(5)=(0.0D0,0.0D0)
      DO 510 J=5,8
      DINTE=DINTE+A(J)
  510 YY(5)=YY(5)+ALP(J)*A(J)
      YY(4)=DINTE-TMCD3*YY(5)
      YY(7)=(0.0D0,0.0D0)
      DTURBE=(0.0D0,0.0D0)
```

```
      DO 520 J=9,12
      DTURBE=DTURBE+A(J)
  520 YY(7)=YY(7)+ALF(J)*A(J)
      YY(6)=DTURBE-TT1*YY(7)
C
C  THE RELATIVE MOVEMENTS ARE NORMALIZED BY THE MAX.VALUE
C
      YYMAX=0.0D0
      DO 530 J=1,7
      YYD=DABS(DREAL(YY(J)))
      IF(YYMAX.GE.YYD) GO TO 530
      YYMAX=YYD
  530 CONTINUE
      DO 540 J=1,7
  540 YY(J)=YY(J)/YYMAX
C
      PRINT 545
  545 FORMAT(/,2X,130('-'))
      PRINT 550
  550 FORMAT(/,2X,'RELATIVE DISPLACEMENTS AND ROTATIONS OF THE FOUR
     *RIGID MASS CENTERS W.R.T. THE FOLLOWING CRITICAL SPEED',/)
      PRINT 560,(YY(J),J=1,7)
  560 FORMAT(90X,2D12.5)
      PRINT 630
  630 FORMAT(7X,'ROT. SPEED (RPM)',4X,'NAT. FREQ. (CPM)',11X,'COMPLEX DE
     *TERMINANT')
      PRINT 640,RPM,NTFPM,DET
  640 FORMAT(2X,'****',2X,F13.6,8X,F10.2,6X,2D17.8,2X,49('*'),/)
      PRINT 545
      MM=MM+1
      IF(MM.EQ.5) GO TO 35
      IF(MM.EQ.9 ) GO TO 800
      ISIGNP=-ISIGNP
      RPMP=RPM+RPMINX/100.0
      GO TO 750
  650 DETIP=DIMAG(DET)
      ISIGN=DETIP/DABS(DETIP)
      IF(DABS(ISIGN+ISIGNP).GT.0.0D0) GO TO 670
      RPMINC=RPMINC/10.0
      RPM=RPMP
      GO TO 200
  670 IF(IDET.NE.0) GO TO 700
      PRINT 690,RPM,DET
  690 FORMAT(8X,F13.6,24X,2D17.8,/)
  700 ISIGNP=ISIGN
      RPMP=RPM
      IF(RPMINC.NE.RPMINX) GO TO 200
  750 CONTINUE
  800 CONTINUE
      PRINT 810
  810 FORMAT(/,2X,10('$'),'NO MORE RETROGRADE CRITICAL SPEEDS
     *< 120,000 RPM',10('$'),/)
      STOP
      END
```

C.4 Forced Whirling Analysis Using the Combined Model

A flow chart for this program is presented in Fig. C11. This program takes approximately 1 minute, 15 seconds of CPU time.

Fig. C11. Flow chart for forced whirling by combined model.

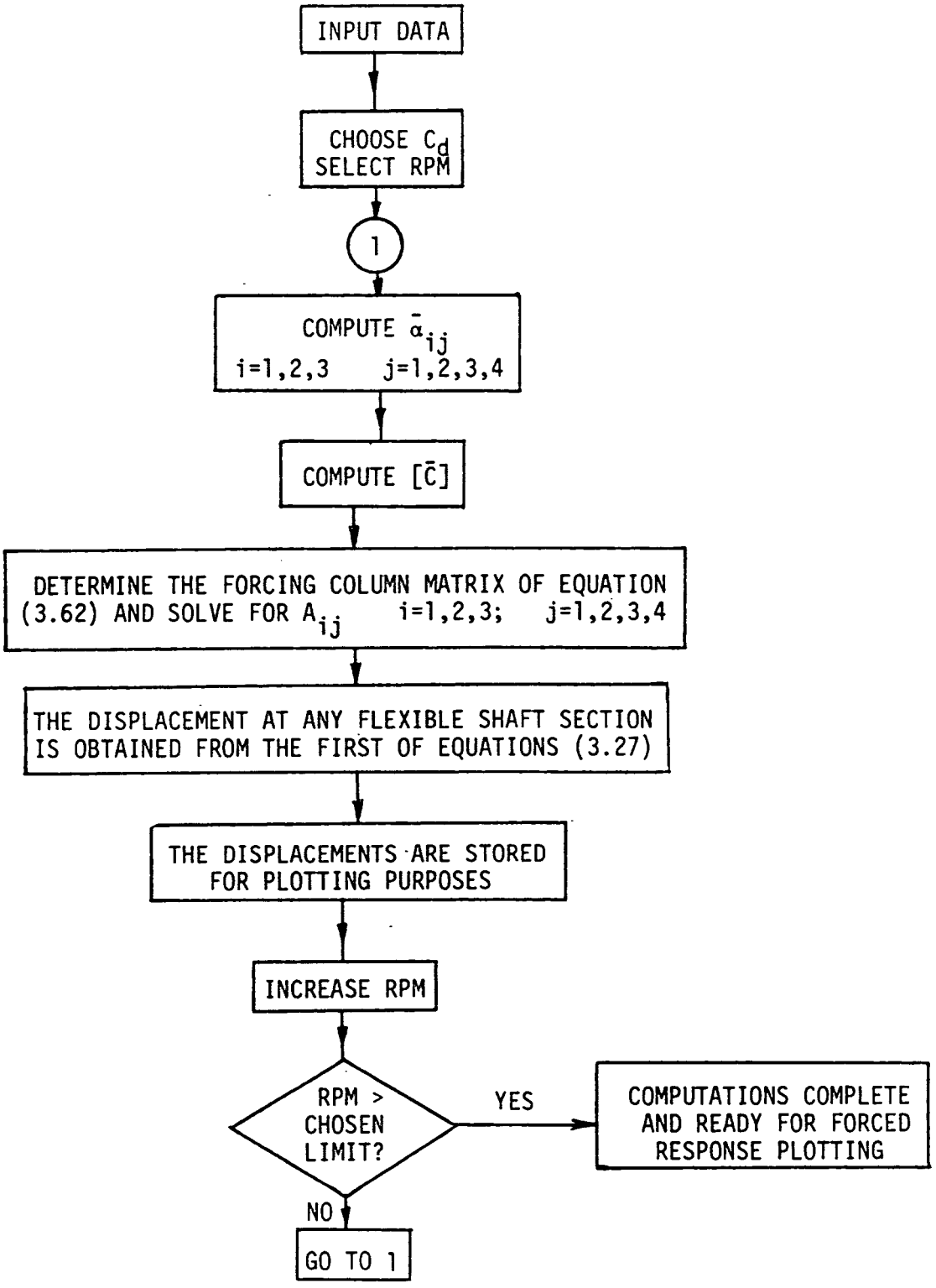

```
C
C           F O R C E D   W H I R L I N G
C           ( C O M B I N E D   M O D E L )
C
C
      IMPLICIT REAL*8(A-H,C-Z)
      REAL*4 BETA,ECCEN,PHIZRO
      REAL*4 AWFWCG(503),AWDAMP(503),ASLFSE(503)
      REAL*4 PHFWCG(503),PHFWSL(503),PHDAMP(503),RPMARY(503)
      REAL*8 N,IA(3),K(3),L(3),KSU,KSL,KNEOP,NOMSQ
      REAL*8 MF,MD,MT
      REAL*8 IDF,IPF,IDD,IPD,IDT,IPT,IEQ,KEQ
      REAL*8 IDMOD,IPMOD,LAC,MMOD
      COMPLEX*16 CDESIN,RACIN,DSOUT1,DSOUT2,ALP(12),C(12,12),B(12),A(12)
      COMPLEX *16 FACTR,PHASE,WFSBGN,WFWCG,WFSEND,SLPFSE
      COMPLEX*16 UNITIM
      COMPLEX*16 WA(168),WK(12)
      DIMENSION DOUT(3),DIN(3),AREA(3),ANUM(3),BB(3),C1(3),C2(3)
C
C
C   SEE ' FREE WHIRLING BY COMBINED MODEL' PROGRAM FOR DEFINITION
C   OF VARIABLES IN THE  DATA STATEMENTS
C
C   FLYWHEEL DATA IN THIS PROGRAM ARE THOSE OF LLNL
C
C   BETA: PHASE LAG OF INITIAL TILT FROM MASS ECCENTRICITY
C   ECCEN: MASS ECCENTRICITY
C   PHIZRO: INITIAL TILT
C
C
C
      DATA E,G,WL/29.5D6,11.5D6,0.283D0/
      DATA DOUT/0.3125D0,0.3125D0,0.7493D0/
      DATA DIN/0.0D0,0.0D0,0.3175D0/
      DATA K/0.885D0,0.885D0,0.6569D0/
      DATA KNEOP/0.0D0/
      DATA MF,MD,MT/0.0336D0,0.002998D0,0.00479D0/
      DATA TF,TD,TT1/3.15D0,1.8332D0,0.8942D0/
      DATA IDF,IPF/0.823D0,1.645D0/
      DATA IDT,IPT/0.003402D0,0.00628D0/
      DATA L/0.7455D0,0.6792D0,2.1269D0/
      DATA KSU,KSL/2.0D6,2.0D6/
      DATA BETA,ECCEN,PHIZRO/3.1415,0.001,0.0025/
      DATA KEQ,LAC,MMOD/0.885D0,3.5969D0,0.000202D0/
      DATA TMOD2,TMOD3,TSP/0.4163D0,0.4352D0,0.2431D0/
      DATA IPMOD,IDMOD/1.15D-05,1.798D-05/
C
C
C
      PII=2.0*DARSIN(1.0D0)
C
C   TO NEGLECT THE RESTORING EFFECT OF GRAVITY ON THE MOTION OF THE DISKS,
C   SET GR = 0.0.
```

```
      GR=386.0
      RHO=WL/386.0
      THETA=BETA
      PHASE=DCMPLX(0.0D0,THETA)
      CD=0.0
      STP1=1.0
      STP2=1.0
      STP3=0.5
      DO 30 J=1,3
      AREA(J)=PII*(DOUT(J)**2-DIN(J)**2)/4.0
      IA(J)=PII*(DOUT(J)**4-DIN(J)**4)/64.0
      ANUM(J)=E*IA(J)
   30 CONTINUE
C
C   CALCULATIONS RELATING TO THE EQUIVALENT QUILL SHAFT INSIDE
C   THE TURBINE SHAFT
C
      IEQ=IA(2)*(L(3)/LAC)**4
      DEQ=(64.0*IEQ/PII)**0.25
      AEQ=PII*DEQ**2/4.0
C
C   K(3),AREA(3),IA(3) ARE  NEWLY DEFINED FOR THE EQUIVALENT SECTION
C   CONTAINING BOTH THE TURBINE SHAFT AND FLYWHEEL SHAFT
C
      K(3)=(KEQ*AEQ+K( 3)*AREA(3))/(AEQ+AREA(3))
      AREA(3)=AREA(3)+AEQ
      IA(3)=IA(3)+IEQ
      ANUM(3)=E*IA(3)
      N=1.0D0
      DO 50 J=1,3
      BB(J)=RHO*IA(J)*N*(N*E/(K(J)*G)+N-2.0)
      C1(J)=(RHO**2)*IA(J)*(N**3)*(N-2.0)/(K(J)*G)
      C2(J)=RHO*AREA(J)*N**2
   50 CONTINUE
      RPM=1980.0
      RPMINC=20.0
      IN=501
      DO 900 I=1,IN
      RPM=RPM+RPMINC
      RPMARY(I)=RPM
      OMEGA=RPM*PII/30.0
      NOMSQ=N**2*OMEGA**2
C
C   COMPUTATION OF ALPHAS
C
      DO 300 J=1,3
      M=4*(J-1)
      DESIN=BB(J)**2-4.0*ANUM(J)*(C1(J)-C2(J)/(OMEGA**2))
      CDESIN=DCMPLX(DESIN,0.0D0)
      RADIN=CDSQRT(CDESIN)
      DSOUT1=(-BB(J)+RADIN)/(2.0*ANUM(J))
      DSOUT2=(-BB(J)-RADIN)/(2.0*ANUM(J))
      ALP(M+1)=OMEGA*CDSQRT(DSOUT1)
      ALP(M+2)=-ALP(M+1)
```

```
      ALP(M+3)=OMEGA*CDSQRT(DSOUT2)
      ALP(M+4)=-ALP(M+3)
  300 CONTINUE
      DO 350 J=1,12
      DO 350 M=1,12
  350 C(J,M)=(0.0D0,0.0D0)
C
C   DEFINING THE CBAR MATRIX
C
      DO 400 J=1,4
      C(1,J)=(RHO*AREA(1)/ALP(J)+MF*(1.0+ALP(J)*(TF-GR/NOMSQ)))*CDEXP(AL
     *P(J)*L(1))
      C(2,J)=(E*IA(1)*(ALP(J)**2/NOMSQ+RHO/(K(1)*G))+RHO*AREA(1)*TF/ALP(
     *J)-(IDF-IPF/N)*ALP(J))*CDEXP(ALP(J)*L(1))
      C(3,J)=(1.0D0,0.0D0)
      C(3,J+4)=-CDEXP(ALP(J+4)*L(2))
      C(4,J)=ALP(J)
      C(6,J+4)=ALP(J+4)*CDEXP(ALP(J+4)*L(2))
      C(7,J+4)=-ALP(J+4)
      C(7,J+8) =ALP(J+8)*CDEXP(ALP(J+8)*L(3))
      C(8,J+4)=1.0-(TMOD2+TMOD3)*ALP(J+4)
      C(8,J+8)=-CDEXP(ALP(J+8)*L(3))
      C(9,J+4)=-RHO*AREA(2)/ALP(J+4)-KSL/NOMSQ*(1.0-(TMOD2+TMOD3-TSP)*AL
     *P(J+4))+MMOD*(1.0-TMOD2*ALP(J+4))
      C(9,J+8)=RHO*AREA(3)/ALP(J+8)*CDEXP(ALP(J+8)*L(3))
      C(10,J+4)=E*IA(2)*(ALP(J+4)**2/NOMSQ+RHO/(K(2)*G))-TMOD2*RHO*AREA(
     *2)/ALP(J+4)+ALP(J+4)*(IDMOD-IPMOD/N)+KSL/NOMSQ*(TMOD3-TSP)*(1.0-(T
     *MOD3+TMOD2-TSP)*ALP(J+4))
      C(10,J+8)=(-E*IA(3)*(ALP(J+8)**2/NOMSQ+RHO/(K(3)*G))-TMOD3*RHO*ARE
     *A(3)/ALP(J+8))*CDEXP(ALP(J+8)*L(3))
      C(11,J+8)=-(RHO*AREA(3)/ALP(J+8)+MT*(GR*ALP(J+8)/NOMSQ-1.0+TT1*ALP
     *(J+8))+KSL/NOMSQ)
      C(12,J+8)=E*IA(3)*(ALP(J+8)**2/NOMSQ+RHO/(K(3)*G))-TT1*RHO*AREA(3)
     */ALP(J+8)-KSL*TT1/NOMSQ+ALP(J+8)*(IDT-IPT/N)
  400 CONTINUE
      DO 403 J=1,12
  403 B(J)=(0.0D0,0.0D0)
      B(1)=-MF*ECCEN
      B(2)=PHIZRO*(IDF-IPF)*CDEXP(-PHASE)
      UNITIM=(0.0D0,1.0D0)
      DO 410 J=1,4
      C(5,J)= RHO*AREA(1)/ALP(J)+KNECP/NOMSQ+UNITIM*CD/(N*OMEGA)-MD
      C(5,J+4)=-RHO*AREA(2)/ALP(J+4)*CDEXP(ALP(J+4)*L(2))
  410 CONTINUE
      JN=12
      IJCB=0
      M=1
C
C   LEQ2C: IMSL SUBROUTINE FOR SOLUTION OF LINEAR ALGEBRAIC EQUATIONS
C
      CALL LEQ2C(C,JN,JN,B,M,JN,IJCB,WA,WK,IER)
      DO 420 JR=1,12
      A(JR)=B(JR)
  420 CONTINUE
```

```
      WFSBGN=(0.0D0,0.0D0)
      DO 450 JQ=1,4
      WFSBGN=WFSBGN+A(JQ)
  450 CONTINUE
      WFSEND=(0.0D0,0.0D0)
      SLPFSE=(0.0D0,0.0D0)
      DO 484 JQ=1,4
      FACTR=A(JQ)*CDEXP(ALP(JQ)*L(1))
      WFSEND=WFSEND+FACTR
      SLPFSE=SLPFSE+ALP(JQ)*FACTR
  484 CONTINUE
C
C  NOTE: ALL VARIABLES ENDING WITH 'FWCG' ARE RELATED TO THE GEOMETRIC
C  CENTER OF THE FLYWHEEL.
C  WFSEND: DISPLACEMENT AT FLYWHEEL SHAFT END
C  SLPFSE: SLOPE AT FLYWHEEL SHAFT END
C
C  AWFWCG(I): ARRAY OF ABSOLUTE VALUE OF FLYWHEEL CG DIPLACEMENT
C  AWDAMP(I): ARRAY OF ABSOLUTE VALUE OF DAMPER DISPLACEMENT
C  ASLFSE(I): ARRAY OF ABSOLUTE VALUE OF SLOPE AT THE END OF FLYWHEEL
C  SHAFT
C  ARRAYS BEGINNING WITH 'PH' ARE RELATED TO PHASE LAGS
C
      WFWCG=WFSEND+TF*SLPFSE
      AWFWCG(I)=CDABS(WFWCG)
      AWDAMP(I)=CDABS(WFSBGN)
      ASLFSE(I)=CDABS(SLPFSE)
      PHFWCG(I)=DATAN2(DIMAG(WFWCG),DREAL(WFWCG))*180.0/PII*(-1.0)
      PHFWSL(I)=DATAN2(DIMAG(SLPFSE),DREAL(SLPFSE))*180.0/PII*(-1.0)
      PHDAMP(I)=DATAN2(DIMAG(WFSBGN),DREAL(WFSBGN))*180.0/PII*(-1.0)
      IF(PHFWCG(I).GT.-1.0E-03.AND.PHFWCG(I).LT.1.0E-04) PHFWCG(I)=0.0
      IF(PHFWSL(I).GT.-1.0E-03.AND.PHFWSL(I).LT.1.0E-04) PHFWSL(I)=0.0
      IF(PHDAMP(I).GT.-1.0E-03.AND.PHDAMP(I).LT.1.0E-04) PHDAMP(I)=0.0
      IF(PHFWCG(I).LT.0.0) PHFWCG(I)=360.0+PHFWCG(I)
      IF(PHFWSL(I).LT.0.0) PHFWSL(I)=360.0+PHFWSL(I)
      IF(PHDAMP(I).LT.0.0) PHDAMP(I)=360.0+PHDAMP(I)
      IF(PHFWCG(I).EQ.360.0) PHFWCG(I)=0.0
      IF(PHFWSL(I).EQ.360.0) PHFWSL(I)=0.0
      IF(PHDAMP(I).EQ.360.0) PHDAMP(I)=0.0
  900 CONTINUE
      PRINT 910
  910 FORMAT(8X,3('ABSOLUTE',7X,'PHASE LAG',8X))
      PRINT 920
  920 FORMAT(8X,'FWCGDISP',9X,'(DEG)',10X,'DAMPDISP',9X,' DEG',9X,'FWS S
     *LOPE',9X,'(DEG)',11X,'RPM',//)
      DO 940 I=1,IN
      PRINT 960,AWFWCG(I),PHFWCG(I),AWDAMP(I),PHDAMP(I),ASLFSE(I),
     *PHFWSL(I),RPMARY(I)
      IF(AWFWCG(I).GT.STP1) AWFWCG(I)=STP1
      IF(AWDAMP(I).GT.STP2) AWDAMP(I)=STP2
      IF(ASLFSE(I).GT.STP3) ASLFSE(I)=STP3
  940 CONTINUE
  960 FORMAT(6X,6(E11.4,4X),F7.1,6X,/)
      CALL SETMSG(45,'PLEASE SET THE STEPSIZE TO .005 INCHES.THANKS')
      CALL PLOT(0.0,-40.0,-3)
```

```
 CALL PLOT(4.0,4.0,-3)
 CALL FACTOR(1.3)
 RPMARY(502)=2000.0
 RPMARY(503)=1000.0
 AWFWCG(502)=0.0
 AWFWCG(503)=0.5
 ASLFSE(502)=0.0
 ASLFSE(503)=0.25
 AWDAMP(502)=0.0
 AWDAMP(503)=0.5
 PHFWCG(502)=0.0
 PHFWCG(503)=180.0
 PHFWSL(502)=0.0
 PHFWSL(503)=180.0
 PHDAMP(502)=0.0
 PHDAMP(503)=180.0
 CALL PLOT(0.0,10.0,-3)
 CALL AXIS(0.0,0.0,'RF (INCHES)',11,2.0,90.0,AWFWCG(502),AWFWCG(503
*))
 CALL AXIS(0.0,0.0,'OMEGA (RPM)',-11,10.0,0.0,RPMARY(502),RPMARY(50
*3))
 CALL LINE(RPMARY,AWFWCG,501,1,0,0)
 CALL DLINE(RPMARY,PHFWCG,501,1,5)
 CALL AXIS(10.5,0.0,'PHASE LAG (DEG.)',-16,2.0,90.0,PHFWCG(502),PHF
*WCG(503))
 CALL PLOT(10.0,0.0,3)
 CALL PLOT(10.0,2.0,2)
 CALL PLOT(0.0,2.0,2)
 CALL SYMBOL(0.125,1.75,0.08,'PHIZRO =',0.0,8)
 CALL NUMBER(999.0,1.75,0.08,PHIZRO,0.0,4)
 CALL SYMBOL(0.125,1.60,0.08,'ECCEN =',0.0,7)
 CALL NUMBER(999.0,1.60,0.08,ECCEN,0.0,3)
 CALL SYMBOL(0.125,1.45,0.08,'BETA =',0.0,6)
 CALL NUMBER(999.0,1.45,0.08,BETA,0.0,4)
 CALL PLOT(0.0,-3.5,-3)
 CALL AXIS(0.0,0.0,'PHIF (RAD)',10,2.0,90.0,ASLFSE(502),ASLFSE(503)
*)
 CALL AXIS(0.0,0.0,'OMEGA (RPM)',-11,10.0,0.0,RPMARY(502),RPMARY(50
*3))
 CALL LINE(RPMARY,ASLFSE,501,1,0,0)
 CALL DLINE(RPMARY,PHFWSL,501,1,5)
 CALL AXIS(10.5,0.0,'PHASE LAG (DEG.)',-16,2.0,90.0,PHFWSL(502),PHF
*WSL(503))
 CALL PLOT(10.0,0.0,3)
 CALL PLOT(10.0,2.0,2)
 CALL PLOT(0.0,2.0,2)
 CALL PLOT(0.0,-4.0,-3)
 CALL AXIS(0.0,0.0,'RD (INCHES)',11,2.0,90.0,AWDAMP(502),AWDAMP(503
*))
 CALL AXIS(0.0,0.0,'OMEGA (RPM)',-11,10.0,0.0,RPMARY(502),RPMARY(50
*3))
 CALL LINE(RPMARY,AWDAMP,501,1,0,0)
 CALL DLINE(RPMARY,PHDAMP,501,1,5)
 CALL AXIS(10.5,0.0,'PHASE LAG (DEG.)',-16,2.0,90.0,PHDAMP(502),PHD
*AMP(503))
```

```
CALL PLOT(10.0,0.0,3)
CALL PLOT(10.0,2.0,2)
CALL PLOT(0.0,2.0,2)
CALL PLOT(0.0,0.0,999)
STOP
END
```

APPENDIX D - EFFECTS OF FLYWHEEL DEAD WEIGHT AND TORQUE ON THE LOWEST FIRST-ORDER FORWARD CRITICAL SPEED OF A PENDULOUSLY SUPPORTED FLYWHEEL

D.1 Effect of Flywheel Dead Weight

For a pendulously supported flywheel, i.e., one supported from above by a vertical cantilever shaft, the dead weight of the flywheel can have an effect on the critical speeds. The reason for this effect is that the dead weight acts through a moment arm equal to the horizontal distance of the flywheel center of gravity from any arbitrary point on the flywheel shaft. Thus, a moment, varying along the length of the shaft, is produced. In the case of a pendulously supported flywheel, this moment acts in such a sense that it is a restoring moment and thus stiffens the flywheel shaft (so-called tie-bar action). If the flywheel were supported from below, this moment would be the opposite of a restoring moment and thus would unstiffen the flywheel shaft (column action).

In modes of whirling higher than the lowest one, the flywheel does not deflect significantly from its original position, as can be seen in Fig. 4.5. Hence, the dead-weight effect is significant only in the lowest mode. Only a very few papers in the literature even mention the dead-weight effect. For example, Ref. 11 mentioned it and stated that Ref. 47 showed that it affects the displacements less than 3 percent for the small-scale, research-type flywheel system investigated in [11,47]. Actually, Ref. 47 gave a linear analysis and the effect was 2.6% on the dispalcements (and thus on the flexibility); therefore, it affected the critical speeds only 1.3% approximately, due to the square-root relationship of flexibility and natural frequency ($\sqrt{1.026} \approx 1.013$).

Table D.1 presents the lowest first-order forward critical speeds for the three Systems A, B, and C, with and without the effect of flywheel dead

Table D.1. Lowest First-Order Forward Critical Speeds With and Without the Flywheel Dead-Weight Effect, for the Three Systems A,B, and C, as Computed Using the Combined-Model Analysis

	Flywheel System		
	A	B	C
Ω_g (with dead weight), rpm	1,038	1,907	14,230
Ω_o (without dead weight), rpm	1,030	1,903	14,228
Ratio Ω_g/Ω_o	1.0078	1.0021	1.0001

weight. The critical speeds were obtained using the combined model. Here, Ω_g denotes a critical speed calculated with the flywheel dead weight included and Ω_o stands for a critical speed when the pendulum effect of the flywheel weight is not used.

This pendulum effect, for a simple cantilevered flywheel system, was studied quantitatively by Greenhill many years ago and more recently by Kung [48]. Kung showed that the ratio Ω_g/Ω_o satisfies the following relation, in the absence of applied torque:

$$(\Omega_g/\Omega_o)^2 = 1 + (\bar{P}/P_{cr}) \tag{D-1}$$

where $\bar{P}$ = weight of flywheel and P_{cr} = absolute value of the critical buckling load for the system. The system for which P_{cr} has to be calculated in the present case is shown in Fig. D1(a). This system is equivalent to that shown in Fig. D1(b). By the principle of virtual work, the following equation, which equates the bending strain energy in the beam to the sum of the external work done by the force $\hat{P}$ and the moment $\hat{M}$, is obtained:

$$\int_0^{\ell} (EI/2)\left(\frac{d^2w}{dx^2}\right)^2 dx = (\hat{P}/2)\int_0^{\ell} \left(\frac{dw}{dx}\right)^2 dx + (\hat{M}/2)\,\frac{dw}{dx}\,(\ell) \tag{D-2}$$

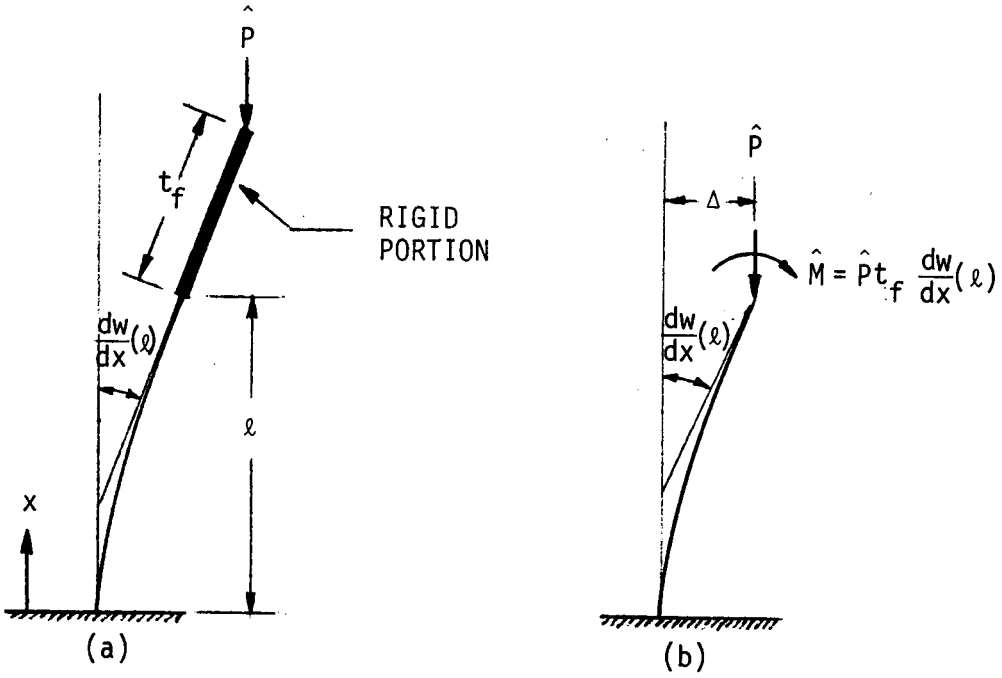

Fig. D1. (a) Actual system for which P_{cr} is desired; (b) equivalent system for which P_{cr} is determined. For convenience, the systems are shown upside down from the orientation in the actual spin-test setup.

where w = lateral deflection of the beam and EI = flexural rigidity of the beam.

Assuming that, at the instant of instability, the deflection curve can be approximated by

$$w = \Delta(1 - \cos \frac{\pi x}{2\ell}) \tag{D-3}$$

where Δ is the deflection as shown in Fig. D1(b), we obtain the following approximate expression for P_{cr}

$$P_{cr} = \hat{P} = (\pi^2/4)(EI/\ell)(\ell + 2t_f)^{-1} \tag{D-4}$$

In Sections 4 and 5, it was shown that in the first mode for Systems A and B, the damper was essentially stationary. Hence, these two systems can be

modeled as a flywheel cantilevered at the damper. Thus, ℓ = 0.7455 in. is used in equation (D-4). For System C a more active participation of the damper was predicted in the first mode. However, in the absence of a suitable equivalent length, the same ℓ used for Systems A and B is also used for System C. The results are tabulated in Table D.2. Comparison of Tables D1 and D2 show reasonably close values for Systems A and B. However,

Table D.2. Simplified Calculation of the Pendulum Effect Using Equation (D-1) (EI = 13,806 lb-in^2)

	Flywheel System		
	A	B	C
Weight $\bar{P}$, lb	36.7	22.2	13.0
t_f, in.	7.05	3.45	3.15
Ratio Ω_g/Ω_0	1.0059	1.0019	1.0010

for System C, the agreement is rather poor. This discrepancy can be explained by noting the significant damper displacement associated with the lowest first-order forward mode shape for this system. In other words, Kung's analysis, which assumes a shaft with all of the mass action lumped at the lower end, is not applicable when there is significant motion of another mass at some other location (like at the damper, in this case).

In summary, it was shown that the effect of including the flywheel dead weight (as was done in obtaining all of the numerical results presented in the other parts of this report) is very small. In fact, it was calculated to be less than 1% even in the most significant case (System A). It was shown further that the relative values obtained from the accurate combined

model analysis could be predicted reasonably accurately, at least for Systems A and B, by a simplified analysis due to Kung.

D.2 Effect of Load Torque

In spin testing of flywheels, the torque during normal, steady running is small (only 7.5 to 8.0 lb-in. for the Oak Ridge spin-test facility), since it has to overcome only the ball-bearing, damper, and windage losses (exceedingly small due to high vacuum). However, to accelerate rotationally, i.e., to increase the rotational speed, some additional torque capacity is required. For the Oak Ridge facility, the maximum torque capacity (available in the lower speed range) is on the order of 17 lb-in.

The question arises as to the effect of the aforementioned torques on the critical speeds. This can be estimated for a simple uniform-diameter shaft by Kung's version [48] of Greenhill's formula:

$$(\Omega_T/\Omega_{oT})^2 = 1 - (T/T_{cr})^2 \qquad \text{(D-5)}$$

Here, $T \equiv$ applied torque, $T_{cr} \equiv$ critical buckling torque, and Ω_T and Ω_{oT} are the critical speeds respectively with and without torque. The general expression for T_{cr} is

$$T_{cr} = \pi k E I/\ell \qquad \text{(D-6)}$$

where $k \equiv$ dimensionless buckling coefficient which depends upon the way in which the torque is applied, as well as the boundary conditions, as was discussed by Ziegler [49]. Here, we conservatively assume that the torque is applied semitangentially in Ziegler's terminology and that the support conditions are those of a cantilever. Then $k = 1$, according to [49].

For the Oak Ridge system, $E = 29.5 \times 10^6$ psi, $I = (5/16)^4/64 = 0.000468$ in.^{4}, $\ell = 0.745$ in. Thus, the critical speed is lowered only 43 parts in 10^9, even when the maximum available torque of 17 lb-in. is used. Obviously, this is certainly a negligible effect from an engineering standpoint.

APPENDIX E - LIST OF SYMBOLS

A_i	cross-sectional area of the shaft sections (i=1,2,3)
A'_j	cross-sectional areas at various stepped sections of the turbine shaft (j=1,2,3) (see Appendix A.2)
A_t	cross-sectional area of the uniform shaft equivalent to the stepped turbine shaft
A	amplitude of w in the first of equations (B-23)
$\hat{A}$	cross-sectional area of shaft (Appendix B.2)
A_{eq}	cross-sectional area of the modified quill-shaft sections inside the turbine shaft (Fig. B1)
$\bar{A}_j$	coefficient appearing in the first of equations (B-25), (j=1,...,4)
A_{ij}	coefficients appearing in the first of equations (B-27) and Appendix B (i=1,2,3), (j=1,...,4)
$\overline{AA}$	$(\ell_3/K_3A_3G) + (\ell_3^3/3EI_3)$
a_i	length parameters appearing in equations (A-1), (i=1,...,4)
B	amplitude of ψ in the second of equations (B-23)
B_j	coefficient appearing in the second of equations (B-25), (j=1,...,4)
B_{pj}	coefficient appearing in the second of equations (B-27), (p=1,2,3), (j=1,...,4)
$[B_1],[B_2]$	matrices defined in equations (2.11)
$[B_1^*],[B_2^*]$	matrices appearing in equation (2.19)
C_d	damping coefficient of external damper
$[C]$	damping matrix defined in equation (2.15)
$[\bar{C}]$	coefficient matrix appearing in equation (B-55)
d'_1,d'_2,d'_3,d_i	diameters defined in Fig. A1
d_o	outer diameter of the equivalent uniform turbine shaft
E	Young's modulus of shaft material

E^*	complex Young's modulus of shaft material
e	base of the natural logarithms
F_j	lateral forces acting in lumped model (j=d,f,i,t)
F_o	arbitrary lateral force acting through the turbine center of mass (see Appendix A.2)
F_r	elastic restoring force in a whirling shaft (section 4)
$\bar{F}_d$	side force due to hysteretic damping
$\hat{F}$	total force acting on a whirling shaft element (section 4)
$\{F\}$	generalized-force excitation vector defined in equation (2.21)
G	shear modulus of shaft material
G^*	complex shear modulus of shaft material
g	gravitational acceleration
$[G]$	gyroscopic matrix defined in equation (2.4)
I	area moment of inertia of shaft cross section about a diametral axis
I_d, I_p	diametral and polar mass moments of inertia of a shaft element of length dz
I_{dj}, I_{pj}	respective diametral and polar mass moments of inertia of components (j=f,i,t)
I_i'	area moments of inertia about a diameter of the various stepped portions of the turbine shaft (i=1,2,3) (see Appendix A.2)
I_i	area moment of inertia about a diameter of the ith shaft section (i=1,2,3)
I_t	area moment of inertia about a diameter of the equivalent turbine shaft
$[I]$	identity matrix (main diagonal elements are all unity, remaining elements are all zero)

I_{eq}	area moment of inertia of the modified flywheel shaft, inside the turbine shaft, about a diameter
I_{ac}	area moment of inertia of the actual flywheel shaft, inside the turbine shaft, about a diameter
i	$\sqrt{-1}$
K_{eq}	transverse shear correction coefficient of the modified quill shaft within the turbine shaft
K, K_i	transverse shear correction coefficients, (i=1,2,3)
K_t	transverse shear correction coefficient of the equivalent turbine shaft
K_{neop}	spring rate of neoprene-rubber washer in external damper
$K_{s\ell}, K_{su}$	spring rates of the lower and upper bearings, respectively
K_i'	transverse shear correction coefficients of the various stepped cross sections of the turbine shaft (i=1,2,3) (see Appendix A.2)
$[K]$	stiffness matrix appearing in equation (2.1)
$[\bar{K}]$	$[\alpha]^{-1}$
$[K^*]$	complex stiffness matrix appearing in equation (2.14)
k	dimensionless buckling coefficient (see Appendix D.2)
L_{ac}	length defined in Fig. B1
L_i	lengths appearing in Appendix B (see Fig. 3.1) (i=1,2,3)
ℓ	length of flexible shaft (shown in Fig. D1)
ℓ_a, ℓ_b, ℓ_c ℓ_g, ℓ_3	lengths (see Fig. 2.1)
ℓ_1', ℓ_2'	lengths defined in Fig. A1
M, M_x, M_y	total bending moment and its components about the x and y axes
$\hat{M}$	moment used in Appendix D.1

M_o	an arbitrary moment acting on the turbine wheel (see Appendix A.2)
M_j	bending moments at components (j=d,f,i,t) of lumped model
M_i, M_{ix}, M_{iy}	total bending moment and its components about the x and y axes acting on the ends of shaft i (i=1,2,3) (Appendix B.3)
[M]	mass matrix defined in equation (2.3)
$m, \bar{m}$	ratios of inside diameter to outside diameter
m_j	masses of components (j=d,f,i,t) in the lumped model
n	ω/Ω
[0]	zero matrix (all elements are zero)
{0}	zero column matrix
P	axial force in shaft
$\bar{P}$	weight of flywheel
$\hat{P}$	axial force used in Appendix D.1
P_{cr}	absolute value of the critical buckling load for a flywheel system
$\{\bar{p}\}$	$\omega\{\bar{q}\}$
{q}	generalized displacement vector defined in equation (2.2)
$\{\bar{q}\}$	generalized displacement amplitude vector
R_1, R_2	turbine-bearing reactions (see Fig. 2.2)
R_i, R_o	inner and outer radii of a shaft element
r_e	mass eccentricity
r_j	translational displacements of components (j=d,f,i,t) in the lumped model
r_o	deflection of turbine center of mass when subjected to a force F_o and moment M_o (see Appendix A.2)
t	time
T	applied torque on the turbine wheel

T_{cr}	critical buckling torque (see Appendix D.2)
t_1, t_2, t_3 t_d, t_f, t_s, t_t	thickness parameters defined in Fig. 2.1
U	total strain energy in the system
U^*	strain energy in the turbine shaft; equation (A-9)
V, V_x, V_y	total shear force and its components in the x and y directions
V_i, V_{ix}, V_{iy}	total shear force and its components in the x and y directions acting on the ends of shaft i (i=1,2,3) (Appendix B.3)
w, w_x, w_y	lateral displacement of a shaft element and its components in the x and y directions
w_i, w_{ix}, w_{iy}	lateral displacement and its components in the x and y directions of specific locations on the ith shaft (i=1,2,3) as defined in Appendix B.3
w_p	deflection distribution of shaft section p (p=1,2,3); see equation (B-27)
$\bar{w}, \bar{w}_x, \bar{w}_y$	lateral displacement of flywheel center of mass and its components in the x and y directions
$\bar{w}', \bar{w}'_x, \bar{w}'_y$	lateral displacement of intermediate mass center and its components in the x and y directions
$\bar{w}_s, \bar{w}_{xs}, \bar{w}_{ys}$	displacement of the lower spring attachment point and its components in the x and y directions
$\bar{w}'', \bar{w}''_x, \bar{w}''_y$	displacement of turbine center of mass and its components in the x and y directions
$\bar{w}_1$	displacement of the flywheel center of mass when $r_e = 0$
x, y, z	Cartesian coordinates in a reference frame attached to the deflected shaft, tilting, but not rotating, with it

x_o, y_o, z_o	Cartesian coordinates in an inertial reference frame
z^*	an arbitrary point in any of the three shaft sections
z_p	position coordinate z in shaft p (p=1,2,3)
α_{ij}	compliance coefficients defined in equations (A-7), (i,j=1,...,8)
$\bar{\alpha}$	coefficient appearing in equations (B-23)
$\bar{\alpha}_j$	coefficients appearing in equations (B-25), (j=1,...,4)
$\bar{\alpha}_{pj}$	coefficients appearing in equations (B-27) and Appendix B, (p=1,2,3), (j=1,...,4)
$\alpha^*_{11}, \alpha^*_{12}, \alpha^*_{22}$	compliances for the equivalent uniform turbine shaft (see Appendix A.2)
$[\alpha]$	compliance matrix appearing in equation (2.5) and Appendix A
$\alpha'_{11}, \alpha'_{12}, \alpha'_{22}$	compliances defined in Appendix A.2 for the actual stepped turbine shaft
β	phase lag of flywheel initial tilt relative to the mass eccentricity
$\gamma, \gamma_x, \gamma_y$	total shear strain and its components in the yz and xz planes
γ_s	loss tangent (= $\bar{F}_d/F_r$)
Δ	deflection of flywheel shaft end (see Appendix D.1)
$\Delta\Omega$	increments in Ω to plot whirl diagrams
δ	angle between the deflected flywheel center line and the axis of rotation (see Fig. B9)
ν	Poisson's ratio of shaft material
ρ	density of shaft material
ϕ_j	tilting angles of components (j=d,f,i,t) in the lumped model
$\bar{\phi}_o$	rotation of turbine wheel when subjected to a force of F_o and a moment of M_o (see Appendix A.2)

ϕ_o	initial tilt of flywheel with respect to axis of rotation
$\vec{\phi}_o$	initial tilt of flywheel defined as a vector
ψ, ψ_x, ψ_y	bending slope and its components in the x and y directions
$\psi_i, \psi_{ix}, \psi_{iy}$	bending slope and its components in the x and y directions at specified locations as defined in Appendix B.2
ψ_p	bending-slope distribution of shaft section p (p=1,2,3); see equation (B-27)
θ	a factor defined in equation (A-12) for the actual stepped turbine shaft
θ^*	a factor equal to θ for the equivalent uniform turbine shaft
Ω	rotational speed
Ω^*	an arbitrary rotational speed within the range of operation
Ω_{11}	lowest first-order critical speed
Ω_{21}	second lowest first-order critical speed
Ω_g	lowest first-order critical speed with the effect of flywheel deadweight included
Ω_o	lowest first-order critical speed without the effect of flywheel deadweight
Ω_{oT}	lowest first-order critical speed without the effect of applied torque being considered
Ω_T	lowest first-order critical speed with the effect of applied torque
ω	natural frequency of vibration
ω_I, ω_R	imaginary and real parts of ω
$(\dot{\ })$	derivative with respect to time

APPENDIX F - SUGGESTIONS FOR FURTHER RESEARCH ON ANALYSIS OF FLYWHEEL ROTOR DYNAMICS

The following are some areas in which further research could be conducted to extend usefulness of the present state of the art of knowledge on flywheel rotor dynamics:

1. The effect of power take-off or power feed-in, as a steady torque, on the system dynamics. In the present work, the applied torque at the turbine wheel was neglected, based on the analysis of Appendix D.2. However, in some vehicular applications, this could become a more significant factor.

2. The effect of accelerating through the critical speeds, for which the torque available at the turbine is the limiting factor. In the present work, transients [50] have not been considered.

3. The use of magnetic bearings and the corresponding use of active control to prevent whirl instability [51]. In the present work, whirl instability is controlled only by the external viscous damper, which is a passive one.

4. The use of a nonlinear model of the squeeze-film damper action, in which the damping coefficient C_d increases when the damper disk approaches the housing wall [19], rather than the present equivalent viscous damper. However, recent research [52] has shown that even the currently accepted nonlinear hydrodynamic theory for finite-length squeeze-film bearings is inadequate to predict quantitative response.

5. Study of excitation and response of nonsynchronous whirling.

6. Effect of Coulomb damping due to relative motion between flywheel components as a function of rotational speed. This may be important in only certain flywheel systems.

7. Effect of the increase in flywheel moment of inertia due to the radial growth due to centrifugal action. This is believed to be a negligible effect on all current flywheels known to the present authors.